

THESIS

QUANTIFICATION OF PERFORMANCE, DAMAGE, AND RISK TO LIGHT WOOD
FRAME BUILDINGS SUBJECTED TO TORNADOES AND EXPANSIVE SOILS

Submitted by

Timothy D. Maloney

Department of Civil and Environmental Engineering

In partial fulfillment of the requirements

For the Degree of Master of Science

Colorado State University

Fort Collins, Colorado

Fall 2017

Master's Committee:

Advisor: Hussam N. Mahmoud

Co-Advisor: Bruce R. Ellingwood

John W. van de Lindt

Sammy Zahran

Copyright by Timothy D. Maloney 2017

All Rights Reserved

ABSTRACT

QUANTIFICATION OF PERFORMANCE, DAMAGE, AND RISK TO LIGHT WOOD FRAME BUILDINGS SUBJECTED TO TORNADOES AND EXPANSIVE SOILS

Each year, damage to infrastructure caused by the uncorrelated hazards of tornadoes and expansive soils is on the order of billions of dollars. The monetary losses caused by each hazard alone are reason for concern. For tornados, however, the impact can be devastating and extend beyond monetary loss. Furthermore, the presence of expansive soils can exacerbate life-safety concerns during a tornado by limiting construction of underground shelters such as basements. It is not uncommon for communities to be crippled by damage to critical infrastructure such as businesses, homes, utility networks, and emergency facilities. This destruction can limit a community's ability to support its population in the short-term which can lead to significant outmigration that may be difficulty to recover from. The ability of a community to plan for and recover from such hazards is referred to as community resilience. The major goal of this research is to contribute to the development of a set of standards and guidelines for resilient community design. Specifically, this study aims to link the performance of individual building components to building system performance, so that the effect of implementing a change in standard construction techniques (i.e. recommending that homes be constructed with hurricane clips) can be quantified. The work herein focuses on light wood frame residential buildings constructed with methods typical in the American heartland.

The research approach taken herein was to develop detailed finite element (FE) models to capture building system performance and individual building component behavior under

expansive soil and tornado loading. The level of detail used in the FE models allows the interaction between building components to be captured to a higher degree than previously possible. Knowledge of the demand on building components gained from the FE analysis was then applied to perform statistical analysis to quantify the performance of several building archetypes chosen to represent the residential building portfolio in a typical community located in the US heartland. The performance of the typical archetypes was then analyzed to identify deficient building components and compared to target resilience performance levels provided by research partners at the University of Oklahoma. The effect of implementing various improved construction techniques was then examined in an effort to meet the resilience performance targets.

This study revealed that, typically, light wood frame residential construction that is common in tornado prone areas of the U.S. is not sufficient to meet the resiliency goals considered in this study. This is unsurprising considering the historical lack of consideration given to tornado hazards in U.S. design codes and standards. Similarly, it was found that typical masonry block basement wall construction was insufficient to withstand loading from expansive soils without sustaining damage. This is also not surprising because many people in expansive soil prone areas choose to forgo constructing basements due to the likelihood of damage. The study also revealed, however, that resilience target performance levels can be achieved using existing construction techniques. This suggests that resilient community design is a goal that is already within reach at the current state of the art.

ACKNOWLEDGEMENTS

First, I would like to recognize my advisors, Dr. Hussam Mahmoud and Dr. Bruce Ellingwood for their support and guidance throughout my graduate studies. I have learned far more during my time working with them than I could have imagined at the beginning of my graduate education at Colorado State University (CSU). The knowledge and insight into structural engineering and general problem solving that they have shared with me has been truly eye-opening and the work ethics that they display has been inspirational. The work presented in this thesis would not have been possible without them, and I am very grateful for having been given the opportunity to learn from them.

I would also like to acknowledge the financial and logistical support of the National Science Foundation (NSF) under grant award # 1452725 without which this research would not be possible. Additionally, I would like to recognize our NSF collaborators here at CSU and at the University of Oklahoma, the University of Washington, and the University of Colorado for the support and expertise that they have provided.

Finally, I want to acknowledge the life-long support of my family. In particular I want to thank my parents Dr. Daniel J. Maloney and Christina B. Maloney for instilling the values of hard work and education in me and my siblings from an early age and for providing us with love and support in all of our endeavors. You have provided me with examples of these values throughout my life in both your words and your actions and by doing so you have given me a solid foundation upon which to build my career and my life. I also want to thank my girlfriend, Allison for her patience, understanding, and love throughout this process. Together, you have acted as the support structure that I have needed to make it through my graduate studies.

TABLE OF CONTENTS

ABSTRACT.....	ii
ACKNOWLEDGEMENTS.....	iv
LIST OF TABLES.....	x
LIST OF FIGURES.....	xii
CHAPTER 1 INTRODUCTION.....	1
1.1 Problem Statement.....	1
1.2 Research Objective and Scope.....	3
1.3 Organization of Thesis.....	6
CHAPTER 2 BACKGROUND AND LITERATURE REVIEW.....	7
2.1 Hazard Quantification and Existing Treatment in U.S. Codes.....	7
2.1.1 Tornado Hazards.....	8
2.1.2 Expansive Soil Hazards.....	17
2.2 Typical Residential Home Construction in Norman, OK.....	20
2.2.1 Common Construction Practice.....	21
2.2.2 Observed Building Failures under Tornado Action.....	24
2.2.3 Observed Expansive Soil Damage.....	27
2.2.4 Existing Mitigation Techniques: Tornado Hazards.....	28
2.2.5 Existing Mitigation Techniques: Expansive Soils.....	30
2.3 Material Parameters and Connection Strengths.....	32
2.3.1 Building Materials.....	32
2.3.2 Experimental Connection Strength Values.....	34
2.3.3 Component Resistance Statistical Parameters.....	38
CHAPTER 3 BUILDING ARCHETYPES, QUALITY LEVELS, AND MODELING APPROACH.....	42
3.1 Analysis Program: ABAQUS.....	42

3.2 Building Archetypes	42
3.2.1 Archetype 1: Small, 1-Story, Hip Roof Home (Figure 3.1).....	42
3.2.2 Archetype 2: Small, 2-Story, Gable Roof Home (Figures 3.2 and 3.3).....	44
3.2.3 Archetype 3: Medium, 1-Story, Hip Roof Home (Figure 3.4).....	46
3.3 Quality of Construction.....	48
3.3.1 Basic Construction Quality	48
3.3.2 Quality Levels 1 (Enhanced), 2 (Improved), and 3 (Resistant)	48
3.4 Modeling Techniques/Element Types	49
3.4.1 Fastener Modeling.....	49
3.4.2 Masonry Basement Wall Modeling.....	51
CHAPTER 4 MODEL VALIDATION	55
4.1 Component Level Model Validation	55
4.1.1 Shear Wall Model Validation.....	56
4.1.2 Roof Sheathing Panel Model Validation.....	61
4.1.3 Basement Masonry Wall Model Validation.....	66
4.2 Building System Level Model Validation	70
4.2.1 Fundamental Frequency Validation (<i>f</i>)	70
4.2.2 Earthquake Response Validation	73
CHAPTER 5 BASIC QUALITY ARCHTYPE PERFORMANCE	78
5.1 Building Damage Quantification	78
5.1.1 Roof Cover Failure.....	79
5.1.2 Window/Door Failure	79
5.1.3 Roof Deck Failure	80
5.1.4 Missile Impact on Walls.....	80
5.1.5 Roof Structure Failure.....	80
5.1.6 Wall Structure Failure	80
5.1.7 Building System Damage.....	81
5.2 Building Quality Level Targets	82

5.3 Building System Mean Value Analysis and Statistical Modeling – Component Level	84
5.3.1 Roof Panel Failure.....	86
5.3.1.1 Archetype 1, Basic Quality (A1-BQ)	86
5.3.1.2 Archetype 2, Basic Quality (A2-BQ)	88
5.3.1.3 Archetype 3, Basic Quality (A3-BQ)	89
5.3.2 Rafter to Top Stud-Sill Connection Failure	91
5.3.2.1 Archetype 1, Basic Quality (A1-BQ)	93
5.3.2.2 Archetype 2, Basic Quality (A2-BQ)	100
5.3.2.3 Archetype 3, Basic Quality (A3-BQ)	109
5.3.3 Bottom Stud-Sill to Foundation Connection Failure	109
5.3.3.1 Archetype 1, Basic Quality (A1-BQ)	112
5.3.3.2 Archetype 2, Basic Quality (A2-BQ)	114
5.3.3.3 Archetype 3, Basic Quality (A3-BQ)	114
5.3.4 Wall Sheathing Damage.....	115
5.3.4.1 Archetype 1, Basic Quality (A1-BQ).....	116
5.3.4.2 Archetype 2, Basic Quality (A2-BQ).....	123
5.3.4.3 Archetype 3, Basic Quality (A3-BQ).....	125
5.3.5 Window/Door Pressure Failure.....	126
5.3.5.1 Archetype 1, Basic Quality (A1-BQ).....	127
5.3.5.2 Archetype 2, Basic Quality (A2-BQ).....	127
5.3.5.3 Archetype 3, Basic Quality (A3-BQ).....	127
5.3.6 Roof Cover Failure.....	128
5.3.6.1 Archetype 1, Basic Quality (A1-BQ).....	128
5.3.6.2 Archetype 2, Basic Quality (A2-BQ).....	129
5.3.6.3 Archetype 3, Basic Quality (A3-BQ).....	129
5.3.7 Summary of Component Fragilities	129
5.3.7.1 Archetype A1-BQ Component Fragilities	129
5.3.7.2 Archetype A2-BQ Component Fragilities	139

5.3.7.3 Archetype A3-BQ Component Fragilities	145
5.4 Building System Level Fragility Analysis	148
5.4.1 Archetype A1-BQ Building System Fragilities	149
5.4.2 Archetype A2-BQ Building System Fragilities	152
5.4.3 Archetype A3-BQ Building System Fragilities	154
5.4.4 Building System Fragility Archetype Comparison	155
5.5 Masonry Basement Wall Mean Value Analysis and Statistical Modeling	158
5.5.1 Masonry Block Basement Wall Mean Value Analysis.....	159
5.5.2 Masonry Block Basement Wall Statistical Analysis.....	163
CHAPTER 6 PROPOSED BUILDING IMPROVEMENTS	165
6.1 Building System Improvements to Meet Target Fragilities	165
6.1.1 <i>Enhanced</i> Quality Target	171
6.1.1.1 Archetype A1	171
6.1.1.2 Archetype A2	173
6.1.1.3 Archetype A3	176
6.1.2 <i>Improved</i> Quality Target	178
6.1.2.1 Archetype A1	178
6.1.2.2 Archetype A2	180
6.1.2.3 Archetype A3	183
6.1.3 <i>Resistant</i> Quality Target.....	184
6.1.3.1 Archetype A1	185
6.1.3.2 Archetype A2	187
6.1.3.3 Archetype A3	189
6.2 Building System Improvements Summary	190
6.3 Masonry Basement Wall Improvements	191
CHAPTER 7 CONCLUSIONS AND RECOMMENDATIONS FOR FUTURE RESEARCH	195
7.1 Summary	195
7.2 Conclusions.....	196

7.2.1 Basic Quality Archetypes	196
7.2.2 Enhanced, Improved, and Resistant Quality Archetypes	197
7.3 Recommendations for Future Research	197
REFERENCES	200
APPENDIX A FASTENER SPECIFICATIONS	204
APPENDIX B CLEVELAND COUNTY, OKLAHOMA SOIL SURVEY DATA	205

LIST OF TABLES

Table 2.1	Summary of Wind Load Parameter Statistics; All Archetypes	12
Table 2.2	Aerodynamic Coefficients for Building Archetypes 1 & 3	13
Table 2.3	Aerodynamic Coefficients for Building Archetype 2	14
Table 2.4	Summary of relevant building material parameters.....	33
Table 2.5	Component resistance statistics; all archetypes	40
Table 2.6	Masonry block basement wall component material property statistics	40
Table 3.1	Masonry block wall component material properties	52
Table 3.2	ABAQUS CDP model input parameters	53
Table 4.1	Model roof panel failure pressures for different failure criteria	64
Table 5.1	HAZUS hurricane module damage states (HAZUS Table 6-9)	78
Table 5.2	Modified HAZUS hurricane module damage states	81
Table 5.3	A1-BQ F_p factors	98
Table 5.4	A2-BQ F_p factors	106
Table 5.5	Foundation connection uplift resistance accounting for shear-uplift interaction (Alfano 2016).....	110
Table 5.6	Wall line load percentages	111
Table 5.7	Drift induced wall sheathing cracking; worst case wind direction	116
Table 5.8	A2-BQ wall sheathing damage critical story	124
Table 6.1	10th percentile failure wind speed comparison; A1-BQ lower bound <i>versus</i> Li (2005).....	167
Table 6.2	A1 enhanced quality improvements	171
Table 6.3	A1 enhanced quality improvements (lower bound).....	172
Table 6.4	A2 enhanced quality improvements	174
Table 6.5	A2 enhanced quality improvements (lower bound)	174
Table 6.6	A3 enhanced quality improvements	176
Table 6.7	A3 enhanced quality improvements (lower bound).....	176

Table 6.8	A1 improved quality improvements	178
Table 6.9	A1 improved quality improvements (lower bound).....	179
Table 6.10	A2 improved quality improvements	180
Table 6.11	A2 improved quality improvements (lower bound).....	181
Table 6.12	A3 improved quality improvements	183
Table 6.13	A3 improved quality improvements (lower bound).....	183
Table 6.14	A1 resistant quality improvements	185
Table 6.15	A1 resistant quality improvements (lower bound).....	185
Table 6.16	A2 resistant quality improvements	187
Table 6.17	A2 resistant quality improvements (lower bound).....	187
Table 6.18	A3 resistant quality improvements	189
Table 6.19	A3 resistant quality improvements (lower bound).....	189
Table 6.20	Concrete Block Masonry Basement Wall Improvements.....	194
Table A.1	Nail Sizing Chart.....	204
Table A.2	Hurricane Clip Specifications (from Simpson Strong-Tie)	204
Table B.1	Relevant Cleveland County Soil Parameters (from USDA Soil Survey Data) ...	205

LIST OF FIGURES

Figure 1.1	Construction quality and standards for each archetype	5
Figure 2.1	EF Scale	11
Figure 2.2	Wind pressure zones for (a) wind effects on MWFRS and (b) C&C (after ASCE 7-10)	15
Figure 2.3	Areas in the continental U.S. susceptible to expansive soils (FHWA).....	17
Figure 2.4	Soil pressures acting on basement wall	18
Figure 2.5	Typical roof panel nailing pattern.....	21
Figure 2.6	Typical rafter to sill connection detail	22
Figure 2.7	Typical exterior wall sheathing detail.....	23
Figure 2.8	Typical roof panel failure (RoofingAnnex.com)	25
Figure 2.9	Typical roof-wall connection failure (newson6.com).....	25
Figure 2.10	Typical wall collapse failure (Denver.cbslocal.com)	26
Figure 2.11	Typical wall-foundation connection failure (van de Lindt et al. (2013))	26
Figure 2.12	Typical masonry basement wall cracking due to expansive soils (basement systems.ca).....	27
Figure 2.13	Typical foundation slab cracking due to expansive soils (nachi.org).....	28
Figure 2.14	Typical hurricane strap (Simpson Strong-Tie)	29
Figure 2.15	Typical foundation tie (Simpson Strong-Tie).....	30
Figure 2.16	Roof and wall sheathing nail pullout load-displacement curves	35
Figure 2.17	Gypsum nail tear-through load-displacement curve	37
Figure 2.18	Wood to wood toe nail pullout load-displacement curve	38
Figure 3.1	Archetype 1 layout (a) complete, (b) w/out roof, (c) w/out wall sheathing	44
Figure 3.2	Archetype 2 roof truss.....	45
Figure 3.3	Archetype 2 layout.....	46
Figure 3.4	Archetype 3 layout (a) plane view and (b) bird’s-eye view.....	47
Figure 3.5	3-dimensional nail – spring model orientation	51
Figure 3.6	Masonry wall composite material compressive and tensile stress-strain curves ..	53
Figure 3.7	Masonry wall composite material compressive and tensile damage-strain curves	54

Figure 4.1	Model validation shear wall layout (Bahmani and van de Lindt (2014))	56
Figure 4.2	ABAQUS shear wall model.....	57
Figure 4.3	ABAQUS shear wall model – deformed shapes (x-z view, y-z view, x-y view) ..	58
Figure 4.4	Model versus experimental in plane shear wall load-displacement	59
Figure 4.5	Gypsum board fastener shear load-displacement	60
Figure 4.6	Roof sheathing edge rotation restriction	61
Figure 4.7	Roof panel failure criterion sequence	65
Figure 4.8	Roof panel model deformed shape and stress contours	66
Figure 4.9	Masonry wall test setup (Bui et al. (2013))	66
Figure 4.10	Masonry wall test pressure setup and transducer location (Bui et al. (2013)).....	67
Figure 4.11	Masonry wall model validation pressure-displacement curves	68
Figure 4.12	Masonry wall damage: experimental <i>versus</i> model.....	69
Figure 4.13	Fundamental period calculation: simplified setup	71
Figure 4.14	1994 Northridge Earthquake – Canoga Park station ground motion acceleration scaled to PGA 0.3g	73
Figure 4.15	Earthquake response ceiling level drift measurement node (from Isoda et al. (2002), Fig. 3.2)	75
Figure 4.16	Drift-time history: ABAQUS model <i>versus</i> CUREE-Caltech poor CQL	76
Figure 4.17	Drift-time history: ABAQUS model <i>versus</i> CUREE-Caltech typical CQL	76
Figure 5.1	Construction Quality Level 1 (Enhanced) damage state target fragilities	83
Figure 5.2	Construction Quality Level 2 (Improved) damage state target fragilities	83
Figure 5.3	Construction Quality Level 3 (Resistant) damage state target fragilities	84
Figure 5.4	Pressure <i>versus</i> displacement A1-BQ initial roof panel failure	87
Figure 5.5	A1-BQ roof panels considered in statistical analysis and first roof panel to fail ..	88
Figure 5.6	A2-BQ roof panels considered in statistical analysis and first roof panels to fail ..	89
Figure 5.7	A3-BQ roof panel layout	90
Figure 5.8	Rafter-Sill connection, worst case wind direction	92
Figure 5.9	A1-BQ L_p <i>versus</i> P_w/P_l for the five most critical rafters	95

Figure 5.10	Single rafter failure load redistribution analysis	96
Figure 5.11	A1-BQ rafter-sill connection critical rafter determination	97
Figure 5.12	A2-BQ identification of critical rafters	101
Figure 5.13	A2-BQ L_p versus P_w/P_l five most critical rafters	103
Figure 5.14	A2-BQ rafter-sill connection fragility: logarithmic fit L_p versus $L_p = 0.30$	104
Figure 5.15	Governing equations for F_p for tributary panel loss or adjacent panel loss	105
Figure 5.16	A2-BQ rafter-sill connection fragility: accounting for and not accounting for failure of adjacent roof panels	106
Figure 5.17	A2-BQ single panel failure case projected L_p value	107
Figure 5.18	A2-BQ multiple panel failure case projected L_p value	108
Figure 5.19	Wall to foundation shear-uplift interaction curves (Alfano 2016).....	110
Figure 5.20	Wall sheathing cracking due to wall racking fragilities versus other critical failure mode fragilities	119
Figure 5.21	A1-BQ Roof panel fragilities; DS-1	130
Figure 5.22	A1-BQ Roof panel fragilities; DS-2	130
Figure 5.23	A1-BQ Roof panel fragilities; DS-3	131
Figure 5.24	A1-BQ Roof panel fragilities; DS-4	131
Figure 5.25	A1-BQ Rafter-sill connection fragilities; DS-1 - 4.....	132
Figure 5.26	A1-BQ Foundation connection fragilities; DS-1 - 4.....	133
Figure 5.27	A1-BQ Wall sheathing fragilities; DS-1.....	134
Figure 5.28	A1-BQ Window/door pressure fragilities; DS-1	135
Figure 5.29	A1-BQ Window/door pressure fragilities; DS-2	135
Figure 5.30	A1-BQ Window/door pressure fragilities; DS-3	136
Figure 5.31	A1-BQ Roof cover fragilities; DS-1	137
Figure 5.32	A1-BQ Roof cover fragilities; DS-2.....	137
Figure 5.33	A2-BQ Roof panel fragilities; DS-1	139
Figure 5.34	A2-BQ Roof panel fragilities; DS-2	140

Figure 5.35	A2-BQ Roof panel fragilities; DS-3	140
Figure 5.36	A2-BQ Roof panel fragilities; DS-4	141
Figure 5.37	A2-BQ Rafter-sill connection fragilities; DS-1 - 4.....	141
Figure 5.38	A2-BQ Foundation connection fragilities; DS-1 - 4.....	142
Figure 5.39	A2-BQ Wall sheathing fragilities; DS-1.....	143
Figure 5.40	A2-BQ Window/door pressure fragilities; DS-1	143
Figure 5.41	A2-BQ Window/door pressure fragilities; DS-2	144
Figure 5.42	A2-BQ Window/door pressure fragilities; DS-3	144
Figure 5.43	A2-BQ Roof cover fragilities; DS-1	145
Figure 5.44	A2-BQ Roof cover fragilities; DS-2.....	145
Figure 5.45	A3-BQ Foundation connection fragilities; DS-1 - 4.....	146
Figure 5.46	A3-BQ Wall sheathing fragilities; DS-1.....	146
Figure 5.47	A3-BQ Window/door pressure fragilities; DS-1	147
Figure 5.48	A3-BQ Window/door pressure fragilities; DS-2	147
Figure 5.49	A3-BQ Window/door pressure fragilities; DS-3	148
Figure 5.50	A1-BQ upper bound damage fragilities w/out windborne debris breach	149
Figure 5.51	A1-BQ lower bound damage fragilities w/out windborne debris breach	150
Figure 5.52	A1-BQ upper bound fragility comparison; no debris breach <i>versus</i> debris breach cases	151
Figure 5.53	A1-BQ lower bound fragility comparison; no debris breach <i>versus</i> debris breach cases	151
Figure 5.54	A2-BQ upper bound damage fragilities	152
Figure 5.55	A2-BQ lower bound damage fragilities	153
Figure 5.56	A3-BQ upper bound damage fragilities	154
Figure 5.57	A3-BQ lower bound damage fragilities	155
Figure 5.58	DS-1 building system fragility archetype comparison	156

Figure 5.59	DS-2 building system fragility archetype comparison	156
Figure 5.60	DS-3 building system fragility archetype comparison	157
Figure 5.61	DS-4 building system fragility archetype comparison	157
Figure 5.62	Tensile damage gradation: masonry block basement wall	162
Figure 6.1	A1-BQ upper and lower bound fragilities versus Roueche et al. (2017) comparable damage states	168
Figure 6.2	A1 upper bound enhanced quality fragilities	172
Figure 6.3	A1 lower bound enhanced quality fragilities	173
Figure 6.4	A2 upper bound enhanced quality fragilities	175
Figure 6.5	A2 lower bound enhanced quality fragilities	175
Figure 6.6	A3 upper bound enhanced quality fragilities	177
Figure 6.7	A3 lower bound enhanced quality fragilities	177
Figure 6.8	A1 upper bound improved quality fragilities	179
Figure 6.9	A1 lower bound improved quality fragilities	180
Figure 6.10	A2 upper bound improved quality fragilities	181
Figure 6.11	A2 lower bound improved quality fragilities	182
Figure 6.12	A3 upper bound improved quality fragilities	184
Figure 6.13	A3 lower bound improved quality fragilities	184
Figure 6.14	A1 upper bound resistant quality fragilities	186
Figure 6.15	A1 lower bound resistant quality fragilities	186
Figure 6.16	A2 upper bound resistant quality fragilities	188
Figure 6.17	A2 lower bound resistant quality fragilities	188
Figure 6.18	A3 upper bound resistant quality fragilities	190
Figure 6.19	A3 lower bound resistant quality fragilities	190

CHAPTER 1

INTRODUCTION

1.1 Problem Statement

More than 90% of the investment in building construction in the United States is in light-framed residential construction. Buildings such as these are simple, quick, and generally relatively inexpensive to construct, so their appeal to both home buyers and developers is obvious. Unfortunately, because the buildings are generally not engineered or designed for specific hazards, their performance under such hazards is often difficult to quantify. What is apparent is that these structures, at times may be inadequate to ensure even the most basic standard of engineering design - life safety, let alone enhanced performance objectives such as reparability and continued occupancy and function in the event of an extreme natural hazard. As observed in the case of disasters such as the Joplin, Missouri tornado in 2011, which took 161 lives and caused nearly \$3 billion in damages (Kuligowski et al. (2014)), when buildings fail to provide adequate shelter, the results can be tragic. Not only are lives lost as a result of the disaster, but the long term effects on the community can result in serious economic and social issues. For example, if people are forced from their homes due to serious damage that requires extensive and costly repairs, or the construction of a new home altogether, their daily lives as productive members of the community will be disrupted, even if losses are insured. Similarly, the longer that schools and businesses are closed, the more likely it is that people will leave the community to resume their lives elsewhere. The functionality of other essential community features such as hospitals, fire stations, and water and power facilities can be even more critical

to the health and well-being of the community in a disaster scenario, however these facilities do not typically utilize light wood frame construction, and thus are not the focus of this study.

A community's ability to plan for the impact of extreme hazard events and to recover from them is referred to as community resilience (Presidential Policy Directive 21). Design for resilience should be aimed at preventing an extreme event from becoming a disaster. Community resilience is a relatively new consideration in building design and construction because up to this point, building codes and regulatory processes have focused on the design of individual buildings, not building portfolios and their primary design concern has been life safety, not functionality, reparability, or economic loss. Most of the resiliency research that has been done to this point has considered actions and policies to achieve community resilience objectives (Bruneau, 2003; McAllister, 2013). Little work has been done to explore the link between individual building performance and community resilience as a whole (Lin and Wang 2016), and thus there is a lack of quantitative knowledge about this relationship. Without this knowledge, it is not possible to evaluate the community wide benefit of implementing individual building improvements and so it is difficult to assert as to which of these improvements may be economically and practically worthwhile in a given community subject to unique hazards. This gap in the knowledge base represents a significant road block to the realistic development of more resilient communities.

Although communities across the country can be subject to a wide range of potential hazards, such as earthquakes, tornados, hurricanes, and floods, among others, the scope of this study focuses on two types of natural hazards: tornados and expansive soils. This combination of hazards was selected for several reasons. For one, vast sections of the interior United States are subject to both hazards and light wood frame construction is particularly susceptible to tornado

damage. Additionally, the threat to life safety during a tornado is compounded by the presence of expansive soils, which make it difficult and expensive to construct and/or maintain basements. Basements and similar subgrade structures are perhaps the most common and reliable way to shelter people safely in the event of a tornado and because expansive soils prohibit, or at least discourage basement construction, they can go from being a nuisance to legitimately effecting life safety in tornado prone regions.

1.2 Research Objective and Scope

The research reported herein is part of a larger study aimed at bridging the knowledge gap that currently exists between individual building performance and overall community resilience. More specifically, the objective of this thesis is to provide a blueprint for quantifying this link through the development highly detailed finite element (FE) models. The models are constructed for three representative building archetypes and allow the system performance, localized behavior, and primary failure modes of the buildings to be captured when subject to tornado winds and expansive soil pressures, hazards specific to a sample community modeled after Norman, OK. The level of detail being used in the FE models is unprecedented to this point, and allows for capturing the failure modes and sequences to a greater degree than previously possible for light-frame wood construction. This facilitates the development of physics-based models of residential building performance under tornado and expansive soil loads. Previous models have utilized individual component performance (roof panels, rafter-sill connections, foundation-wall connections) and assumed failure sequences. This is a reasonable approach, but it does not have the ability to capture actual interaction between the components and realistically model system performance. Based on the data acquired from the FE models, statistical models are constructed to formulate fragilities which quantify the failure probabilities of the buildings at varying wind

speeds. Using the fragilities developed herein, the effects of individual components on total building performance are quantified, deficient components are identified, and improvements are proposed to meet performance goals (target fragilities) for varying levels of resilience set by our research partners at the University of Oklahoma.

The enhanced level of modeling detail used in this study allows for quantification of the effect that different building enhancements have on the performance of a residential building, and thus the overall community, to a degree that has not been possible until now. A better understanding of this relationship will permit the development of standards and guidelines for residential construction to determine which building improvements, corresponding to a specific level of resilience, are economical, sustainable, and feasible for a given community that is vulnerable to tornado hazards coupled with the presence of expansive soils. Once such standards and guidelines are developed, they can be utilized by local community planners and engineers nationwide to improve the resilience of their communities and to make them less vulnerable to the potentially devastating effects of tornadoes. The research presented herein is limited to quantifying the performance of several light-frame wood residence archetypes which represent different types of typical residences in Norman, OK

In the research described subsequently, the finite element software, ABAQUS, is used to create and validate accurate, highly detailed models of the selected light-frame wood residence archetypes and subject them to tornado wind loading and expansive soil pressures to gauge their performance quantitatively. The following three basic archetypes will be used: (1) small footprint (1200 sf) single-story, hip roof; (2) small footprint two-story, gable roof; and (3) large footprint (2400 sf) single-story, hip roof. Each of these archetypes can be considered with and without a masonry block wall basement but the analysis of the basement under expansive soil

loading will be performed separately. The basement is assumed not to affect the performance of the structure during a tornado so long as it is not damaged extensively to the point where the foundation anchorage is compromised. Therefore, the presence of a basement is simply a life-safety enhancement because it provides a place for occupants to shelter. Four different levels of construction quality will be explored for each archetype, these include: (A) Typical or Basic Quality; (B) Enhanced Quality (focus on life-safety); (C) Improved Quality (focus on reparability); and (D) Resistant Quality (focus on continued occupancy/function). The target performance for construction quality levels (CQLs) B, C, and D is provided to us by our NSF project partners at the University of Oklahoma. Figure 1.1 illustrates the archetype-CQL schemes considered in this study (excluding the basic CQL archetypes).

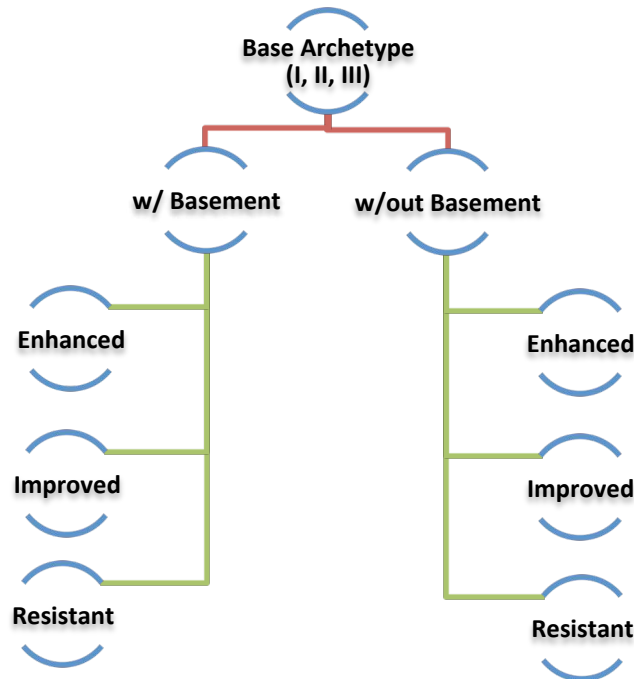


FIGURE 1.1 – Construction quality and standards for each archetype

Once the archetypes and their respective CQLs are constructed, fragilities are developed for each. The fragilities will show an archetype's probability of failure versus increasing wind speed. The definition of "Failure" as it pertains to the fragilities will be discussed later on. These fragilities will then be used in the future, as part of the larger project, to help tie individual building performance to overall community resilience measures.

1.3 Organization of Thesis

This thesis includes seven chapters. Chapter 1 provides a concise statement of the problem that this research addresses and states the scope and objectives of the research. Chapter 2 discusses the background information and a review of the literature that is relevant to the research. This includes information about light wood frame building component performance and behavior, masonry basement wall performance and behavior, tornado wind pressures, expansive soil pressures, and statistical data regarding loads and component resistances. Chapter 3 describes the three building archetypes analyzed in this study and outlines the modeling techniques used to create the ABAQUS models for each. Chapter 4 covers the validation of the ABAQUS models for individual building components and building system behavior using experimental data. Chapter 5 discusses the findings of the analyses of the basic quality archetype models which are based on typical current construction techniques. Analysis results from the ABAQUS models, using mean values for loads and resistances and MATLAB statistical models are discussed in this chapter. Chapter 6 addresses the deficiencies of the basic quality archetypes and provides some suggestions for meeting the Enhanced, Improved, and Resistant quality targets. Chapter 7 summarizes the work presented in this thesis and makes suggestions for future research to expand upon the findings of this study.

CHAPTER 2

BACKGROUND AND LITERATURE REVIEW

2.1 Hazard Quantification and Existing Treatment in U.S. Codes

Two hazards are considered in this study; tornados and expansive soils. These hazards are inherently different in their nature. The probability of a tornado passing through a community is low but the consequences if one occurs may be very severe, conversely, many communities throughout the heartland of the U.S. are impacted by expansive soils but the consequences of this affliction are relatively low compared to a tornado event. While it may be tempting and somewhat natural to be more concerned about tornados and view expansive soils as a mere inconvenience, this presents an interesting dichotomy between the two hazards. The annual cost of expansive soil related damage in the U.S. alone has been estimated from about \$2.3 billion (Gromko (1974)) to \$9 billion (Jones and Jones (1987)). The Insurance Information Institute reports that the average insured loss between 1993 and 2012 was \$7.78 billion for severe thunderstorms including tornadoes. Considering these values, the annual monetary damages related to each hazard are comparable. This means that from an economic standpoint they may be equally destructive, despite the impressive nature of a tornado. Even from a life-safety perspective, expansive soils may have a larger impact than it would seem on the surface because their presence in many tornado prone areas often prevents people from constructing basements and other subsurface structures that could protect and shelter them in the event of a tornado.

One commonality that does exist between the two hazards considered in this study is that there is currently a significant lack of knowledge and understanding associated with both of

them. With that lack of knowledge in mind, this section will discuss their respective treatment in current practices and codes.

In general, design codes such as ASCE 7-10 weigh the probability of the occurrence of an event against the potential consequences of failure given its occurrence in determining the design loading for a structure. For example, if the probability of occurrence of an event is small, the event may not be accounted for in the design of a typical structure such as a commercial office building or home. If, however, a hospital, a nuclear power plant or some other critical facility is constructed in the same location, subject to the same hazards, it may be recommended or required by code that the event be designed for due to the high consequences associated with failure of the critical facility.

2.1.1 Tornado Hazards

Of the two hazards considered in this study, tornado winds are certainly the most destructive. While the likelihood of a tornado's path passing through Norman, OK or a geographically similar region is considerably lower than the likelihood of that community being affected by expansive soils, the level of destruction associated with a tornado (even a mild one), would almost certainly be significantly higher.

Most structures are not designed specifically for tornado loading. This is due in large part to the generally low probability of a given structure being located in the path of a tornado, although even critical structures are not currently required to be designed to withstand tornado winds. Some studies have been performed in an attempt to better understand the distribution and magnitude of tornado pressures on buildings, including one by Haan et al (2010) which suggests a modification factor to be applied to the ASCE-7 design wind pressures to account for tornado

loading. Although some studies such as this have been performed, there currently is no generally used and accepted method to account for tornado loading.

Other factors such as wind-borne debris also make it difficult to model the effects of tornadoes on buildings. Wind-borne debris can have a vast range of shapes and sizes and can cause various levels of damage to a building upon impact. It is conceivable that a large projectile could itself do considerable structural damage to a building but perhaps the larger concern is the internal pressurization of a structure that can occur due to a breach of the building envelope. This can result from even small projectiles impacting and breaking windows during high winds. The breach can result in an internal pressure increase of about 200% and can initiate failure of building components. Because wind-borne debris impact is largely random, it cannot be physically quantified and must instead be accounted for probabilistically.

Although tornadoes spin in a cyclical motion, they are usually large enough that their direct wind effect on a building structure is similar to that of straight line winds (unless the building is located directly in the path of the tornado), meaning that the building aerodynamics are approximately the same as they would be under normal, high wind conditions. A few distinctions from normal conditions (stipulated in ASCE 7-10) are the increased wind speeds and the variability in wind direction during a tornado, as well as the wind speed profile near the ground. The aerodynamic similarities allow for the use of ASCE 7-10 in determining the approximate wind pressure distributions and magnitudes anticipated during the storm. Thus, for this study, tornado loading will be determined using the same procedure applied by Alfano (2016). This procedure utilizes the ASCE 7 wind loads modified by the Haan et al. (2010) tornado loading coefficient. There is still considerable uncertainty about the effects of tornado pressure loading versus straight line wind pressure loading, so the case which utilizes the Haan factor will be

considered the upper bound case and the lower bound case will use the ASCE 7-10 wind loads with no modification.

To determine tornado loads on the main wind force resisting system (MWFRS), the directional procedure is applied from chapter 27 of ASCE 7-10. For the components and cladding (C&C), the loads are determined from chapter 30. In each case, the wind pressure for a given building zone, P (psf), is equal to:

$$P = [q_z GC_p - q_h GC_{pi}]; \text{MWFRS Wind Pressure} \quad (2.1)$$

$$P = q_h [GC_p - GC_{pi}]; \text{C and C Wind Pressure} \quad (2.2)$$

where, for buildings less than 60' in height, GC_p is the external aerodynamic coefficient, GC_{pi} is the internal pressure coefficient, q_z is the velocity pressure at a given height, and q_h is the velocity pressure at the building's mean roof height, as calculated by:

$$q_z = 0.00256 K_c K_z K_{zt} K_d V^2; \text{Velocity Pressure} \quad (2.3)$$

where K_z is the velocity pressure exposure coefficient, K_{zt} is the topographic factor, K_d is the wind directionality factor, K_c is the modification factor for tornado loading provided by Haan et al (2010), and V is the 3-s gust wind speed expressed in miles per hour. For this study, V will be considered as a range of deterministic values based on the Enhanced Fujita (EF) tornado scale, which is commonly used to classify the intensity of a tornado based on the level of damage it causes. The tornado's 3-s gust wind speed is inferred from the damage level (making it compatible for use with the ASCE 7-10 procedures without adjustment). The EF scale is shown in Figure 2.1.

ENHANCED FUJITA SCALE		DAMAGE
EF-0	(65-85 MPH)	LIGHT
EF-1	(86-110 MPH)	MODERATE
EF-2	(111-135 MPH)	CONSIDERABLE
EF-3	(136-165 MPH)	SEVERE
EF-4	(166-200 MPH)	DEVASTATING
EF-5	(200+ MPH)	INCREDIBLE

FIGURE 2.1 – EF Scale (weather.com)

K_d accounts for the reduced probability of the maximum wind speeds coming from any given direction and the reduced probability of the maximum pressure coefficient occurring for any given wind direction. Because the maximum wind speed can occur in any direction during a tornado and thus the maximum pressure may be exerted on the building from any direction, the directionality factor is conservatively neglected and set equal to 1.0 (Alfano, 2016). The topographic factor, K_{zt} , is set equal to 1.0 under the assumption that the site is relatively flat. The remaining variables in the wind pressure calculation (G , C_p , GC_{pi} , K_c) account for the statistical uncertainty in the wind pressure loading. The parameters and distribution types for all of these variables except for K_c are obtained using the methods from Lee and Rosowsky (2005), which are modified based on Ellingwood and Tekie (1999). The parameters and distribution for K_c are taken from Haan et al (2010) and Alfano (2016). A summary of the statistical parameters and distributions for the variables that can be applied universally, to all building types is shown in Table 2.1:

TABLE 2. 1 – Summary of Wind Load Parameter Statistics; All Archetypes

Parameters	Category		Nominal	Mean	SD	COV	Dist.
^a K _z	33 ft high		1	0.93	0.13	0.14	Normal
G _{cpi}	Enclosed	(+)	0.18	0.15	0.05	0.33	Normal
	Partially Enclosed	(+)	0.55	0.46	0.15	0.33	
G	Rigid Structure		0.85	0.82	0.08	0.10	Normal
K _c Roof	MWFRS - Roof		1.8-3.2	-	-	-	Uniform
	C & C - Roof		1.4-2.4	-	-	-	
K _c Walls	MWFRS - WW & LW		1.5	-	-	-	Uniform
	C & C - WW & LW		1.3	-	-	-	
	MWFRS - SW		1	-	-	-	
	C & C - SW		1	-	-	-	

a) Assume boundary layer effects are negligible during a tornado, thus nominal K_z is 1.0 any height.

The values of GC_p depend on prevailing wind direction, building geometry, and location on the building wall or roof (denoted by wind zones in ASCE 7-10). These values are tabulated in Table 2.2 for archetypes 1 and 3 and Table 2.3 for archetype 2. Archetypes 1 and 3 are geometrically similar enough that the same values of GC_p apply to each.

TABLE 2.2 – Aerodynamic Coefficients for Building Archetypes 1 and 3

Parameters	Category	Nominal	Mean	SD	COV	Dist.
MAIN WIND FORCE RESISTING SYSTEM						
Wind Normal to Long Side						
C_p (MWFRS)	Windward Wall	0.8	0.69	0.10	0.14	Normal
	Leeward Wall	-0.5	-0.46	0.07	0.15	
	^a Side Walls	-0.7	-0.64	0.10	0.15	
	Windward Roof	-0.62	-0.61	0.12	0.20	
	Leeward Roof	-0.48	-0.40	0.04	0.10	
Wind Normal to Short Side						
C_p (MWFRS)	Windward Wall	0.8	0.70	0.10	0.14	Normal
	Leeward Wall	-0.43	-0.41	0.06	0.15	
	^a Side Walls	-0.7	-0.66	0.10	0.15	
	Roof (0-h/2)	-0.9	-0.80	0.13	0.16	
	Roof (h/2 - h)	-0.9	-0.80	0.13	0.16	
	Roof (h - 2h)	-0.5	-0.43	0.04	0.10	
	Roof (> 2h)	-0.3	-0.26	0.03	0.10	
COMPONENTS & CLADDING						
GC_p (C&C)	Zone 1 (Roof)	-0.85	-0.81	0.10	0.12	Normal
	Zone 2 (Roof)	-1.44	-1.36	0.16	0.12	
	^b Zone 3 (Roof)	-2.3	-2.18	0.26	0.12	
	Zone 4 (Wall - Short)	-0.87	-0.78	0.09	0.11	
	Zone 4 (Wall - Long)	-0.85	-0.77	0.09	0.11	
	Zone 5 (Wall -Short)	-0.93	-0.89	0.10	0.11	
	Zone 5 (Wall - Long)	-0.9	-0.86	0.10	0.11	

a) Statistics not specified in Ellingwood & Tekie (1999), assuming same mean to nominal, and COV as leeward wall.

b) Per ASCE 7-10, for a hip roof with slope less than 25 degrees, Zone 2 is equivalent to Zone 3.

c) Note that GC_p (C&C) values vary slightly for the windows and doors due to the differing component areas, the values shown are for the stucco wall sheathing.

TABLE 2.3 – Aerodynamic Coefficients for Building Archetype 2

Parameters	Category	Nominal	Mean	SD	COV	Dist.
MAIN WIND FORCE RESISTING SYSTEM						
Wind Normal to Long Side						
C_p (MWFRS)	Windward Wall	0.8	0.69	0.10	0.14	Normal
	Leeward Wall	-0.5	-0.46	0.07	0.15	
	^a Side Walls	-0.7	-0.64	0.10	0.15	
	Windward Roof	-0.82	-0.81	0.16	0.20	
	Leeward Roof	-0.54	-0.45	0.04	0.10	
Wind Normal to Short Side						
C_p (MWFRS)	Windward Wall	0.8	0.70	0.10	0.14	Normal
	Leeward Wall	-0.43	-0.41	0.06	0.15	
	^a Side Walls	-0.7	-0.66	0.10	0.15	
	Roof (0-h/2)	-0.9	-0.80	0.13	0.16	
	Roof (h/2 - h)	-0.9	-0.80	0.13	0.16	
	Roof (h - 2h)	-0.5	-0.43	0.04	0.10	
	Roof (> 2h)	-0.3	-0.26	0.03	0.10	
COMPONENTS & CLADDING						
GC_p (C&C)	Zone 1 (Roof)	-0.85	-0.81	0.10	0.12	Normal
	Zone 2 (Roof)	-1.44	-1.36	0.16	0.12	
	Zone 3 (Roof)	-2.3	-2.18	0.26	0.12	
	Zone 4 (Wall - Short)	-0.87	-0.78	0.09	0.11	
	Zone 4 (Wall - Long)	-0.85	-0.77	0.09	0.11	
	Zone 5 (Wall -Short)	-0.93	-0.89	0.10	0.11	
	Zone 5 (Wall - Long)	-0.9	-0.86	0.10	0.11	

a) Statistics not specified in Ellingwood & Tekie (1999), assuming same mean to nominal, and COV as leeward wall.

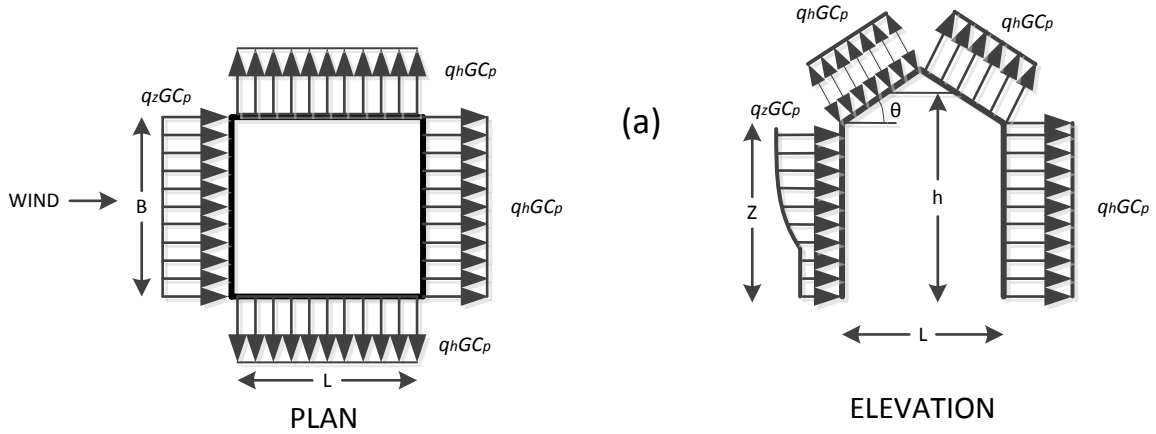
b) Note also that GC_p (C&C) values vary slightly for the windows and doors due to the differing component areas, the values shown are for the stucco wall sheathing.

c) Note that GC_p (C&C) values vary slightly for the windows and doors due to the differing component areas, the values shown are for the stucco wall sheathing.

The wind loads calculated using the equations above will be applied to the building archetypes in accordance with the ASCE 7-10 figures shown below for the MWFRS and C&C respectively. To remain consistent with previous studies, (Alfano (2016), Amini and van de

Lindt (2014)) the roof-wall connections and wall-foundation connections will be modeled under MWFRS wind loads while the roof and wall sheathing will be modeled under C&C wind loads.

MWFRS WIND PRESSURE ZONES



C&C WIND PRESSURE ZONES

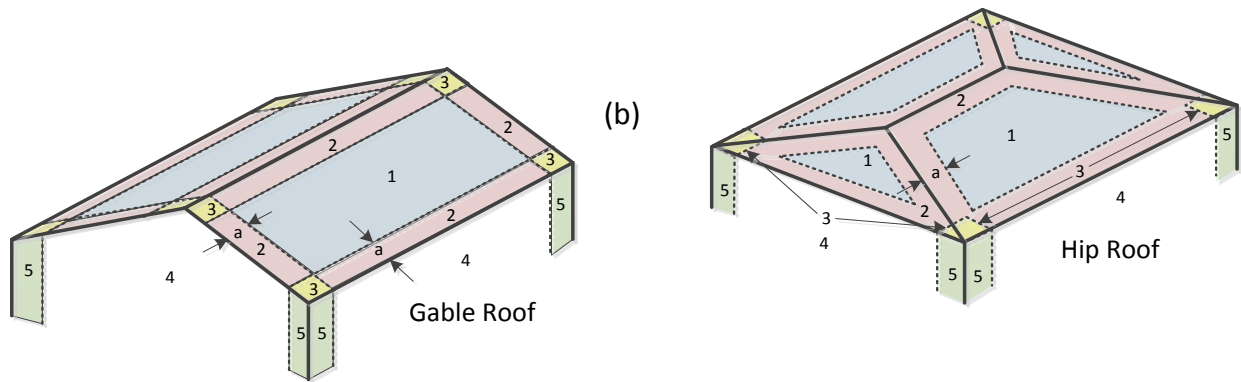


FIGURE 2. 2 – Wind pressure zones for (a) wind effects on MWFRS and (b) C&C (after ASCE 7-10)

Several other assumptions were made in the tornado wind load analysis. First, it was assumed that the archetype homes are of ordinary importance, or are risk category (RC) II, and thus the

importance factor (I) = 1. This is a reasonable assumption for any single-family home or multi-family dwelling. Second, it was assumed that the buildings are located in an exposure category C location as defined in ASCE 7-10 (urban or suburban area) and that $K_z = 1.0$. The K_z value for Exposure C at a mean roof height of 33' is used because surface roughness, which would typically reduce the value of K_z near the ground, is assumed not to have much effect during a tornado. While portions of the prototype community, Norman, OK, may actually fall into exposure category B, surrounding features are not expected to have a significant impact on tornado winds as they would with typical, straight line winds. Additionally, assuming category C with $K_z = 1.0$ is conservative for residential buildings that typically are less than 35 ft. high.

With the wind pressures, including their statistical variability, applied as described above, the remaining consideration for tornado loading is deciding the wind speed at which the building envelope is likely to be breached, causing internal pressures to rise. Alfano (2016) does not consider this case and Lee and Rosowsky (2005) consider the envelope breach to occur with the loss of the first roof sheathing panel. It is not unlikely, however, that the envelope breach could occur prior to the loss of a roof sheathing panel. For example, the loss of a door or window could lead to internal pressurization which may then *cause* a roof sheathing panel (or other component) to fail, starting a cascading failure effect. For this reason, it is important to consider the effect of an envelope breach in the form of broken doors or windows in the analysis. Because of the randomness of the wind-borne debris impacts that may cause the envelope breach, statistical data can be used to determine the wind speed at which a breach-causing impact is “expected” to occur but accurate probabilistic modeling of debris impacts can be very complex and is outside the scope of this study. Therefore, to account for these effects, two cases will be considered for each archetype. The first case will assume that windows and doors are not broken by flying debris,

and that internal pressure increases are only initiated by roof panel failure or window/door pressure blowout. The second case assumes that at least one window or door is breached by debris impact and the internal pressure is elevated from the beginning of the analysis. This approach does not include the probability of debris impact into the total probability of failure of a component but it does show the effect of a breach versus no breach situation, which gives an understanding of the importance of preventing such an event.

2.1.2 Expansive Soil Hazards

The second hazard considered in this study is expansive soil. Expansive soils are a significant concern in many regions of the United States, especially in the south-central portion of the country. The map shown in Figure 2.3 illustrates the distribution of expansive soil prone areas throughout the U.S.

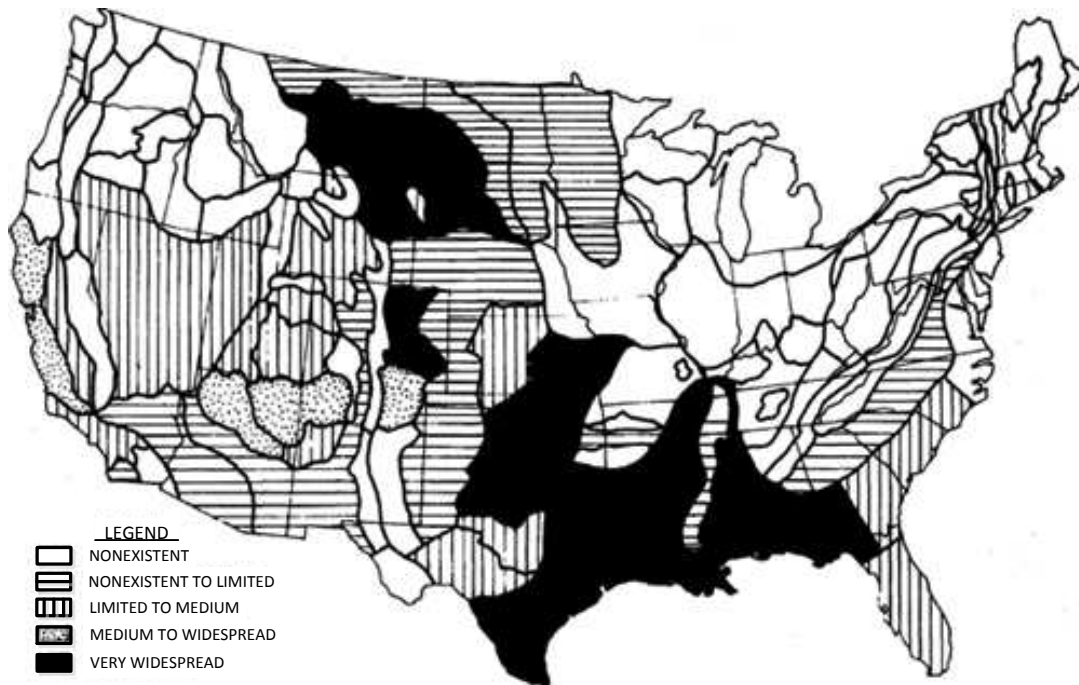


FIGURE 2. 3 – Areas in the continental U.S. susceptible to expansive soils (FHWA)

While damage associated with expansive soils is significantly less severe than damage associated with a tornado, the likelihood that a community will be affected by this problem is far higher and its economic impact is substantial. Furthermore, life-safety issues associated with a tornado can be compounded by the presence of expansive soils because people are less likely to construct basements or underground tornado shelters in affected areas due to the damage that these soils can cause to subterranean structures. Constructing and maintaining these structures can become expensive, so many people opt out of them despite the life-saving potential of the shelter in the event of a tornado.

In order to quantify the pressures exerted on a basement wall by expansive soils, two different types of pressures are considered; (1) typical at rest soil pressure and (2) expansive swell pressure surcharge. These pressures are illustrated in Figure 2.4 below.

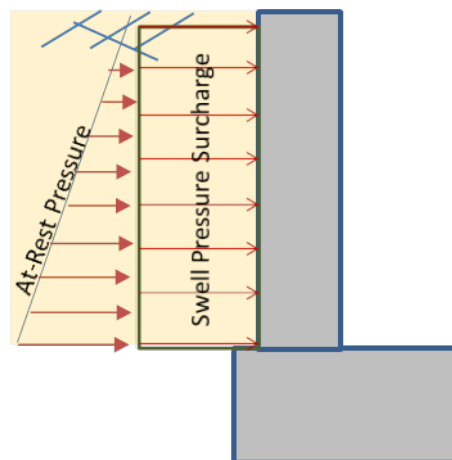


FIGURE 2. 4 – Soil pressures acting on basement wall

At rest earth pressure as a function of soil depth is calculated using equations 2.4 and 2.5, and the uniform swell pressure surcharge is found using equations 2.6 (Erzin and Erol (2007)) and 2.7 (Lytton et al. (2005)).

$$P_o = K_o \gamma H; \text{ **At – rest soil pressure** } \quad (2.4)$$

where P_o is pressure, K_o is equal to $(1-\sin(\phi'))$, ϕ' is the effective soil friction angle, γ is soil density, and H is soil depth. Soil friction angle, ϕ' , can be calculated using the plasticity index (PI) using the relationship in equation 2.5.

$$\phi' = 0.0016(PI)^2 - 0.30(PI) + 36.21; \text{ **Soil Friction Angle (degrees)** } \quad (2.5)$$

$$\text{Log}(P_s) = -3.72 + 0.011(PI) + 2.08\gamma_d + 0.24\text{Log}(s); \text{ **Swell Pressure (kg/cm}^2\text{)}** } \quad (2.6)$$

where P_s is swell pressure, γ_d is dry soil density (g/cm^3) and s is soil suction (bar), calculated using equation 2.7.

$$\text{Log}(s) = 2.02 + 0.0060(PI) - 0.077W; \text{ **Soil Suction (bar)** } \quad (2.7)$$

where W is moisture content. The relationships shown in equations 2.6 and 2.7 are assumed to apply for swell pressures less than 100 kPa or 20.89 psf (Erzin and Erol (2007)).

The soil parameters in the equations above are defined using the U.S. Department of Agriculture (USDA) soil survey data for Cleveland County, OK. Norman is the county seat of Cleveland County, and occupies a large portion of it. Mean soil parameters including PI , W , and γ are available from the USDA database for 81 separate locations in Cleveland County. It is assumed that the archetype buildings in this study are randomly located within Cleveland County and that all 81 soil types represented in the USDA database are equally likely to be present at the

random site. This is probably not the case in reality, as the total area and population density in each of the 81 USDA survey locations would affect the probability of a building being built on a given soil type but that level of detail is beyond the scope of this analysis. Because the USDA soil parameters are likely to be correlated, the statistical analysis is not performed by assigning statistical parameters to each soil parameter and then randomly generating the parameters independent of one another. Instead, 1 of the 81 sites is randomly selected according to a uniform distribution and the soil parameters associated with that site are used. A list of the soil parameters for all 81 sites is provided in the Appendix B.

2.2 Typical Residential Home Construction in Norman, OK

This section outlines what were found to be construction practices in communities similar to Norman, OK. in size, demographics, and geographic location. Because such a wide variety of homes exist in a given community due to factors like age, home value, and contractor, it is difficult to define exactly what constitutes “typical” construction. In this study, typical construction is assumed to consist of affordable, non-engineered light wood frame homes that have not been constructed or retrofitted in any way to mitigate the risks associated with tornado events or expansive soils. Many of the construction techniques used for the baseline archetypes are taken from CUREE publication No. W-29 because the small, single story home detailed in the report fits the basic description of typical construction and because experimental results reported by the CUREE-Caltech wood frame project provide a means to validate the building system performance. Other construction techniques are taken from typical details found online. The common construction practices used for each component examined in this study are listed in section 2.2.1. These are the practices used for the basic CQL of each archetype. The resistance

characteristics and statistical information for each of the typical quality components are detailed in section 2.4.

2.2.1 Common Construction Practice

Typical construction practices for each component considered in this study are detailed below.

Roof Panel to Rafter Connections (Figure 2.5): Each roof panel consists of a 15/32" thick, 4'x8' plywood sheet. The sheet is fixed to the spruce pine-fir (SPF) wood rafters by 8d nails spaced along the rafters at 12" in the interior and 6" around the exterior of each panel. The rafters are spaced at 24" on center.

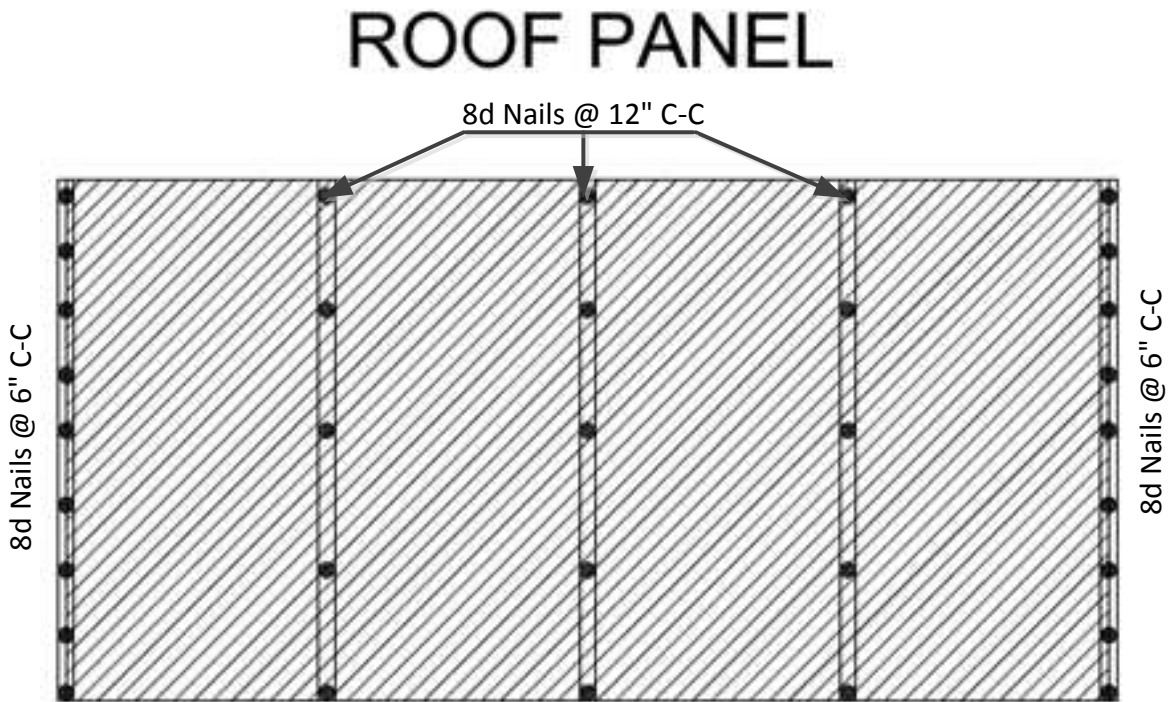


FIGURE 2.5 – Typical roof panel nailing pattern

Rafter to Wall Connections (Figure 2.6): The rafters are connected to the SPF top stud sills by three 16d toe-nails.

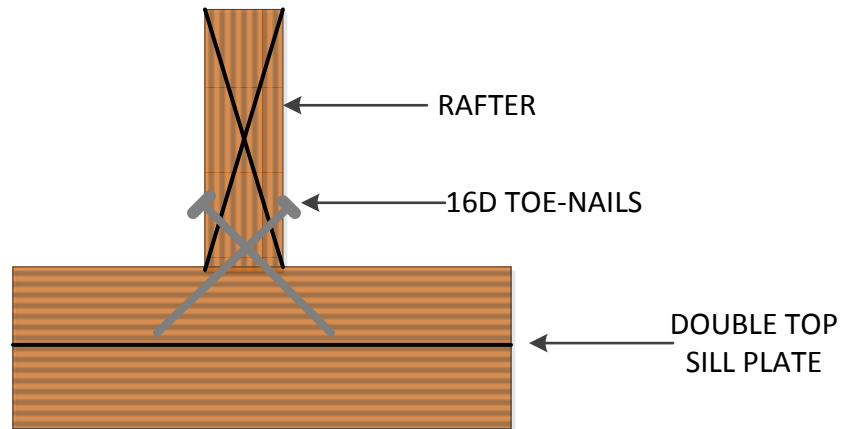


FIGURE 2. 6 – Typical rafter to sill connection detail

Bottom Stud-Sill to Foundation Connection: The bottom stud still plate is connected to the building's concrete foundation by $\frac{1}{2}$ " diameter steel anchor bolts spaced at 6" on center.

Wall Sheathing (Figure 2.7): The interior walls are sheathed by 0.5" thick gypsum board on either side. The gypsum board is fixed to the SPF studs (at 16" on center) by 5d gypsum screws spaced at 7" on center. The panels are each 4'x8'.

The exterior walls are sheathed by 0.5" thick gypsum on the interior with the same fastener schedule as the interior walls, and by a 1.0" thick coat of stucco on the exterior. The stucco is backed by stucco lath which is fixed to the SPF studs by 6d nails spaced at 6" on center.

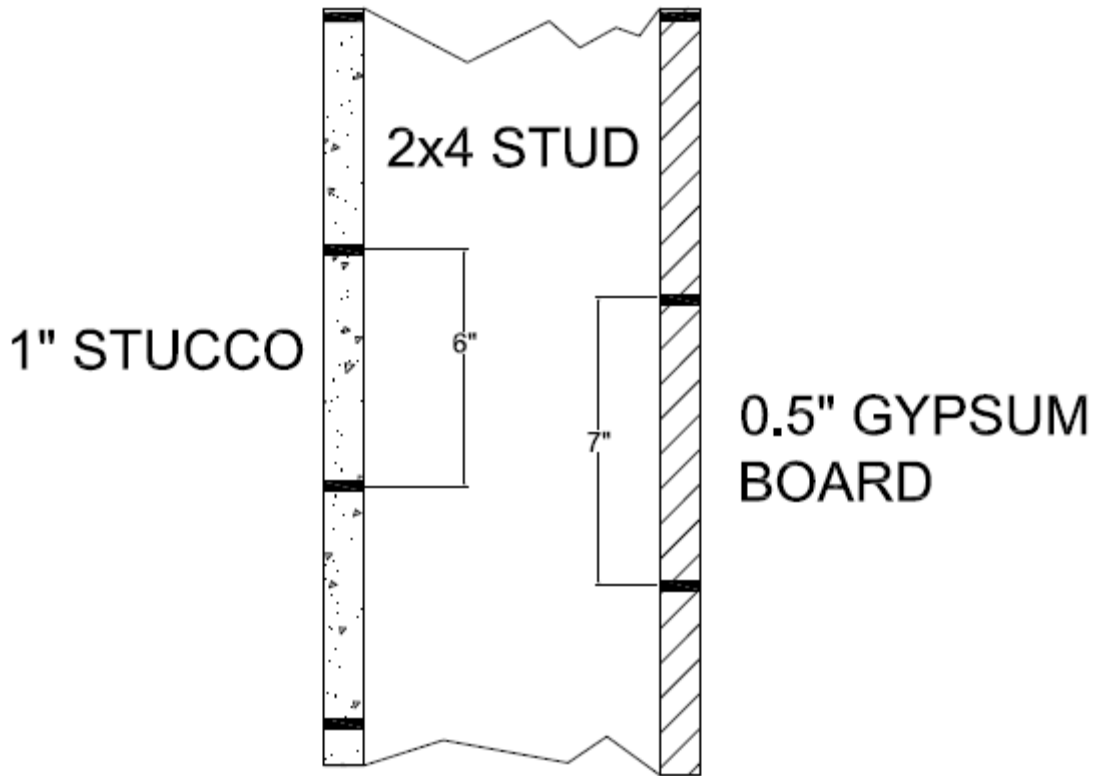


FIGURE 2. 7 – Typical exterior wall sheathing detail

Windows/Doors: The basic quality windows are assumed to be DP25 windows and doors are assumed to have an allowable pressure rating of 50 psf per the HAZUS hurricane module (HAZUS).

Roof Cover: Typical roof cover is assumed to be 1’x0.5’ class D asphalt shingles. The resistance statistics for individual roof shingles found in Table 2.5 are taken from Huang et al. (2015), based on data from Romero (2012) which performed field experiments on shingles that had been in-situ for approximately 9 years.

Basement Wall: It is common for residential buildings in expansive soil prone areas not to be constructed with basements at all. For this study, it is assumed that the typical basement wall

consists of unreinforced concrete masonry block and mortar. This is a bare minimum assumption that sets a baseline for any potential improved basement wall system to be compared to.

2.2.2 Observed Building Failures under Tornado Action

Although one purpose of this study is to better understand the failure modes and sequences that occur in residential wood frame building construction during a tornado, previous research and field observations can provide an indication of likely residential building performance. A typical failure sequence outlined in an issue of “Popular Mechanics” by Tim Reinhold, the senior vice president of the Insurance Institute for Business and Home Safety (IBHS) seems to be generally supported by other literature, including to some degree, the findings by Alfano (2016). According to Reinhold, as the tornado approaches, a building is struck by flying debris, damaging the building envelope and likely breaching it (breaking windows). When the envelope is breached, the building is internally pressurized. This significantly increases the load on the walls and ceiling/roof causing the relatively weak connections between the roof and walls to fail resulting in damage or removal of the roof. With the loss of the roof and ceiling diaphragm, the walls lose their lateral bracing and may become unstable. The sidewalls generally fail first due to large suction pressures, followed by the windward wall and finally the leeward wall and interior walls. This can all occur within a span of about 5 seconds. Images and brief descriptions of more critical failure modes examined in this study are shown below.

- 1) Roof Sheathing Panel Failure (Figure 2.8):** Typically occurs when the fasteners attaching a roof panel to a rafter pull-out of the rafter wood. Failure of one panel may not seem disastrous, but leads to internal pressurization which can cause a cascading failure effect. Additionally, if the tornado is accompanied by rain, as is often the case, one panel

failure can lead to extensive water damage. Such failures generally initiate at the eaves where local pressures are amplified by wind-flow separation effects.



FIGURE 2. 8 – Typical roof panel failure (RoofingAnnex.com)

- 2) **Roof-Wall Connection Failure (Figure 2.9):** is another common failure mode. It generally follows envelope breach, when large suction pressures cause the relatively weak connection between the rafters and top sill plate to fail, resulting in extensive damage or removal of the roof.



FIGURE 2. 9 – Typical roof-wall connection failure (newsons6.com)

- 3) **Wall Collapse (Figure 2.10):** generally occurs once the wall stability is lost as a result of the loss of the roof/ceiling diaphragm.



FIGURE 2. 10 – Typical wall collapse failure (Denver.cbslocal.com)

- 4) **Wall-Foundation Connection Failure (Figure 2.11):** occurs when the connection between the foundation and the bottom stud-sills fails, the entire home may shift off its foundation. Per Alfano (2016), this mode can occur due to pure shear, or a combination of uplift and shear.

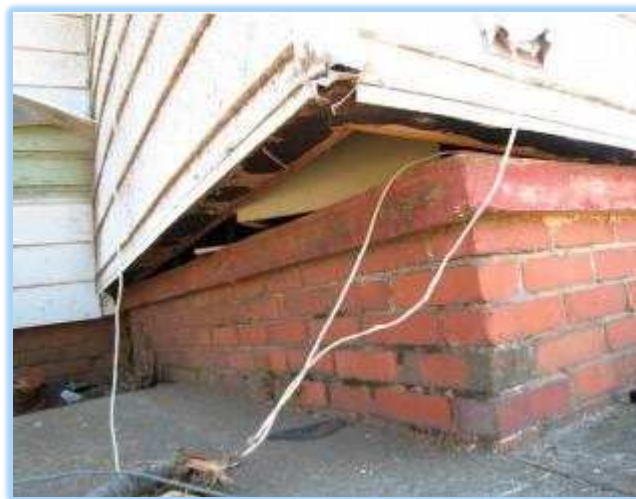


FIGURE 2. 11 – Typical wall-foundation connection failure (van de Lindt et al. (2013))

Other less common or critical damage states, such as wall sheathing damage, roof cover failure, and window or door pressure blowout will also be examined in this study. These damage

states are important to perform life-cycle cost analysis, but they are not designated as “critical” failure modes that would cause extensive damage or life-safety issues.

2.2.3 Observed Expansive Soil Damage

Unlike tornado related damage, expansive soil damage often initiates and worsens over time as the soils surrounding the home cyclically expand and contract. Often times, basement walls and foundation slabs will crack due to expansive soil pressure and the initial crack or cracks will propagate with each shrink/swell cycle. This can lead to water entry into the home which can damage or destroy property and may require costly repairs to mitigate. Water entry can even lead to mold growth that can be harmful to the health of the home’s occupants. Figures 2.12 and 2.13 below depict damage commonly associated with expansive soils.



**FIGURE 2. 12 – Typical masonry basement wall cracking due to expansive soils
(basementsystems.ca)**



FIGURE 2. 13 – Typical foundation slab cracking due to expansive soils (nachi.org)

Although two common damage modes associated with expansive soil pressures are shown above, the only mode examined in this study is masonry wall cracking.

2.2.4 Existing Mitigation Techniques: Tornado Hazards

Because there are currently no national code design requirements specific to tornado winds, there is not an abundance of mitigation techniques geared specifically toward tornado winds either. There are, however, existing construction techniques in common use that are designed to mitigate risks associated with high winds in hurricane prone areas. There is no reason to believe that these same techniques cannot be applied to address concerns about tornado winds as well. Some known construction techniques used in high wind areas for each component discussed in this study are listed below.

Roof Panels: In order to mitigate the effect of high wind pressure, the roof panel nailing schedule, or the nail gauge can be increased to strengthen the connection. Increasing the specific gravity of the rafter wood species can also increase connection strength (NAHB (2002)).

Roof to Wall Connection: Similar to the roof panel connections, the roof to wall connection strength can be improved by adding additional toe-nails to the connection, increasing the nail gauge, or increasing the sill plate wood specific gravity. To improve connection strength even more, hurricane straps can be used on one or both sides of a rafter. Figure 2.14 depicts a typical hurricane strap, although many variations exist.

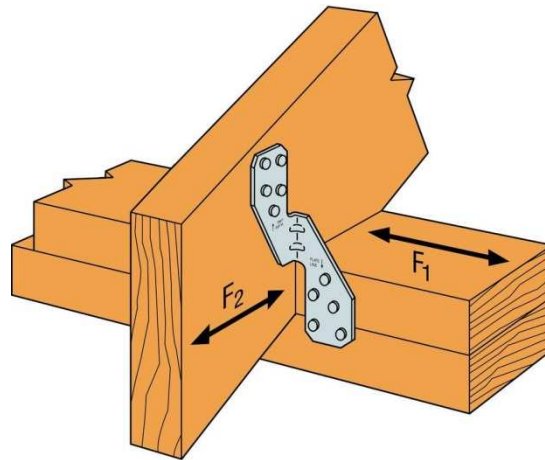


FIGURE 2. 14 – Typical hurricane strap (Simpson Strong-Tie)

Wall to Foundation Connection: The wall to foundation connection can be bolstered in many ways. The most basic technique is simply to increase the number or size of the anchor bolts that make up the connection. Foundation ties are also used to strengthen this connection. Figure 2.15 depicts one type of foundation tie.

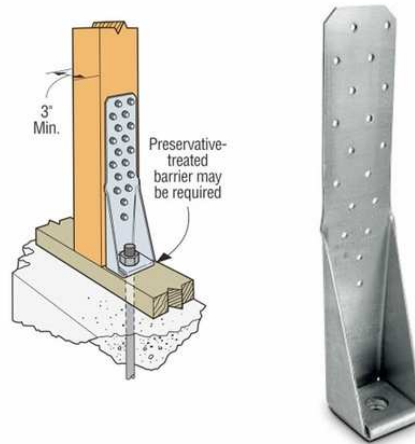


FIGURE 2. 15 – Typical foundation tie (Simpson Strong-Tie)

Mitigation techniques exist for the less critical components considered in this study as well. For example, wind resistant doors, windows, and shingles are commercially available and widely used in high wind areas.

2.2.5 Existing Mitigation Techniques: Expansive Soils

There are many new and innovative techniques currently being developed to mitigate the effects of expansive soil pressures on basement walls and foundations by reducing soil swell pressure or increasing the strength of the wall. A number of common techniques are summarized in this section.

Chemical Soil Stabilization: Chemical soil treatments are designed to alter the clay mineralogy to reduce the potential for expansion. Treatments using calcium-oxide (lime) are the most common, but alternatives using stabilizers such as silica fume and fly-ash are being developed as well.

Moisture Control: Soil swell pressures occur due to changes in the soil water content in an expansive soil. Preventing large fluctuations in the soil's water content can help to mitigate swell pressures. This can be done in two basic ways; (1) Subgrade Irrigation, in which the soil surrounding the basement/foundation is kept hydrated at a consistent water content by irrigation with a network of pipes and (2) Water Diversion, in which excess ground water is diverted away from the soils surrounding the basement by surface grading, drains, cutoff walls, etc.

Non-Expansive Backfills: The in-situ expansive soils surrounding a basement wall can be excavated and replaced with other natural non-expansive soils or man-made backfills. Depending upon the volume of material requiring replacement and the type of replacement backfill selected, this can be a costly option. New and experimental recycled backfills such as tire derived aggregate (TDA) could provide a sustainable and cost effective alternative to that problem. A study by Seda et al. (2007) shows a 75% reduction in swell pressures with the use of an expansive soil-rubber (ESR) mixture as backfill.

Basement Wall Reinforcement: The masonry block basement wall's resistance to damage can be improved by adding vertical reinforcement in the form of rebar. The rebar is placed in the block openings and spans the height of the wall. Rebar is grouted in place in the block openings and the size and spacing can vary based on desired wall strength. Another form of reinforcement used to increase wall resistance to out of plane loading is the application of fiber reinforced polymer (FRP) strips. Bui et al. (2013) demonstrated that FRP strips increased the bearing capacity of a concrete masonry block wall subject to out-of-plane loading by about 135% prior to the first observed cracking.

If the desired wall strength cannot be achieved using a masonry block wall, a reinforced concrete basement wall can be implemented but this study will focus on mitigating expansive soil pressure damage to masonry basement walls.

2.3 Material Parameters and Connection Strengths

2.3.1 Building Materials

The building material parameters used to perform the structural analysis for all three basic quality archetypes for this study are experimental mean values, rather than nominal (or specification) design values in order to more realistically capture the structure behavior. Building materials include Spruce-Pine Fir lumber, which is used for all framing components, gypsum wall board used for ceiling and interior wall sheathing, 15/32” plywood used for roof sheathing, and stucco used for exterior wall sheathing. Non reinforced concrete masonry block walls are used in all basic quality models with basements. Table 2.4 summarizes the building materials and relevant parameters (density, modulus of elasticity, etc.). Note that the masonry wall parameters used in the model are composite parameters that represent the coupled performance of the masonry blocks and mortar.

TABLE 2. 4 – Summary of relevant building material parameters

Material	Parameter	Value	Reference
^a SPF (Southern) Framing Wood	E (ksi)	1353	Wood Handbook (2010)
	Density (pcf)	25.9	Wood Handbook (2010)
	Specific Gravity	0.37	NAHB (2002)
^a DF Plywood Roof Sheathing	E (ksi)	1080	Wood Handbook (2010)
	Density (pcf)	32.2	Wood Handbook (2010)
Gypsum Wall Board	E (ksi)	234	^b Typical Value
	Density (pcf)	50	Typical Value
Exterior Wall Stucco	E (ksi)	275	Typical Value
	Density (pcf)	118	Typical Value
Ceiling Insulation	Density (pcf)	28.2	CUREE Publication No. W-29
Masonry Block Wall	E (ksi)	2296	Jankowiak and Lodygowski (2005) Kmiecik and Kaminski (2011) Abdelnaby and Elnashai (2013)
	f_c (ksi)	1.01	
	f_t (ksi)	0.51	
	Density (pcf)	59.5	
a) Assume 12% moisture content, per Wood Handbook (2010)			
b) Not a lot of data for mechanical properties			

Materials in this study are idealized as isotropic for simplicity. Most of these materials are also highly variable in their properties. There are limited data available for the mechanical properties of gypsum wallboard or stucco, so “typical” values are assumed for these materials based upon a variety of sources including manufacturer websites. The dead load includes the weight of ceiling insulation which is assumed based upon CUREE Publication No. W-29. The weight of the roof shingles is conservatively neglected under the assumption that the shingles have peeled off prior to the onset of the more critical damage states of concern to this paper, so the shingle density is not included in the Table 2.4.

The material densities listed in Table 2.4 allow ABAQUS to calculate total building mass and weight. For the purposes of the statistical analysis, the variability in the dead load of the

building components also has an effect on the probabilities of failure for different damage states. This will be accounted for in the statistical analysis by subtracting the random dead load from the random wind pressure uplift load such that the basic formulation of each failure limit state is:

$$g(x) = R - (W - D); \text{Failure Limit State} \quad (2.8)$$

where R is the component resistance discussed in sections 2.3.2 and 2.3.3, W is the wind pressure load effect found using the using the statistical parameters in section 2.1.1, and D is the dead load effect discussed in this section. The dead load statistical parameters and distributions used in this analysis are taken from Tables 3.5 and 3.6 of Alfano (2016) which summarizes dead load statistics per studies by Ellingwood et al. (2004), Lee and Rosowsky (2005), and others. These tables show that the coefficient of variation (COV) and distribution for each component (roof sheathing, whole roof, walls, and floor) is the same. The distribution is assumed to be normal for each component and the COV of each is equal to 0.10 (Ellingwood et al. (2004)). These statistical parameters will be applied to the total building dead load taken from the ABAQUS analysis to generate random values in subsequent Monte-Carlo simulation to determine fragilities.

2.3.2 Experimental Connection Strength Values

The strengths of individual fasteners (nails, straps, etc.) are taken from pre-existing experimental testing data. Figures 2.15, 2.16, and 2.17 below show load displacement relationships for critical connection types used in the ABAQUS archetype models.

Figure 2.16 depicts the load versus displacement curves used to model nail pullout between the 15/32" plywood roof panels and rafters, wall studs and gypsum panels (interior walls), and walls studs and stucco panels (exterior walls) respectively. The base experimental data for these

curves is taken from Dao and van de Lindt (2008). The base curve was then modified per NAHB (2002) to reflect the change in wood species (from Hem-Fir to SPF). The base curve is for 8d nails, so the curve for the roof panel connectors did not need to be modified any further. The load-displacement curves for the gypsum board and stucco fasteners was modified to adjust for the reduced fastener diameters, 5d and 6d respectively by multiplying by the ratio of the new diameter to the original (5d/8d or 6d/8d). This adjustment is based on the assumption that most of the nail pullout resistance comes from friction between the nail and its embedment material (in this case SPF wood); therefore, a reduction in the circumference of the nail and its corresponding reduction in contact area between the nail and wood correlates directly to a reduction in the nail's friction-based pullout resistance.

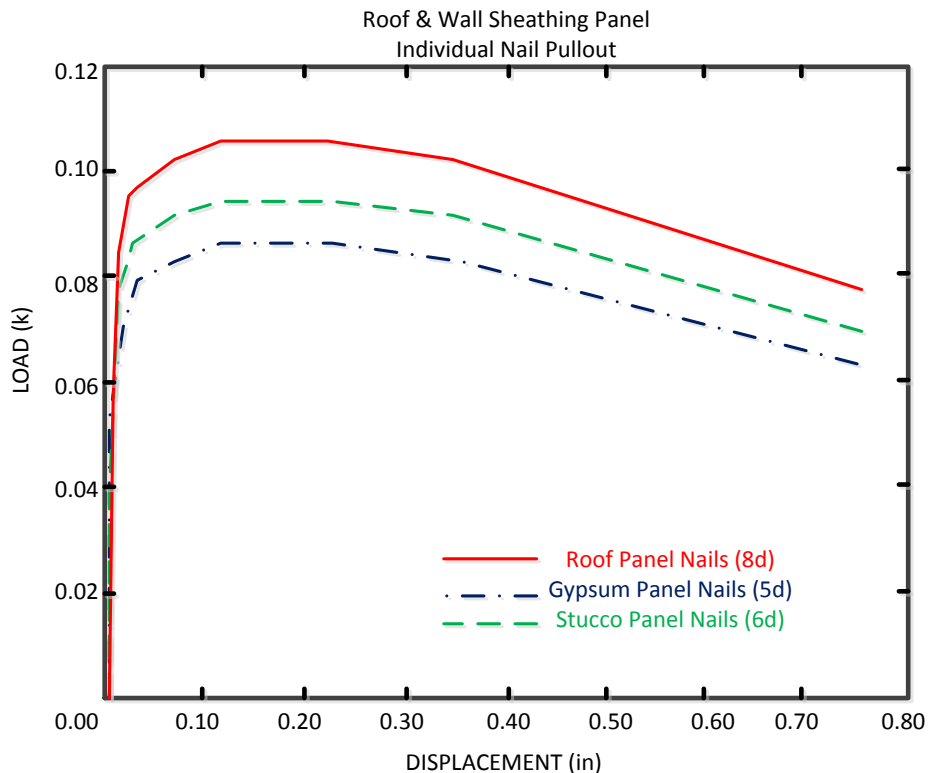


FIGURE 2. 16 – Roof and wall sheathing nail pullout load-displacement curves

The in-plane shear resistance for the plywood and stucco sheathing panels is represented by a linear stiffness value in accordance with Gruber (2012). The lateral stiffness for the 8d and 6d nails are taken to be 9.75 k/in and 8.73 k/in respectively. These values are adjusted for nail size from the Gruber (2012) value of 12 k/in for a 16d nail. The size adjustment multiplies the original (16d) value by the ratio of the new nail's cross sectional area to the 16d's cross sectional area. This is because lateral resistance is assumed to be governed by shear failure of the nail which is dependent upon cross sectional area; thus, a reduction in cross sectional area correlates directly with a reduction in lateral resistance. Note also that roof and stucco sheathing panel failures are not expected to occur due to insufficient resistance to in-plane shear, so pullout resistance is considered the more important variable in these cases.

The gypsum board in-pane shear resistance plays a large role in dictating the in-plane stiffness of the walls, particularly the interior walls which are sheathed on both sides with gypsum board. The lateral load versus displacement curve for the gypsum fasteners is found primarily from the equations provided by Grenier (2014). The curve in Figure 2.17 has been modified from these equations in accordance with observations made during the validation of an ABAQUS shear wall model described in Chapter 4. Because an understanding of these modifications relies on an understanding of the validation process, a description of the modifications will not be provided here, but in Chapter 4.

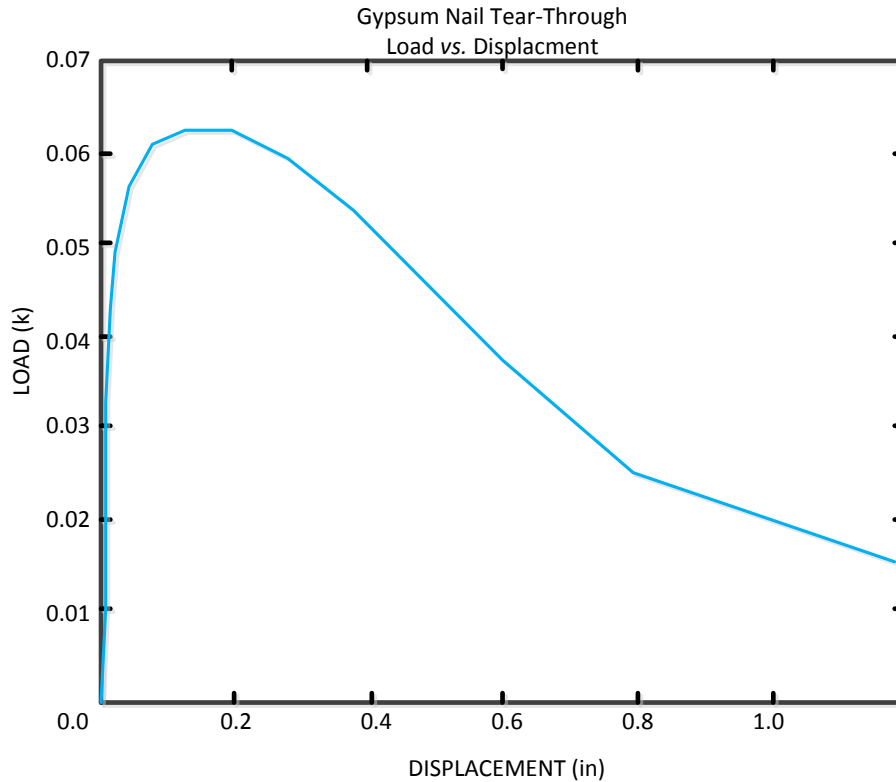


FIGURE 2. 17 – Gypsum nail tear-through load-displacement curve

The pullout resistance for toe nailed wood-wood connections, which include rafter-sill, stud-sill, joist-sill, and other connections throughout the structure is modeled using the average load versus displacement curve taken from NAHB (2002) for two pneumatically driven (nail-gun) 16d toe-nails. It is assumed that the toe nails in the NAHB (2002) test set-up bear the load relatively equally, and thus, the strength for a single nail is assumed to be half of this test value. Upon making this modification, the curve from NAHB (2002) is very similar to the one used for a single 16d nail in Gruber (2012) for the same wood species. NAHB (2002) uses SPF wood and 16d nails, so no specific gravity or nail size adjustment was necessary.

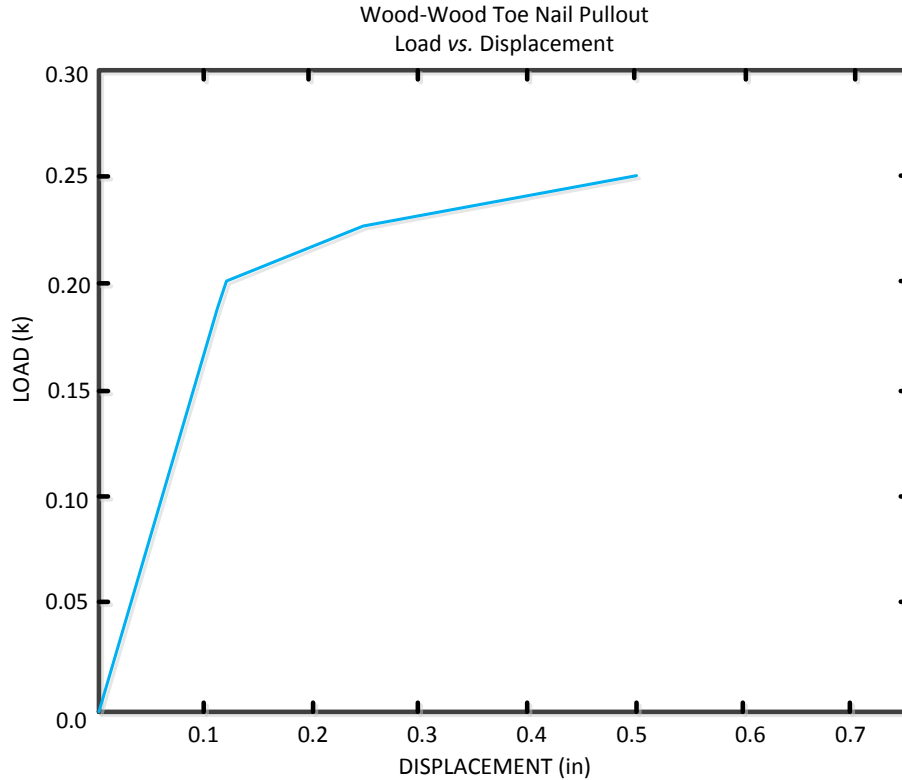


FIGURE 2.18 – Wood to wood toe nail pullout load-displacement curve

The in-plane shear resistance for these wood-wood connections is taken from Gruber (2012) for 16d nails as a 12 k/in.

2.3.3 Component Resistance Statistical Parameters

In order to construct the building system-level fragilities, statistical data describing the resistance of each component is required. Because the finite element models used in this study are detailed down to the individual nail level, the resistances for many important components depend upon the individual fastener (nail or other component, hurricane strap, etc.) connection strengths; thus the component strength is not simply assigned directly from experimental component failure test data, as was the case in previous studies (Lee and Rosowsky (2012),

Alfano (2016), Amini (2012), etc.). This being the case, statistical information for coefficients of variation (COVs) and probability distributions must be either established or assumed for the modeled component resistances. This would not be necessary if it were computationally feasible to run the simulation of each model enough times to produce adequate data to perform a statistical analysis. Unfortunately, however, the models used in this study are far too computationally expensive to make this a reasonable approach.

To resolve this issue, it will be assumed that the COVs and probability distributions associated with component experimental data can be applied to the modeled component resistance as well. Using this approach the ABAQUS model can be executed only a handful of times using the mean values for the connection strengths, dead loads, material strengths, and loads. From these “mean value” ABAQUS simulations, a mean resistance value, or equation defining the resistance value can be identified for each critical component. The corresponding COV and probability distribution can then be taken from the experimental data and applied to the modeled component resistance so that a statistical analysis can be performed using the combination of the mean resistance value or equation taken from the ABAQUS analysis and the distribution and COV from the experimental data.

The statistical parameters and probability distributions associated with each building system component resistance are shown in Table 2.5.

TABLE 2. 5 – Component resistance statistics; all archetypes

Parameters	Category	Unit	Mean	SD	COV	Dist.	Ref.
^b R _{sh}	Roof Sheathing	psf	63	12.6	0.2	Normal	Lee & Rosowsky (2005)
R _{Raft1}	Rafter- Top Sill; 3 d16 toe nails	lb	747	119.5	0.16	Normal	Alfano (2016)
WD _{GC}	Gypsum Drift Cracking	% drift	0.28%	0.15%	0.51	Lognormal	CUREE W-23
WD _{SC}	Stucco Drift Cracking	% drift	0.20%	0.10%	0.51	Lognormal	Arnold et al (2003)
R _{FN}	Foundation Conn. No Reinf.	kips	Alfano Eqn.	-	0.388	Normal	Alfano (2016)
^c WS _{SC}	Stucco Bending Stress	psi	530	-	-	-	Typ.
R _p	Window Pressure	psf	40	8	0.2	Normal	HAZUS
R _D	Door Pressure	psf	50	10	0.2	Normal	HAZUS
R _S	Shingle Pressure	psf	74	22.2	0.3	Normal	Huang et al. (2015)
R _{HC}	H2.5 Hurricane Clip	lb	1312	157.44	0.12	Normal	Reed et al. (2008)

a) Mean values taken from ABAQUS analysis.
b) Mean value for first failure panel.
c) No experimental/statistical data available. Assume typical value from manufacturer websites.

The variance in component resistance for the masonry block basement wall is accounted for by using statistical data for the variation in material properties of the components which make up the wall; concrete block and mortar. Table 2.6 shows the statistical parameters associated with the relevant concrete block and mortar material properties.

TABLE 2. 6 – Masonry block basement wall component material property statistics

Component	Parameter	E	f _t	f _c	Sources
	-	ksi	ksi	ksi	
Mortar	mean	2532	0.51	2.39	Bui et al. (2013); IBC; Melchers (1999); Kassem et al. (2013)
	COV	0.08	0.2	0.2	
	Dist.	Normal	Normal	Normal	
	SD	203	0.10	0.48	
Block	mean	2285	0.60	1.95	
	COV	0.08	0.2	0.1	
	Dist.	Normal	Normal	Normal	
	SD	183	0.12	0.20	

1) The mortar COV is consistent with "poor" quality control while the block COV is for "excellent" control. This is because the block is assumed to be formed in a factory, while the mortar would be mixed on-site

The mean values for the strength properties are taken from the International Building Council (IBC) and Bui et al. (2013). The coefficients of variation and statistical distributions are general values for concrete taken from tables compiled by Melchers (1999) and Kassem et al. (2013).

CHAPTER 3

BUILDING ARCHETYPES, QUALITY LEVELS, AND MODELING APPROACH

3.1 Analysis Program: ABAQUS

The ABAQUS finite element software program was used to develop and analyze the building archetype models. ABAQUS was selected for its user friendly CAE interface, its versatility, and its stability for complex analysis. The CAE interface allows the building models to be constructed in a three dimensional physical layout (similar to AutoCAD) instead of in a purely numerical format which would become complex and difficult to visualize for structural models of this size and level of detail. Furthermore, the versatility of the program allows for the creation of specialty elements necessary to capture accurate and realistic behavior of connections and other components.

The only potential drawback to choosing ABAQUS is the amount of run-time required to analyze the complex models considered in this research. This makes it impractical to rely on the ABAQUS models alone to perform the statistical analysis of the building archetypes. Therefore, the physical information gained using the ABAQUS models is interpreted and used to perform Monte-Carlo simulations with MATLAB to formulate component and building system level fragility curves.

3.2 Building Archetypes

3.2.1 Archetype 1: Small, 1-Story, Hip Roof Home (Figure 3.1)

The first model considered is a small (30'x40'), single story light wood frame home with a hip roof. The building layout and basic details/dimensions are taken from CUREE Publication

No. W-29 (Reitherman and Cobeen (2003)). This building was selected, in part, because the results of the ABAQUS analysis can be compared with data from the CUREE-Caltech Wood frame Project (C-C) to validate the model. The basic dimensions of the building are: 40'Lx30'Wx13'H. The roof has a rise of 4.5', has no overhang at the edges, and is sloped at 3V:12H. The framing system for this archetype consists mainly of structural lumber members ranging from 2x4's to 2x8's, various sheathing materials, and various sized nails (primarily 16d).

Some deviations from the C-C layout were made out of necessity while others were based on judgment. For example, details were not provided in Reitherman and Cobeen (2003) regarding window and door openings in the walls, so typical, generic construction details were used for these features. An example of a deviation based on judgement was the use of plywood sheathing panels for the roof sheathing, which are more representative of typical modern construction practice in most parts of the U.S. than the 1x6 sheathing boards specified in the C-C project. The rafters spanning normal to the long dimension are supported at intermediate points by truss members that are connected to the main partition stud and the rafters spanning normal to the short dimension are supported intermediately by posts connected to the ceiling joists.





FIGURE 3. 1 – Archetype 1 layout (a) complete, (b) w/out roof, (c) w/out wall sheathing

3.2.2 Archetype 2: Small, 2-Story, Gable Roof Home (Figures 3.2 and 3.3)

The second archetype selected for this study has the same 30'x40' footprint as the first. The same basic construction techniques and materials are assumed to be used for the baseline version of this archetype as well. The floor plan for each story of the two-story home is simply a copy of the floor plan used for the small single story home.

Despite the similarities between archetypes 1 and 2, several new considerations were made for the 2-story archetype. The first of these considerations was the first-second story connection, and the second was the alternate roof type. The details of these components are discussed below.

First-to-Second Story Connection: The inter-story connection was taken from generic typical details acquired online. The connection between the top stud sill of the first floor and the base of the second floor is made by 0.5" diameter steel anchor bolts spaced at 6' on center. The connection bolts are placed all along the perimeter sill plates of the building as well as along the main partition stud sill plate. The second floor joists are supported at the edges by the top stud sill plate of the first floor and intermediately by three generic steel beams which span the 30' length of the structure (perpendicular to the joists). The steel beams are supported at each end by the first floor top stud sill plates and intermediately by the main partition stud sill plate. Note that

there is assumed to be a joint in the exterior stucco between the first and second story meaning that stresses are not transferred between the stucco panels of the first and second floor. The connection is assumed to be fairly rigid.

Gable Roof: The 2-story archetype features a gable roof as opposed to a hip roof like archetype 1. This was done to represent both common roof types in this study, as the wind pressures vary with the change in roof type. The archetype 2 gable roof consists of 3V:12H sloped trusses spaced at 24" on center, maintaining the slope and spacing of the hip roof rafters used for archetype 1. The rafter member size (2x6) and baseline material (SPF) are also consistent with archetype 1. The trusses are connected by a 1x8 SPF ridge board at the peak of the roof as well. The roof sheathing (including fasteners) is the same as for archetype 1, as are the rafter-sill connections for the basic quality model. In addition, note that beam elements were used to model the truss members for this archetype as opposed to the shell elements used to model the rafters in archetype 1. It is assumed that the trusses are prefabricated with steel truss joint connections that will not fail prior to the rafter-sill connections. A typical truss is shown in Figure 3.2 and is a generic shape consistent with typical trusses found online.

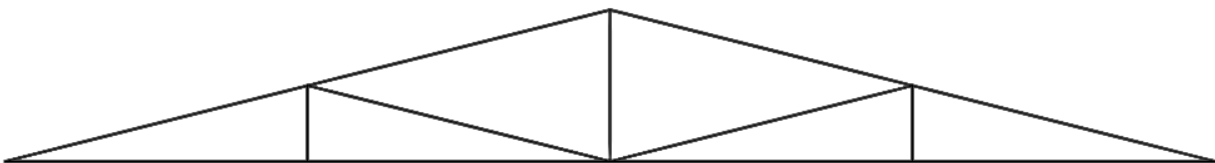


FIGURE 3. 2 – Archetype 2 roof truss

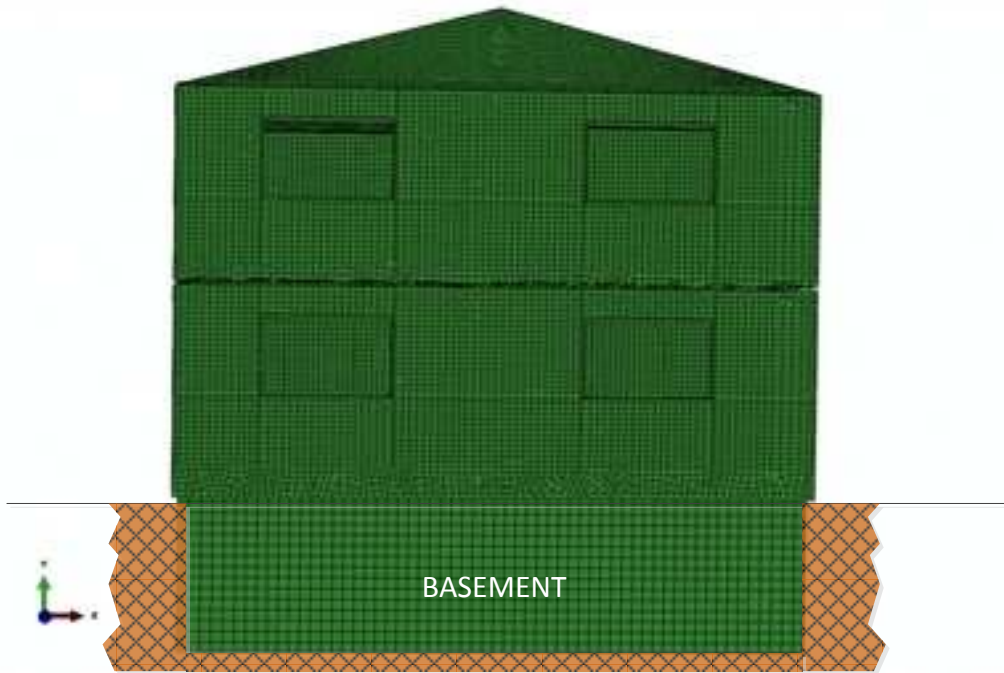


FIGURE 3.3 – Archetype 2 layout

The assembled second story archetype (including the basement) is shown in Figure 3.3 above.

3.2.3 Archetype 3: Medium, 1-Story, Hip Roof Home (Figure 3.4)

The third archetype examined in this study is a single story, medium sized home with a footprint of 60'x80' and a hip roof identical to the one used for archetype 1. The floorplan is staggered, so the footprint of the house is not rectangular. Figure 3.4 shows the layout of archetype 3.

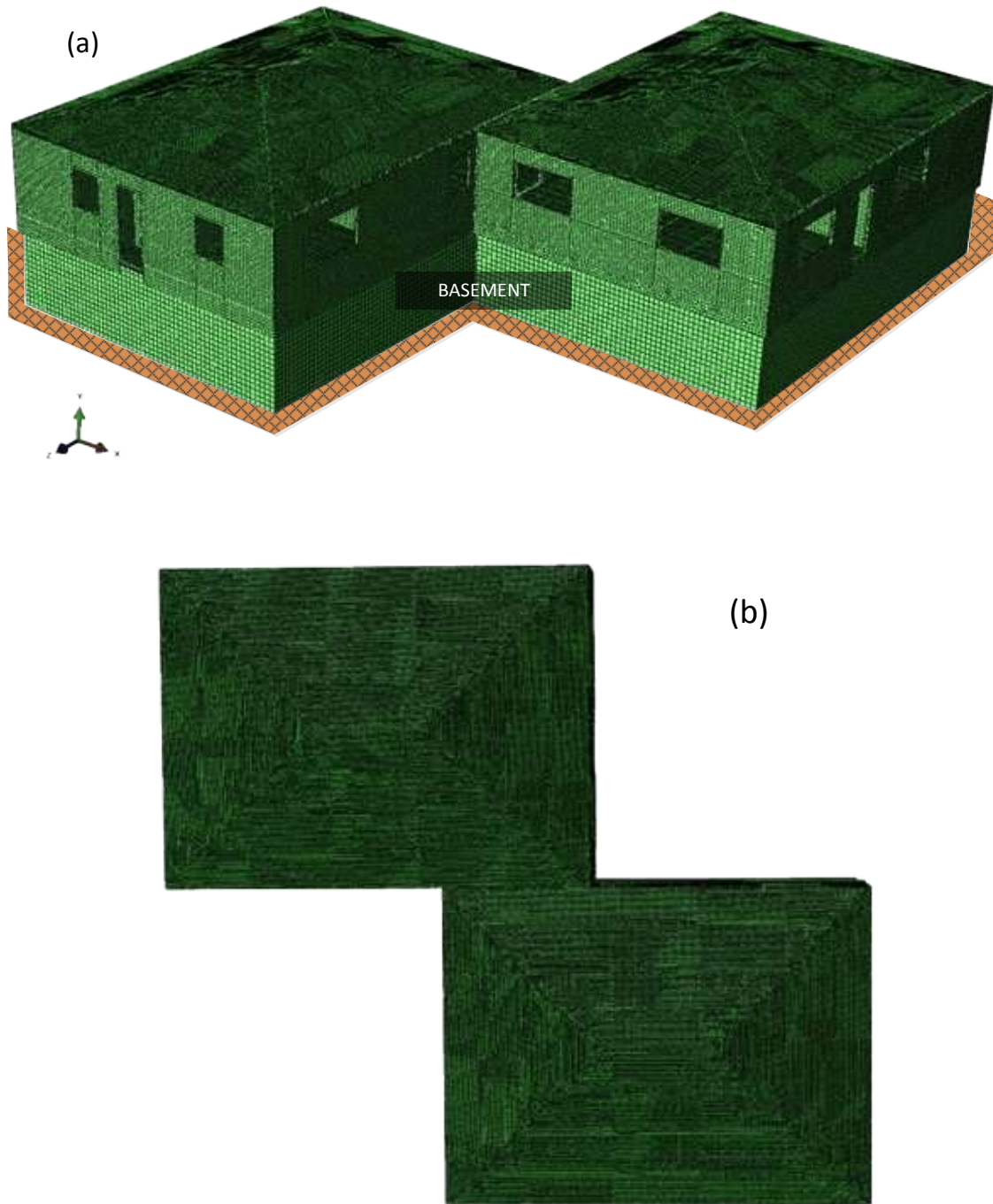


FIGURE 3. 4 – Archetype 3 layout (a) plane view and (b) bird's-eye view

The floor plan for each unit of archetype 3 is the same as for archetype 1, and the two building sections are connected at what had been the large glass door opening for archetype 1. This

opening was turned into a hallway, and a rigid connection between the two buildings was assumed so that the loads will be transferred through the connection directly from one section of the building to the other.

3.3 Quality of Construction

Each building archetype was analyzed for four levels of construction quality: basic, enhanced (focus on life safety), improved (focus on reparability), and resistant (focus on continued function). Only the basic quality construction is discussed in detail. Providing such information for the other levels of quality would require an in-depth design and cost-benefit analysis to identify optimized combinations of components for each performance target and that is beyond the scope of this thesis. However, initial recommendations are made for these different levels of quality in Chapter 6 to illustrate the kinds of measures that might be taken to meet each target construction quality level.

3.3.1 Basic Construction Quality

The basic construction quality level (CQL) for all three archetypes in this study is based on existing construction practices. The details of the components used to construct the basic quality archetypes are provided in Chapter 2, section 2.2.1. The building material properties are shown in Table 2.4 and the component resistances and statistical parameters are given in Table 2.5.

3.3.2 Quality Levels 1 (Enhanced), 2 (Improved), and 3 (Resistant)

The total building performance goals to be achieved for each CQL are defined by performance targets provided by our system analysis collaborators at the University of Oklahoma. Many different types of modifications could be made to a given archetype to meet the

target for each CQL. The modifications should be made such that the cost is optimized while performance targets are still being met. Suggested, non-optimized, modifications are discussed in Chapter 6. Note that each CQL has four damage states; slight, moderate, extensive, and complete.

3.4 Modeling Techniques/Element Types

To strike a balance between computational efficiency and accuracy, the models were optimized by choosing the element types that would best represent each component of the building. Generally, all studs, posts, beams, sheathing, rafters, hips, joists, blocking, and sills/plates are shell elements. Due to complexities in roof geometry, the portions of the rafters that connect to the hips and the portion of the hips that connect to the ridge are modeled as solid elements. These elements were created in AutoCAD and imported into ABAQUS so that the geometry would be exact. Fasteners (nails) are modeled as spring elements with specified nonlinear behavior. This process and the spring parameters are discussed in further detail below.

3.4.1 Fastener Modeling

The behavior of different nailed connections is dependent upon the elements the nail is connecting, as well as the orientation and size of the nail. Data for the nail behavior is obtained from experimental testing and previously performed work such as that done by Grubler (2012) and Vieira and Schafer (2009). Load-displacement curves for the common nailed connection types used in this stud were provided in Chapter 2.

Each connector is modeled with three springs, one for each dimension in space. The nails are assigned local orientations instead of using the global orientation because in a 3-d model, nails in the same set may mirror each other. This means that if they are specified in global dimensions,

the nail properties on the mirrored side of the model may be opposite of what they should be. Also, roof nails are slanted and thus will not be oriented parallel to any of the global axes, which would complicate the spring behavior if the global orientation were to be used. The local coordinate system used to model the nails is cylindrical with the radial and tangential directions being directions “1” and “2” in ABAQUS and the axial direction corresponding to the “3” direction in ABAQUS. This allows the nail properties specified in the three different directions to remain dependent upon the nail orientation, instead of becoming distorted and inaccurate if the nail, or the member to which it is attached, shifts out of plane due to deformation during the analysis. It is also important to note that not all of the spring elements are modeled nonlinearly. According to Grubler (2012), certain configurations, can be modeled accurately with a linear spring. The two primary connection types in the models are wood-wood connections and wood-sheathing connections; these connection types and details of the failure modes associated with them are described below.

Springs – Wood to Wood: In general, for wood-wood (not including wooden sheathing) nailed connections, the failure modes are nail pullout (tensile loading), nail shear (transverse loading) and wood crushing (compression loading). The third of these options is rare, and will likely not control in most cases but is accounted for in the analysis. Nonlinear behavior is generally associated with a nail being loaded in tension/compression (pullout or crushing of member) while the linear behavior is associated with a nail that is being loaded in shear (Grubler (2012)). As oriented in the models, the transverse (shear) stiffness is applied to the radial and tangential directions, the tensile (pullout) stiffness is applied to the positive axial direction and the compressive (crushing) stiffness is applied to the negative axial direction.

Springs – Wood to Sheathing: The primary failure modes for the wood-to-sheathing connections are nail pullout of the wood member (tension), nail pull through of the sheathing member (tension), crushing of the wood member or sheathing (compression), and nail tear out of the sheathing (transverse loading). Nonlinear behavior is generally associated with all of these failure modes. As the nails are oriented in ABAQUS, the tensile and compressive modes (pull out, pull through and crushing) will be oriented in the axial direction, while the transverse loading modes (tear out) will be oriented in the radial and tangential directions.

A diagram depicting the orientation of the springs relative to the nail that they model is shown in Figure 3.8.

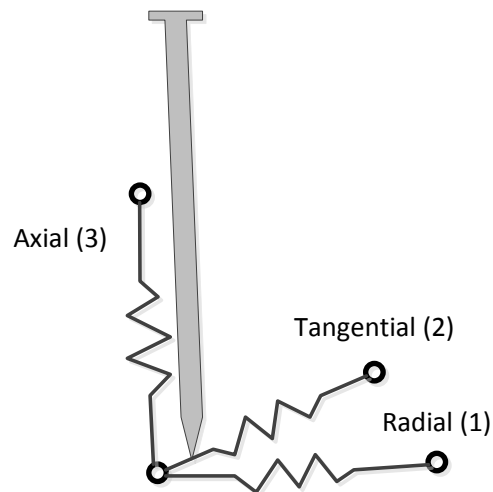


FIGURE 3. 5 – 3-dimensional nail – spring model orientation

3.4.2 Masonry Basement Wall Modeling

The effect of expansive soils on a typical basement wall must be modeled so that the effects of proposed improvements to basement construction (wall reinforcement, non-expansive backfills, etc.) can be examined subsequently and quantified. The basement walls considered

herein are typical cement block/mortar walls with typical material properties. The blocks are 8"x8"x20" with a void area of $\approx 56\%$. The material properties of the blocks and mortar are taken from the International Building Council (IBC) and Bui et al. (2013). These values are shown in Table 3.1.

Rather than modeling the wall as separate mortar and block elements with interaction properties governing their behavior, the wall is modeled as a single shell element. This involves deriving "composite" material parameters to be assigned to the shell element that represent the composite behavior of the blocks and mortar. The composite material derivation procedure detailed in Abdelnaby and Elnashai (2013) has been used in numerous other studies and has been shown to give good results. The mortar, block, and composite properties are shown below:

TABLE 3. 1 – Masonry block wall component material properties

KEY MASONRY MATERIAL PROPERTIES			
Material	E	Comp. Strength	Tensile/Bond Strength
-	ksi	ksi	ksi
Mortar	2532	2.39	0.51
Block	2285	1.95	0.6
Composite	2296	1.01	0.51

The wall shell element thickness in the model was adjusted to an effective thickness based on the ratio of void volume to block volume (i.e. the effective thickness is $\approx 40\%$ the actual thickness, as the block volume is only $\approx 40\%$ solid and 60% void).

After the material parameters were determined, the tensile and compressive stress-strain curves were calculated based on the recommendations in Kmiecik and Kaminski (2011). The "Majewski formula" was used to calculate the compressive stress with respect to strain. The

compressive and tensile stress-strain curves and the corresponding damage-strain curves for each are shown in Figures 3.9 and 3.10.

The damage parameters were determined in accordance with Jankowiak and Lodygowski (2005) and Kmieciak and Kaminski (2011). With this information, all necessary inputs for use of the concrete damaged plasticity (CDP) model in ABAQUS are known and the CDP model is used to model the plastic/damaged behavior of the masonry wall. The ABAQUS CDP damage parameter inputs are shown in Table 3.2.

TABLE 3. 2 – ABAQUS CDP model input parameters

ABAQUS CDP INPUTS				
K_c	ϵ	σ_{b0}/σ_{c0}	ψ	μ
-	-	-	deg	-
0.667	0.503	1.16	36	0

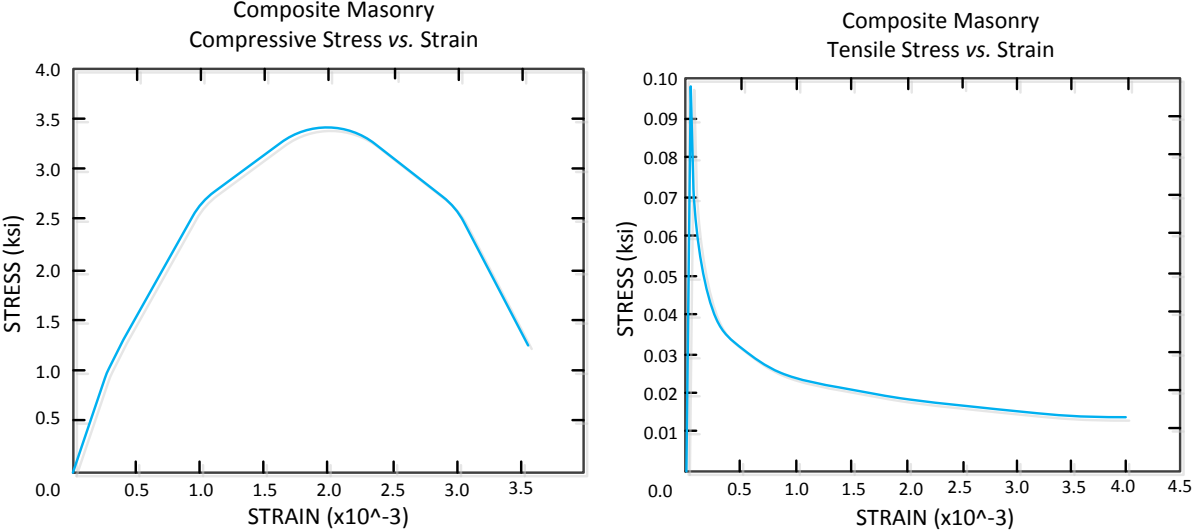


FIGURE 3. 6 – Masonry wall composite material compressive and tensile stress-strain curves

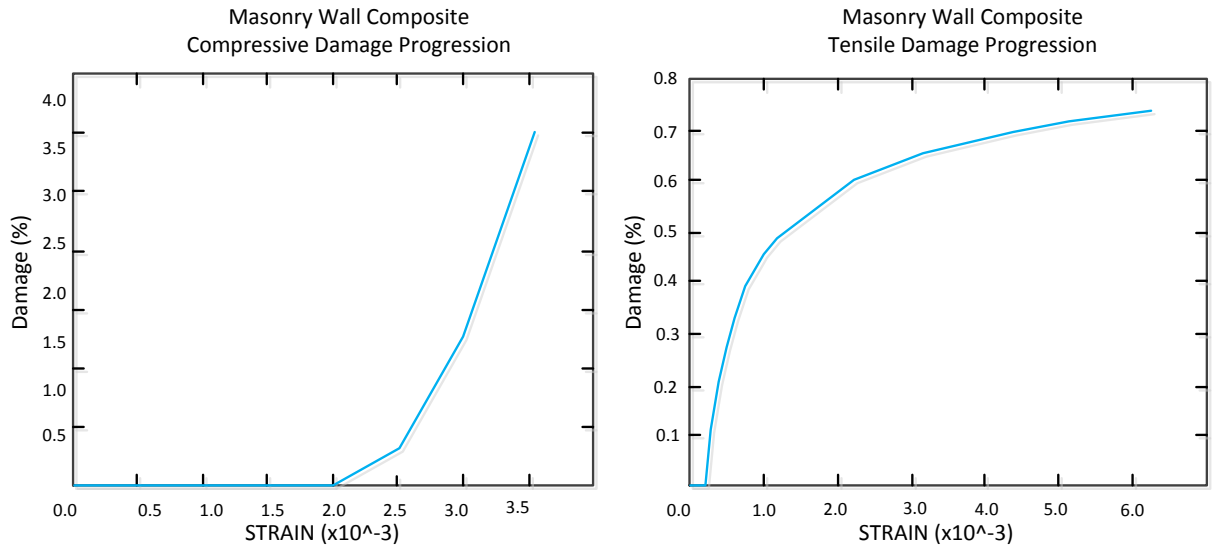


FIGURE 3. 7 – Masonry wall composite material compressive and tensile damage-strain curves

CHAPTER 4

MODEL VALIDATION

The ABAQUS finite element models developed in this thesis are validated by comparison of the model predictions with existing experimental data. By performing this validation on different scales ranging from individual components to fully assembled buildings, we can determine whether the finite element models applied on a small scale (individual nail/connection modeling) are yielding results that are consistent with actual experimental results on the large scale. The component validation is performed for shear walls, masonry walls, roof panels, etc. This approach makes it easier to troubleshoot modeling issues on relatively simple systems. Furthermore, more experimental data is available on the failure modes and behaviors of these components because it is easier and less expensive to test them in the lab than it is to perform testing on complete, full scale homes. Validation for individual component models inherently increases confidence in the accuracy of the fully assembled wood frame system models and is therefore a valuable part of this research.

4.1 Component Level Model Validation

We start the ABAQUS model validation process by considering separate, smaller and less complex elements of a light wood frame homes prior to delving into the larger and more complex complete home models. In addition to increasing confidence in the accuracy of the complete home models, the component modeling allows for refinement of modeling efficiency techniques on a smaller scale which can then be implemented in the home models. To this end, a number of components were modeled to validate the results of the ABAQUS model by replicating their experimentally observed behaviors.

4.1.1 Shear Wall Model Validation

The layout, materials, dimensions and other specifications for the shear wall considered are taken from Bahmani and van de Lindt (2014). The specimen (identified as test specimen G-01) was selected for its simplicity and consists of a shear wall that is roughly 8'x8'. The wall consists of 2x4 studs, 2x4 sill plates (top and bottom) and 0.5" thick gypsum sheathing panels on only one side of the wall. HDU8 steel hold downs are placed in the bottom interior corners of the wall, connecting the exterior double studs to the bottom sill plate. The wall is held together primarily by 16d common nails and is anchored to a steel base plate by 8 - 5/8" dia. steel anchor bolts. The gypsum wallboard is fixed to the studs using #6 drywall screws. The wall is loaded in-plane by load bolts placed through the double top sill. The experimental test layout, upon which the model was based, is shown in Figure 4.1:

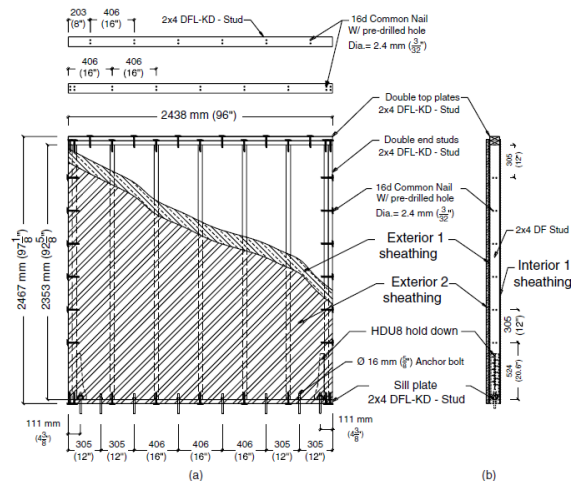


FIGURE 4.1 – Model validation shear wall layout (Bahmani and van de Lindt (2014))

In order to remain consistent with the modeling techniques used for the residential framing systems, the 2x4's and the sheathing are modeled as shell elements. The HDU8 hold downs have

a complex geometry, and were modeled in AutoCAD then imported to ABAQUS as solid elements. The nails, screws, and bolts were all initially modeled as beam elements of various diameters. The model layout is pictured in Figure 4.2:

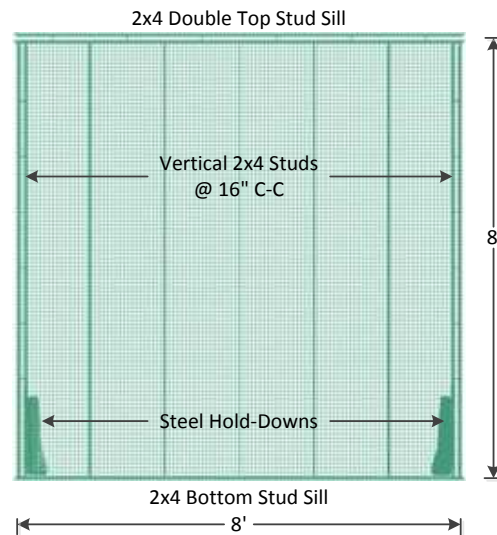


FIGURE 4. 2 – ABAQUS shear wall model

The load in the model is applied to the three nodes (top, middle, bottom) of each of the 6 evenly spaced load bolts as a concentrated force. The load bolts span vertically between the two shell elements that represent the 2x4 stacked top sills. The boundary conditions are applied as follows:

- 1) Encastré (fixed) along the entirety of the steel baseplate.
- 2) Restricted from translation in the “Z” (out of plane) direction at each load bolt.

The loading and boundary conditions were selected to best represent the actual experimental conditions used in Bahmani and van de Lindt (2014).

With the initial use of beam elements to model the nails and screws, the linear behavior of the wall was captured with good accuracy. From Table 3 of Bahmani and van de Lindt (2014),

specimen G-01 has an initial stiffness of 0.42 k/in/ft. When multiplied by 8' (wall length), the stiffness of the wall is approximately 3.36 k/in experimentally while the linear model predicts an average linear stiffness of 3.38 k/in. The linear model deformed shape in from three different perspectives is shown in Figure 4.3 below. Note that the deformed shape for the nonlinear model is visually similar and so it is not shown. A simple ramped static load was used to model the loading for the linear case, because only the initial stiffness was replicated.

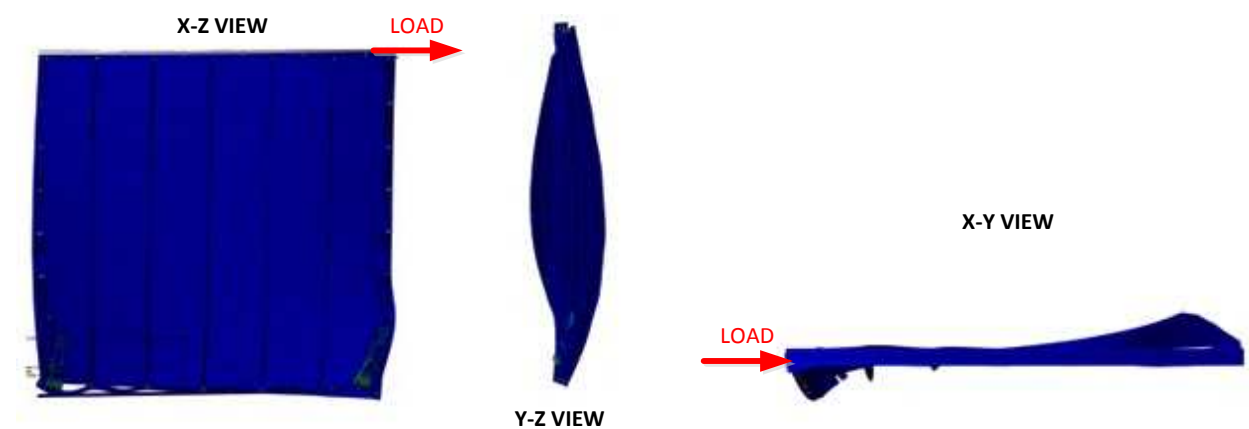


FIGURE 4. 3 – ABAQUS shear wall model – deformed shapes (x-z view, y-z view, x-y view)

After the linear behavior was captured, the nonlinear behavior was replicated using spring elements to model the fasteners as described in Chapter 3. In order to recreate the backbone curve found in Bahmani and van de Lindt (2014) for specimen G-01, the model was tested in displacement control (displacement is specified and the corresponding loads are calculated and recorded.) Displacement control allows for the capture of the fully nonlinear behavior, and shows the decrease in stiffness that occurs at higher displacements. Figure 4.4 shows the comparison between model and experimental load-displacement for the shear wall.

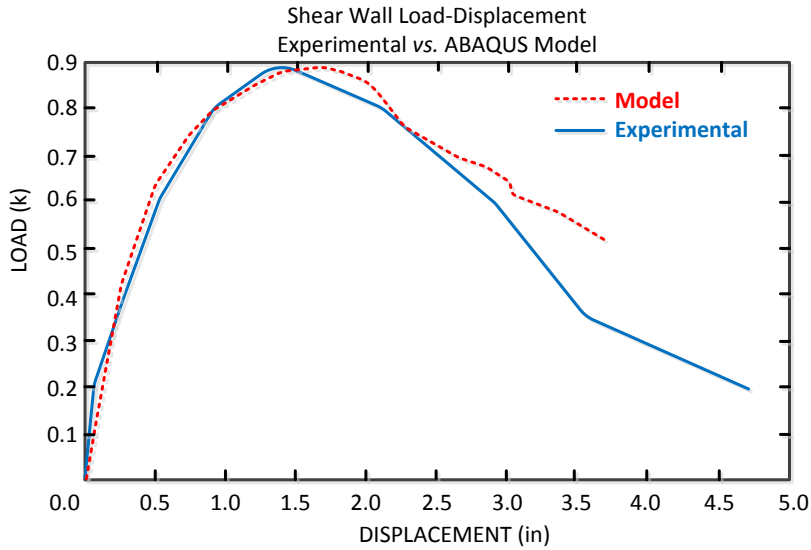


FIGURE 4. 4 – Model versus experimental in plane shear wall load-displacement

The model predictions agree reasonably well with the experimental results up through a displacement of approximately 3” (3% story height of the wall), and particularly up to the peak load capacity of the wall. It was observed that the load-displacement specified for the gypsum screws in the transverse directions was the critical variable in this analysis.

The “idealized” load-slip equation specified by Grenier (2014), Eq. 3.2 for Group-2 (corner gypsum screws with 10mm side distance) appears to give the best results when compared to experimental testing and is used subsequently to define the behavior of the gypsum fasteners in this study. The Grenier (2014) values were modified in the following ways to better match experimental data:

- The load capacity was increased by 10%. This is thought to be justifiable because a 10% increase is relatively small and considering the variability associated with construction of

a shear wall (screw diameter, quality of construction, material inconsistencies, etc.), the increase seems reasonable.

- A “tail” was added after a displacement of 0.2” is reached. Because experimental data for corner and end screws shows a major drop in load carrying capacity between 0.1-0.2”. The shape chosen for this tail falls between the idealized value and the observed edge and corner fastener values for load capacity with respect to displacement and appears to recreate experimental data reasonable well. Figure 4.5 depicts the load-displacement for the idealized equation, the experimental end and corner fasteners, and the modified curve used in this thesis.

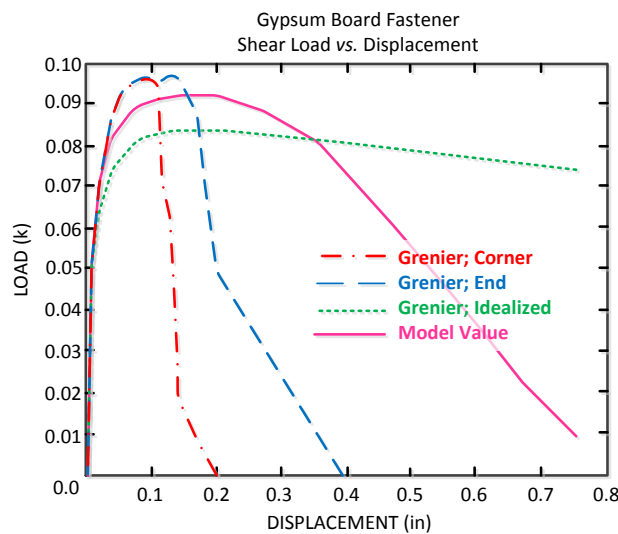


FIGURE 4.5 – Gypsum board fastener shear load-displacement

Note that the modified curve shown in Figure 4.5 is for 6d drywall screws (consistent with Bahmani and van de Lindt (2014)) but the load-displacement response shown for transverse loading of drywall fasteners in Figure 2.17 is for 5d nails (per CUREE Publication No. W-29).

This is why the curves differ. The reduction in shear load capacity for the 5d nails is assumed to

be proportional to the reduction in shear area and thus fastener diameter. 6d screws are approximately 25% larger in diameter than 5d nails; thus they have approximately 25% more shear capacity. If pullout or tear through were being analyzed, the difference between a nail and a screw would be more complex, but it is assumed that for transverse loading this adjustment can be used.

4.1.2 Roof Sheathing Panel Model Validation

Prior to attempting to model the roof as a whole, a single sheathing panel subjected to pressure loading was validated against experimental data from Hill et al. (2009) and NAHB (2002) and verify the accuracy of the model panel behavior. The simple model consists of a single 48"x96"x15/32" plywood sheet modeled with a shell element and 8d nails (modeled using 3 directional springs) spaced at 6" on the edges and 12" in the interior.

The rafter ends of the nail springs are totally fixed and a uniform pressure load is applied to the panel. The primary failure mode is nail pullout in accordance with the tests performed by Hill et al (2009) and NAHB (2002). Panel rupture was also explored as a potential failure mode. An additional boundary condition was also applied to the transverse (48" long) edges of the panel. This condition restricts rotation about the transverse axis to simulate the rotational limit that the edge rafter will impose on the panel at each edge. Figure 4.6 illustrates this condition:

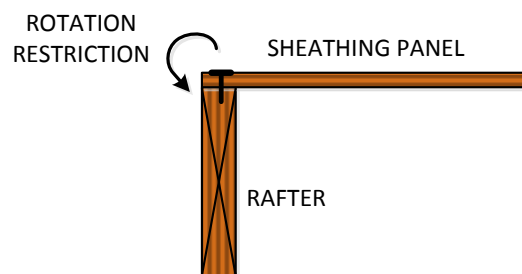


FIGURE 4. 6 – Roof sheathing edge rotation restriction

The panel model is load controlled since the panel displacements and deformed shape are unknown. A dynamic, implicit load step was used so that the full load versus displacement behavior with decreasing stiffness could be captured without modeling errors.

Each experimental test considered was performed using the same parameters. The tests subjected a 48"x96"x15/32" plywood panel to uniform pressure loading (by an inflatable airbag). The experimental nailing patterns used for each test were consistent with the ABAQUS model pattern. Note that only the tests performed by Cunningham (1993), Mizzell (1994), Jones (1998), and Sutt (2000) were used, as the others are inconsistent with the parameters mentioned herein (i.e. different panel thickness, rafter spacing, and/or nail size were used).

The failure criterion used for each experimental test considered is the "first nail failure" criterion or, FC-1b, as it will be denoted subsequently. This is a common criterion in the literature reviewed for this study and in NAHB (2002), it is explicitly stated that this is because total panel failure follows closely after the failure of the first nail (usually located in the interior of the panel) due to load redistribution to the remaining nails. The results of the ABAQUS analysis of the single sheathing panel support this claim, as will be shown in this section.

The experimental data shows significant variation in panel failure pressure values, ranging from 130 psf (Cunningham (1993)) to 61 psf (Mizzell (1994)), with a weighted average of 74 psf. This discrepancy is explained in NAHB (2002). The variability is a result of the different species of rafters supporting the sheathing panels in the different experiments. A denser wood will result in a greater nail pullout capacity. NAHB (2002) specifically sites the correlation between the Cunningham (1993) data and Mizzell (1994) data. While these data sets show the largest discrepancy between panel failure pressures (Cunningham = 130 psf, Mizzell = 61 psf),

the correlation between them is good considering the density of the wood species used for rafters in each study. For Cunningham (1993), the rafter wood was DF-L with specific gravity (G) ≈ 0.50 . For Mizzell (1994), SPF with $G \approx 0.37$ was used. Considering these values and rearranging NAHB (2002) equation 2, the following ratio is shown to find equivalent failure pressures for varying specific gravities.

$$P_1 = P_2 * \left[\frac{G_1^{2.5}}{G_2^{2.5}} \right]; \text{ Panel Specific Gravity Adjustment (NAHB (2002))} \quad (4.1)$$

Using this ratio, and the specific gravities listed above for DF-L and SPF, the Cunningham and Mizzell failure pressures match almost exactly (with the ratio, Mizzell failure pressure = 61.2 psf). This relationship allows for the use of variable wood species without the need for experimental data specific to each species.

In the roof panel validation model, the pullout load-displacement relationship of the fastener springs from the rafters was developed assuming that the rafter wood species was hem-fir. This relationship was taken from Grubler (2012). Three failure criteria were considered. These criteria are:

- FC-1a: Total Panel Release - every nail fails.
- FC-1b: First Nail Failure – the failure of the first sheathing nail corresponds to total panel failure, popular in literature/experimental sources.
- FC-2: Panel Rupture – Section of panel ruptures due to stresses exceeding plywood modulus of rupture ≈ 5 ksi (Kretschmann (2010)).

Subjecting the model to a uniform pressure load (consistent with the experimental test methods discussed earlier) and considering the failure criteria above, the failure pressures were in Table 4.1 were observed:

TABLE 4. 1 – Model roof panel failure pressures for different failure criteria

SUMMARY		
Criteria	Failure Pressure	xW1
-	psf	-
1a	103.14	2.40
1b	90.64	2.11
2	97.38	2.26

Note that xW1 represents a factor of safety on the design panel load. In the table above, the design load is considered as the load on a 4’x8’ panel subjected to a uniform “Zone 2” wind pressure load of 0.043 ksf. The “xW1” metric means that the failure load on the panel was that many times the design load. This is used as an extra check on the results. The factor of safety values are between 2.4 and 2.11 which is reasonable, creating more confidence to the accuracy of the model. In addition, note that the data above represents values from the middle “strip” of the panel, where the stresses are the highest and failure occurs first. One node from the center of the panel and one node from the edge are considered to encompass all failure modes (i.e. FC-1b occurs when the middle-center nail releases, while FC-1a occurs when the center-edge nail releases).

As stated earlier, FC-1b is a common failure criterion in the literature reviewed for this thesis. The graph below shows the sequence of the modeled failure criteria and supports the claim in NAHB (2002) that panel failure follows closely after the first nail failure. For this reason, FC-1b will be the primary failure criterion considered for the roof sheathing panels

modeled in the more advanced building system models discussed in Chapters 5 and 6 of this study. Figure 4.7 illustrates the sequence in which the three considered criteria occur.

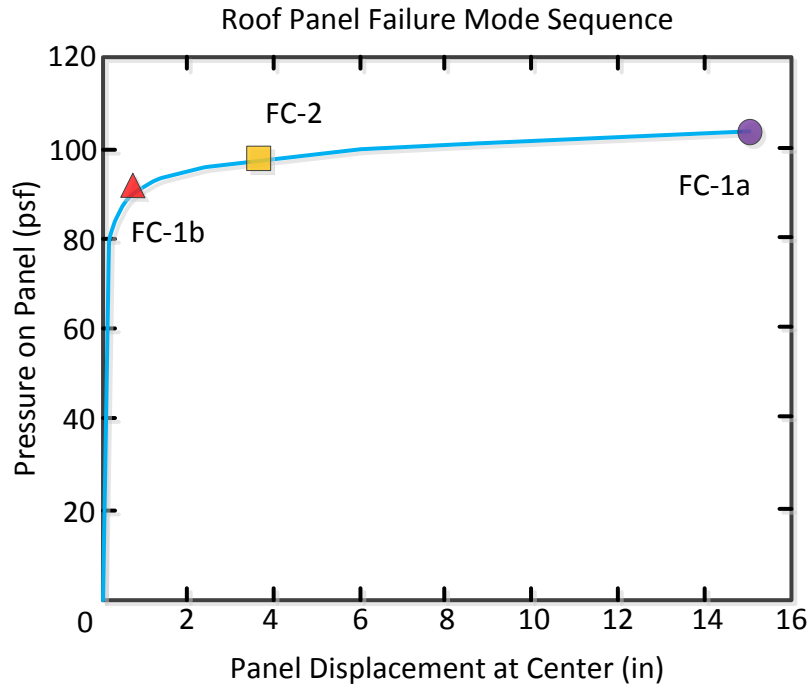


FIGURE 4. 7 – Roof panel failure criterion sequence

Using the FC-1b failure criterion, the model data appears to correlate with the experimental data extremely well. First, as shown earlier, the “factor of safety” check was reasonable at about 2.11x the design value. Second, the failure pressure value is in the middle of the range of experimental values at 90.64 psf. Third and most importantly, when the failure pressure is adjusted for the specific gravity of the hemlock-fir rafter wood used in the model ($G \approx 0.43$), we get a theoretical failure pressure ≈ 89 psf. This adjustment can be made from either the Cunningham (1993) or Mizzell (1994) data with approximately the same result. Clearly, when compared to the model value of 90.64 psf, the correlation between the model and experimental failure pressures is excellent and the parameters used for the single roof panel sheathing model

can justifiably be applied to the larger models discussed in this study. The deformed shape of the panel model and the stress contours at failure are shown in Figure 4.8.

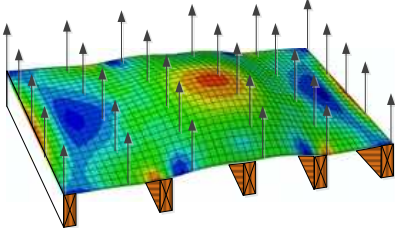


FIGURE 4. 8 – Roof panel model deformed shape and stress contours

4.1.3 Basement Masonry Wall Model Validation

Experimental test results from Bui et al (2013) were used to compare with the model results and validate the masonry wall model performance. An equivalent ABAQUS model of a masonry wall was constructed to recreate the test using the same procedures and material properties described in Chapter 3. The dimensions of the wall are as shown in Figure 4.9.

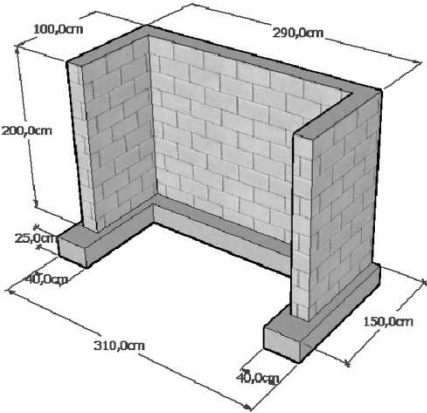


FIGURE 4. 9 Masonry wall test setup (Bui et al. (2013))

The wall referred to as “Wall 1” in Bui et al. (2013) was selected for the purpose of model validation. This wall is unreinforced and fixed to its base with a simple mortar bond, making it a good candidate to validate the model against, since no reinforcement is assumed for the typical masonry basement wall in this study. The block and mortar dimensions and material properties used for the testing are consistent with those used in the model (model values were primarily taken from Bui et al. (2013)).

The test specimen was loaded over most of its front face with a uniform pressure applied by water bags as shown in Figure 4.10. The pressure and out-of-plane displacement of the wall were measured at several locations using a series of transducers.

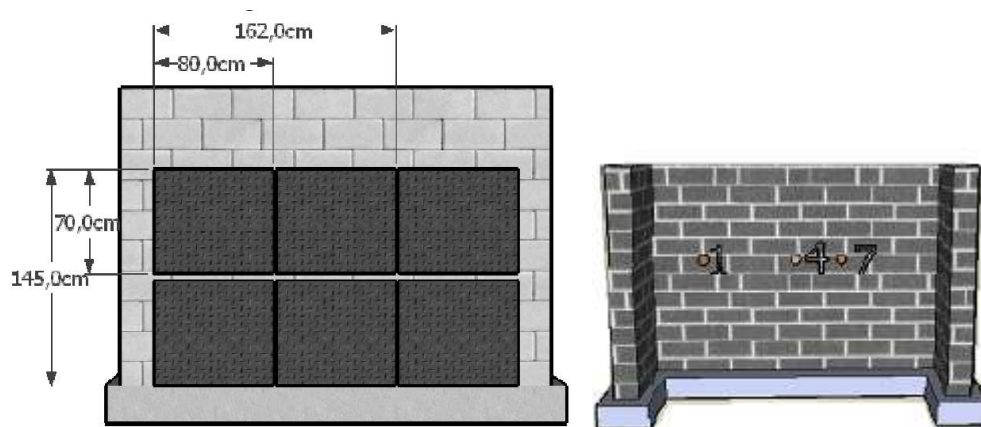


FIGURE 4. 10 – Masonry wall test pressure setup and transducer location (Bui et al. (2013))

A uniform pressure load was applied in the ABAQUS model over the same area to recreate the test condition. The pressure was measured by dividing the model’s base reaction force by the area over which the load was applied. Bui et al. (2013) presents pressure versus displacement curves for transducers 1, 4, and 7 which are located about 43 inches above the base of the wall. Transducer 4 is the centrally located instrument and thus captures the maximum out-of-plane

displacement. For this reason, the model deformation was measured at the location of transducer 4 (43" above base, in center of wall).

The base of Wall 1 was not fully restrained; thus the base boundary condition of the model was somewhere between fixed and pinned, and so the model was executed with each boundary condition. The results of this analysis confirm that the actual boundary condition is between fixed and pinned as shown in Figure 4.11.

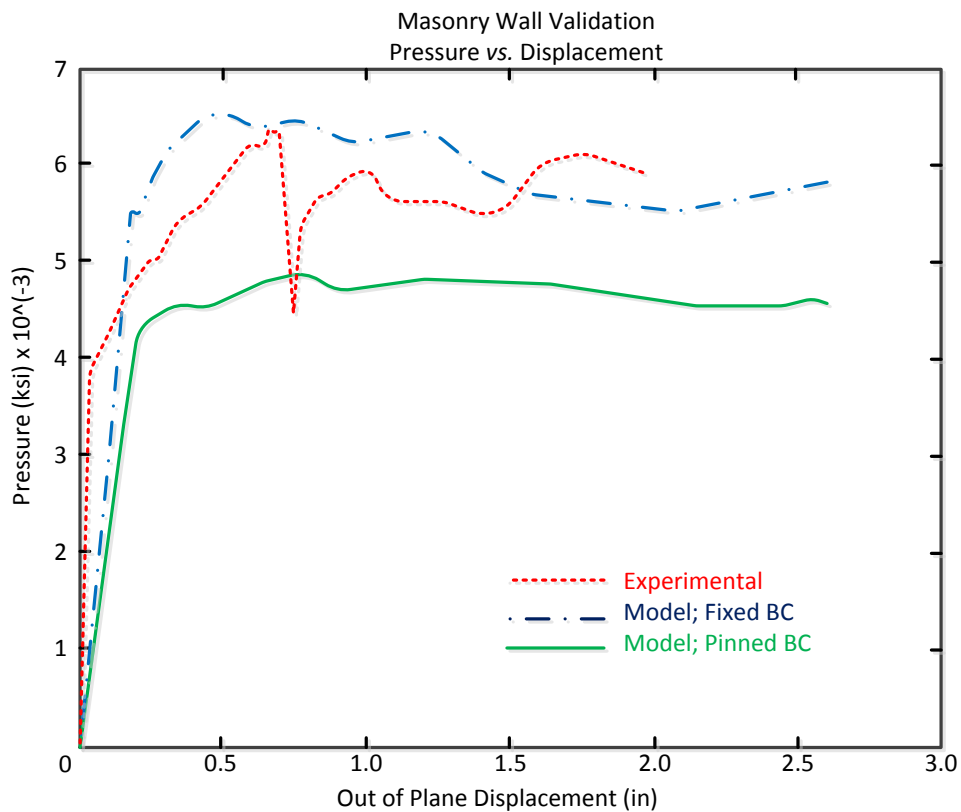


FIGURE 4. 11 – Masonry wall model validation pressure-displacement curves

The shape of both curves seems reasonable. The pinned condition will be conservatively assumed to apply for this study.

In addition to evaluating the pressure-displacement behavior of the wall tested and its ABAQUS model, the failure/damage patterns of the two were also compared, as shown in Figure 4.12. The experimental and computational damage patterns show good agreement, with the same basic inverted “y” shape observed in both.

The combination of these two analyses indicates that the physical behavior of the wall is being captured reasonably well by the ABAQUS model. Comparisons of both the pressure versus displacement and the damage patterns reveal discrepancies between the model and experimental behavior. These discrepancies are believed to be due to: (1) The oversimplified base boundary condition of the wall model, and (2) the uncertainty associated with the construction of a masonry wall, material strength variability, and other similar factors which led to the symmetrical failure pattern shown in Figure 4.12. Considering these factors, the basement wall model appears to be performing to a suitable level.

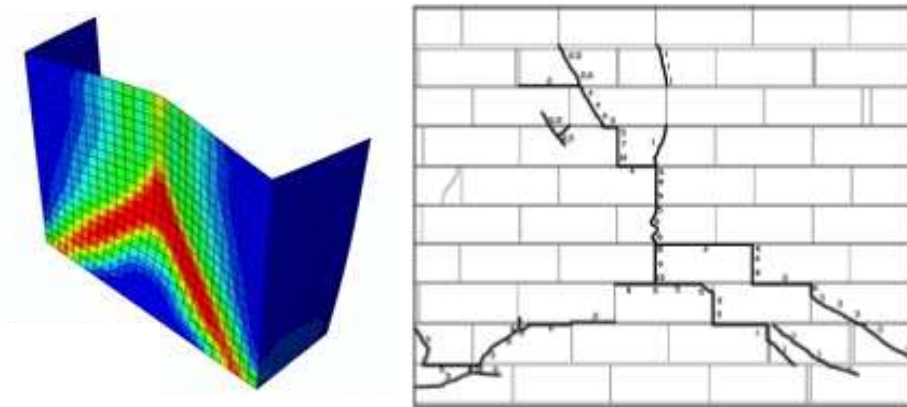


FIGURE 4. 12 – Masonry wall damage: experimental *versus* model

4.2 Building System Level Model Validation

To validate the model of the wood frame residence as a complete system, the model was subject to the earthquake excitation used in CUREE Publication No. W-12 (Isoda et al. (2002)). The fundamental frequency of the model and the earthquake response were compared to the results of Isoda et al. (2002). Because the model was built according to the CUREE-Caltech layout and specifications the results should be comparable to those shown in Isoda et al. (2002). The validation of the building system is described in this section.

4.2.1 Fundamental Frequency Validation (f)

The fundamental frequency (f) of the building system model was calculated in two different ways. The first method determined f using the stiffness from a static lateral pushover test. The second method was an ABAQUS frequency analysis. For both methods, the fasteners are modeled as beam elements because a frequency value associated with the initial stiffness of the building (prior to onset of fastener failure and associated nonlinearities, which are modeled by the springs) is desired.

The fundamental frequency of the building structure is determined using the basic structural vibrations formula:

$$f = \frac{1}{2\pi} * \sqrt{\frac{K}{M}}; \text{ Fundamental Frequency (Hz)} \quad (4.2)$$

where K is the lateral stiffness (kips/ft) and M is the mass (kslugs) of the structure. In order to simplify the analysis, the house was idealized as a 1-DOF system. Twenty-one individual point loads of 1 kip each were spaced evenly (one at the location of each rafter) along the top sill plate on the long side of the building (consistent with the direction of ground motion used in Isoda et

al (2002). The attachment of the building to the foundation was assumed to be rigid, and a static analysis was performed using ABAQUS. The simple diagram shown in Figure 4.13 illustrates the setup.

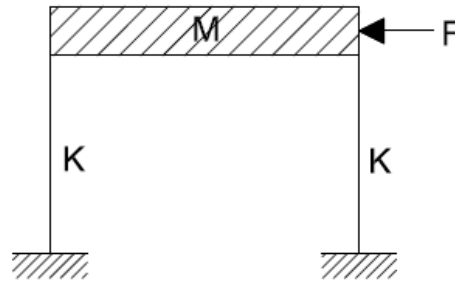


FIGURE 4. 13 – Fundamental period calculation: simplified setup

The total stiffness of the system was calculated by taking the average of the displacements at the far end, middle, and near end of the house and dividing the total load (21 kips) by the average displacement. The mass of the model was taken as the total mass minus the floor mass. Note that the mass of non-structural components such as the roof shingles, ceiling insulation, and re-roof are lumped into the mass of the plywood roof sheathing for the dynamic analysis. The mass of the structural model considered for the frequency analysis is 1,211 slugs while the CUREE specified mass (minus the floor) is 1,160 slugs (within about 5% of each other).

The entire floor diaphragm is assumed to be rigid. This assumption is enforced by applying a fixed boundary condition to the floor from the joists up to the base stud sills (for the earthquake excitation, acceleration time history is applied to the entire floor diaphragm, rather than just its base). This assumption is supported by Isoda et al. (2002) which states that of 16 different floor diaphragm configurations tested, only 2 did not qualify as “rigid” according to the 1997 Uniform

Building Code (UBC) method of classification. Both diaphragms that were not considered rigid lacked blocking and subfloor adhesive, and the model building does not.

Using the stiffness and mass values, and the boundary conditions discussed above, the fundamental frequency of the structure was found to be about 6.4 Hz from the pushover analysis. The ABAQUS frequency analysis returned a large number of modes, so the value chosen is the value associated with the fundamental mode as determined by the mass participation. The fundamental mode from the ABAQUS frequency analysis was 6.2 Hz. As anticipated, the primary mode is a racking mode with a shape similar to the deformed shape observed in the pushover analysis.

The Caltech-CUREE wood frame project provided a regression analysis for fundamental period, T , based on earthquake building response data using building height as the only independent variable. From CUREE Publication No. W-11 (Camelo et al. (2002)), equation 19, the best-fit curve for the data set gives the median T value for a given building height to be:

$$T = 0.032h^{0.55} \quad (4.3)$$

Using this equation, we calculate a theoretical $T = 0.131$ s ($f = 7.62$ Hz), given a building height of about 13 ft, close to the values obtained from the static pushover and the ABAQUS frequency analysis. More importantly, Isoda et al. (2002) provides the fundamental frequencies of the CUREE-Caltech Small-Index Building for the three different levels of construction quality used in that study as: *Poor Quality* – 5.58 cps; *Typical Quality* – 6.13 cps; *Superior Quality* – 10.5 cps. So our ABAQUS model appears to be closest to the CUREE-Caltech typical construction quality level (CQL) based on the frequency analysis. Note that the CQLs used in the CUREE-Caltech wood frame project are not to be confused with the CQLs used in this study.

The modified versions of the poor and typical quality CUREE-Caltech CQLs are being used for comparison and validation. This is because the modified versions feature braced cripple walls while the original versions have unbraced cripple walls. Because the ABAQUS model does not include a cripple wall, the modified versions are a better comparison. The superior CQL was not modified because it does not have a cripple wall.

4.2.2 Earthquake Response Validation

The second level of validation for the building system model is the earthquake response and its comparison with the CUREE-Caltech model values shown in Isoda et al. (2002). The building system ABAQUS model was subjected to the ground motion acceleration record from the 1994 Northridge Earthquake at the Canoga Park station, scaled to a peak ground acceleration (PGA) of 0.3g. The acceleration-time history is shown in Figure 4.14:

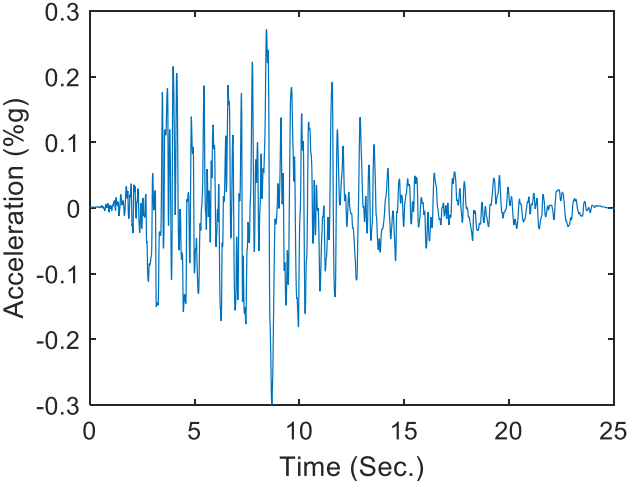


FIGURE 4. 14 – 1994 Northridge Earthquake – Canoga Park station ground motion acceleration scaled to PGA 0.3g

The same assumptions regarding the boundary conditions and masses made for the frequency analysis were applied to the model. The acceleration record shown in Figure 4.14 was applied to the rigid floor system normal to the long dimension of the building in the form of an acceleration boundary condition. The rigid floor system was fixed in all other degrees of freedom so that the floor and ground motion are the same (i.e. the floor is rigid and moves directly with the ground with negligible local deformations within the floor diaphragm). Although the acceleration record is available through 25 seconds, the analysis was cut to 10 seconds due to the large computational and time costs associated with the implicit numerical scheme employed by ABAQUS to solve this dynamic problem. The peak excitation occurs prior to the 10 second mark, at approximately 8.7 seconds, so it is assumed that the peak response occurs prior to 10 seconds and it is suitable to use the abridged record for the purpose of model validation. Consistent with the CUREE-Caltech model, 1% Rayleigh damping was assumed. The Rayleigh damping coefficients were estimated from the procedure outlined by Chowdhury and Dasgupta (2008) for structures with a large number of modes. The modes and associated circular natural frequencies (ω) were taken from the ABAQUS frequency analysis. The damping parameters were calculated to be:

$$\alpha = 0.24133; \beta = 0.00035$$

where α is the mass matrix coefficient and β is the stiffness matrix coefficient.

In accordance with Isoda et al. (2002), the displacement was measured at the base and at a centrally located node along the top stud-sill of the building. The base node selection is arbitrary because the base displacement is uniform. The top displacement is taken at the location shown in Figure 4.15.

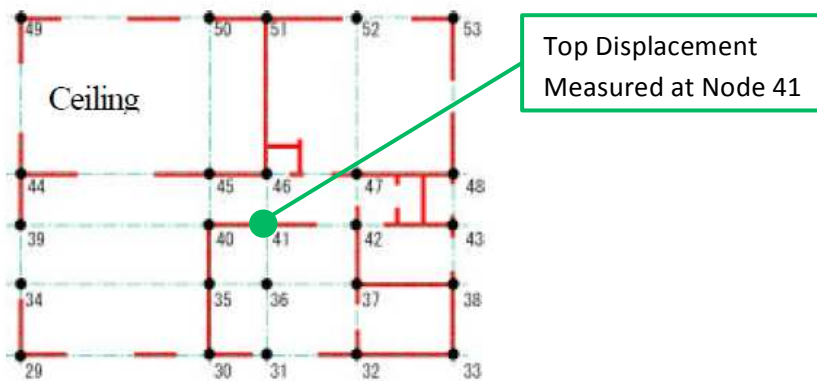


FIGURE 4. 15 – Earthquake response ceiling level drift measurement node (from Isoda et al. (2002), Fig. 3.2)

The base displacements are subtracted from the top displacements to get the drift-time history for the ABAQUS model subject to earthquake excitation.

The drift-time history for the ABAQUS model is plotted against the drift-time histories of the poor and typical CUREE-Caltech CQLs in Figures 4.16 and 4.17 below. The superior CQL is not shown here because the drift was virtually non-existent. Moreover, the frequency of the ABAQUS model (presented in the previous section) is closest to the typical CQL.

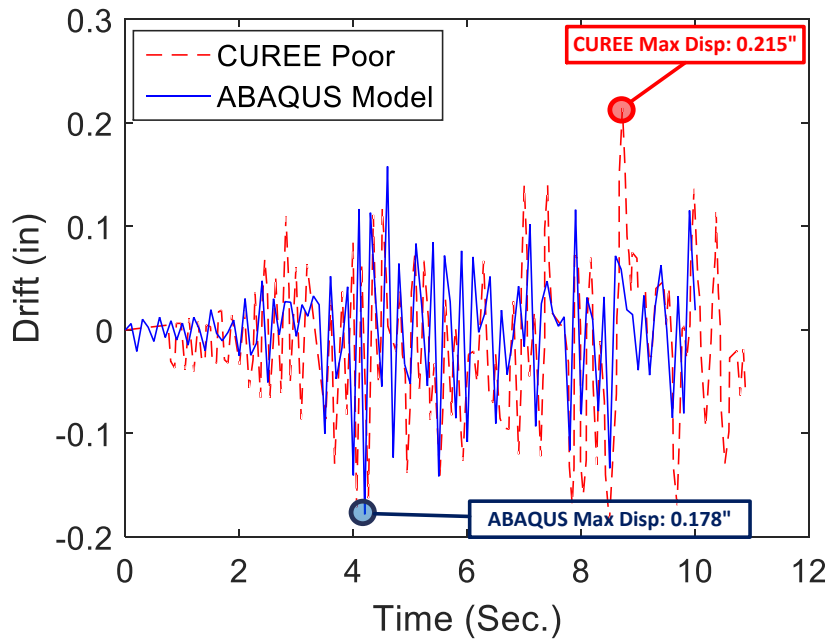


FIGURE 4. 16 – Drift-time history: ABAQUS model *versus* CUREE-Caltech poor CQL

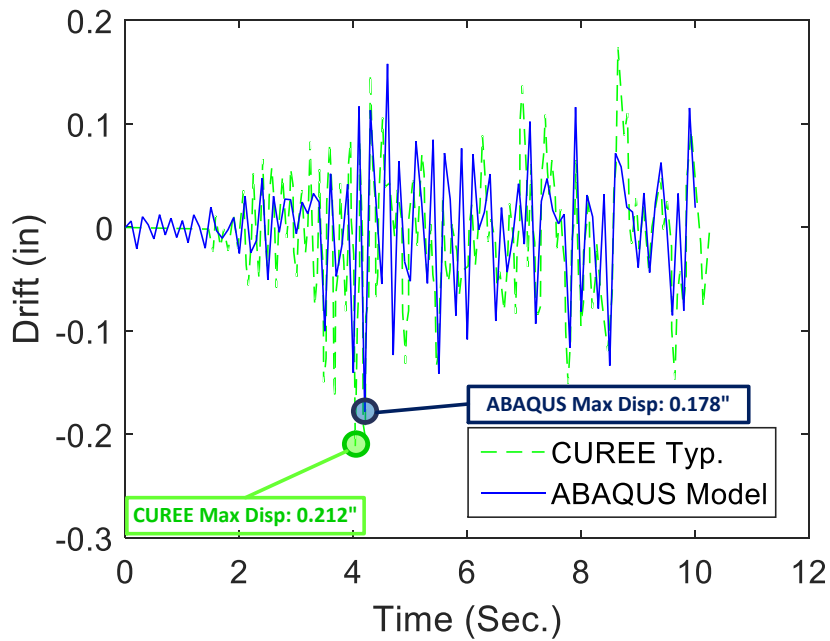


FIGURE 4. 17 – Drift-time history: ABAQUS model *versus* CUREE-Caltech typical CQL

Figures 4.16 and 4.17 show that the drift-time history for the ABAQUS model fits reasonably well with both the poor and typical CUREE-Caltech CQLs. The typical CQL appears to be the closer fit, which makes sense given that the fundamental frequencies of the two are so close (6.2 Hz and 6.13 Hz respectively). Considering the inherent differences between the two models used to predict the building response (simplified CUREE-Caltech and detailed ABAQUS) and the necessary assumptions made to fill in the gaps in the available CUREE-Caltech documentation (certain construction details, material parameters, etc.), the agreement is sufficient to consider the performance of the building as a complete system to be validated for the purposes of this investigation.

CHAPTER 5

BASIC QUALITY ARCHETYPE PERFORMANCE

5.1 Building Damage Quantification

In order to quantify the damage states for the building as a whole, and its individual components, total damage states 0-4 (None-Very Minor, Minor, Moderate, Severe, Destruction) were borrowed from the HAZUS hurricane module. This is because no similar, well established module is currently available for tornado damage at this point in time. Table 5.1 summarizes HAZUS hurricane damage states for residential construction.

TABLE 5. 1 – HAZUS hurricane module damage states (HAZUS Table 6-9)

Table 6-9. Damage States for Residential Construction Classes

Damage State	Qualitative Damage Description	Roof Cover Failure	Window Door Failures	Roof Deck	Missile Impacts on Walls	Roof Structure Failure	Wall Structure Failure
0	No Damage or Very Minor Damage Little or no visible damage from the outside. No broken windows, or failed roof deck. Minimal loss of roof over, with no or very limited water penetration.	≤2%	No	No	No	No	No
1	Minor Damage Maximum of one broken window, door or garage door. Moderate roof cover loss that can be covered to prevent additional water entering the building. Marks or dents on walls requiring painting or patching for repair.	>2% and ≤15%	One window, door, or garage door failure	No	<5 impacts	No	No
2	Moderate Damage Major roof cover damage, moderate window breakage. Minor roof sheathing failure. Some resulting damage to interior of building from water	>15% and ≤50%	> one and ≤ the larger of 20% & 3	1 to 3 panels	Typically 5 to 10 impacts	No	No
3	Severe Damage Major window damage or roof sheathing loss. Major roof cover loss. Extensive damage to interior from water.	>50%	> the larger of 20% & 3 and ≤50%	>3 and ≤25%	Typically 10 to 20 impacts	No	No
4	Destruction Complete roof failure and/or, failure of wall frame. Loss of more than 50% of roof sheathing.	Typically >50%	>50%	>25%	Typically >20 impacts	Yes	Yes

For the purposes of this study, these guidelines are used with some moderate modification to define component and building system damage states. The modifications to the HAZUS table and the justifications for them are listed below by damage state. These modifications are primarily related to the reduction in water damage anticipated during a tornado as opposed to a

hurricane. It is likely that heavy precipitation will accompany each type of storm but the duration of the precipitation associated with a tornado is likely to be on the order of minutes or hours, as opposed to days for a hurricane. The extended duration of precipitation during a hurricane is assumed to significantly increase the level of water damage associated with certain types of component damage, thus making such component damages less catastrophic in the case of a tornado. Future work should seek to gain a quantitative understanding of the anticipated differences in water damage caused by a tornado versus a hurricane but for now judgement was used to estimate the water related damage state severity reductions associated with a tornado.

5.1.1 Roof Cover Failure

It is assumed that significantly less water damage is sustained as a result of the loss of roof cover during a tornado than would be for a hurricane for the reasons discussed above regarding duration of precipitation. For this reason, the HAZUS table will be adjusted such that damage state (DS) 0 is now considered to be 0-15% loss, DS-1 is 15-50% loss, DS-2 is 50%+, and DS-3 and 4 cannot be sustained solely due to roof cover damage.

5.1.2 Window/Door Failures

Using the same rationale that was used for the roof cover failure damage state modifications, less water is expected to penetrate the building envelope during a tornado than a hurricane due to window and door breaches. Therefore, the HAZUS table will be modified such that DS-0 applies for no window or door failures, DS-1 applies for 1-3 (or 20% if $3 < 20\%$) failures, DS-2 applies for 3 (or 20%) to 50% failures, DS-3 applies for $\geq 50\%$ failures, and DS-4 cannot be sustained solely due to window/door failures.

5.1.3 Roof Deck Failure

Again, due to the reduction in the anticipated duration of precipitation, the HAZUS table will be modified as follows, DS-0 and DS-1 apply for no roof panel loss, DS-2 applies for 1 panel-25% panel loss, DS-3 applies for 25%-50% panel loss, and DS-4 applies for $\geq 50\%$ panel loss.

5.1.4 Missile Impact on Walls

For reasons discussed previously, relating to the complexity of modeling missile impact, this category is not considered in the damage state quantification for this study. Instead, the two cases considering missile impact and no missile impact are shown separately. This category is instead replaced by a category for wall exterior wall damage. Damage is quantified for each of the four sides of the building. DS-0 applies for damage to 1-2 sides, DS-1 applies for damage on 3-4 sides, and DS-3, DS-4 cannot be sustained solely due to wall damage.

5.1.5 Roof Structure Failure

Because this is a structural damage state, water damage is assumed to be a secondary concern. Therefore this category is not modified from the HAZUS table.

5.1.6 Wall Structure Failure

Again, because this is a structural damage state, water damage is a secondary concern. Therefore this category is not modified from the HAZUS table. This category is assumed to apply to the wall-foundation connection failure mode, not the wall collapse failure mode, as discussed in Chapter 2.

5.1.7 Building System Damage

The damage sustained by the entire building system is assumed to be defined by the worst component damage that the building has sustained. For example, if 75% of the roof shingles are missing and no roof panels are missing, the building system has sustained “moderate” damage but if 30% of the roof panels are missing and only 40% of the roof shingles are gone, the building system has sustained “extensive” damage.

The modified HAZUS damage states to be used for the purpose of quantifying component and building system damage in this study are shown in Table 5.2.

TABLE 5. 2 – Modified HAZUS hurricane module damage states

MODIFIED DAMAGE STATES							
Damage State	Damage Description	Roof Cover Failure	Window & Door Failures	Roof Deck	Exterior Wall Damage	Roof Structure	Wall Structure Failure
0	None to Very Minor	0-15% Shingle Failure	No Damage	No Roof Panel Loss	Cracking on 1-2 Sides	No Damage	No Damage
1 - Slight	Minor	15-50% Shingle Failure	1-3>20%	No Roof Panel Loss	Cracking on 3-4 Sides	No Damage	No Damage
2 - Moderate	Moderate	50%+ Shingle Failure	3≥20% - 50%	1 - 25% Panel Loss	-	No Damage	No Damage
3 - Extensive	Severe	-	≥50%	25% - 50% Panel Loss	-	No Damage	No Damage
4 - Complete	Destruction	-	-	≥50% Roof Panel Loss	-	Rafter-Sill Failure	Fndn. Connection Damage

The masonry basement wall will be analyzed separately from the rest of the building system because the hazard that causes damage to the basement (expansive soil) is different than the hazard that causes damage to the rest of the building system (tornado). Additionally, the performance of the basement is generally not expected to impact the performance of the rest of the building system, so the analysis has been uncoupled for the purpose of this study. Therefore, no considerations for basement wall damage are made in the evaluation of building system damage and the basement wall is not considered to be a part of the “building system”.

The addition of a basement to any of the 3 archetypes serves as an added life safety measure in the event of a tornado but will not be assumed to satisfy or improve the quality of the archetype. In other words, the enhanced quality target cannot be met simply by adding a basement. The home must be designed to satisfy life safety concerns on its own, above ground level. The analysis of the basement wall performance under expansive soil loads in this chapter is limited to performing an ABAQUS mean value analysis of the typical masonry basement wall under anticipated in-situ soil conditions for Norman, OK and then analyzing the likelihood of basement wall damage over a period of time. Considerations for potential basement wall improvements will be made in Chapter 6.

5.2 Building Quality Level Targets

The building performance targets for each construction quality level (CQL) were introduced in Chapter 3 but will be explored in greater detail in this section. The CQL performance targets were provided in the form of damage state fragilities by our research partners at the University of Oklahoma. The damage state fragilities plot the cumulative probability of damage for a given damage state against tornado wind speed, providing an understanding of how the likelihood of damage changes as the magnitude of a tornado increases.

The performance target fragilities are provided herein for comparison to the basic quality archetype fragilities that are calculated using the methods described later in this chapter. In Chapter 6, improvements necessary to meet the performance target fragilities will be discussed. The performance target fragilities for damage states slight, moderate, extensive, and complete for each CQL are shown in Figures 5.1 – 5.3.

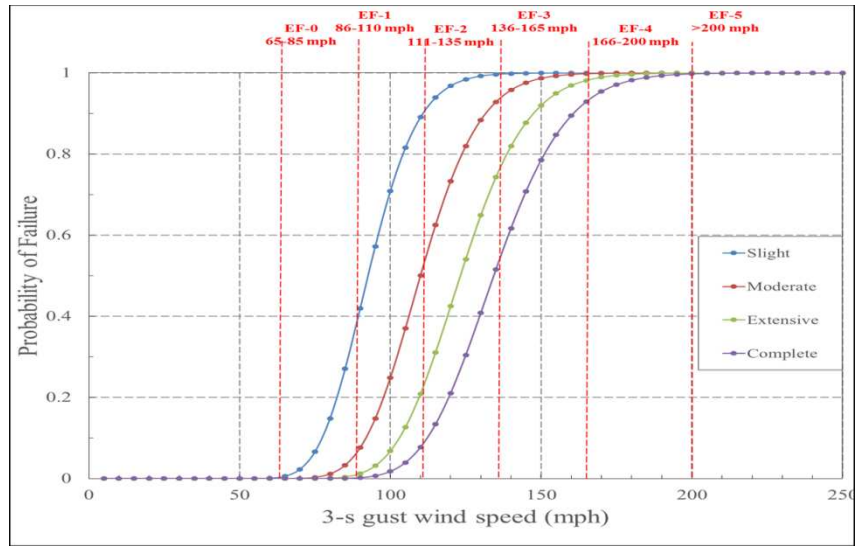


FIGURE 5. 1 - Construction Quality Level 1 (Enhanced) damage state target fragilities

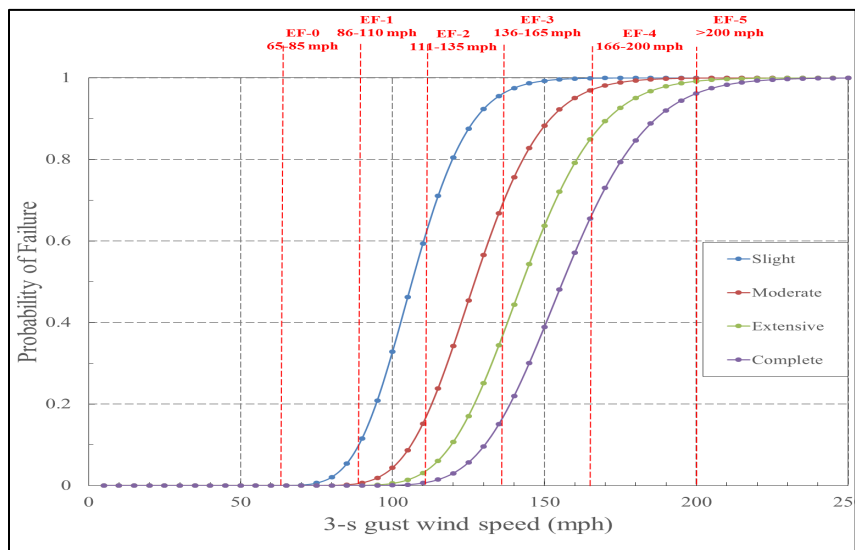


FIGURE 5. 2 – Construction Quality Level 2 (Improved) damage state fragilities

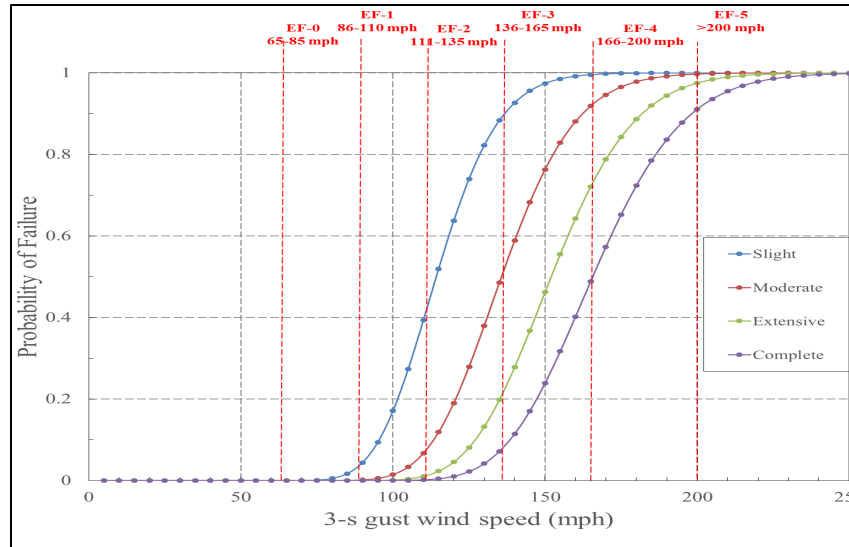


FIGURE 5.3 – Construction Quality Level 3 (Resistant) damage state fragilities

5.3 Building System Mean Value Analysis and Statistical Modeling – Component Level

This section details both the ABAQUS mean value analysis and MATLAB statistical analysis of the basic quality building archetype components. Although the ABAQUS mean value runs are performed on the building system as a whole, only the individual performance of the components that make up the system is analyzed in this section. In other words system level behavior is captured, but performance is quantified for each individual component. System level performance is quantified later on in this chapter.

Mean Value Analysis (Tornado Hazard): The mean value analysis for each building system model is performed by using the mean wind pressure loads or expansive soil loads, individual fastener resistances, and building material parameters found using the information in Chapter 2 as inputs. For the tornado hazard case, the wind speed is ramped up during the ABAQUS run. This allows for the analysis of each archetype model under average anticipated conditions at varying wind speeds; thus it allows the mean resistance of each critical component

and the demand on that component as a function of wind pressure to be determined for use in the MATLAB statistical models. The mean value analysis also allows for capturing the nonlinearity in component demand as the wind pressures on the building system change (i.e. when roof panels fail, load demand on the rafter-sill connections tributary to those panels is reduced). The ABAQUS mean value runs are generally performed assuming no building envelope breach although for some components it was necessary to consider different pressure cases.

Statistical Analysis (Tornado Hazard): The statistical analyses of component performance are done using Monte-Carlo methods in MATLAB to construct damage and failure fragilities dependent upon wind speed. To generate fragilities, 1000 iteration simulations are used. Each simulation ramps 3s gust wind speeds up in 5 mph intervals. For each component, random wind pressures are determined using the statistical information provided in Chapter 2. Random resistances and demands are found by using the mean resistances and demands determined based on the mean value ABAQUS simulations. For the resistances, the coefficients of variation and statistical distributions given for experimental component resistances in Table 2.5 are applied to the mean values determined by the ABAQUS mean value runs as described in Chapter 2. The variability in demand is accounted for by the wind pressure variability, as demand is a function of wind pressure. The MATLAB simulations account for the nonlinear component demand relationships that change as a function of wind pressure or other factors.

Because a breach of the building envelope affects virtually every component by increasing the internal pressure coefficient, envelope breach by roof panel failure or window/door pressure blowout is accounted for in the MATLAB models for each component by increasing the internal pressure coefficient for subsequent wind speeds after a breach is determined to occur. As discussed in Chapter 2, debris impact is not being accounted for statistically, so building

envelope breach by debris impact is considered as a separate case. Separate cases are also analyzed statistically for the “upper” and “lower” bounds of wind pressure. The upper bound case includes the Haan tornado amplification factor while the lower bound case does not. This means that a total of 4 statistical cases are analyzed; (1) upper bound, without debris breach, (2) upper bound, with debris breach, (3) lower bound, without debris breach, and (4) lower bound, with debris breach. Cases 2 and 4 will only be analyzed for archetype 1. The reason for this is described later in this section.

5.3.1 Roof Panel Failure

In this section, the ABAQUS mean value analysis and MATLAB statistical analysis for roof panel failure in each basic quality archetype is discussed. For the roof panel failure, no “worst case” wind direction scenario needs to be considered because the C&C pressures from ASCE 7-10 are used and these do not vary by wind direction.

5.3.1.1 Archetype 1, Basic Quality (A1-BQ)

For A1-BQ, the first panel observed to fail during the ABAQUS mean value analysis (assuming no prior envelope breach) is located along the edge of the roof in pressure zone 2. This failure occurs at a wind speed of approximately 85 mph (corresponding to an EF-1 tornado). Note that per ASCE 7-10, the zone 3 pressures located in the corners of the roof would usually be the highest pressures but for the hip roof considered in this archetype, the pressures in zones 2 and 3 are equal.

Roof sheathing failure is considered to occur upon failure of the first nail in the sheathing panel, as discussed in Chapter 4. The first nail is considered to fail when it reaches a withdrawal displacement of approximately 0.75”. The ABAQUS static analysis runs terminated when nail

spring axial displacements reached $\approx 0.65''$. This is a limitation of the model. At this level of nail axial displacement, the slope of the nail load-displacement curves becomes negative and any further increase in load causes the panel's pressure-displacement curve to plateau, signifying that any further pressure increase or even continued application of the current pressure will lead to failure. Figure 5.4 illustrates this behavior for the first panel to fail.

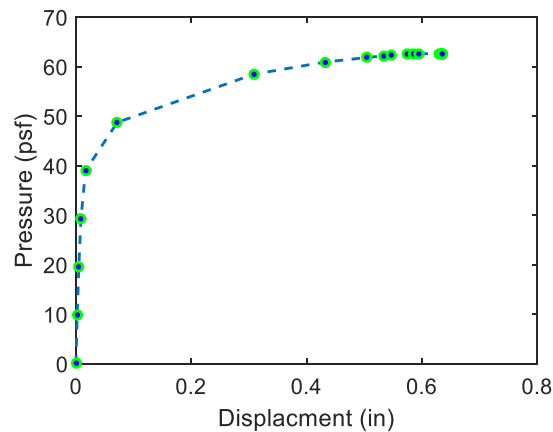


FIGURE 5. 4 – Pressure *versus* displacement A1-BQ initial roof panel failure

Panels near the perimeter of the roof are located in multiple pressure zones. Therefore, in order to determine the “equivalent” pressure on these panels, the weighted average method was used in accordance with Lee and Rosowsky (2005). For A1-BQ, the first panels fail at a mean equivalent pressure of 63 psf, which is consistent with the 61 psf observed in the Mizzell (1994) experimental data for the SPF rafters used in this archetype. Other panels were analyzed to determine if a significant variation of panel resistances exists based on panel location and fixity (i.e. the nailing is slightly different for panels located tributary to a ridge) but it was determined that this is not the case.

Only half of the panels are considered in the construction of the roof panel fragilities for panel failure. It was found that half of the roof is a sufficient representative sample for the entire roof (i.e. the probability that 10% of the panels on a single half fail is approximately equal to the probability that 10% of the panels on the whole roof fail). Therefore, to save computational effort, the second half was not included in the MATLAB simulations. The panels included in the analysis are shown shaded in Figure 5.5 below. The first panel to fail is highlighted in the figure as well.

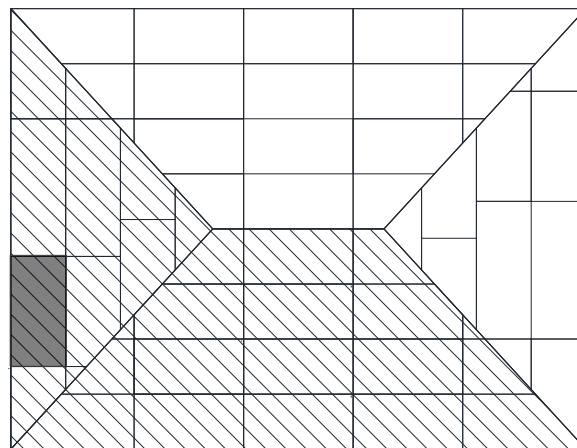


FIGURE 5. 5 – A1-BQ roof panels considered in statistical analysis and first roof panel to fail

5.3.1.2 Archetype 2, Basic Quality (A2-BQ)

As expected, the ABAQUS analysis revealed that the typical roof panel for A2-BQ fails at an equivalent panel pressure of approximately 60 psf, so the same mean roof panel resistance value (63 psf) that was used for A1-BQ will be used for A2-BQ. The first panels to fail during the ABAQUS mean value analysis for this archetype were located at the edges of the roof ridge, primarily in C&C zones 2 and 3 (see Figure 5.6) but with a small portion of the panel located in

zone 1. These panels are the logical “first-failure” panels due to their location and the amount of zone 2 and 3 area that they occupy. The panels are estimated to fail at approximately 85 mph (corresponding to an EF-1 tornado).

As discussed under A1-BQ above, modeling the roof panels on one side of the building is a sufficient to represent the entire roof. Therefore only half of the panels are considered in the MATLAB simulations. The panels considered are shown shaded in Figure 5.6 with the first panels to fail highlighted as well.

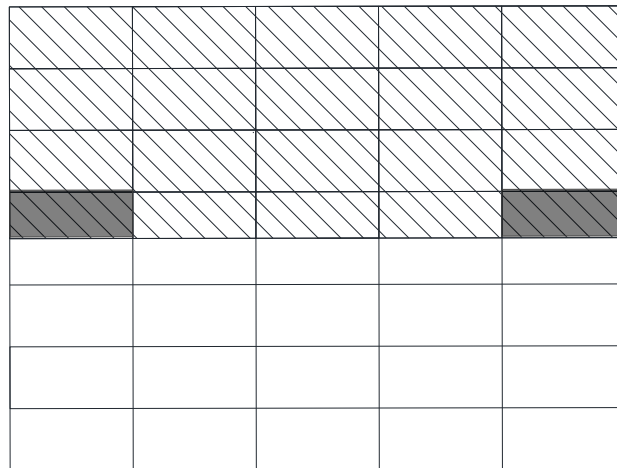


FIGURE 5. 6 – A2-BQ roof panels considered in statistical analysis and first roof panels to fail

5.3.1.3 Archetype 3, Basic Quality (A3-BQ)

The A3-BQ roof consists of two staggered sections that are each identical to the A1-BQ roof layout. The roof layout is pictured in Figure 5.7.

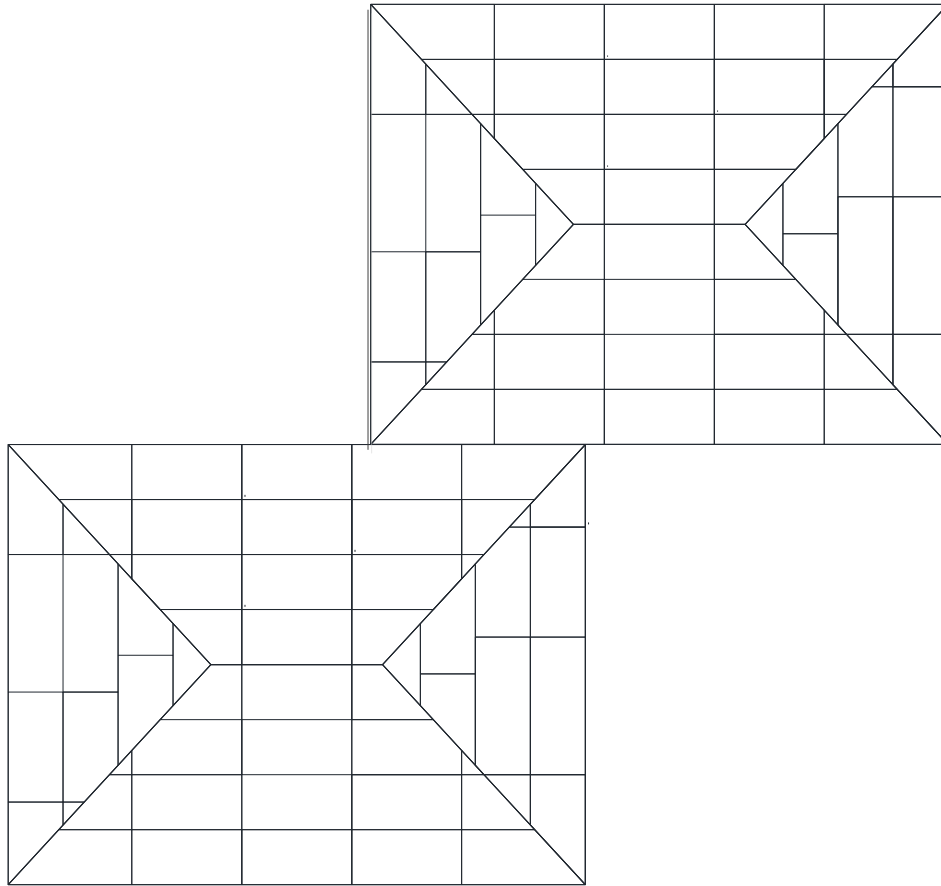


FIGURE 5. 7 – A3-BQ roof panel layout

In reality, there would likely be some unique wind pressures in the center area between the two roof sections, but the roof pressure zones for both the MWFRS and C&C for A3-BQ are assumed to remain the same as for A1-BQ because without a wind tunnel study there is no way to determine what these unique pressures would be. Additionally, because the 27 roof panels considered in the A1-BQ Monte-Carlo simulation were shown to be a representative sample for the entire roof, this assumption should hold true for A3-BQ because the roof and wind pressure zone proportions are the same and we have simply doubled the roof area. Essentially the roof has

been scaled up in size, but not fundamentally changed. Therefore, there is no need to re-evaluate roof panel failure for A3-BQ and the analysis for A1-BQ is considered sufficient to quantify panel failure for both of these archetypes. Therefore, the A1-BQ value of 63 psf is considered to be the mean panel resistance for A3-BQ as well.

5.3.2 Rafter to Top Stud-Sill Connection Failure

The rafter to top-sill (R-TS) connection failure under basic quality conditions (3-16d pneumatically driven toe-nails) is assumed to occur when any of the three nails in the connection reach a nail pull-out deflection of about 0.5” per NAHB (2002). The ABAQUS model indicates the other two nails in the connection withdraw 0.5” very shortly after the initial nail, providing additional justification for this metric. The R-TS connection resistances and demands determined by the mean value analysis for each archetype are discussed below. The “worst-case” wind direction was determined by subjecting each structure to wind coming from the four primary directions specified by the directional procedure in ASCE 7-10. The wind speeds that caused the most damage defined the “worst-case” wind direction. Based on this, the worst case was determined to occur when the wind force is perpendicular to the long side opposite the large sliding glass door. Figure 5.8 illustrates the findings of the worst case wind direction analysis.

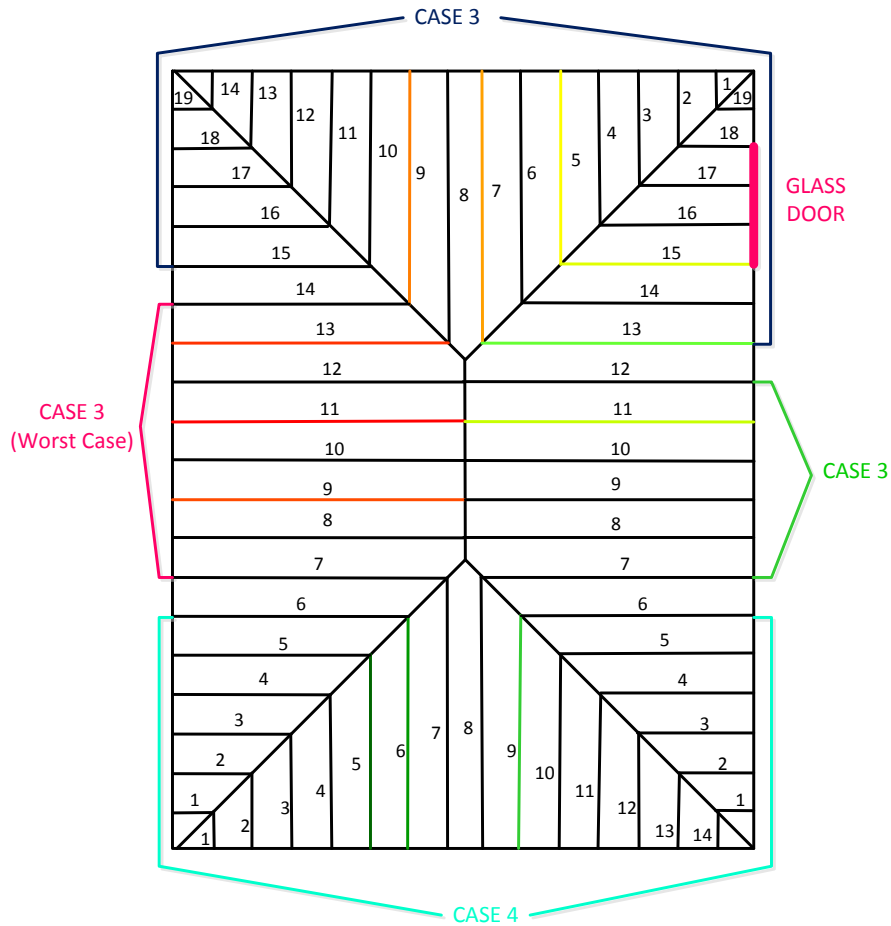


FIGURE 5. 8 – Rafter-Sill connection, worst case wind direction

The color gradation from red to green represents the sequence of failure with red signifying the earliest failure and green signifying the last. For clarity, only the first three rafter failures for each wind direction case are shown. Cases 1-4 are shown with their labels on the windward side of the building under each case. As can be seen, the first three failures occur under Case 2 conditions, with the wind normal to the long side of the building opposite the large sliding glass door, so this will be considered the “worst-case” scenario for rafter-sill connection failure. Although it may seem unnecessary to display any case other than Case 2, the purpose of Figure 5.8 is to display the relative severity of each wind direction case.

5.3.2.1 Archetype 1, Basic Quality (A1-BQ)

For A1-BQ, under mean conditions the first rafter failure occurs along the windward side near the center of the building, as shown in Figure 5.8, reflecting the fact that the eave region on the windward side of the building is subject to larger suction pressures and the rafters in the center of the roof have the largest tributary area. The failure occurs at a wind speed of about 110 mph, which is in the EF-1 tornado range. Considerations are also made below in this section to account for the effect of the loss of sheathing panels tributary to a rafter. This effect is two-fold, as it results in a load reduction due to the loss of pressure bearing area but also a separate load increase after the loss of the first roof panel due to the internal pressure spike associated with breach of the building envelope.

To perform the Monte-Carlo statistical analysis for the R-TS connections, it is necessary to convert the statistically determined wind pressure into a force that is applied to the rafter to sill connection. The nonlinear behavior of the fasteners and the configuration of the hip roof make this difficult to do without the aid of a program such as ABAQUS. Therefore, the ABAQUS model was used to determine the relationships between wind pressure and load demand on the R-TS connections. First, reaction forces were taken for the rafter-sill connection. Next, the overall tributary pressure uplift load on the rafter was determined using the known input pressure and the tributary area of each rafter and subtracting the mean dead load. Finally, the load on the connection was taken as a percentage of the total load on the rafter at each time step as the load was ramped up. It was found that the percentage of load acting on the connection was, in most of the “mean value” cases, around 40%-50% of the total load tributary to the rafter (this varies based on the rafter location and time step). The load of interest, however is the load at the time of rafter failure. This percentage can be applied as a “factor” to the tributary rafter load calculated

randomly in the statistical analysis; thus by multiplying the random pressure by the rafter's tributary area and this factor (L_p), an equivalent random load demand can be determined for the rafter-sill connection. The factor L_p also changes as the ratio between the windward and leeward pressures on the roof changes. To account for this, the minimum and maximum pressure ratios (P_w/L_w) were determined from by Monte-Carlo simulation (100,000 samples). The maximum and minimum values were observed to be approximately 2.5 and 0.5 respectively. Then, ABAQUS simulations were performed at intermediate pressure ratios by leaving the windward pressure as the mean value and calculating the leeward pressure at intermediate points (7 in all) between the maximum and minimum ratios. The respective values of L_p were determined for each ratio. The values of L_p were then plotted against the P_w/L_w ratio and fit with a polynomial equation to yield a numerical relationship between P_w/L_w and L_p . This accounts for the variability in the random wind pressures in the determination of L_p and thus the rafter-sill connection resistance. The conversion from random wind pressure to equivalent connection force and the L_p versus P_w/L_w plots for the five most critical rafters on the "worst-case" pressure side of the roof are shown in Figure 5.9 and equation 5.1 respectively.

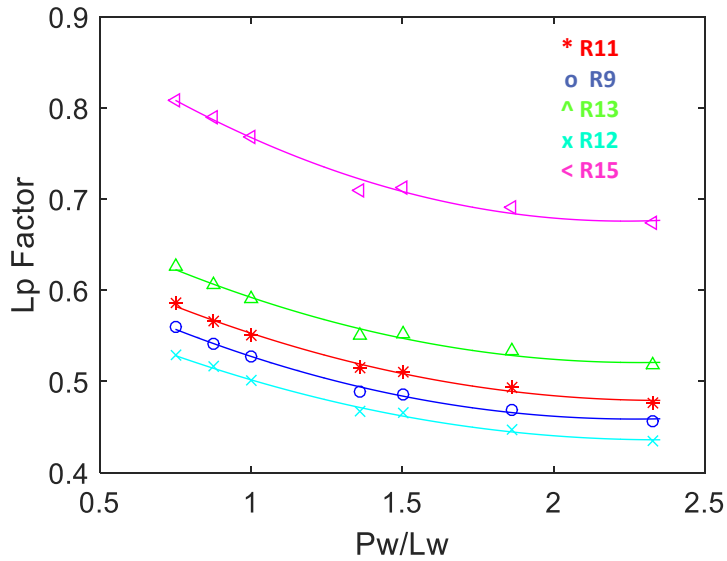


FIGURE 5.9 – A1-BQ L_p versus P_w/P_l for the five most critical rafters

$$L_r = [\cos(14)P_r A_T - D]L_p \quad (5.1)$$

where L_r is random connection load, P_r is random wind pressure, A_t is tributary area, D is random dead load, and L_p is the load percentage factor discussed above. P_r is multiplied by the cosine of the roof slope (14 degrees) to “normalize” the pressure into a pure uplift pressure.

After the failure of the first rafter, the other rafters in the same roof zone will fail quickly due to the redistribution of loads between rafters which support common sheathing panels (similar to the way a roof sheathing panel fails after the loss of the first nail). This assumption is supported by a simplified ABAQUS analysis, in which rafters were removed after they reached failure load to determine how the load redistribution affects the remaining rafters. This analysis revealed that the remaining rafters could not support a load equivalent to that required to fail the first rafter, let alone any increase in the load, this is illustrated in Figure 5.10. Thus, it will be assumed that

failure of the first rafter is tantamount to failure of an entire roof section and that failure of an entire roof section will lead to failure of the roof system.

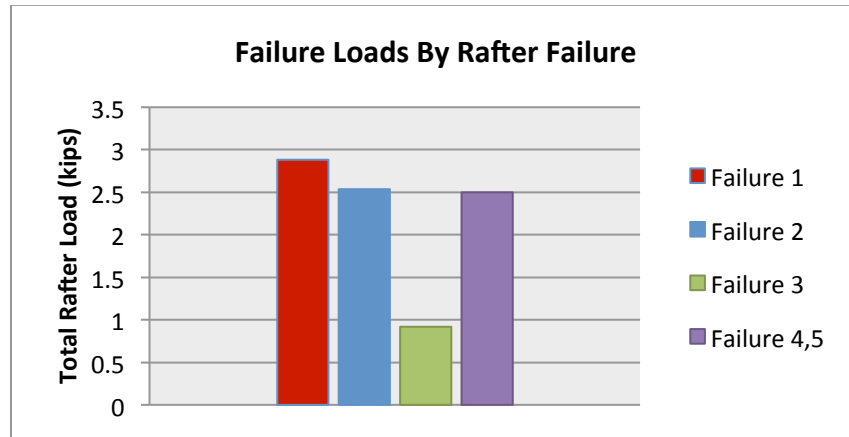


FIGURE 5. 10 – Single rafter failure load redistribution analysis

Only the five most critical rafters are considered in the statistical analysis. Considering all of the rafters complicates the analysis significantly because each rafter has a different L_p value which needs to be evaluated at different values of P_w/P_l . In order to simplify and expedite the analysis, we only wish to consider a limited number of rafters from the mean value analysis but to do this, it is necessary to show that neglecting the probability of other rafters failing first does not significantly impact the overall probability of roof failure. In order to demonstrate this, the preliminary fragility for rafter failure considering only the five most critical rafters as potential “first-failure” rafters is shown in comparison with the fragility for rafter failure considering the first, first three, and first eight most critical rafters. Observe that the differences between the fragilities for the 1-3 most critical and the 3-5 most critical are much more significant than the difference between the 5-8 most critical. Additionally, the magnitude of the difference shrinks considerably between each of these fragilities. The other rafters have increasingly smaller probabilities of failure, so it is assumed that no significant shift will be observed if they are

included in the analysis because no major shift is seen between the 5-8 most critical rafter fragilities, and because the difference will continue to shrink as rafters with smaller individual failure probabilities are considered. Note that the fragilities shown in Figure 5.11 do not make allowance for panel failure.

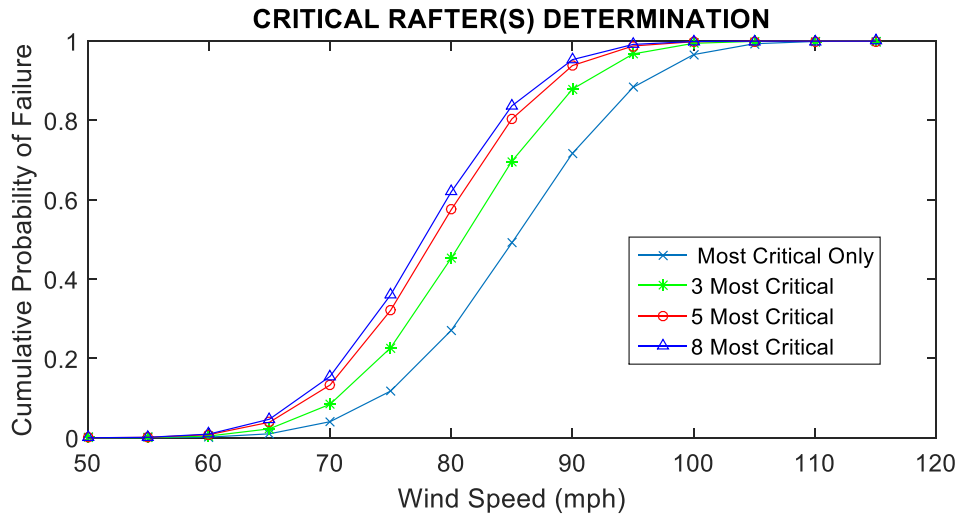


FIGURE 5. 11 – A1-BQ rafter-sill connection critical rafter determination

To include the effect of panel failure on the likelihood of rafter failure in the Monte-Carlo analyses we need to derive a relationship between missing panels and the R-TS connection load demand. It is assumed that the loss of panels reduces the demand on a rafter by reducing the rafter’s tributary area subject to suction pressure, thereby decreasing the likelihood of rafter failure as additional panels fail. Table 5.3 summarizes the decrease in the L_p factor that results from the loss of a given panel, or multiple panels that are tributary to one of the critical rafters. These decreases are determined from ABAQUS mean value analyses with the pressure removed from the respective panels. Initially, the effect of losing panels that are adjacent to a given rafter, but not directly tributary to it were also included but the reduction in demand on the rafter

connections associated with the loss of these panels did not have a significant effect on the rafter failure fragilities. It is assumed that once a rafter has lost all of the panels connected to it, its probability of failure is zero at subsequent wind speeds.

A trend was observed in the L_p reductions taken from the ABAQUS mean value analyses that allows us to “weight” the effect of the loss of certain panels (i.e. the loss of the bottom panels cause significantly higher load reductions than the loss of the upper panels). Assigning these weights allows for the use of equations to quantify the effect of losing multiple panels. These equations (eq. 5.2, 5.3) and Table 5.3, summarizing these weights and the resulting L_p reduction factors, F_p , are shown below. F_p is a percentage of the original L_p value.

TABLE 5. 3 – A1-BQ F_p factors

Critical Roof Section 1, Rafters 9, 11, & 12								
Panel	Area	% Area	Wt.	Eqn. Reduction	Equation F_p	ABAQUS F_p		
-	sf	%	-	-	Raft 9, 11	Raft. 9	Raft. 11	Raft. 12
Top	32	26%	0.19	0.05	0.95	0.95	0.95	0.95
Bot	26.67	22%	0.83	0.18	0.82	0.82	0.83	0.91
Top-1	32	26%	0.31	0.08	0.92	0.92	0.92	0.93
Bot+1	32	26%	0.58	0.15	0.85	0.86	0.86	0.91
Critical Roof Section 2, Rafters 12, 13, & 15								
Panel	Area	% Area	Wt.	Eqn. Reduction	Equation F_p	ABAQUS F_p		
-	sf	%	-	-	-	Raft. 13	Raft. 15	Raft. 12
Top	11.88	12%	0.08	0.01	0.99	0.99	0.99	0.99
Bot	26.67	27%	0.73	0.20	0.80	0.83	0.80	0.90
Top-1	27.12	28%	0.25	0.07	0.93	0.93	0.93	0.94
Bot+1	32	33%	0.43	0.14	0.86	0.86	0.87	0.91

$$F_p = [1 - (W_{p1} * A_{p1} + W_{p2} * A_{p2} + W_{p3} * A_{p3})]; \quad \mathbf{F_p Rafters 9, 11, 13, 15} \quad (5.2)$$

$$F_p = [1 - [(1 - F_{pr1} * F_{pr2} * F_{pr3}) + (1 - F_{pl1} * F_{pl2} * F_{pl3})]]; \quad \mathbf{F_p Rafter 12} \quad (5.3)$$

where W_{pi} is the weight for a given panel, and A_{pi} is the percentage of the total panel area that is tributary to a given rafter. For rafters 9, 11, 13, and 15, the first equation applies using the

weights and percent areas from the tables above. Because rafters 9 and 11 share tributary panels, their weights and percent areas, and thus their resulting F_p values are the same for a given panel loss pattern. This is also true for rafters 13 and 15. As shown above, the equation F_p values are approximately equal to the ABAQUS values. The small difference has virtually no effect on the rafter failure fragilities. Rafter 12 is located at the transition between panels, so it has twice as many tributary panels but the effect of losing each panel is less. The ABAQUS analyses showed a different relationship between panel loss and F_p for rafter 12. This relationship is represented by the second equation shown above. The F_{pri} values in this equation are the ABAQUS values shown in the first table above, associated with losing panels on the right (rafter 9/11) side of rafter 12. The F_{pli} values are the ABAQUS values shown in the second table and are associated with losing panels on the left (rafter 13, 15) side of rafter 12.

The results of the equation are verified by ABAQUS analysis for multiple panel failures (2 and 3 panel failures) as a check and the equation is then used to determine the total reduction in a MATLAB Monte-Carlo simulation which first randomly determines panel failures at a given wind speed and then determines rafter failures using the associated L_p reductions based on the panel failure analysis.

It was noted that a considerable number of nails connecting the upper and lower top stud sill plates along the main partition wall withdraw prior to and during rafter failure. However, the sill plates never appear to fully separate, as nails on either end remain embedded. Furthermore, the flexural stresses in the upper top sill plate do not approach the modulus of rupture of the SPF dimension lumber used for the basic quality archetypes. Based on these observations, the sill plates are likely to remain intact. Improving the connection between these sills (single 16d spaced at 24" on center), may improve the rafter connection's strength, presumably because it

allows the truss member that is fixed to the main partition stud sill plate to carry a larger portion of the wind pressure and the rafter connection failure reflects this behavior. For this reason, sill plate separation is assumed to be included in rafter-to-sill connection failure which is considered the primary measure of major roof damage in this study.

5.3.2.2 Archetype 2, Basic Quality (A2-BQ)

The same failure/damage criteria described above is used in this section and the same methodology is used to determine the L_p and F_p factors for A2-BQ. Assuming the same “worst-case” wind direction as for A1-BQ, the first failure rafters for A2-BQ are the rafters located in the interior of the roof on the windward side. The first 8 rafter connection failures are shown in Figure 5.12 below with color gradation from red to green; red indicates the first failure and green indicates the last. The first to fail is rafter 8, while the eighth to fail is rafter 16. Rafters beyond the eighth failure are not shown because as for A1-BQ, only the first 5 rafters to fail contribute significantly to the cumulative probability of failure for the first rafter failure. This is also illustrated in Figure 5.12. The figure demonstrates that there is not a significant shift in the fragilities considering the 5 most critical rafters and the 7 most critical rafters and that the discrepancy between successive fragilities (i.e. between 5 and 7, or 7 and 9) will continue to shrink even more as additional rafters are considered. Each of the rafters that contribute significantly to the probability of failure of the first rafter to fail are nearly identical in that they share the same rafter tributary area, and connection details (i.e. no panel edge rafters and no rafters connected to roof joists) this is due to the symmetry of the gable roof layout and will make the calculation of L_p and F_p significantly easier as demonstrated in this section.

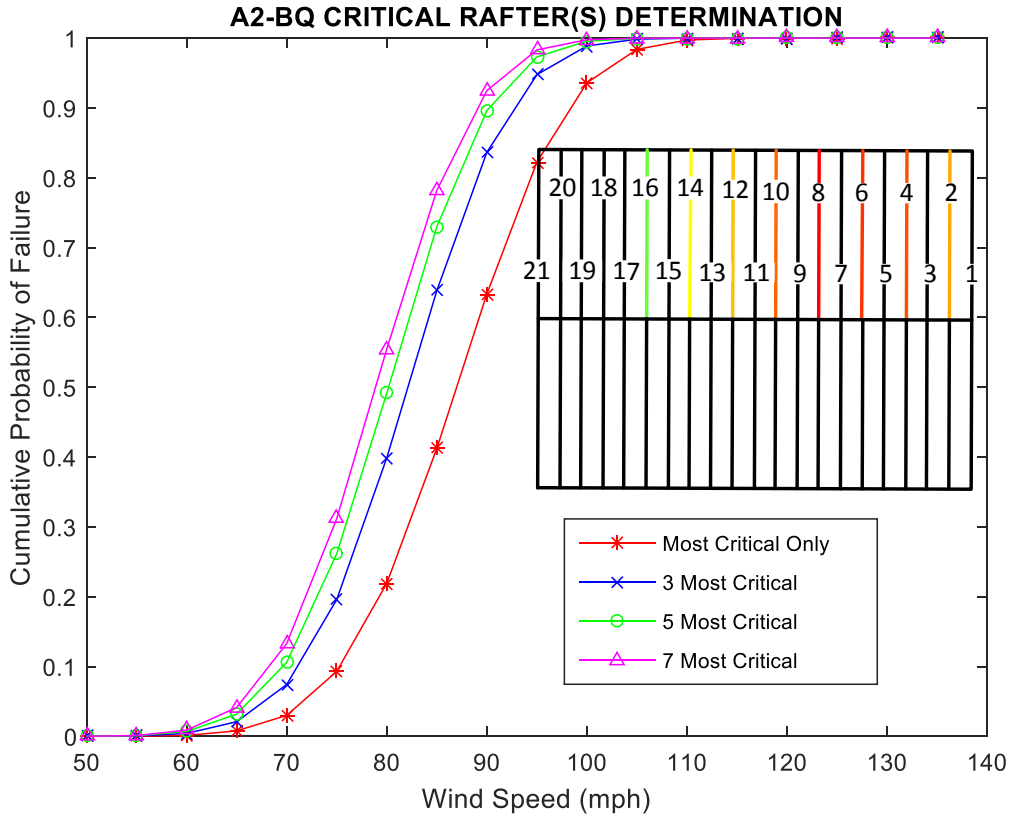


FIGURE 5. 12 – A2-BQ identification of critical rafters

The initial ABAQUS mean value analysis shows that the first rafter-sill connection occurs at a wind speed of approximately 99 mph (EF-1). The assumption made in case A1-BQ, that the failure of the first rafter connection will result in load redistribution and lead to failure of a larger section of the roof, is assumed to apply to A2-BQ as well.

To determine the L_p factor for A2-BQ, the same basic methodology was used as for A1-BQ. An ABAQUS mean value analysis was used to determine the reaction forces at each rafter-sill connection at failure and these reaction forces were then divided by the total force tributary to the corresponding rafter truss. This percentage of total tributary rafter truss load is called L_p and is used to convert the random wind pressures generated in the Monte-Carlo simulations to

random demands on the rafter-sill connections. The tributary area for the typical A2-BQ rafter truss is 2'x30', as the rafters are spaced at 2' with a total length of 30'.

Unlike the case for A1-BQ, where the roof geometry is more complex, L_p will be virtually the same for each rafter, with the exception of rafters on either end of the roof (edge rafters), due to the A2-BQ roof symmetry. This was confirmed by the ABAQUS analysis. The edge rafters do not significantly contribute to the first rafter failure probability, so they need not be considered. The mean value of L_p is equal to approximately 0.30 at failure for the critical rafters.

The variability in the ratio of the randomly generated windward and leeward roof pressures is also considered for A2-BQ. The likely extreme values of P_w/P_l range from 2.5 to 0.75 with a mean value of 1.57. ABAQUS runs were performed at intermediate ratios in this range to determine the effect on L_p . Runs were successfully completed between $P_w/P_l = 1.0$ and 2.5 (upper extreme) resulting in the following logarithmic best fit approximation for L_p as a function of P_w/P_l .

$$L_p = 0.0719 * \ln\left(\frac{P_w}{P_l}\right) + 0.2689 \quad (5.4)$$

The logarithmic fit is plotted against the L_p values extracted from the ABAQUS analysis at varying pressure ratios in Figure 5.13.

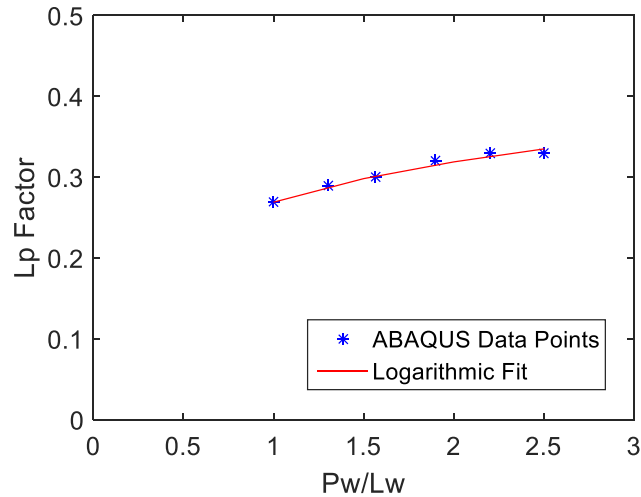


FIGURE 5.13 – A2-BQ L_p versus P_w/P_l five most critical rafters

Some difficulty was encountered in completing the ABAQUS runs through rafter-sill connection failure for pressure ratios less than 1.0 due to modeling limitations, but the ratio will only be less than 1.0 approximately 1.5% of the time so it is not likely to have a significant impact on the rafter-sill connection fragilities. Therefore, it will be assumed for this analysis that the relationship between L_p and P_w/P_l for pressure ratios between 2.5 and 1.0 holds for pressure ratios less than 1.0 as well. From here, equation 5.1 (shown in the previous section) can be used with the A2-BQ L_p value substituted in. It was observed that using the mean value of $L_p = 0.30$ for all pressure ratios makes virtually no difference in the fragility curves (as opposed to using the logarithmic fit as a function of pressure ratio), so the analysis was simplified by assuming a constant L_p value equal to 0.30. A comparison of fragilities using constant L_p versus the logarithmic fit is shown in Figure 5.14.

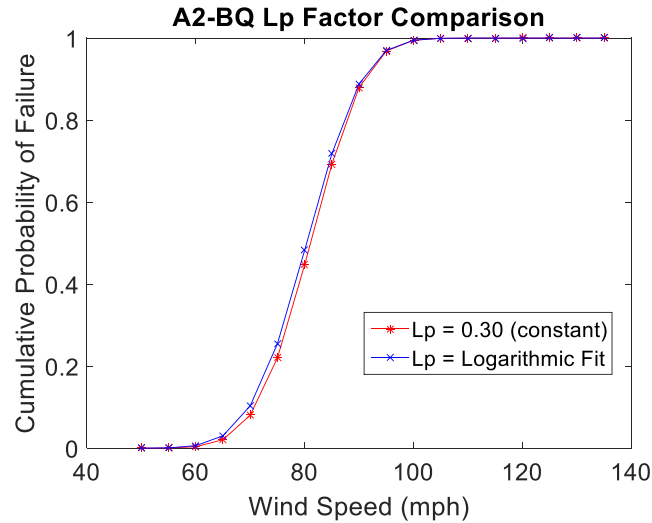


FIGURE 5. 14 – A2-BQ rafter-sill connection fragility: logarithmic fit L_p versus $L_p = 0.30$

The process for quantifying the load reductions on the rafter connections associated with roof panel failures tributary to a given rafter is the same as for A1-BQ. The L_p values were determined by ABAQUS analysis for different combinations of missing panels including scenarios with 1, 2, and 3 missing panels. The ratio of the L_p values to the original value (for no missing panels) is taken as F_p , the panel factor for each combination of missing panels. It was determined that once the individual panel weights were defined for A2-BQ using the ABAQUS analysis, equations 5.2 and 5.3, defined for A1-BQ, could also be applied for A2-BQ to define the panel factor, F_p . Equation 5.2 governs F_p for rafters directly connected to the failed panel and equation 5.3 governs F_p for the rafters which are directly adjacent to the failed panel, as illustrated in Figure 5.15.

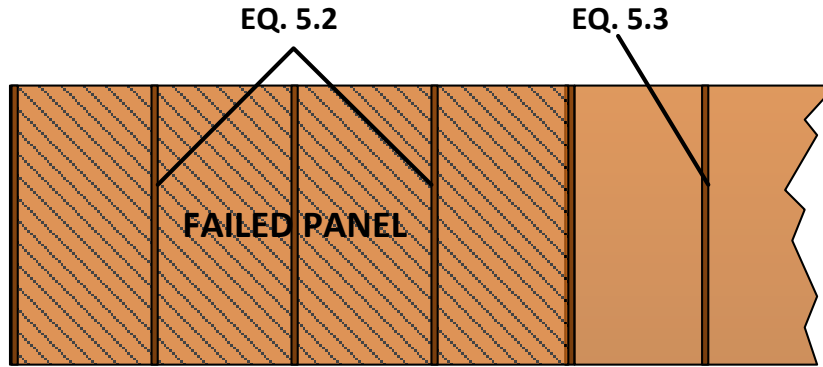


FIGURE 5. 15 – Governing equations for F_p for tributary panel loss or adjacent panel loss

Although equation 5.2 is suitable to quantify the F_p factor for rafters adjacent to a failed panel, it will not be used in the final MATLAB simulations because failed panels adjacent to a rafter have a negligible effect on the rafter-sill connection fragilities, as was the case for A1-BQ. Figure 5.16 shows the rafter-sill connection fragility with and without consideration for failed panels adjacent to a rafter. If all four panels tributary to a given rafter fail, we assume the probability of failure for that rafter becomes zero. Because in this case, none of the critical rafters are located at the intersection of two roof panels, it is not necessary to quantify F_p for such rafters. The Table 5.4 shows the parameters for the A2-BQ panel failure load reduction factor.

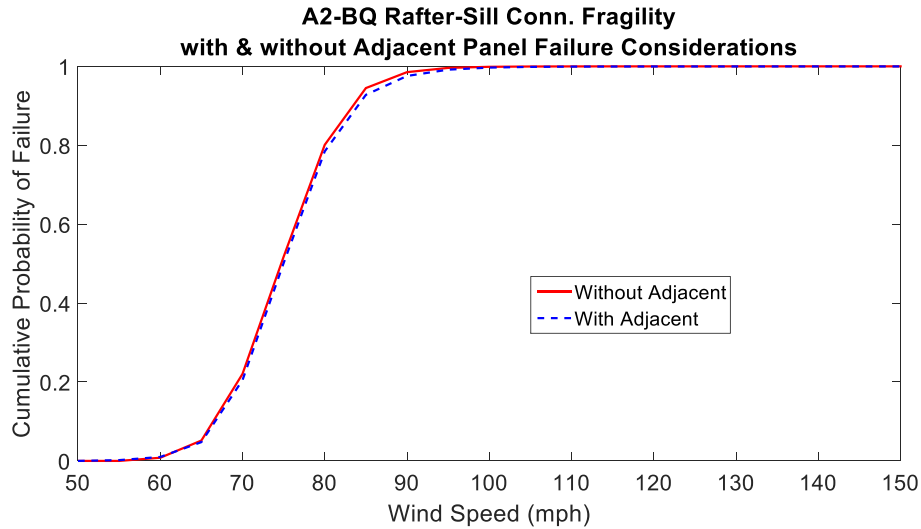


FIGURE 5. 16 – A2-BQ rafter-sill connection fragility: accounting for and not accounting for failure of adjacent roof panels

TABLE 5. 4 – A2-BQ F_p factors

Panel Reduction Factor Stats - Tributary Panels						
Panel	Area	% Area	Wt.	Eqn. Reduction	Equation F_p	ABAQUS F_p
-	sf	%	-	-	-	-
Top	26.7	22%	0.23	0.050	0.95	0.95
Top+1	32	26%	0.38	0.100	0.90	0.91
Bot+1	32	26%	0.57	0.150	0.85	0.86
Bot	32	26%	0.77	0.200	0.80	0.80
Panel Reduction Factor Stats - Adjacent Panels						
Panel	Area	% Area	Wt.	Eqn. Reduction	Equation F_p	ABAQUS F_p
-	sf	%	-	-	-	-
Top	26.7	22%	0.23	0.050	0.95	0.96
Top+1	32	26%	0.19	0.050	0.95	0.95
Bot+1	32	26%	0.19	0.050	0.95	0.94
Bot	32	26%	0.19	0.050	0.95	0.94

Some of the ABAQUS runs used to determine the F_p factors for single panel failures and to validate the F_p equations for multiple panel failures terminated prior to the rafter connections of interest reaching failure deformation. This was the case for the single panel failure scenarios of bottom panel failure and second from bottom panel failure. It was also the case for all of the

multiple panel failures scenarios. When this issue occurred, the ABAQUS F_p value at failure was projected using a combination of the F_p curves from failure scenarios that did reach completion and the data from that ABAQUS run up to the point of termination. Examples of this projection technique are provided in Figure 5.17 below for both the single panel failure scenarios and multiple panel failure scenarios. These projections were performed independently, without use of equations 5.2 and 5.3 for F_p given above. The fact that the projected values match the equation values so well bolsters confidence in the approach.

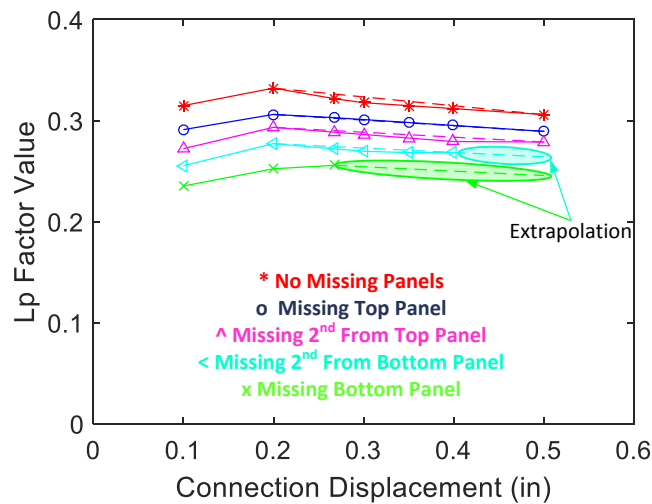


FIGURE 5. 17 – A2-BQ single panel failure case projected L_p value

Figure 5.17 shows the L_p factors as a function of connection displacement for the single missing panel cases (none missing, top missing, bottom missing, intermediate top missing, intermediate bottom missing) from displacement = 0.1 – 0.5” (connection failure). The linear fits for the tails of the cases for no missing panels, top missing and intermediate top missing are also shown on the figure. These cases all ran to completion in ABAQUS, so there was no need for extrapolation. For the cases of missing bottom panel and intermediate bottom panel, the run

terminated prior to completion, so the L_p value was projected based on the available data. The intermediate bottom panel case ran almost all the way to completion, terminating at $d \approx 0.4''$, so the slope of the tail from $d = 0.2'' - 0.4''$ was maintained through $0.5''$ to find the anticipated L_p value. Observe that the slope of each of the linear tail fits is approximately the same, so to find the projected value of L_p for the missing bottom panel case, the intermediate bottom case slope was assumed to be a reasonable approximation for the missing bottom case tail and was used to find the projected L_p value for that case. The F_p value is calculated by dividing the ABAQUS L_p value for a given combination of missing panels by the original ABAQUS L_p value, so F_p is determined from approximating L_p with this method for the cases that terminated prior to completion.

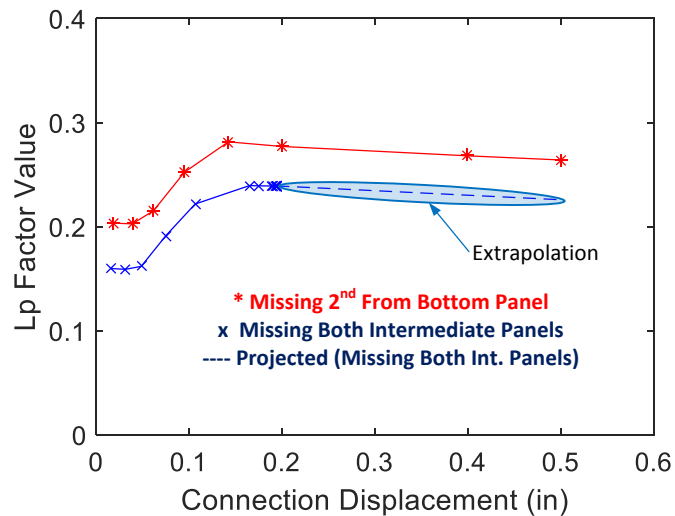


FIGURE 5. 18 - A2-BQ multiple panel failure case projected L_p value

For the cases with multiple panels missing, the ABAQUS trials did not run through completion, so again, the L_p factors were projected based on existing data. Figure 5.18 shows an example of this for the case with both intermediate panels missing. Based on the similarities in

shape to the bottom intermediate missing panel case and the fact that the bottom intermediate panel is expected to have a larger influence on the L_p reduction than the top intermediate panel, the same slope was assumed to apply to the linear tail for the case with both intermediate panels missing. Using this tail slope, the projected L_p value was found. A similar approach was used for the other cases with multiple missing panels, using the tail slopes from the most influential single panel case for a given combination of missing panels (i.e. if the top and bottom panels are missing, use the tail slope for the bottom panel missing case). It is important to reiterate here that using this approach results in projected L_p (and thus F_p) values very similar to those calculated using equations 5.2 and 5.3, which increases the level of confidence in the projections.

5.3.2.3 Archetype 3, Basic Quality (A3-BQ)

A similar situation occurs for the A3-BQ rafter-sill connection failure as for the A3-BQ roof panel failure. Because the roof consists of two sections that are each identical to the A1-BQ roof and the roof pressure zones remain the same as well, a separate analysis does not need to be performed for A3-BQ. As evidence of this, the most likely “first-failure” rafters remain the same. Therefore, the A1-BQ analysis will be used to quantify rafter-sill connection failure for A3-BQ as well.

5.3.3 Bottom Stud-Sill to Foundation Connection Failure

The bottom stud-sill to foundation connection strength is determined from testing performed by Alfano (2016). This testing resulted in the formulation of equations used to determine foundation connection failure strength accounting for both shear and uplift forces. The equations in Table 5.5 determine connection strength per linear foot of wall for the foundation wall connections (Alfano (2016)).

TABLE 5.5 – Foundation connection uplift resistance accounting for shear-uplift interaction (Alfano 2016)

Wall Type	Interaction Curve	COV
A	$R = -0.59 * S + 0.10$	0.704
B	$R = -0.64 * S + 0.12$	0.388
C	$R = -0.66 * S + 0.19$	0.511
D	$R = -0.88 * S + 0.19$	0.205

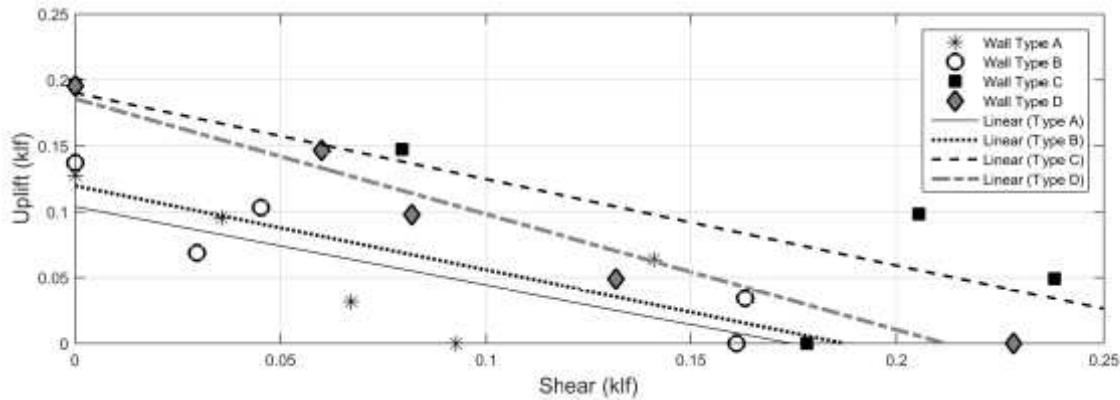


FIGURE 5.19 – Wall to foundation shear-uplift interaction curves (Alfano 2016)

Wall types A and B do not include reinforcing ties, while types C and D do include ties. The walls considered in the determination of failure will be the walls parallel to the wind direction, as these will be the walls that primarily resist shear loading. The walls evaluated by Alfano (2016) have the same anchor bolt size and spacing and base sill material as the walls evaluated in this study. It is assumed that these are the critical components when evaluating foundation connection strength, so it is appropriate to use these equations. As noted in Alfano (2016), until the building uplift is greater than the dead load, the failure will be governed by shear only, with the resistances for a given wall type being equivalent to the experimental values given in the paper for wall tests with no uplift applied. See Figure 5.19 for these values. After this point, uplift governs failure with resistance determined by the equations in Table 5.5. The distribution

type for the foundation connection resistance was assumed by Alfano (2016) to be normal due to a lack of data (only 5 tests were performed for each wall type).

The mean shear and uplift forces induced in the connections are taken from the ABAQUS mean value analyses. Two methods were considered to obtain the percentage of load (shear and uplift) distributed to each wall line. One method considers the horizontal and vertical loads to be applied separately by two separate ABAQUS runs, and the second, more realistically lumps all of the forces considered into a single run. It was concluded that there is very little difference between the shear and uplift load percentages distributed to each wall line determined by using the two methods, so either would be acceptable. Because the coupled ABAQUS run applying all forces together is more realistic, it was used to determine the loads distributed to wall lines as a function of total load. Table 5.6 shows the load percentages for each wall line in archetype 1 for both methods.

TABLE 5. 6 – Wall line load percentages

Isolated Runs		Coupled Run	
Shear % of Total		Shear % of Total	
Short Walls		Short Walls	
GD	OD	GD	OD
18.11%	16.19%	17.46%	14.41%
Uplift % of Total		Uplift % of Total	
Short Walls		Short Walls	
GD	OD	GD	OD
21.59%	19.95%	21.29%	17.40%

In Table 5.6, “GD” stands for the side wall nearest the large glass door, and “OD” is the wall on the opposite side.

Alfano (2016) considered four different cases for foundation connection failure based on the condition of the other critical components (rafter-sill connection and roof panels). These cases vary the enclosure classification (and thus the internal pressure coefficient) and uplift pressure bearing area for different combinations of rafter-sill and roof panel failure conditions. In this study, only the same two cases considered for the other building components are examined which account for (1) the fully enclosed condition with an increase in internal pressure occurring upon the first roof panel failure or window/door pressure failure and (2) the partially enclosed case caused by a window or door breach at the onset of the analysis. It is assumed that if the building enclosure status reaches the “open” condition, the uplift pressure tributary to the anchor bolts does not reduce because a similar uplift pressure will act on some other component (ceiling, floor, etc.) and will still ultimately be transferred into the foundation connection.

5.3.3.1 Archetype 1, Basic Quality (A1-BQ)

The equation in Table 5.6 for wall type B is used for the basic quality foundation connection because no reinforcing ties are used for A1-BQ and type B is more conservative than type A at higher values of shear. It is assumed that either wind direction Case 1 or Case 2 (wind normal to long face) will control this analysis because the larger surface area normal to the wind will produce a larger lateral load. Additionally, the walls perpendicular to the wind direction are shorter, and because connection strength is given per linear foot of wall, they will provide less foundation connection strength. Of these two cases, Case 2 will be selected as the “worst-case” because, while the two cases showed failure at comparable wind speeds, the first failure was observed under Case 2 with the windward side opposite the sliding glass door. The percentage of the total lateral load distributed to each wall does not vary significantly when considering different ratios of windward to leeward wall pressure, so it is not necessary to consider this ratio

in converting total lateral pressure to a wall load. The relationships between total load and wall line load found using the ABAQUS mean value runs will be used to convert random wind pressure loads to wall line loads in the Monte-Carlo simulation. Equations 5.5 – 5.8 relating wall line shear and uplift to total building shear and uplift for the two walls parallel to the wind direction are shown below.

$$S_{w1} = 0.1746 * S_T; \text{ **Wall Line 1 Shear Force** } \quad (5.5)$$

$$U_{w1} = 0.2129 * U_T; \text{ **Wall Line 1 Uplift Force** } \quad (5.6)$$

$$S_{w2} = (0.00008 * S_T^2 + 0.0027 * S_T + 0.0114); \text{ **Wall Line 2 Shear Force** } \quad (5.7)$$

$$U_{w2} = 0.2078 * U_T - 1.0886; \text{ **Wall Line 2 Uplift Force** } \quad (5.8)$$

where S_w is the shear force demand in kips, U_w is the uplift force demand in kips, and S_T and U_T are the total shear and uplift in kips respectively.

Failure for this component is considered to occur when the combined resistance of the wall lines is overcome by the combined load applied to the wall lines. The ABAQUS mean value analysis revealed the onset of foundation connection failure to occur at wind speeds of about 103 mph (EF-1 tornado). Foundation connection failure is very likely to occur after the onset of damage to the roof panels but it is possible that a foundation connection failure could occur first. The basic CQL foundation connection failure seems to occur at a relatively low wind speed, but considering that the connection is only assumed to consist of 0.5” diameter bolts spaced at 6’ o.c., that may not be too surprising.

5.3.3.2 Archetype 2, Basic Quality (A2-BQ)

The procedures for quantifying resistances, demands, and damages for A2-BQ are the same as those used for A1-BQ above. Two ABAQUS mean value runs were performed to quantify demand on the foundation connection for each wall line parallel to the wind direction for A2-BQ. The first run was performed under baseline conditions, assuming no breach and the second run was performed at the elevated internal pressure condition associated with an envelope breach. The two runs revealed that the relationships between the total building uplift and shear loads and the loads transferred to each wall line are virtually unchanged when the windward and leeward pressure ratios are altered. This is consistent with the foundation connection analysis for A1-BQ, where this claim was examined more thoroughly. For this reason, the two ABAQUS runs are assumed to be sufficient to quantify connection demand for A2-BQ. The total load to wall line load relationships taken from the ABAQUS mean value analyses are shown in equations 5.9 – 5.12 for A2-BQ.

$$S_{w1} = 0.31 * S_T; \text{ *Wall Line 1 Shear Force* } \quad (5.9)$$

$$U_{w1} = 0.21 * U_T + 0.61; \text{ *Wall Line 1 Uplift Force* } \quad (5.10)$$

$$S_{w2} = 0.29 * S_T; \text{ *Wall Line 2 Shear Force* } \quad (5.11)$$

$$U_{w2} = 0.21 * U_T - 1.09; \text{ *Wall Line 2 Uplift Force* } \quad (5.12)$$

where units are given in kips and feet.

5.3.3.3 Archetype 3, Basic Quality (A3-BQ)

Again, using the same procedures used for the first two archetypes, foundation connection failure was quantified for A3-BQ with two separate ABAQUS mean value runs. One run each

was performed for the wind pressures associated with the “enclosed” and “partially enclosed” conditions, and both revealed the same approximate linear relationships shown in equations 5.13 – 5.16 relating total building shear and uplift loads to wall line shear and uplift loads.

$$S_{w1} = 0.23 * S_T; \text{ **Wall Line 1 Shear Force** } \quad (5.13)$$

$$U_{w1} = 0.28 * U_T - 1.73; \text{ **Wall Line 1 Uplift Force** } \quad (5.14)$$

$$S_{w2} = 0.21 * S_T; \text{ **Wall Line 2 Shear Force** } \quad (5.15)$$

$$U_{w2} = 0.27 * U_T - 2.41; \text{ **Wall Line 2 Uplift Force** } \quad (5.16)$$

where units are given in kips and feet.

5.3.4 Wall Sheathing Damage

Damage in the form of wall sheathing cracking for both the interior and exterior walls for each basic quality archetype is examined in this section. Only sheathing cracking is considered here, not total wall failure because the walls are not expected to fail and collapse until they have lost the bracing provided by the roof/ceiling diaphragm and lose their overall stability.

Two modes for wall damage are considered herein. The first mode considered is wall racking due to drift caused by the lateral pressures. This mode applies to the walls that are parallel to the wind direction only. The “worst-case” wind direction for this failure mode was determined by measuring the building drifts under loading for each wind direction (from ABAQUS analysis). Similar to the rafter-sill connection failure, the “worst-case” was found to occur under the Case 2 wind direction with wind normal to the long side, opposite the sliding glass door. The MWFRS wind pressures were used for this mode. Table 5.7 below shows the drifts induced by each wind direction loading. The drifts were measured up to the point of rafter to sill connection failure, at

which point wall cracking is not a concern because the building has reached the “complete” damage state. Also, the uplift pressures on the roof are neglected for this analysis. The uplift pressures were shown to slightly decrease the racking displacements if applied. Unlike the other failure modes, wall sheathing damage by racking is not affected by a building envelope breach. This is because the internal lateral pressures parallel to the wind direction act in opposite directions on the leeward and windward sides.

TABLE 5. 7 – Drift induced wall sheathing cracking; worst case wind direction

	Windward Side							
	Edge 1 (GD)		Mid		Edge 2		Average	
	Drift in	Drift %	Drift in	Drift %	Drift in	Drift %	Drift in	Drift %
CASE 1	0.030	0.000	0.143	0.001	0.026	0.000	0.066	-0.07%
CASE 2	-0.035	0.000	-0.162	0.002	-0.027	0.000	-0.075	0.08%
CASE 3	-0.033	0.000	-0.062	0.001	-0.026	0.000	-0.041	0.04%
CASE 4	0.024	0.000	0.042	0.000	0.019	0.000	0.028	-0.03%

The second mode that is considered is wall damage due to the application of out-of-plane wind pressures. This mode applies only to exterior walls, as the interior walls would not be subject to such pressures to a significant degree. Unlike the wall racking mode, envelope breach plays a significant role in the determination of failure for this mode because the pressures of concern are local, not global, and thus the windward and leeward side pressures do not cancel each other out.

5.3.4.1 Archetype 1, Basic Quality (A1-BQ)

Wall damage in the form of gypsum sheathing cracking is considered to occur when the wall drift ratio (wall top displacement in horizontal direction divided by wall height) reaches a mean

value of 0.28% , a value taken from CUREE Publication No. W-15 (McMullin and Merrick (2002)). In McMullin and Merrick (2002), different levels of damage to the gypsum sheathing of shear walls are experimentally quantified. That level of detail is not required here, so the lowest level of damage that would likely require the replacement of a sheathing panel was used. Based on this criterion, the damage state of interest was decided to be “cracking of wallboard at wall penetration”. Out of nine tests, the mean drift ratio that caused this damage state to occur was about 0.28%.

In order to account for the variability in the allowable drift, the mean and standard deviation from the testing performed in McMullin and Merrick (2002) was used to define a lognormal distribution. The lognormal distribution was chosen because in CUREE Publication No. W-23 (Deierlein and Kanvinde (2003)), a lognormal cumulative distribution function (CDF) is used to describe the drift ratios at which different levels of cracking (1” and 12”) occur.

The variability in the wind pressure-induced wall displacement was accounted for by relating the lateral load due to wind pressure to the drift for each wall through the ABAQUS mean value analysis. The analysis revealed an approximately linear relationship between lateral pressure load and drift. This linear relationship is assumed to hold until a major component of the wall fails (i.e. bracing by roof/ceiling diaphragm is lost, or wall develops full yield strength). Under the assumptions of this study, the walls won’t fail (or develop yield strength) until the roof/ceiling diaphragm is gone. As such, a simple factor can be applied to relate the drift of each wall to the lateral pressure load on the building. Using this factor, the random wall pressure can be converted to an equivalent random drift. The random drift value (in inches) can then be divided by wall height (96”) to get the random drift ratio, allowing us to perform a statistical analysis that

accounts for variability in both the wind induced drift in each wall as well as the wall's capacity to withstand drift without cracking. The "random drift ratio" equation is shown below.

$$F_D = L_l R_{pd} / H_w \quad (5.17)$$

where F_D is the random drift ratio, L_l is the random lateral wall pressure load, R_{pd} is the ratio of lateral pressure load to drift for each wall, and H_w is wall height, which in this case will always be 8' (96"). The lateral wall pressure load is calculated by combining the randomly generated lateral pressures (windward wall, leeward wall, and lateral components of windward and leeward roof pressures). The mean R_{pd} is evaluated using the ABAQUS mean value runs. The effect of changing the windward to leeward wall pressure ratio was also examined. This ratio was determined by a Monte-Carlo simulation to be bounded between 0.25 and 1.75 with an average value of ≈ 0.78 . In this range, slight differences were observed in the value of R_{pd} for each wall, but because the differences are slight, assuming that the mean values apply for all windward to leeward pressure ratios does not alter the failure fragilities to a significant degree.

Less data is available regarding the statistical parameters that would quantify stucco damage in the form of cracking. Due to the lack of data, the onset of cracking damage in the stucco sheathing will be assumed to occur at a mean drift ratio of 0.2% (Arnold et al (2003)). To account for the variability in the stucco cracking resistance, the same coefficient of variation and distribution type (lognormal) that was used for gypsum board cracking is assumed to apply to the stucco sheathing as well.

No wall sheathing cracking due to wall racking for gypsum or stucco occurs under the conditions of the ABAQUS mean value analysis for A1-BQ. The maximum gypsum wall drifts from the ABAQUS analysis occur in the interior walls with a magnitude of about 0.12%, below

the mean cracking drift, and the max stucco wall drift in the exterior walls is just 0.08%. These maximums occur at wind speeds of about 160 mph (EF-3), well above the mean failure wind speeds for the other modes (rafter failure, roof panel failure, foundation connection failure, etc.). As shown in Figure 5.20 below, cracking of the wall sheathing due to wall racking seems very unlikely to occur prior to the onset of much more critical roof damage and therefore this damage mode will be ignored.

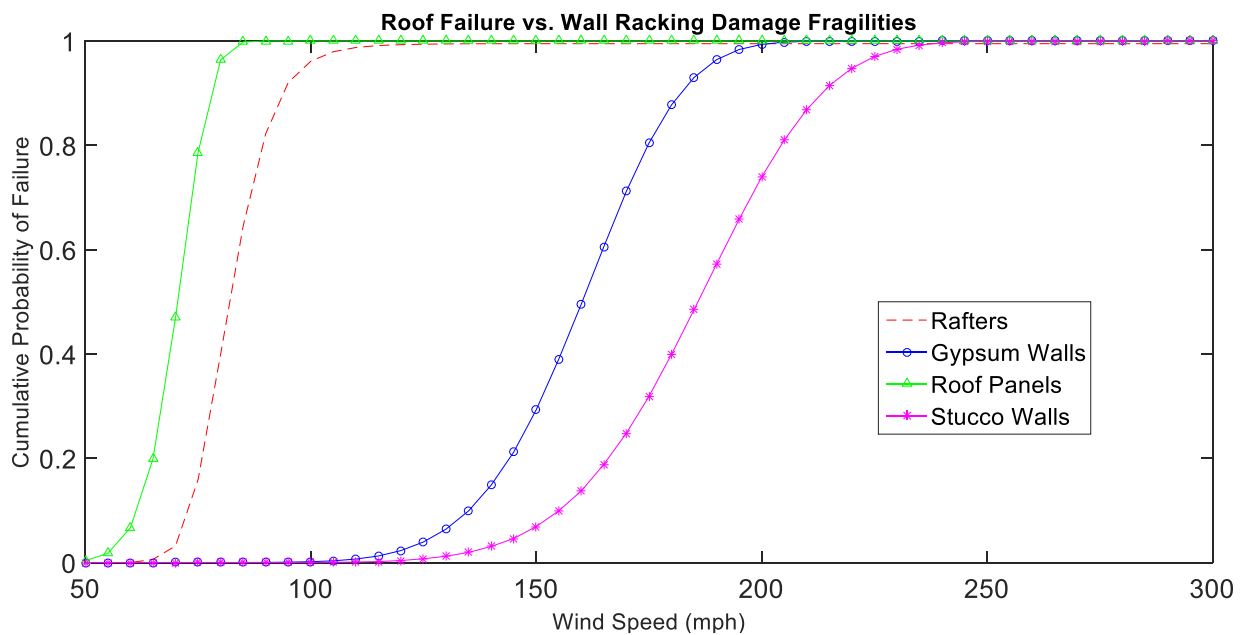


FIGURE 5. 20 – Wall sheathing cracking due to wall racking fragilities *versus* other critical failure mode fragilities

For the second mode considered for wall sheathing failure, which is caused by out-of-plane wind pressures, it was observed through ABAQUS analysis of both cases (MWFRS and C&C) that the stresses caused by the out-of-plane displacements induced in the walls under the MWFRS pressures and the C&C pressures are significantly different. This is because the modes by which wall stresses are generated are different for the MWFRS and C&C respectively. The

C&C wall pressures on each face act independently of the pressures on the other faces of the building, causing bending stresses to develop in the sheathing as a direct function of wind pressure load on each individual wall. These stresses could lead to sheathing rupture, if large enough wind pressures are applied. The C&C wind pressures could also cause sheathing fastener failure directly related to wind pressure if the tensile load generated by the wind pressure is large enough over a given wall face. For the MWFRS case, bending stresses are developed in the wall sheathing due to the drift caused by wind pressure loading which is a function of the total wind pressure load on the building, not only the pressure load tributary to a single wall face. The ABAQUS mean value analyses of each case revealed that significantly larger wall sheathing stresses are created by the flexural stresses generated under MWFRS loading. Additionally, stucco fastener failure does not appear to be a concern until considerably higher wind speeds are reached.

Assuming values of modulus of rupture (MOR) of 530 psi and 750 psi (typical values) for the stucco and gypsum board sheathing respectively, the ABAQUS mean value analysis showed no out-of-plane sheathing failure occurring up to wind speeds of between 125-130 mph (EF-2 tornado), significantly higher than the wind speeds that caused failure for the rafter-sill, roof panel, and foundation connections for the mean value analysis. The stucco is considered to govern failure here, because of its lower MOR. This analysis however assumes (as did all the other mean value analyses) that no envelope breach had occurred. As will be shown below, this failure mode is heavily dependent upon whether or not the buildings envelope remains intact. It is assumed that the flexural stresses induced in the wall sheathings are primarily correlated to the loads induced locally from the roof and wall pressures applied horizontally to that wall (i.e. the

windward wall sheathing stress is related closely to horizontal load induced by the windward wall and roof pressures).

In order to calculate the maximum stresses generated in the wall sheathing for each wall, a number of ABAQUS analyses were performed to derive the relationship between horizontal loads applied to the walls and the maximum stresses generated. The analyses revealed approximately linear relationships between local horizontal loads and maximum stresses for each wall, indicating that a linear fit equation can be applied to the randomly generated wind pressures loads in a Monte-Carlo simulation to determine the random maximum stress in each wall. The equations for these conversions are shown here for each exterior wall.

$$\sigma_{LWmax} = L_{LW} * 4.66 - 9175.7; \text{ **Maximum stucco Stress - leeward wall** } \quad (5.18)$$

$$\sigma_{WWmax} = L_{WW} * 30.07 - 8300.6; \text{ **Maximum stucco stress - windward wall** } \quad (5.19)$$

$$\sigma_{SW1max} = L_{SW1} * 8.0 - 7021.9; \text{ **Maximum stucco stress - side wall 1** } \quad (5.20)$$

$$\sigma_{SW2max} = L_{SW2} * 3.60 - 3692.5; \text{ **Maximum stucco stress - side wall 2** } \quad (5.21)$$

where σ_{max} is the maximum wall stress in psf and L is the local wall load in lbs (windward, leeward, or side) found by multiplying the horizontal component of roof and wall pressures by the areas over which they act.

The load-maximum stress relationships shown above were derived from the enclosed case considering no envelope breach. For this case, the mean windward to leeward wall pressure ratio, $P_{WW}/P_{LW} \approx 0.789$, and the mean windward to leeward roof pressure ratio, $P_{WR}/P_{LR} \approx 1.36$. We also need to consider the case where the building envelope is breached and the enclosure classification is considered partially enclosed to determine if the load-maximum stress

relationships change significantly. For this case, the mean roof pressure ratio does not change very much ($P_{WR}/P_{LR} \approx 1.22$) but the wall pressure ratio does, as it decreases to $P_{WW}/P_{LW} \approx 0.126$. For this reason, a separate ABAQUS analysis was performed to determine the change in the load – maximum stress relationship. In the Monte-Carlo simulation, the enclosed case relationship will be modified per equations 5.22 and 5.23 once the envelope has been determined to have breached by window or door pressure failure, or roof sheathing panel failure. The ABAQUS analyses revealed that for the leeward wall, the load-maximum stress relationship is virtually unchanged under the partially enclosed condition. For the sidewalls, a factor of 0.975 can be applied to the enclosed condition value to adjust for the onset of the partially enclosed condition, and for the windward wall, the relationship changes more significantly and equation 5.23 best fits the load – stress relationship.

Maximum side wall stucco stress; partially enclosed condition;

$$\sigma_{PEC_max} = \sigma_{max} * 0.975 \quad (5.22)$$

Maximum windward wall stucco stress; partially enclosed condition

$$\sigma_{PEC_max} = -L_{Ww} * 15.38 - 8997.7 \quad (5.23)$$

where σ_{PEC_max} is the maximum stress (psf) adjusted for the mean wall and roof pressure ratios associated with the partially enclosed condition, σ_{max} (psf) is the enclosed condition maximum stress calculated using equations 5.18-5.21, and L_{Ww} is the total windward wall load (lb).

The resistance to damage for this mode is governed by the value of the modulus of rupture of the wall sheathing. Some difficulty was encountered locating experimental data on the MOR (flexural strength) for both gypsum board and stucco, so statistical parameters were not obtained.

Instead, a typical value was taken from manufacturer websites to be 530 psi for the stucco sheathing which governs failure. This value is used directly in the Monte-Carlo simulation as a deterministic value, so the variability of the MOR of the sheathing material is not being taken into account in this study. This limitation may have a measureable effect on the outcome of the statistical analysis considering that there is likely to be high variability in stucco sheathing strength due to uncertainties in construction techniques, material properties, and ambient conditions during construction. Fortunately, wall sheathing damage is not one of the more critical failure modes, so it does not affect the total building fragilities much. Never the less, the issue should be addressed in future work when more experimental data becomes available.

5.3.4.2 Archetype 2, Basic Quality (A2-BQ)

The same procedures used to quantify wall sheathing damage for A1-BQ are used for A2-BQ. It is assumed that out-of-plane displacement is the prominent cause of wall sheathing damage for A2-BQ as well. Because this archetype is a two story building, the number of walls considered is doubled. The top and bottom portions of the leeward, windward, and sidewalls were all considered in the initial analysis meaning that 8 total wall sections were analyzed. In order to simplify the analysis and remain consistent with the building system failure criteria used for A1-BQ, only the more critical story (as determined by the ABAQUS mean value analyses) for each face is considered in the development of fragilities. For example, if the highest stress on the entire leeward face is developed in the upper story of the leeward wall during the ABAQUS mean value analysis, only the upper story leeward wall is considered in the statistical analysis. Table 5.8 summarizes the critical story for each face for A2-BQ. Both the enclosed and partially enclosed conditions were considered for the analysis, although the critical story was the same for each case.

TABLE 5. 8 - A2-BQ wall sheathing damage critical story

WALL FACE				
Enclosure Class.	Leeward	Windward	Side Wall 1	Side Wall 2
Enclosed	<i>Upper</i>	<i>Upper</i>	<i>Lower</i>	<i>Upper</i>
Partially Enc.	<i>Upper</i>	<i>Upper</i>	<i>Lower</i>	<i>Upper</i>

Observe that the upper story controls damage/failure for the wall sheathing on all faces with the exception of side wall 1 (the side closest to the large glass door).

For A2-BQ the ABAQUS analysis for the enclosed building with no breach revealed the following approximations for the wall load-maximum stress relationships for each wall face.

Maximum stucco stress - leeward wall;

$$\sigma_{LWmax} = L_{LW} * 5.66 - 9933.1 \quad (5.24)$$

Maximum wall stucco stress - windward wall;

$$\sigma_{WWmax} = -L_{Ww} * 34.07 - 5396.6 \quad (5.25)$$

Maximum wall stucco stress - side wall 1;

$$\sigma_{SW1max} = 0.0002 * L_{Sw1}^2 + L_{Sw1} * 3.98 - 5402.7 \quad (5.26)$$

Maximum wall sheathing stress - side wall 2;

$$\sigma_{SW2max} = L_{Sw2} * 10.26 - 5244 \quad (5.27)$$

The ABAQUS mean value run considering the partially enclosed condition (breached envelope), resulted in the following modified relationships.

Maximum leeward wall stucco stress; partially enclosed condition;

$$\sigma_{PEC_max} = \sigma_{LWmax} * 0.95 \quad (5.28)$$

Maximum windward wall stucco stress; partially enclosed condition;

$$\sigma_{PEC_max} = -L_{Ww} * 9.53 - 4528 \quad (5.29)$$

Maximum side wall 1 stucco stress; partially enclosed condition;

$$\sigma_{PEC_max} = \sigma_{SW1max} * 0.875 \quad (5.30)$$

Maximum side wall 2 stucco stress; partially enclosed condition;

$$\sigma_{PEC_max} = \sigma_{SW2max} * 0.925 \quad (5.31)$$

5.3.4.3 Archetype 3, Basic Quality (A3-BQ)

Using the same procedures to quantify exterior wall sheathing damage for A3-BQ, the relationships shown in equations 5.32 – 5.39 were found to convert the local wall load to maximum wall stress for each wall. These relationships are shown for both the “enclosed” and “partially enclosed” conditions below.

ENCLOSED CONDITION

$$\sigma_{LWmax} = L_{LW} * 2.52 - 8166.8; \text{ Maximum stucco stress - leeward wall} \quad (5.32)$$

$$\sigma_{WWmax} = L_{Ww} * 37.76 - 8893.2; \text{ Maximum stucco stress - windward wall} \quad (5.33)$$

$$\sigma_{SW1max} = L_{SW1} * 4.18 - 8026.3; \text{ Maximum stucco stress - side wall 1} \quad (5.34)$$

$$\sigma_{SW2max} = L_{SW2} * 3.58 - 7212.7; \text{ Maximum stucco stress - side wall 2} \quad (5.35)$$

PARTIALLY ENCLOSED CONDITION

Maximum leeward wall stucco stress; partially enclosed condition;

$$\sigma_{LWmax} = L_{LW} * 2.41 - 10035 \quad (5.36)$$

Maximum windward wall stucco stress; partially enclosed condition;

$$\sigma_{WWmax} = -L_{WW} * 7.06 - 7766 \quad (5.37)$$

Maximum side wall 1 stucco stress; partially enclosed condition;

$$\sigma_{SW1max} = L_{SW1} * 3.93 - 8891.3 \quad (5.38)$$

Maximum side wall 2 stucco stress; partially enclosed condition;

$$\sigma_{SW2max} = L_{SW2} * 3.53 - 10494 \quad (5.39)$$

5.3.5 Window/Door Pressure Failure

As previously noted, it is difficult to quantify the likelihood of window or door breach by windborne debris impact. The probability of windows or doors being damaged by wind pressure, however, is accounted for in this study. Window/door pressure damage is not being modeled in ABAQUS. Instead, statistical data for window and door pressure resistance is taken from the HAZUS hurricane module to quantify failure probabilities. The C&C wind pressures are used for this damage state, and it should be noted that the value of GC_p varies slightly for the differently sized windows and doors.

5.3.5.1 Archetype 1, Basic Quality (A1-BQ)

For archetype A1-BQ, typical door and window pressure resistances are used. The mean values and other statistical data for these features are taken from the HAZUS hurricane module and can be found in Table 2.5. The large sliding glass door in A1-BQ is considered a window, consistent with HAZUS. As discussed above, GC_p varies slightly for the different sizes of windows and doors in the model building. This variation is slight however, and so an average value of 1.05 is used for the zone 4 GC_p . None of the windows or doors is located at a corner of the building, so zone 5 need not be considered.

5.3.5.2 Archetype 2, Basic Quality (A2-BQ)

The same resistance statistics and damage/failure criteria are used for A2-BQ as were used for A1-BQ (described above) to quantify damage for the window/door pressure blowout. The primary difference between A1-BQ and A2-BQ in regards to the windows/doors is that the amount of windows and doors is doubled for the second archetype. As described in Chapter 3, to facilitate timely construction of the second archetype model, the second story is essentially a duplicate of the first story. Because the doors would not exist on the second story (assuming no balcony/porch exists) the second story doors will be considered windows. Because no parameters affecting this damage state are being determined using the ABAQUS model, no further modifications need be made to the model to account for this assumption.

5.3.5.3 Archetype 3, Basic Quality (A3-BQ)

Again, the same resistance statistics and damage/failure criteria are used for A3-BQ as were used for A1-BQ to quantify damage for the window/door pressure blowout. The only differences being that, with the exception of the large glass door present in archetypes 1 and 2, the number of

windows and doors in A3-BQ has been doubled. The large glass door opening has been converted into a hallway to connect the two sections of A3-BQ, so the glass door no longer exists in archetype 3.

5.3.6 Roof Cover Failure

“Roof cover” in this study consists of shingles, roofing paper, and flashing. Roof cover is not to be confused with the roof sheathing discussed earlier in this chapter. Roof cover damage is not modeled using ABAQUS, but is instead accounted for by using statistical resistance data to quantify the probability of failure. The C&C wind pressures are used for this damage state. Due to the large number of shingles on a roof, the Monte-Carlo simulations for roof cover failure do not include the entire number of shingles. Instead, a representative sample size is used for each roof zone, i.e. if there are 100 shingles located in roof zone 1 and 50 located in roof zone 2, a representative model may be used with 20 shingles in zone 1 and 10 shingles in zone 2. Because damage to the roof cover is determined by the percentage of shingles failed, the representative model will accurately approximate the percent failure probability so long as the ratio of shingles in each roof zone is correct.

5.3.6.1 Archetype 1, Basic Quality (A1-BQ)

For the $\frac{1}{2}$ square foot shingles used for the basic quality archetypes, GC_p will be equal to -0.9 in pressure zone 1 and -1.7 in zone 2. For a hip roof with the A1-BQ roof slope (~ 14 deg.), zone 3 is considered to be equal to zone 2. Individual shingle resistances are assumed to be statistically independent. Statistical information for the basic quality asphalt shingle pressure resistance can be found in Table 2.5.

5.3.6.2 Archetype 2, Basic Quality (A2-BQ)

The primary difference between A1-BQ and A2-BQ affecting the roof cover is the change in roof type. Due to the modified roof type (hip for A1-BQ, gable for A2-BQ), the C&C roof pressures and pressure zone configurations vary slightly. The ratio of shingles in each roof pressure zone is adjusted in the Monte-Carlo simulations to reflect the change in pressure zones and accurately model the damage fragilities for A2-BQ. For A2-BQ roof zone 3 must also be considered. The zone 3 $GC_p = -2.6$.

5.3.6.3 Archetype 3, Basic Quality (A3-BQ)

For the same reasons discussed for the A3-BQ roof panel and rafter-sill connection damage quantifications, the A1-BQ roof cover damage analysis is suitable to be used for A3-BQ as well.

5.3.7 Summary of Component Fragilities

The component fragilities formulated using the procedures described in the previous sections of this chapter are shown below.

5.3.7.1 Archetype A1-BQ Component Fragilities

Roof Panel Failure

Figures 5.21 – 5.24 below show the comparison between the fragilities for roof panel damage for damage states 1, 2, 3, and 4.

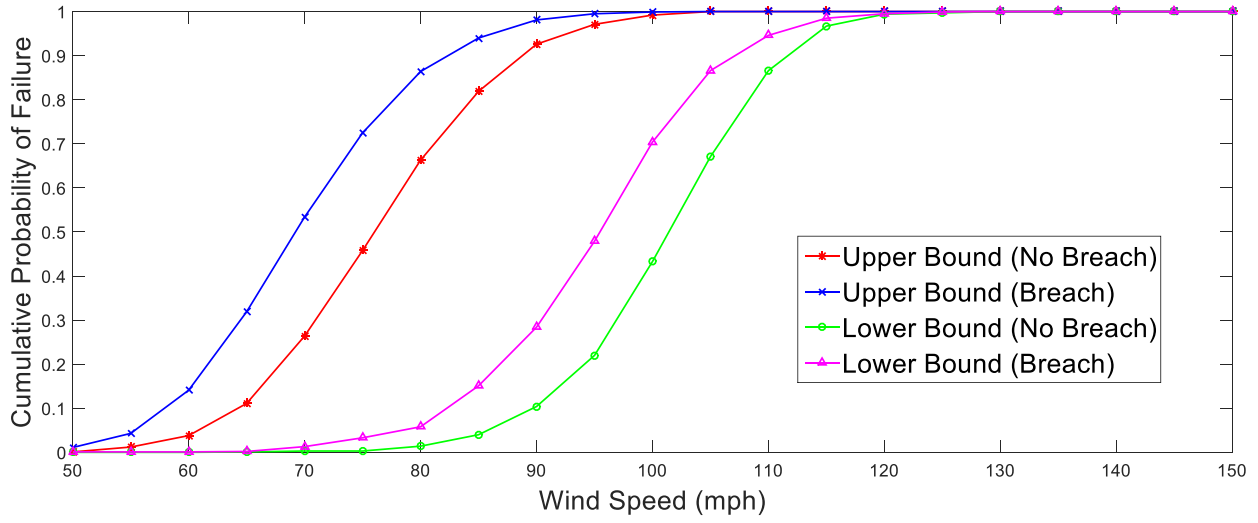


FIGURE 5. 21 – A1-BQ Roof panel fragilities; DS-1

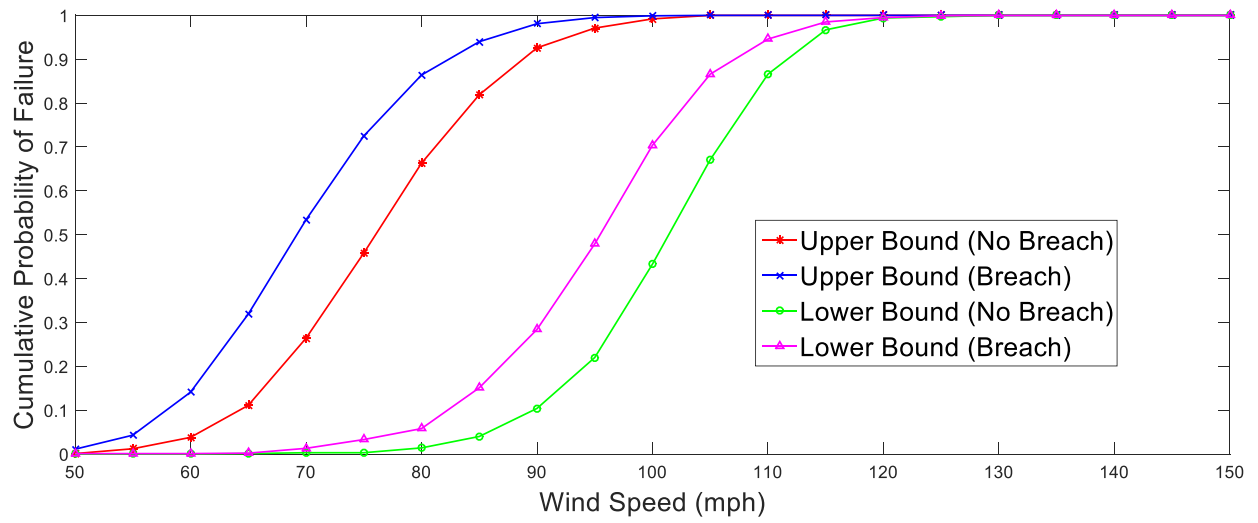


FIGURE 5. 22 – A1-BQ Roof panel fragilities; DS-2

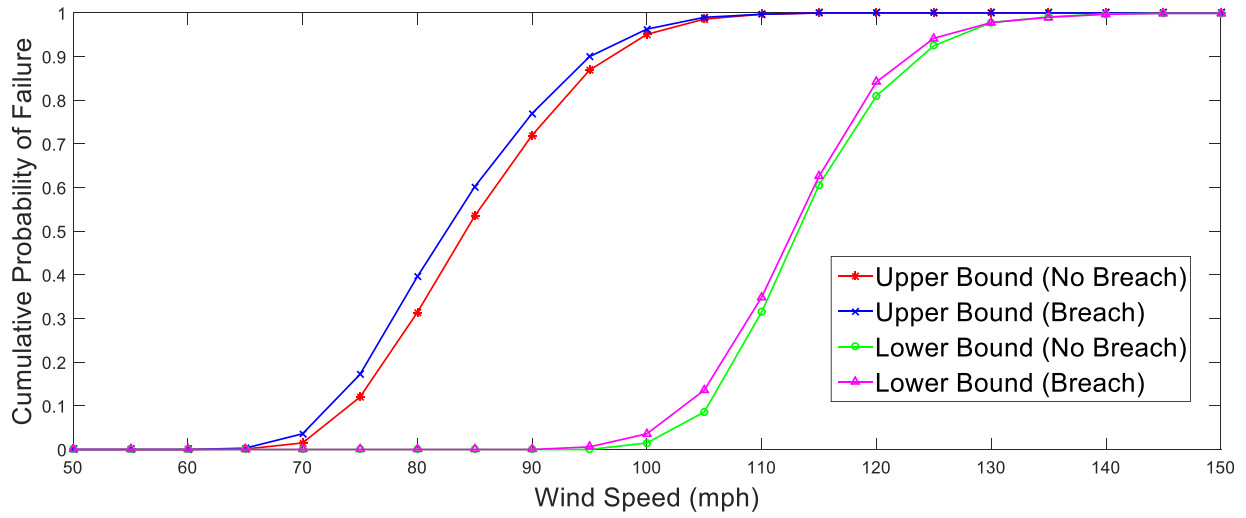


FIGURE 5. 23 – A1-BQ Roof panel fragilities; DS-3

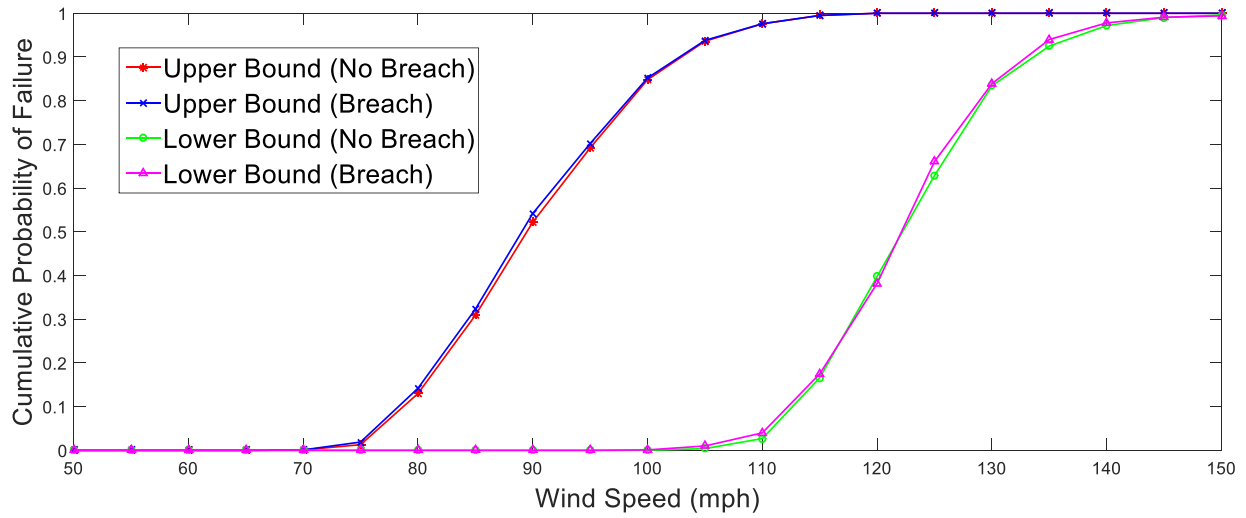


FIGURE 5. 24 – A1-BQ Roof panel fragilities; DS-4

Rafter-Sill Connection Failure

Figure 5.25 below shows comparison between the fragilities for rafter-sill connection failure for all damage states. Only one figure is necessary to represent all damage states for rafter-sill failure because failure of the first rafter-sill connection is considered to result in the most severe damage state and thus there is no gradation of damage for this component.

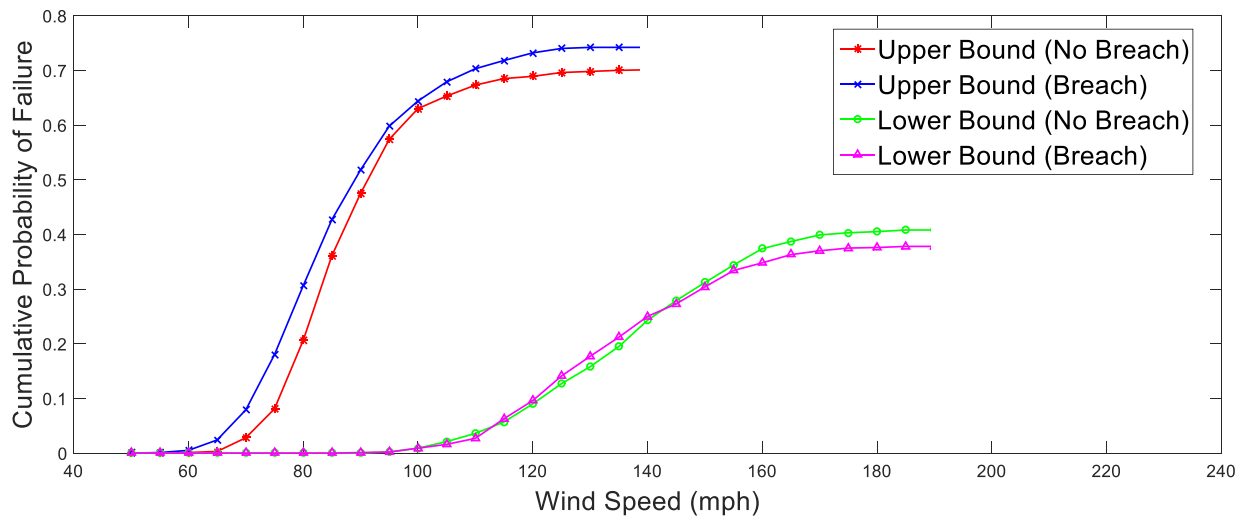


FIGURE 5. 25 – A1-BQ Rafter-sill connection fragilities; DS-1 - 4

The fragilities do not approach a cumulative failure probability equal to 1.0. This is due to the reduction and eventual elimination of load distributed to the rafters as roof panels tributary to those rafters fail and separate from the rafter. Once all the panels have failed, no load is distributed to the rafter, reducing its probability of failure to zero if the rafter has managed to survive up to that point. Under the upper and lower bound conditions this appears to be the case that is likely to occur as wind speeds increase. There is a large difference between the ceiling values for the upper and lower bound cases. The only difference between the two cases is that the Haan Factor for tornado pressure amplification is eliminated for the lower bound case. Because

the Haan Factor is larger for the MWFRS components than for the C&C components, reducing the factor to 1 for both would reduce the loads on the MWFRS more than the loads on the C&C, making it more likely to fail all of the roof panels (C&C) tributary to a given rafter prior to failing the rafter-sill connection (MWFRS).

Foundation Connection Failure

Figure 5.26 shows the comparison between the fragilities for foundation-to-wall connection failure for all damage states. Only one figure is necessary to represent all damage states for foundation connection failure because any failure of the connection is considered to result in the most severe damage state and thus there is no gradation of damage for this component.

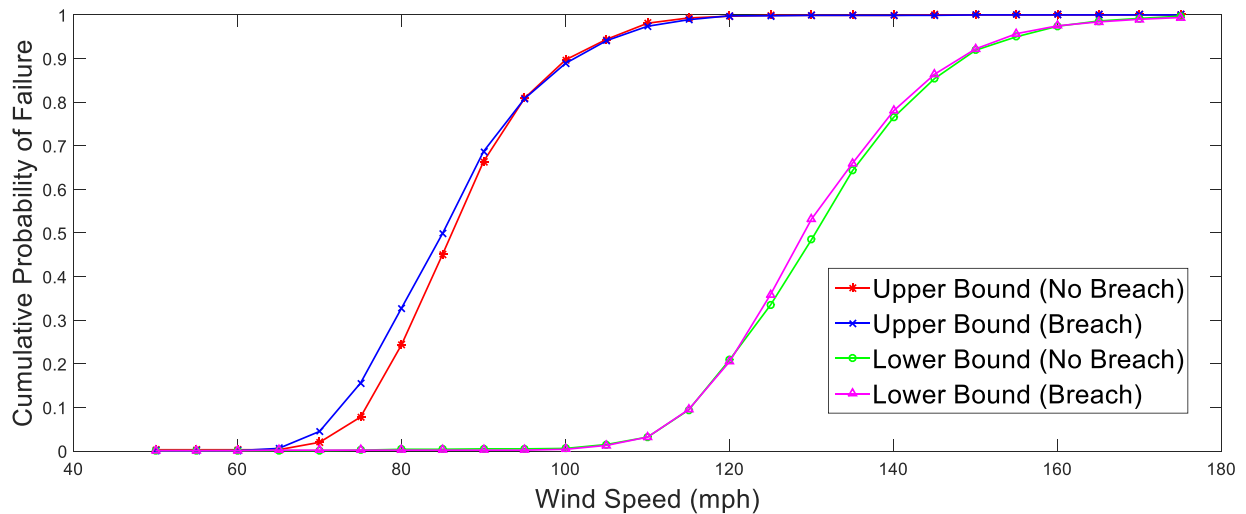


FIGURE 5. 26 – A1-BQ Foundation connection fragilities; DS-1 – 4

Wall Sheathing Damage

Figure 5.27 shows the comparison between the fragilities for wall sheathing damage for damage state 1. Damage states 2, 3, and 4 need not be represented because wall sheathing damage alone cannot cause these states to occur.

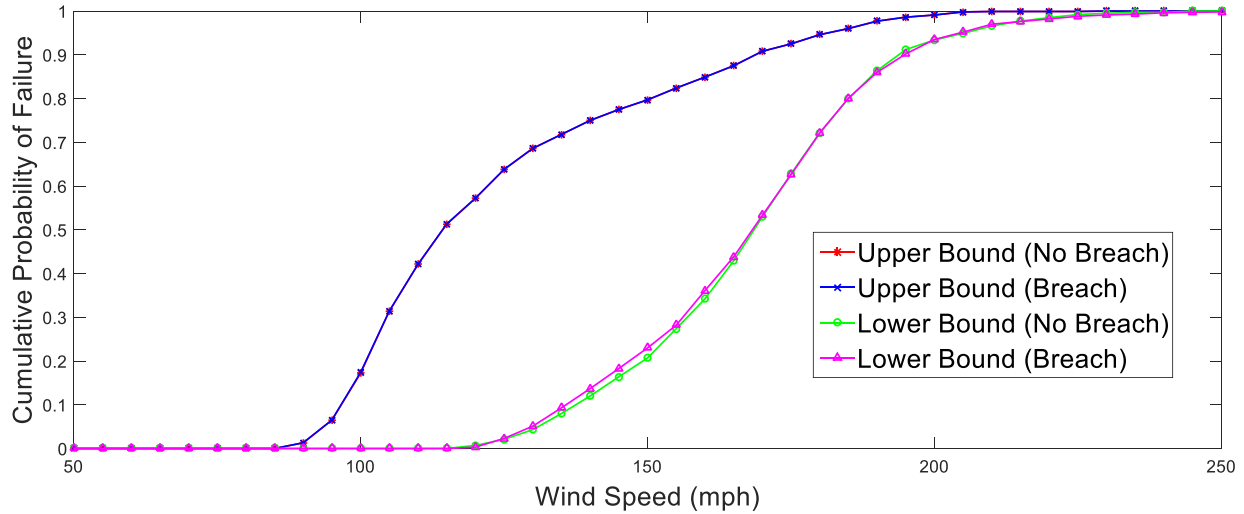


FIGURE 5. 27 – A1-BQ Wall sheathing fragilities; DS-1

Window/Door Pressure Damage

Figures 5.28 – 5.30 show comparison between the fragilities for window/door damage for damage states 1, 2 and 3. Damage state 4 need not be represented because window/door damage alone cannot cause this state to occur.

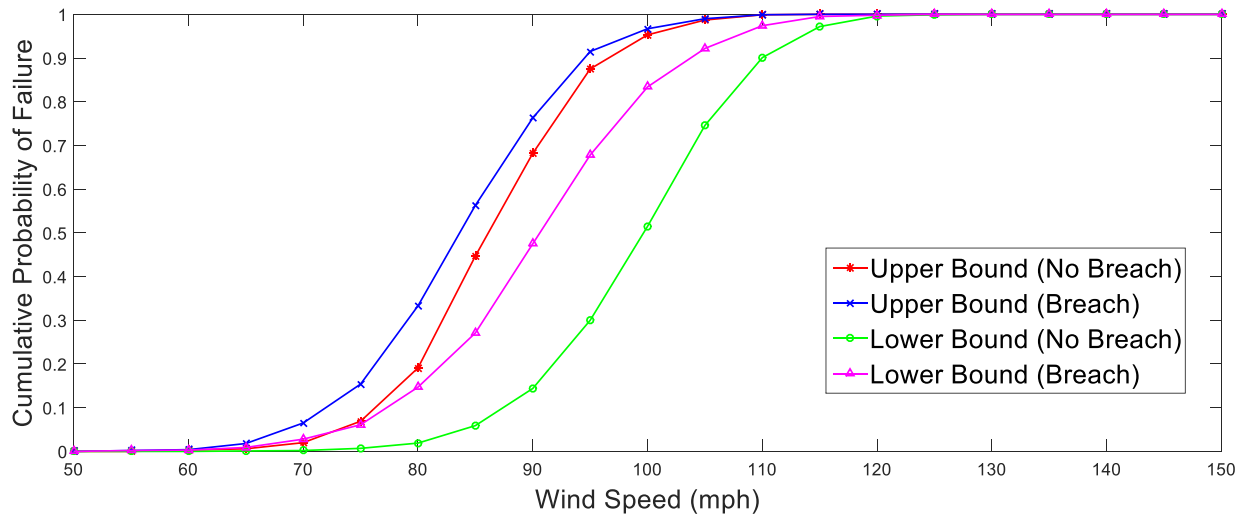


FIGURE 5. 28 – A1-BQ Window/door pressure fragilities; DS-1

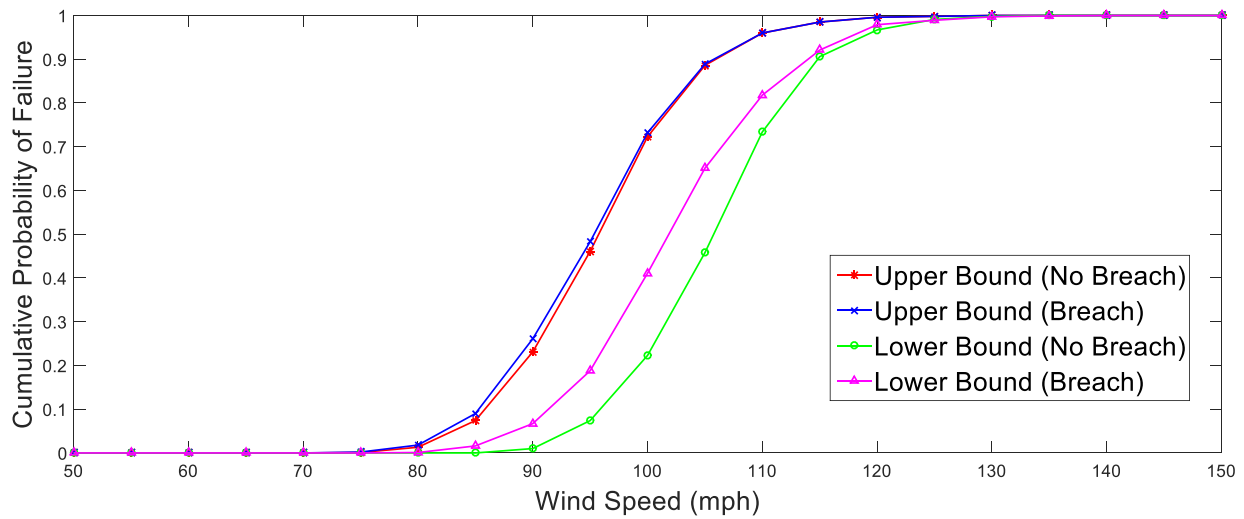


FIGURE 5. 29 – A1-BQ Window/door pressure fragilities; DS-2

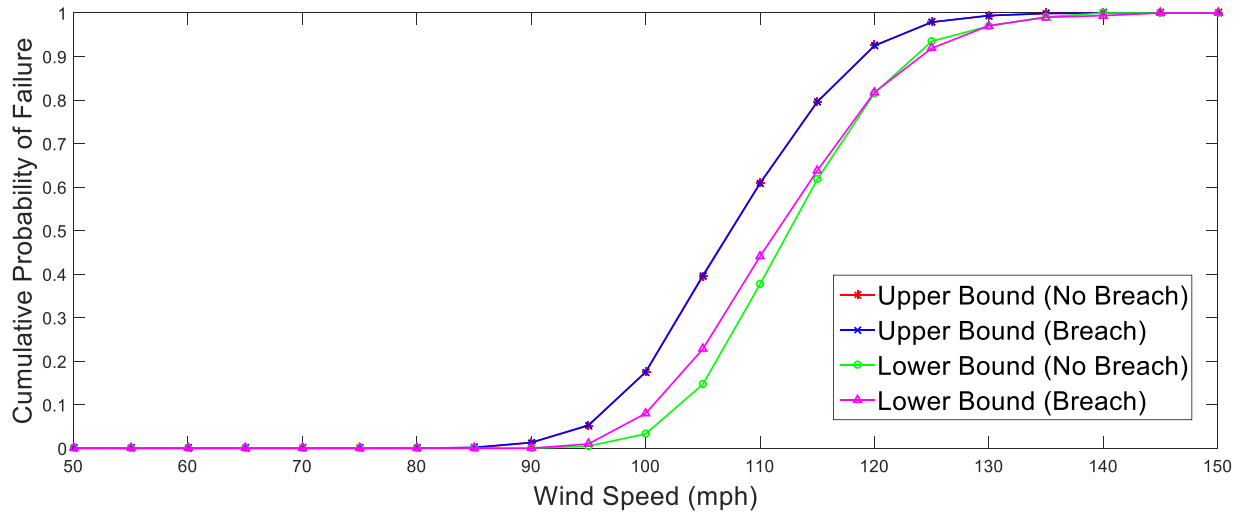


FIGURE 5.30 – A1-BQ Window/door pressure fragilities; DS-3

Roof Cover Damage

The Figures 5.31 and 5.32 show comparison between the fragilities for roof cover damage for damage states 1 and 2, damage states 3 and 4 need not be represented because roof cover damage alone cannot cause these states to occur.

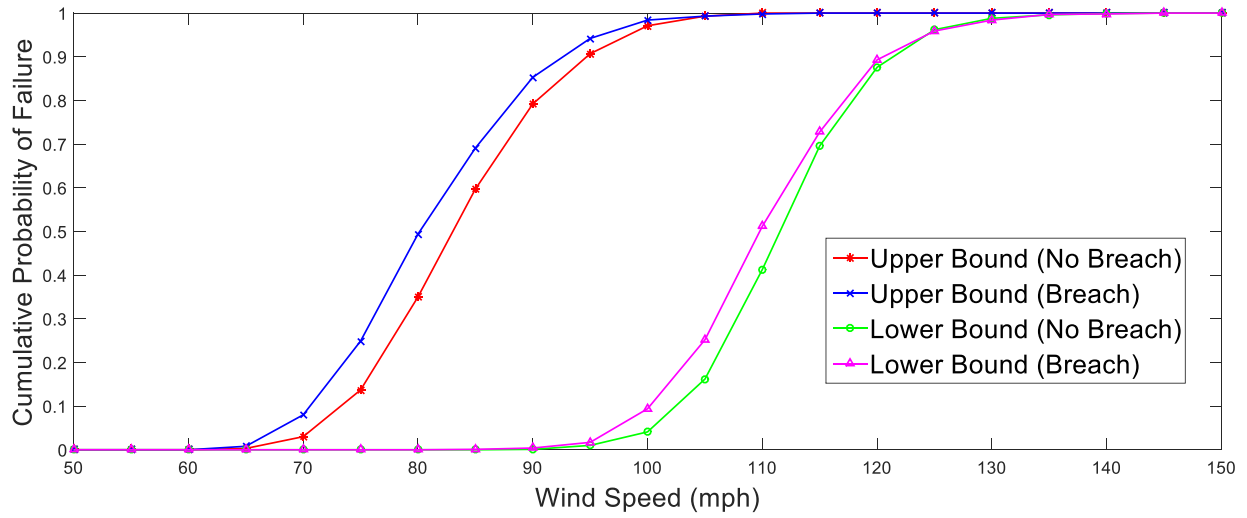


FIGURE 5. 31 – A1-BQ Roof cover fragilities; DS-1

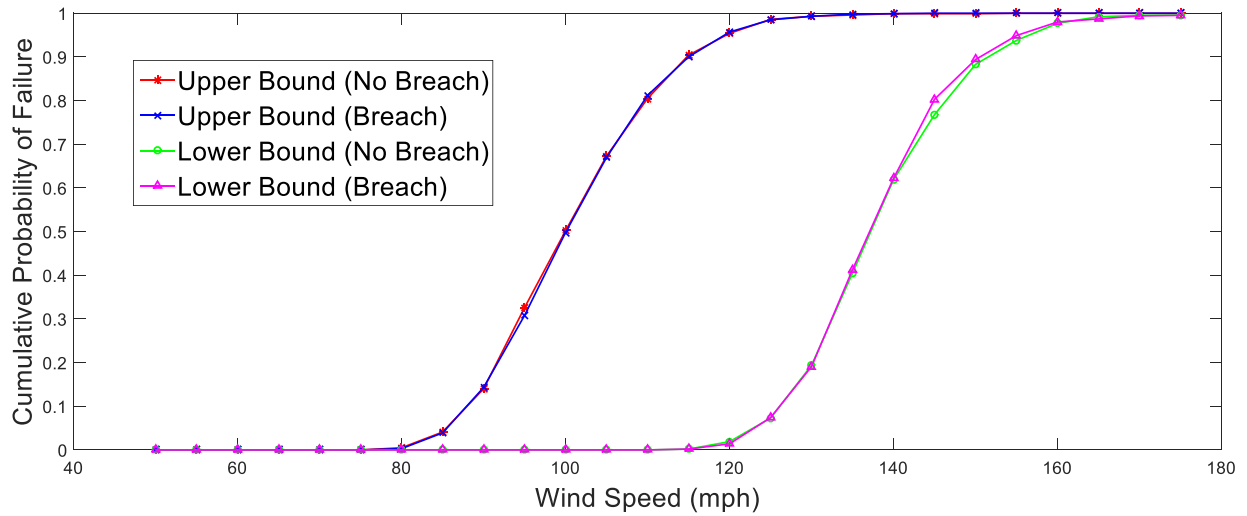


FIGURE 5. 32 A1-BQ Roof cover fragilities; DS-2

As seen by comparison of the missile breach versus no missile breach cases (both upper and lower bound), assuming a projectile breaches the building envelope prior to a window or door pressure failure or a roof panel failure, results in a leftward shift of the damage fragilities. This makes sense because the assumption results in the application of the higher internal pressure coefficient associated with a partially enclosed building occurring at a lower wind speed than it otherwise would; thus the demand on building features is increased earlier and damage is initiated sooner. Observe that debris breach appears to have a significantly larger impact on the lesser damage states (slight and moderate) than it does on the more severe states. This is particularly apparent upon examination of the lower bound fragilities but it is true in both cases. This is because the more severe damage states generally occur at higher wind speeds, at which the building envelope is likely to have been breached by roof panel failure or window/door pressure blowout, even without considering windborne debris breach. In other words, for damage states that are likely to occur after the failure of the first roof panel or window/door pressure blowout, the fragilities are not affected much by assuming wind-borne debris related building envelope breach because the envelope was likely to be breached by other means prior to the onset of these damage states for either case.

A simple and readily applicable solution is proposed to prevent windows from being breached by small projectiles at lower wind speeds; storm shutters could be used to protect the windows from windborne projectiles. The shutters may fail at higher wind speeds due to suction pressure but it is reasonable to assume that they could be designed to withstand at least the wind speeds associated with roof panel failure and/or window pressure blowout. This measure would allow the structure to remain in the enclosed condition longer, delaying the internal pressure increase that often initiates more severe damages. From this point forward, it will be assumed

that one of the improvements made to the buildings considered in this study is the addition of storm shutters and under that assumption, the case considering windborne debris window breach will not be analyzed for archetypes 2 and 3.

5.3.7.2 Archetype A2-BQ Component Fragilities

The damage state fragilities for the upper and lower bound wind pressure cases for each building component are provided in this section.

Roof Panel Failure

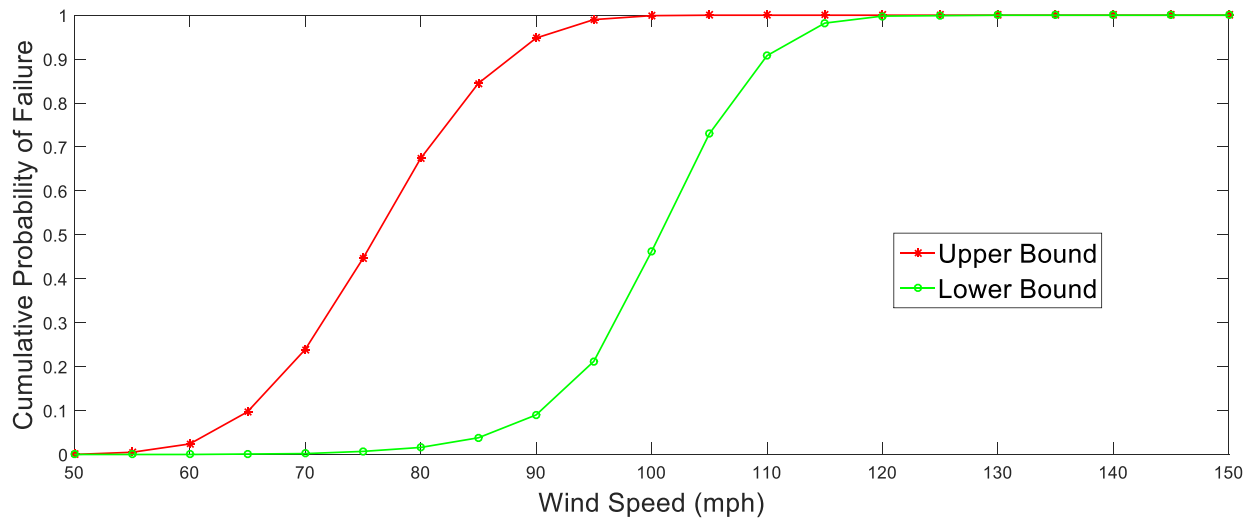


FIGURE 5. 33 – A2-BQ Roof panel fragilities; DS-1

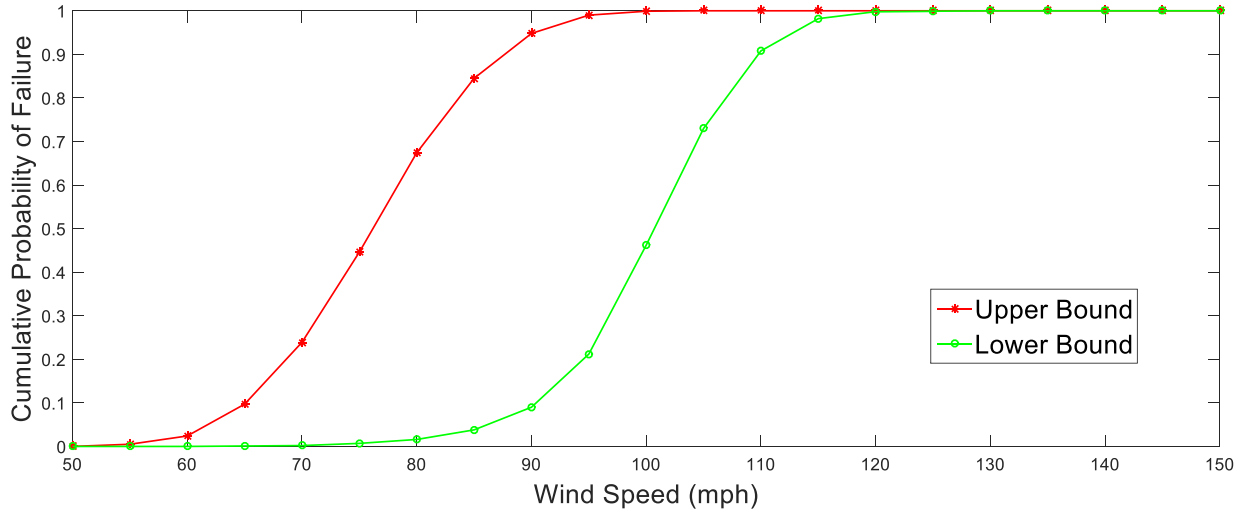


FIGURE 5. 34 – A2-BQ Roof panel fragilities; DS-2

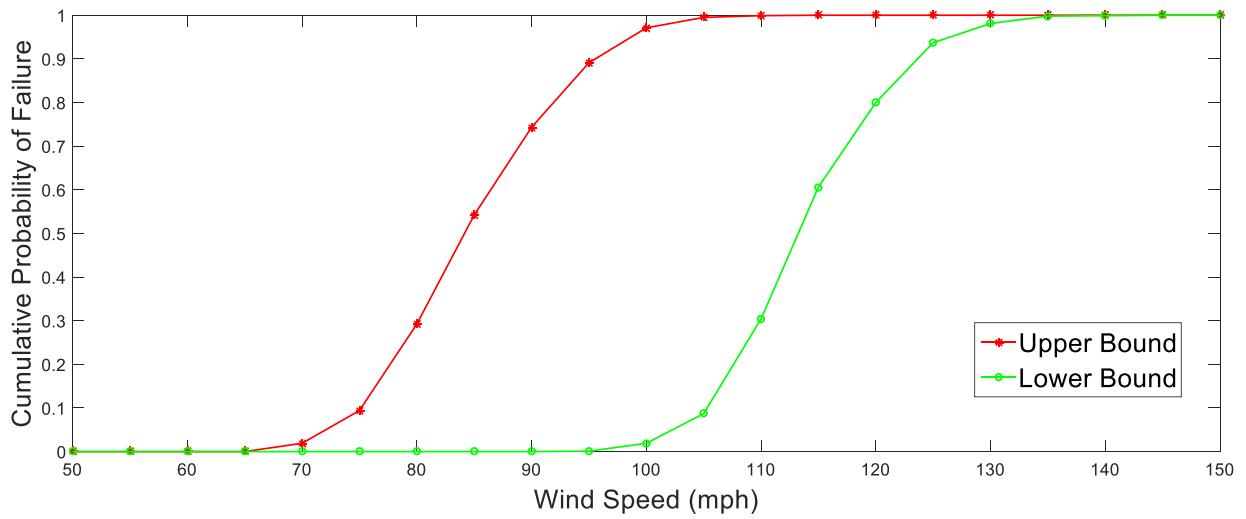


FIGURE 5. 35 – A2-BQ Roof panel fragilities; DS-3

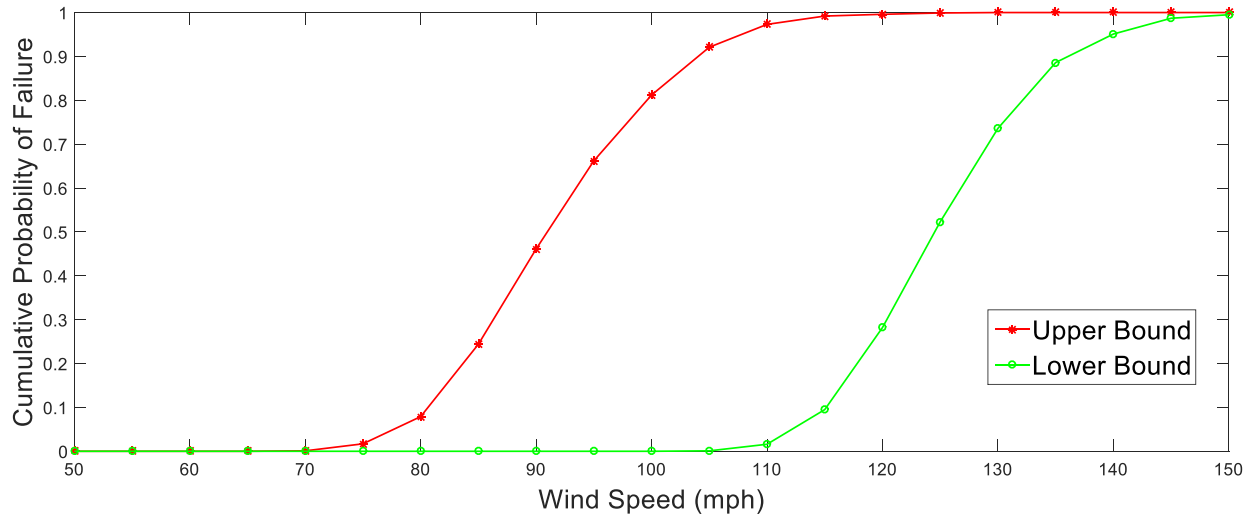


FIGURE 5. 36 – A2-BQ Roof panel fragilities; DS-4

Rafter-Sill Connection Failure

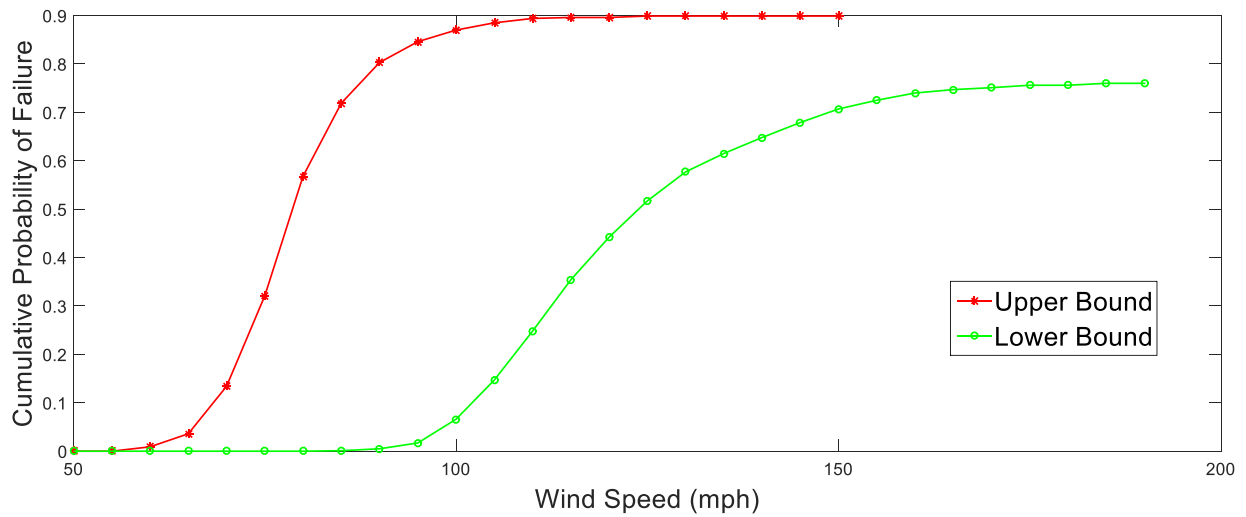


FIGURE 5. 37 – A2-BQ Rafter-sill connection fragilities; DS-1 – 4

Foundation Connection Failure

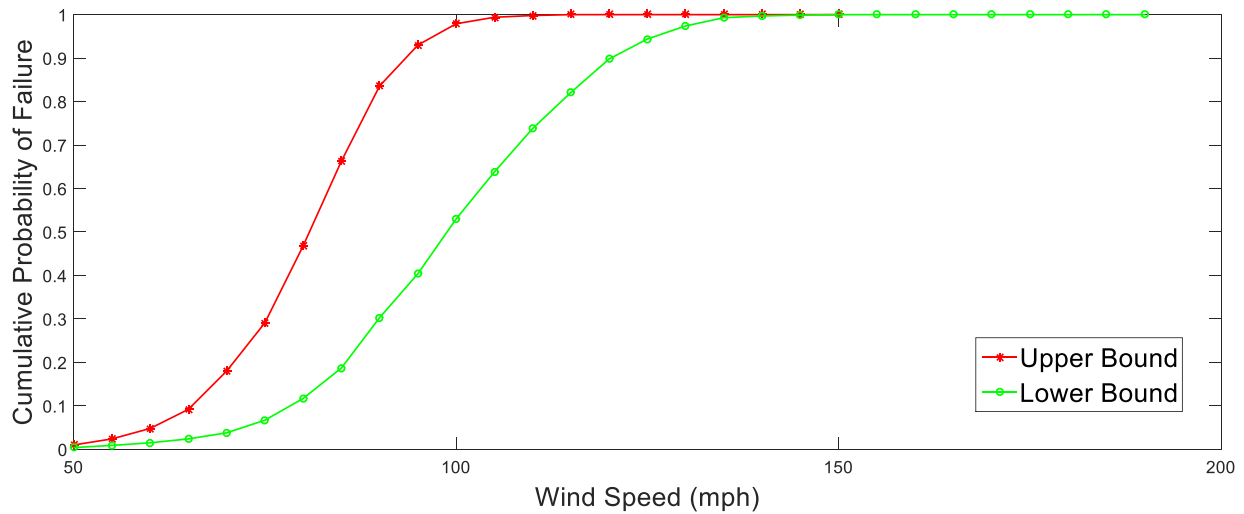


FIGURE 5. 38 – A2-BQ Foundation connection fragilities; DS-1 – 4

Observe that for A2-BQ, the shape of the fragility is different than it was for A1-BQ. This is because the pure shear foundation connection failure mode plays a significantly larger role for archetype 2 than it does for archetype 1 due to the significant increase in area subject to lateral wind pressures. Additionally, the combined uplift and shear mode is less prevalent due to the increased building dead load which acts to counter uplift.

Wall Sheathing Damage

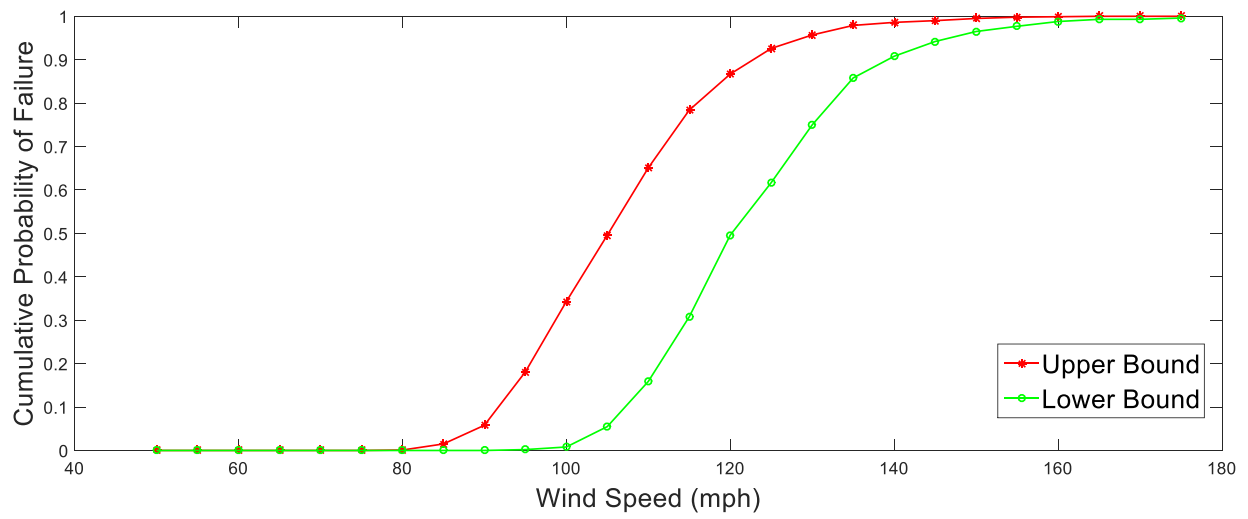


FIGURE 5. 39 – A2-BQ Wall sheathing fragilities; DS-1

Window/Door Pressure Damage

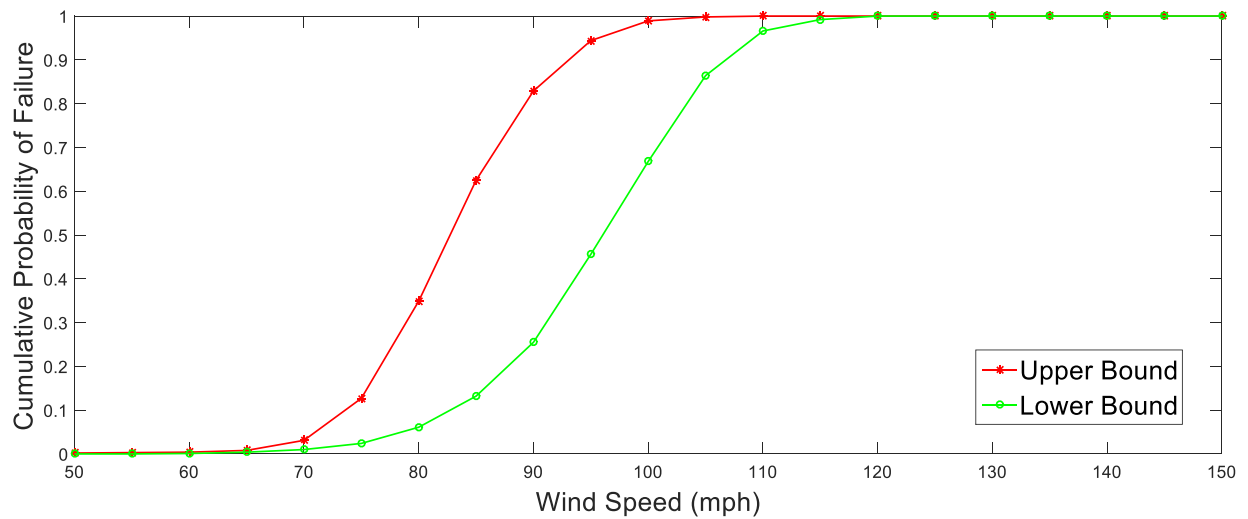


FIGURE 5. 40 – A2-BQ Window/door pressure fragilities; DS-1

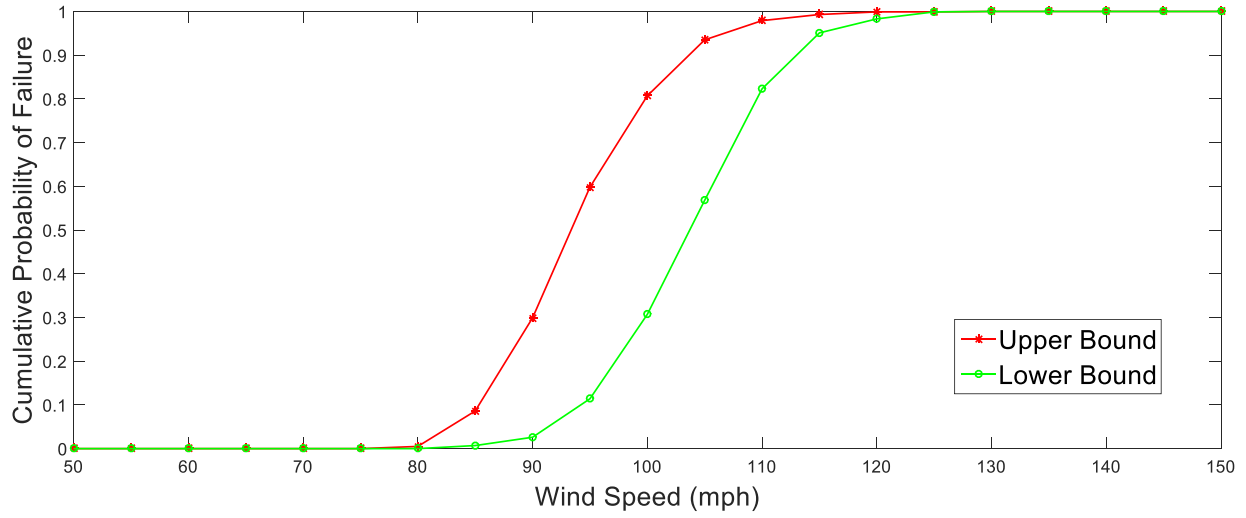


FIGURE 5. 41 – A2-BQ Window/door pressure fragilities; DS-2

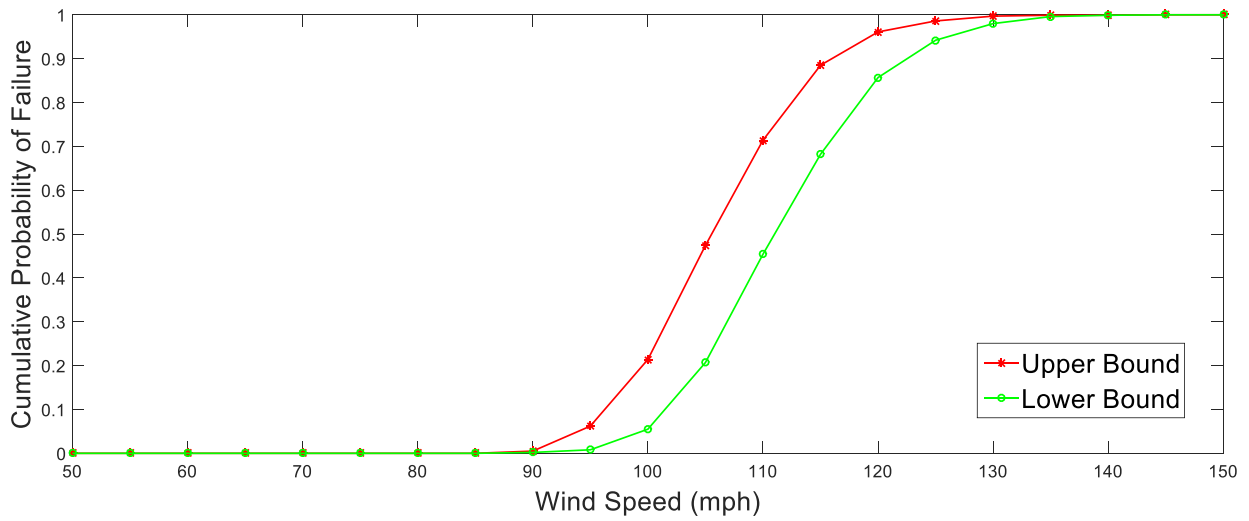


FIGURE 5. 42 – A2-BQ Window/door pressure fragilities; DS-3

Roof Cover Damage

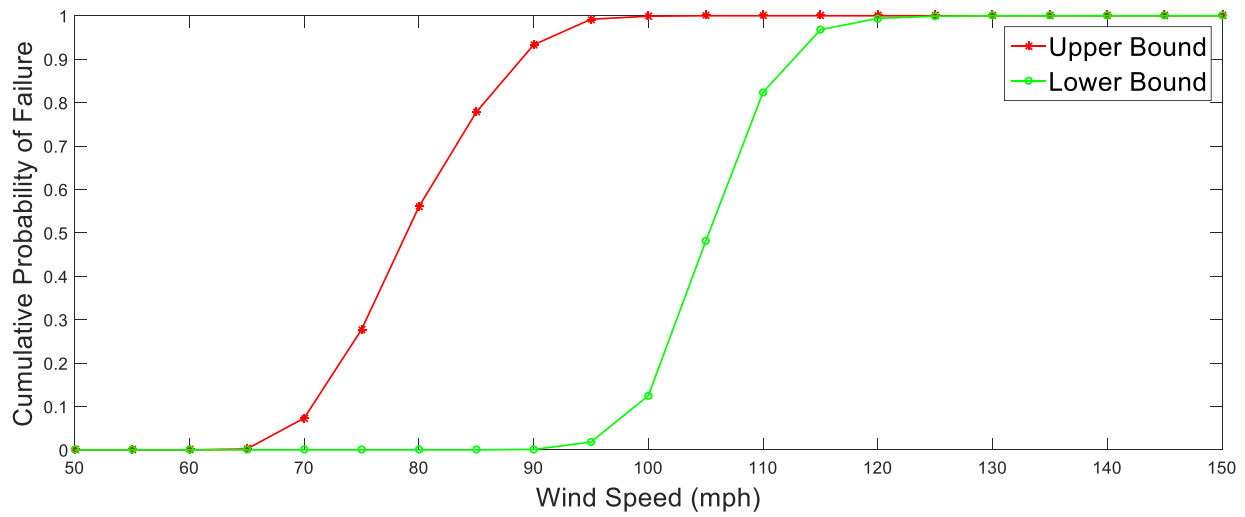


FIGURE 5. 43 – A2-BQ Roof cover fragilities; DS-1

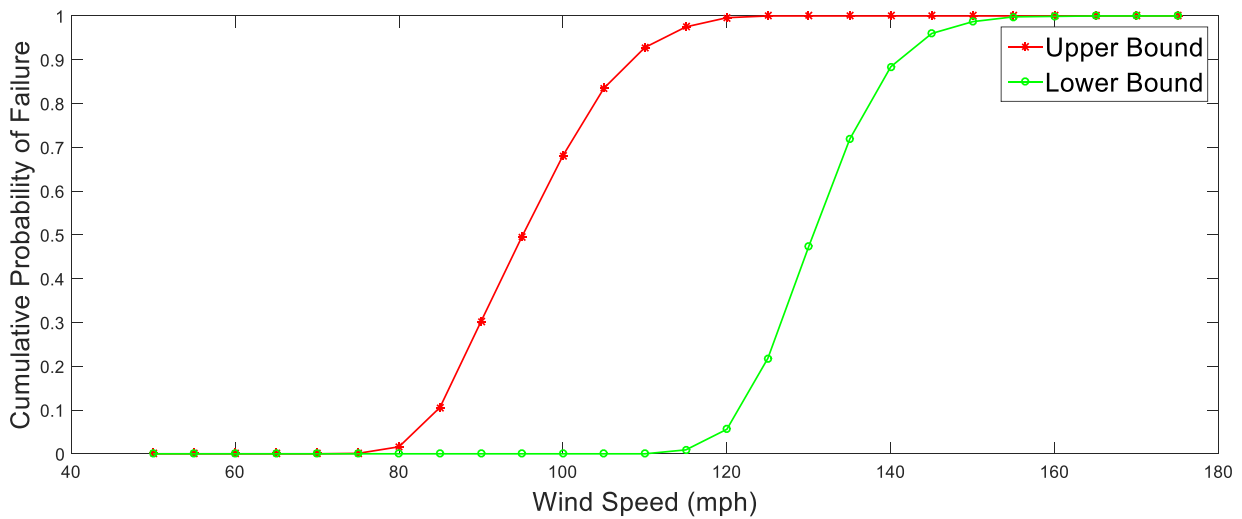


FIGURE 5. 44 – A2-BQ Roof cover fragilities; DS-2

5.3.7.3 Archetype A3-BQ Component Fragilities

Roof Panel Failure: See the A1-BQ fragilities (Figures 5.21 – 5.24).

Rafter-Sill Connection Failure: See the A1-BQ fragilities (Figure 5.25).

Foundation Connection Failure

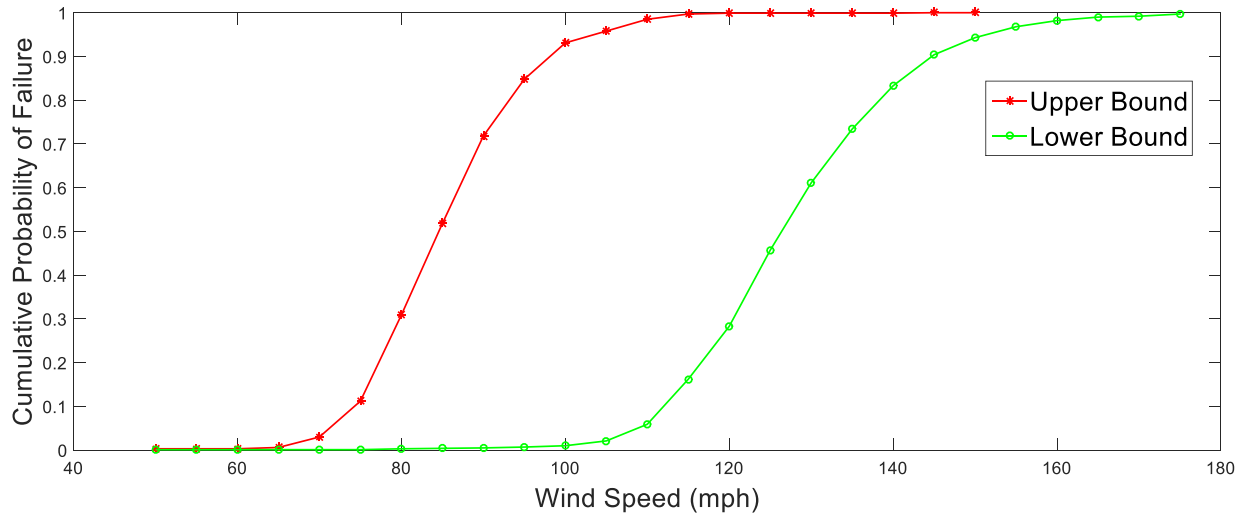


FIGURE 5. 45 – A3-BQ Foundation connection fragilities; DS-1 – 4

Wall Sheathing Damage

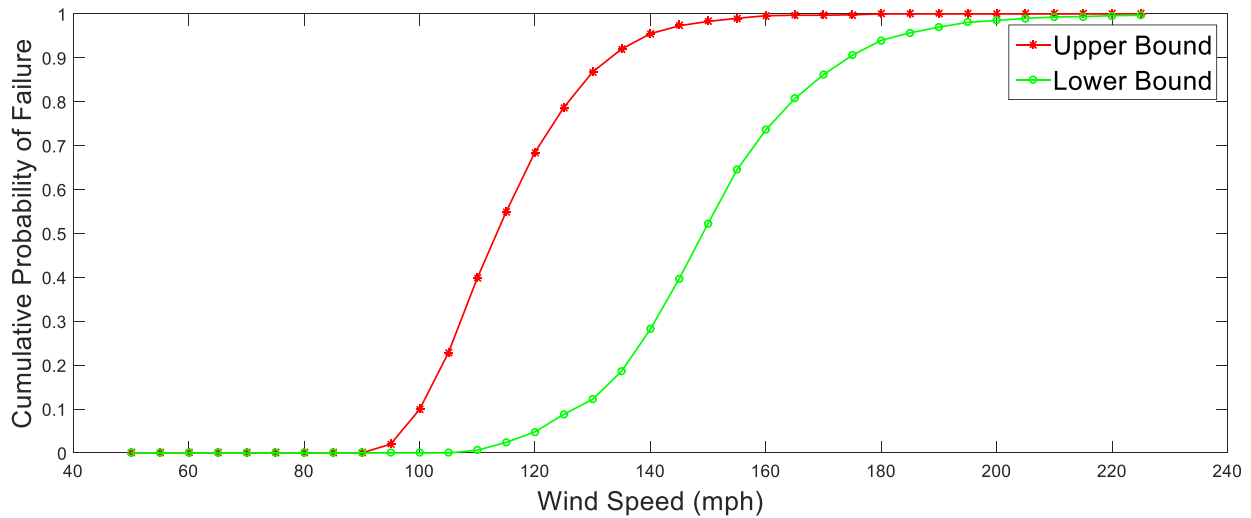


FIGURE 5. 46 – A3-BQ Wall sheathing fragilities; DS-1

Window/Door Pressure Damage

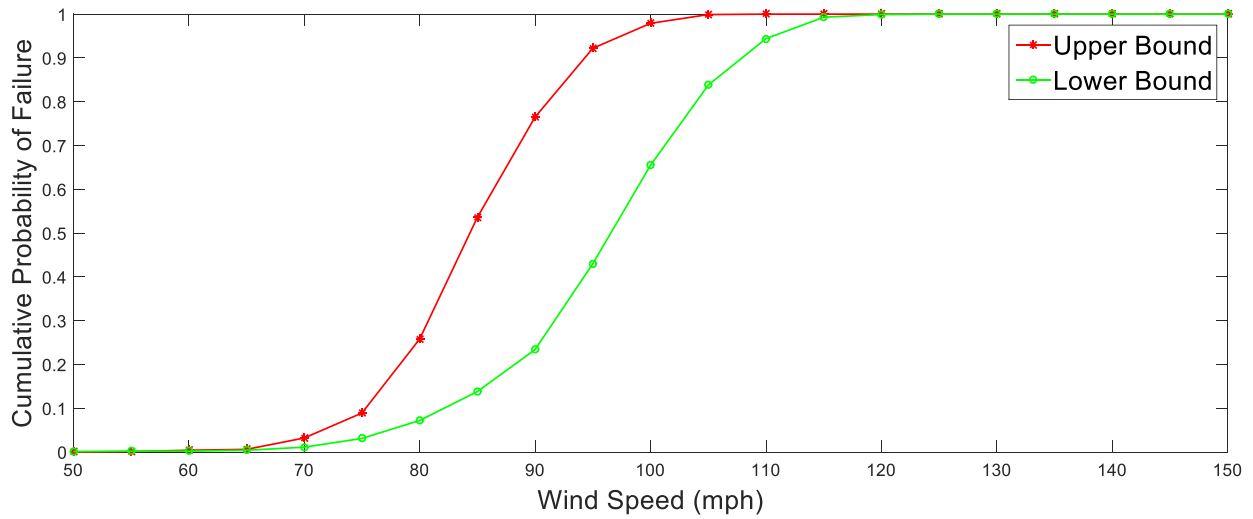


FIGURE 5. 47 – A3-BQ Window/door pressure fragilities; DS-1

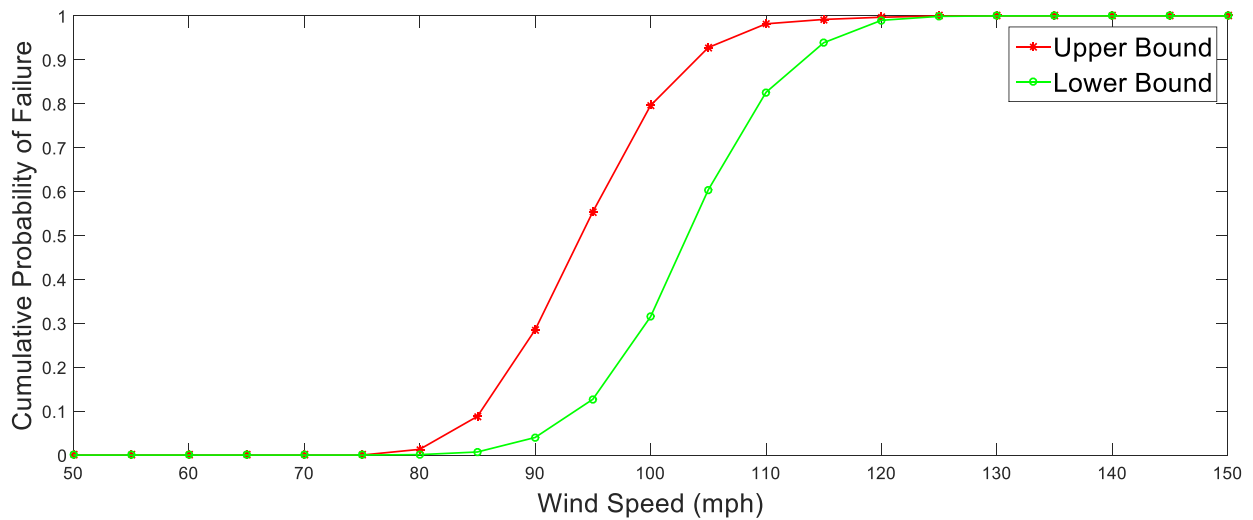


FIGURE 5. 48 – A3-BQ Window/door pressure fragilities; DS-2

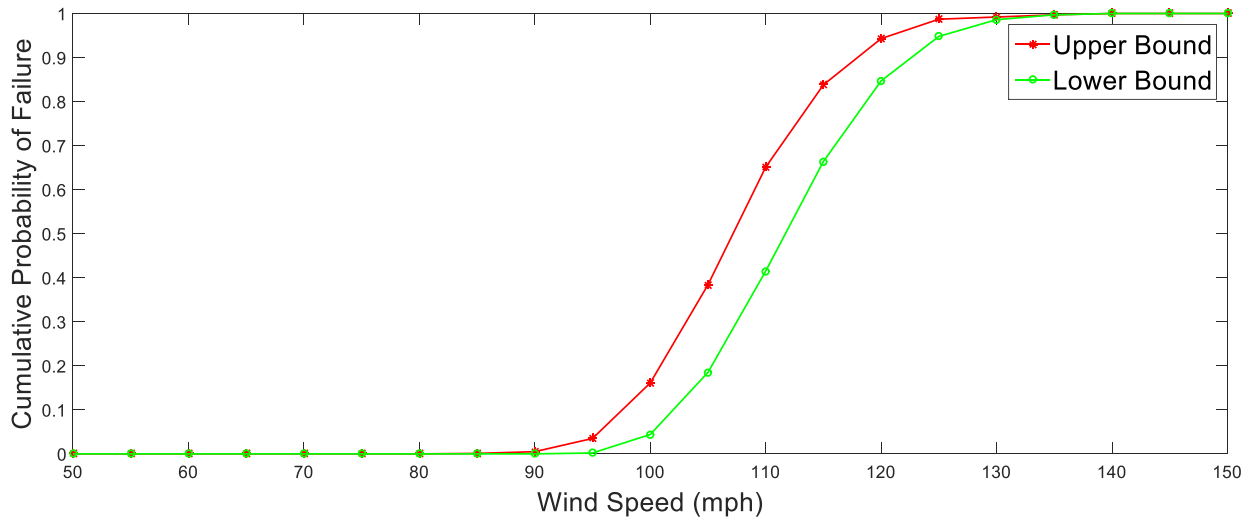


FIGURE 5. 49 – A3-BQ Window/door pressure fragilities; DS-3

Roof Cover Damage: See the A1-BQ fragilities (Figures 5.31 and 5.32)

5.4 Building System Level Fragility Analysis

The total building damage fragilities for damage states slight, moderate, extensive, and complete are shown in this section for each archetype for the upper and lower bound wind pressure cases respectively. Considerations for the wind borne debris breach case are made only for A1-BQ, per the assumptions discussed previously in this chapter. The target fragilities that are shown for comparison are the targets for the “enhanced” CQL.

5.4.1 Archetype A1-BQ Building System Fragilities

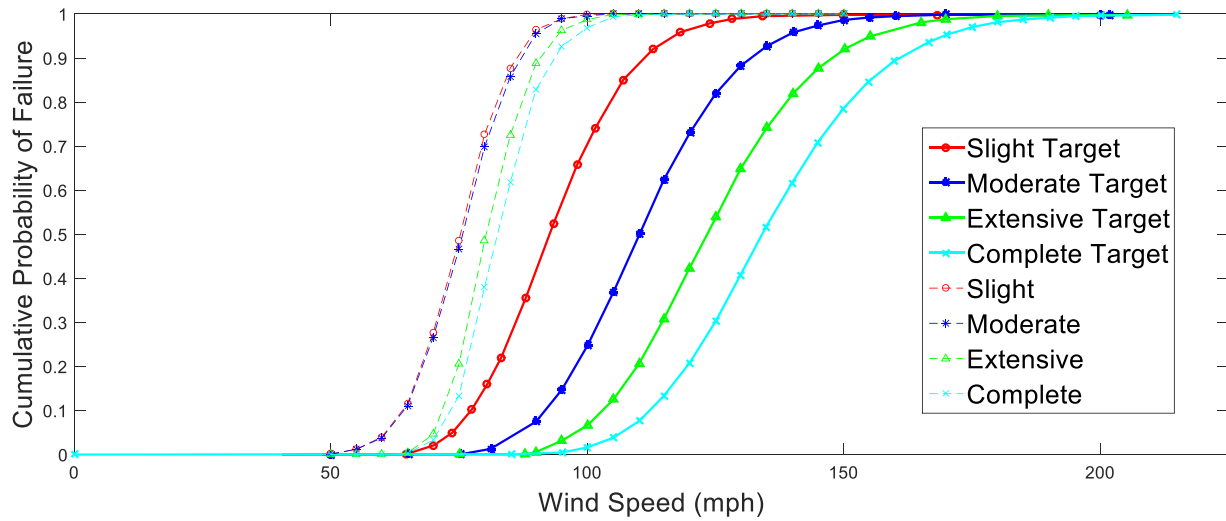


FIGURE 5. 50 – A1-BQ upper bound damage fragilities w/out windborne debris breach

The A1-BQ upper bound damage fragilities are significantly deficient relative to the target fragilities. The reasons for these deficiencies will be discussed in Chapter 6, along with proposed improvements that can help the fragilities meet their targets.

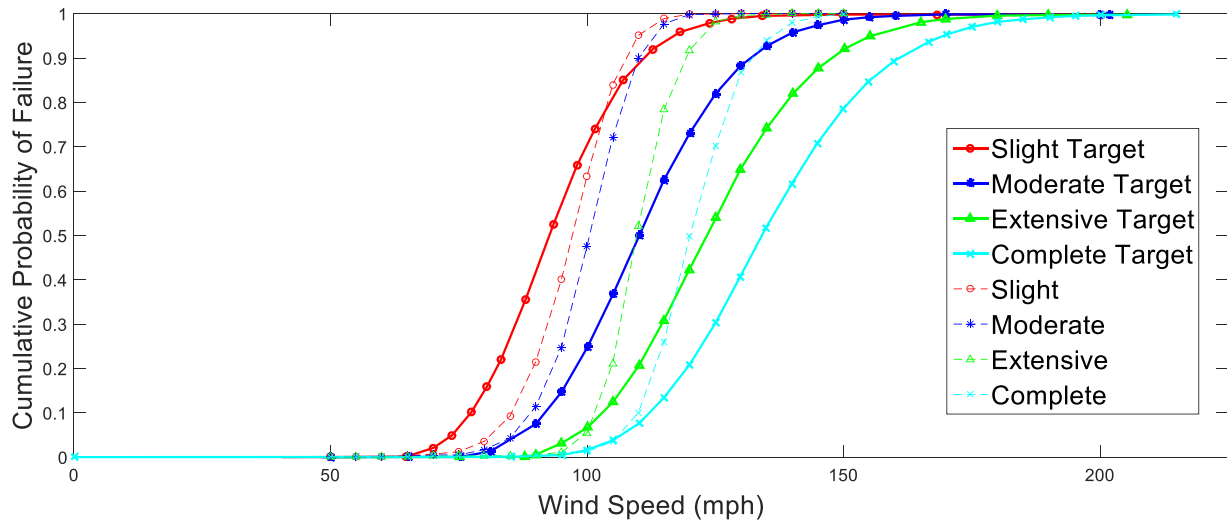


FIGURE 5.51 – A1-BQ lower bound damage fragilities w/out windborne debris breach

As expected, the lower bound fragilities are significantly closer to the targets because the Haan tornado factor is not included for the lower bound case, this is evident by comparison of Figures 5.50 and 5.51. The fragilities are however still deficient.

Figures 5.52 and 5.53 show the fragilities considering envelope breach by windborne debris compared to the fragilities not considering windborne debris breach. The fragilities are shown for the upper and lower bound cases respectively.

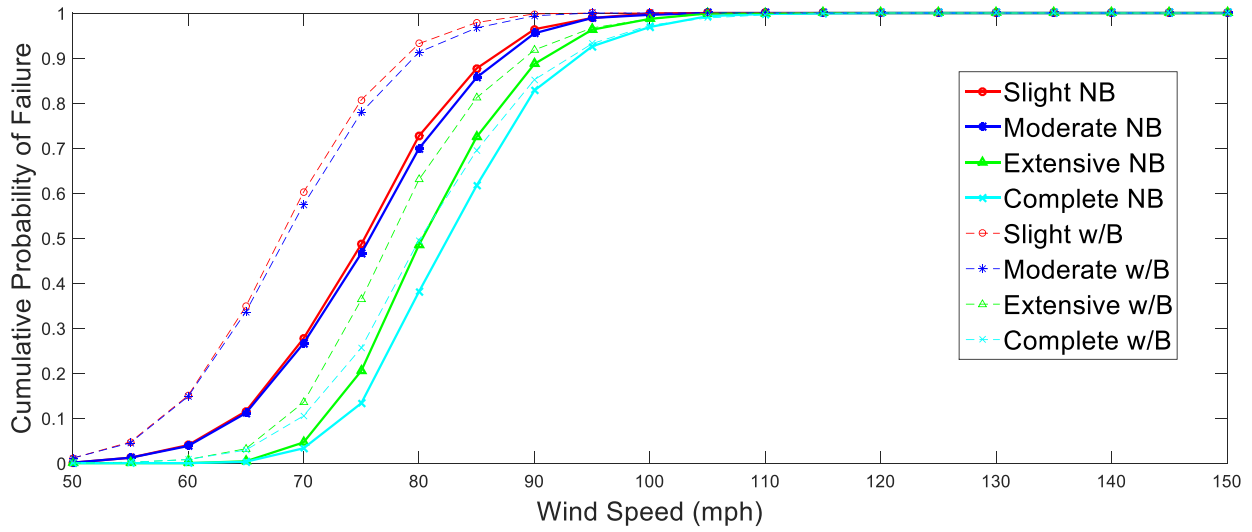


FIGURE 5.52 – A1-BQ upper bound fragility comparison; no debris breach *versus* debris breach cases

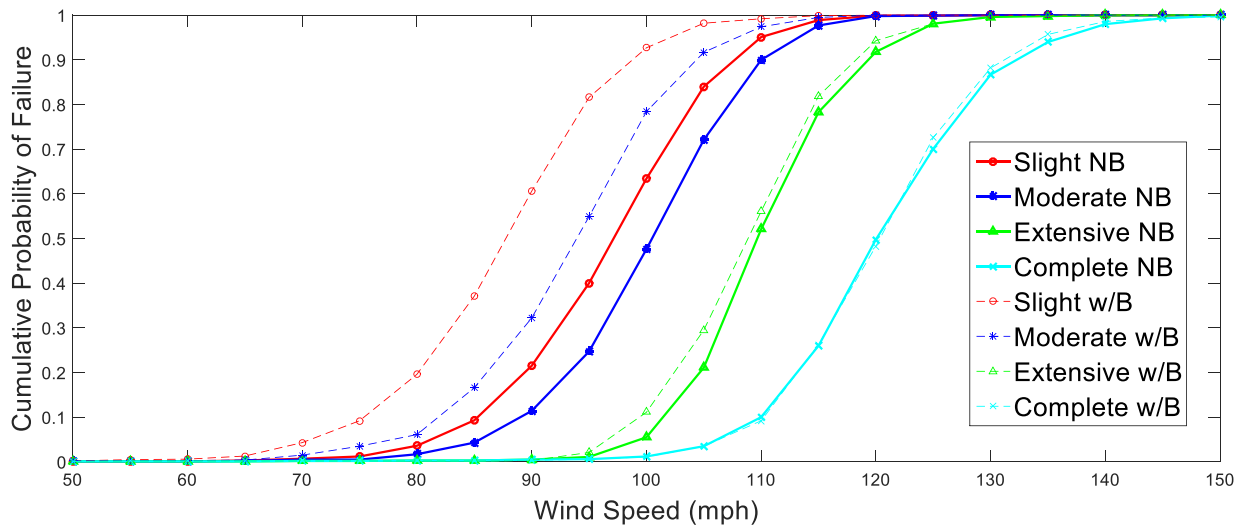


FIGURE 5.53 – A1-BQ lower bound fragility comparison; no debris breach *versus* debris breach cases

5.4.2 Archetype A2-BQ Building System Fragilities

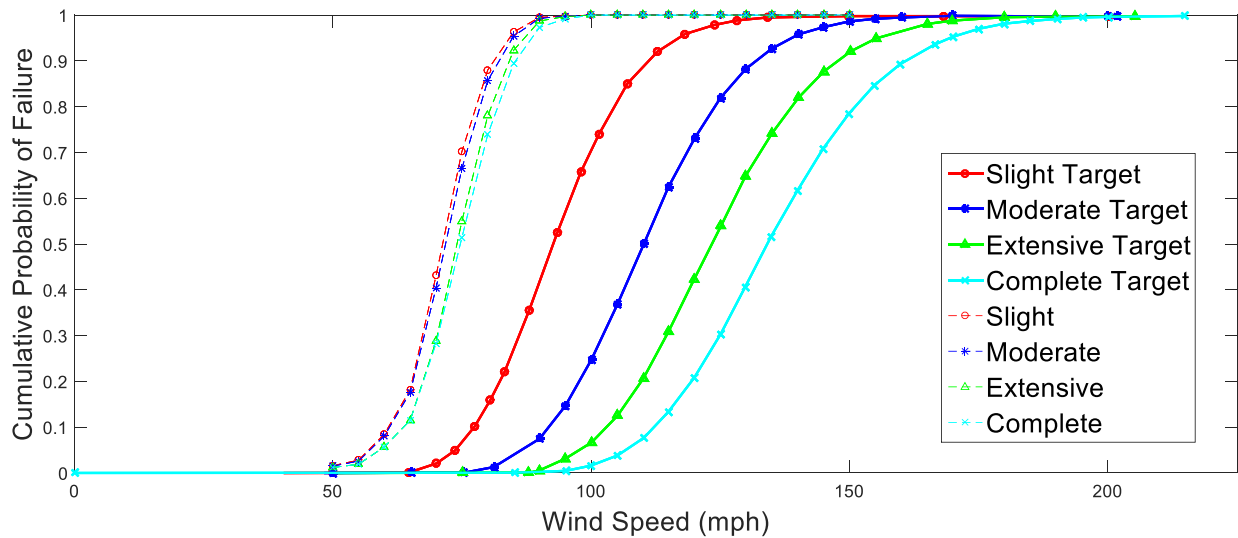


FIGURE 5.54 – A2-BQ upper bound damage fragilities

Again, it is obvious that the A2-BQ upper bound damage fragilities are significantly deficient with respect to the targets. The A2-BQ upper bound fragilities are even slightly left of the A1-BQ fragilities. There are several reasons for these deficiencies which relate primarily to both the roof and foundation components. The roof C&C pressure zones for archetype 2 include zone-3, which was neglected for archetype 1 per ASCE 7-10 specifications. Including the higher pressure zone 3 causes roof panels and shingles to fail begin to fail at slightly lower wind speeds, directly effecting the “slight” and “moderate” damage states and indirectly effecting the more severe damage states by causing the internal pressure coefficient to rise at lower wind speeds. The roof MWFRS pressures are also slightly higher for the A2 gable roof per ASCE 7-10, which causes the rafter-sill connections to fail earlier on. Finally, the foundation connection is also more susceptible to failure for A2-BQ because, while the MWFRS wall pressures do not change from archetype 1, the pressures act over twice the wall area. This causes the foundation connection

failure in pure shear (prior to uplift overcoming the building dead load) to become a bigger issue than it is for archetype 1. This explains why the increased building dead load, with its contribution to overall building stability, does not result in better foundation connection performance. The A2-BQ deficiencies will be discussed further in Chapter 6, along with proposed improvements that can help the fragilities meet their targets.

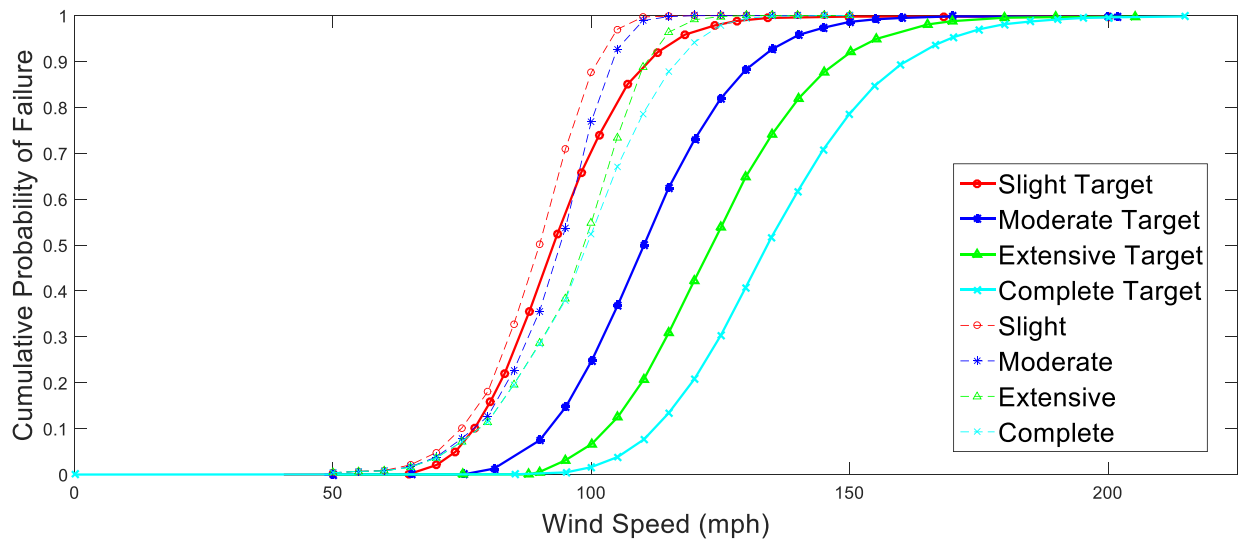


FIGURE 5.55 - A2-BQ lower bound damage fragilities

As expected, the lower bound fragilities are significantly closer to the targets because the Haan tornado factor is not included for the lower bound case. The fragilities are however still deficient.

5.4.3 Archetype A3-BQ Building System Fragilities

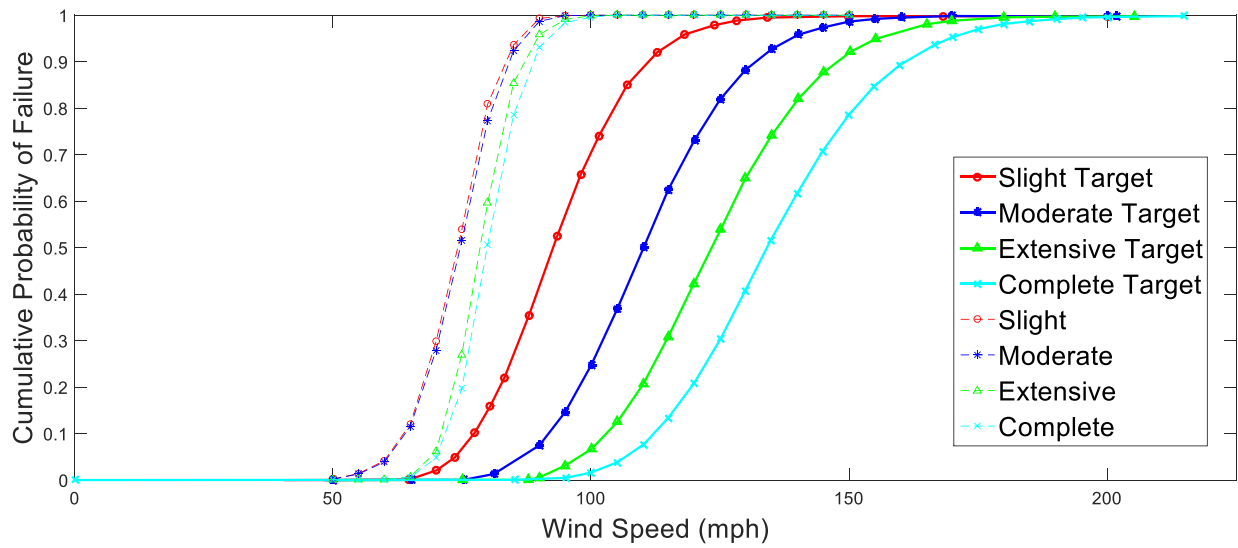


FIGURE 5.56 - A3-BQ upper bound damage fragilities

The A3-BQ upper bound damage fragilities are deficient relative to the target fragilities. Moreover, observe that the A3-BQ fragilities are similar to the A1-BQ fragilities due to the similarities between the two buildings. The A3-BQ deficiencies will be discussed further in Chapter 6, along with proposed improvements that can help the fragilities meet their targets.

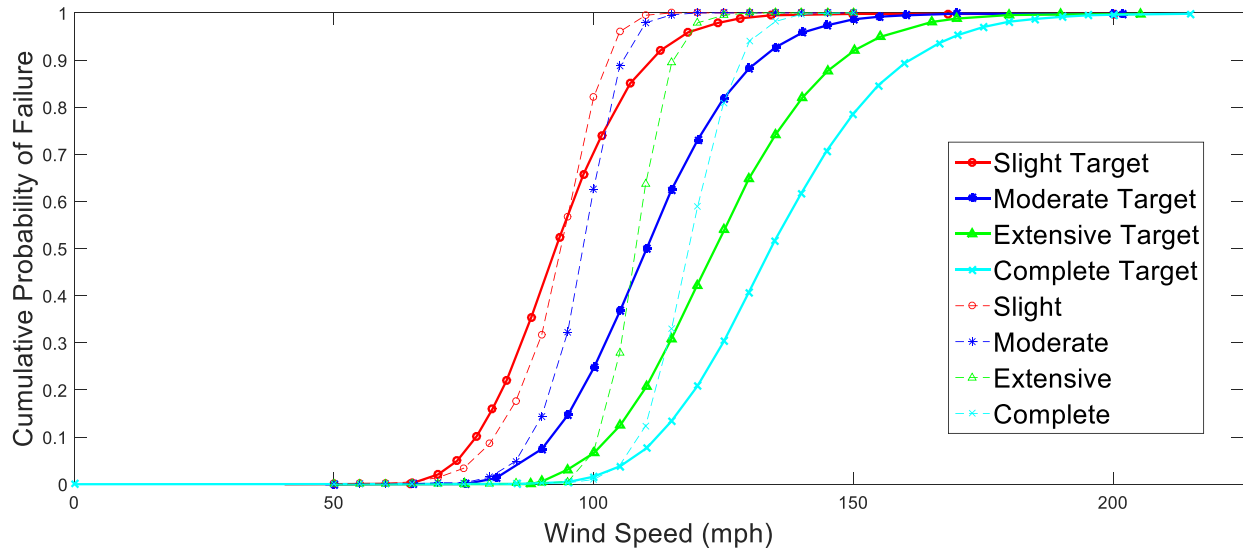


FIGURE 5.57 – A3-BQ lower bound damage fragilities

Again, as expected, the lower bound fragilities are significantly closer to the targets because the Haan tornado factor is not included for the lower bound case. The fragilities are however still deficient.

5.4.4 Building System Fragility Archetype Comparison

Figures 5.58 – 5.61 show comparisons of the upper and lower bound fragilities for archetypes A1-BQ, A2-BQ, and A3-BQ for each damage state.

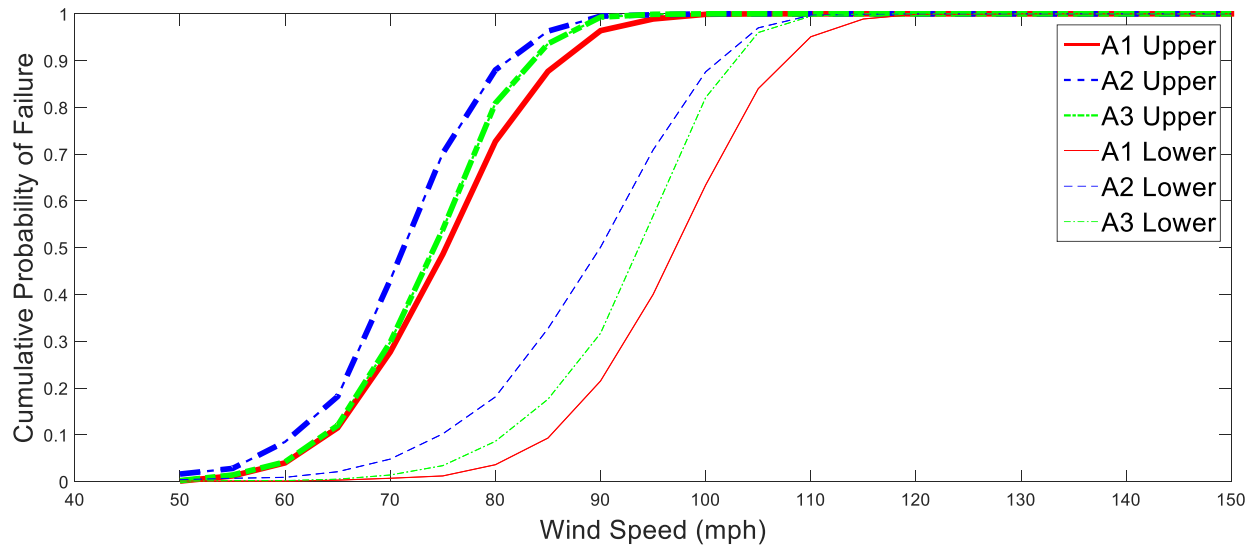


FIGURE 5.58 – DS-1 building system fragility archetype comparison

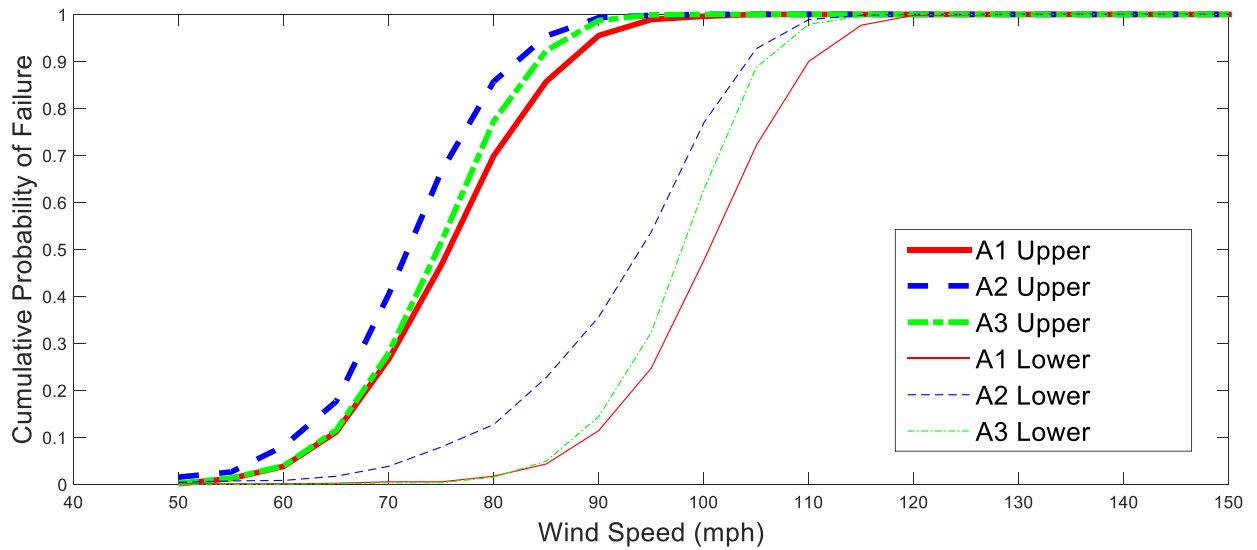


FIGURE 5.59 - DS-2 building system fragility archetype comparison

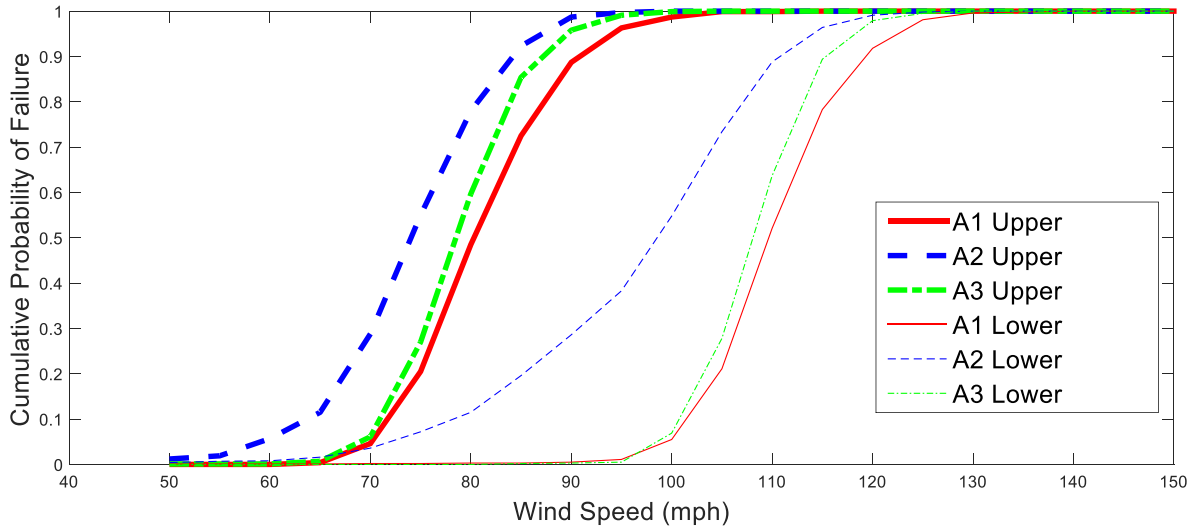


FIGURE 5. 60 - DS-3 building system fragility archetype comparison

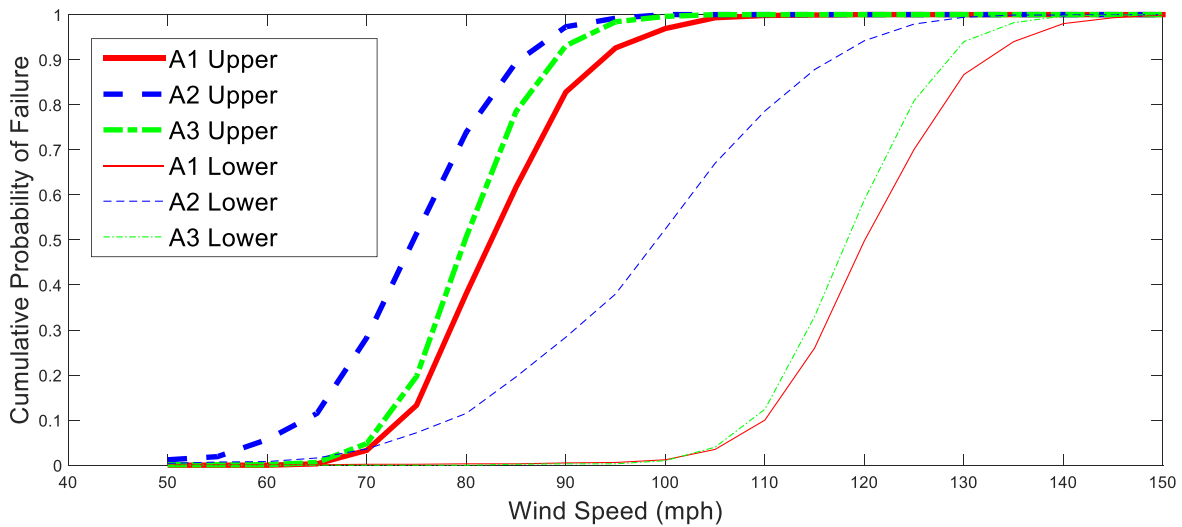


FIGURE 5. 61 - DS-4 building system fragility archetype comparison

To summarize the findings of the building system fragility analyses, several things are clear;

- (1) the building system archetypes are all deficient in comparison to even the lowest of the performance targets (enhanced quality);
- (2) performance under the lower bound wind pressure

case is significantly better than performance under the upper bound case but the basic quality archetypes are deficient under both cases and; (3) There is not a large difference in the performances of the three building system archetypes considered herein.

Another important observation about both the components and building system performance for the basic CQL is that the anticipated failure wind speeds appear to be low in comparison to those found in other studies such as Roueche et al. (2017). Differences in the definition of damage states could partially explain such discrepancies, but the larger issue is perhaps related to the tornado amplification factor used to modify the ASCE 7-10 wind pressures. Roueche et al. (2017) proposed the use of amplification factors that are significantly lower than the Haan factors used in this study. As can be seen by comparison of the upper and lower bound wind pressure case fragilities, the level of amplification assumed for tornado wind pressures can have a large effect on the damage state fragilities. Therefore, if the Haan factors over-predict this amplification, the effect could be a significant leftward shift of the fragilities.

5.5 Masonry Basement Wall Mean Value Analysis and Statistical Modeling

This section describes the ABAQUS mean value analysis and MATLAB statistical modeling methods used to quantify the performance of the basic quality masonry block wall subject to expansive soil pressures. The methods herein are similar to those used for the building system and its components but differ slightly. As for the building system, the ABAQUS mean value runs are performed using the mean expansive soil and masonry block wall strength parameters discussed in Chapters 2 and 3 respectively. The statistical analysis is performed using the USDA soil survey data for Cleveland County, OK, and the statistical strength parameters for concrete block and mortar found in Chapter 2. The variation in the composite masonry block wall strength

is accounted for by the variation in the individual block and mortar components. The random block and mortar strengths generated in a Monte-Carlo analysis will be converted to a composite wall resistance using the methods discussed in Chapter 3.

The approach to the ABAQUS mean value analysis for the masonry block wall is essentially the same as it was for the building system and its components. The statistical analysis for the masonry block wall differs from the building system statistical analysis more significantly. Instead of constructing fragility curves for the basement wall, the probability of failure for a basement constructed at a random location in Cleveland County is calculated. As discussed briefly in Chapter 2, this approach assumes that each soil type surveyed by the USDA at the 81 locations in Cleveland County has an equi-probable chance of occurring at a given building site. The locations, 1-81, are given a uniform probability distribution and sites are randomly selected in the Monte-Carlo simulations. The relevant soil parameters that govern the soil pressures exerted on the wall correspond to the USDA soil parameters for the randomly selected site. There is no specified target for reliability associated with the basement wall performance as there was for the building system. Therefore, in this study, we will assume that a reasonable performance target is a 2% probability of damage, i.e. only 1 out of every 50 masonry block wall basements constructed in Cleveland County will experience damage due to expansive soil pressures. This value should be modified in future work to optimize reliability.

5.5.1 Masonry Block Basement Wall Mean Value Analysis

To quantify damage to the masonry block basement wall, a mean value analysis was performed on the long (40') side of the typical basement wall. Only the long wall was considered because both walls are subject to the same pressures, but the long wall has a larger unsupported

length, making it more critical than the short wall. Because each archetype has virtually the same basement one analysis is considered to be sufficient for all three. The basement for archetypes 1 and 2 is identical and for archetype 3 it varies slightly (assuming the basement underlies the entire building footprint) but still consists of a series of 40' and 30' long walls.

In the ABAQUS analysis, each wall is assumed to be restricted by pinned connections along the bottom and sides. This is consistent with the assumptions made for the validation of the masonry block wall model discussed in Chapter 4, assuming mortar joints connect the wall to the slab and to intersecting walls at the corners of the building. The top boundary condition consists of anchor bolts cast in mortar which connect the basement wall to the bottom sill plate of the building. It is assumed that this connection behaves as “fixed” because the moment resistance allowed by the cast in-place anchors is presumably larger than the moment resistance provided by the mortar joints at the other boundaries and, as shown in Chapter 4, the mortar joint itself performs at a level somewhere between that of a pure fixed and pure pinned connection. Therefore an improvement in the connection’s moment resistance should bring it closer to the idealized fixed condition.

The mean value analysis is used to derive the relationship between total wall load and the maximum tensile stress generated in the wall. This relationship is shown in equation 5.40.

Total Basement Wall Load – Maximum Stress Conversion

$$S_{max} = (M_{Swell}W_{Swell} + M_{At-Rest}W_{At-Rest})L_T; \quad (5.40)$$

where S_{max} is the maximum tensile stress generated in the wall in ksi and W_{Swell} and $W_{At-Rest}$ are the weights of swell load and at-rest load taken by dividing each individual load by the total load, L_T in kips. M_{Swell} and $M_{At-Rest}$ are the Swell and At-Rest pressure factors determined by ABAQUS

analysis to best fit the basement wall load-maximum stress relationship. For the typical case, M_{Swell} and $M_{at-Rest}$ are equal to 0.0068 and 0.0081 respectively. Tensile stress is the primary concern because both the masonry wall validation and the ABAQUS mean value analysis revealed that tensile damage is the controlling damage mode under out of plane pressure loading.

As shown in Chapter 3, the strain associated with the peak tensile stress from the stress-strain curve is the strain at which the onset of tensile damage occurs. In other words, the onset of tensile damage is associated with the peak tensile stress. For this analysis, the onset of damage constitutes failure. The mean value analysis was performed for several cases considering various swell to at-rest loading ratios. This was done to determine whether or not a change in the soil pressure profile shape would have an effect on the wall load-maximum tensile stress relationship. It was determined that the relationship identified in equation 5.40 is valid at any swell to at-rest pressure load ratio.

The static ABAQUS mean value analysis terminates shortly after the stress-strain relationship becomes nonlinear. This is not a problem because the nonlinearity does not occur until after the peak allowable tensile stress is reached; thus, the wall load-maximum tensile stress relationship is captured through the point of peak allowable tensile stress and consequently up to point of damage initiation. Since we do not need to quantify anything past the point of damage initiation, capturing the behavior up to the point of peak allowable tensile stress is sufficient.

The ABAQUS mean value analysis shows that the lower portion of the center of the wall is the spot that is most susceptible to tensile damage. Figure 5.62 illustrates the gradation of tensile damage in the wall under mean swell and at-rest pressure conditions.

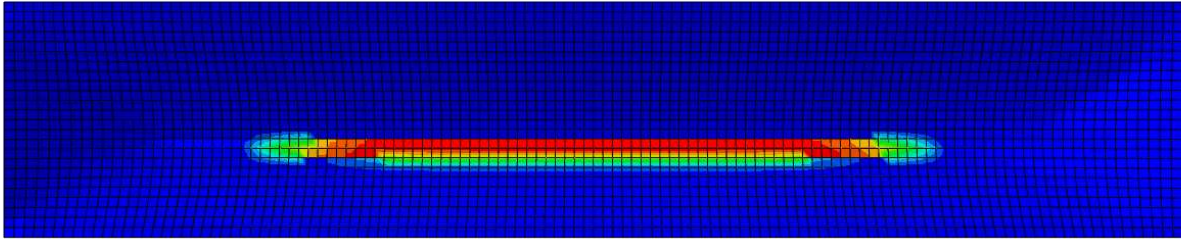


FIGURE 5. 62 – Tensile damage gradation: masonry block basement wall

When the swell pressure is removed, the damage gradation looks similar but is shifted slightly lower on the wall because the triangular at-rest soil pressure profile has more influence when acting alone than it does when coupled with the significantly larger, rectangular swell pressure profile.

Under mean conditions, the ABAQUS analysis revealed that the typical, unreinforced masonry basement wall is significantly deficient to resist damage due to expansive soil pressures. The basement wall was able to withstand a total load of approximately 73 kips (acting over 320 sf of wall) which is equivalent to approximately 19% of the total wall load that is exerted on the basement wall. Without the swell pressures considered, the basement wall survives at-rest pressure loading free of damage under mean conditions.

It was expected that the unreinforced masonry basement walls would be insufficient to withstand the swell pressures associated with expansive soils in the Norman region based on the lack of basements and other underground structures that are currently built in Norman and other areas that are prone to expansive soils. There two additional considerations that may help to explain the modeled deficiencies; (1) the wall chosen to represent “typical quality” is totally unreinforced by rebar and (2) the bottom and side boundary conditions are assumed to be pinned

and, as shown in Chapter 4, this is a conservative assumption that reduces modeled damage resistance.

5.5.2 Masonry Block Basement Wall Statistical Analysis

For the purposes of the Monte-Carlo simulations, the relationship in equation 5.40 allows us to convert random expansive soil pressure loading to random maximum wall tensile stress. We then get the random peak allowable tensile stress by following the methods discussed in Chapter 3 using the random block and mortar strength parameters given in Chapter 2. If the random tensile stress generated in a given iteration of the Monte-Carlo simulation exceeds the peak allowable tensile stress, the basement wall is considered to have been damaged for that iteration. A 100,000 sample Monte-Carlo simulation is used to evaluate the probability of failure for the typical unreinforced masonry block basement wall because the statistical model is computationally inexpensive.

The statistical analysis for the unreinforced masonry block basement wall revealed that there is virtually no chance of such a wall going undamaged in Norman, OK. Even considering at-rest soil pressure alone, the analysis determined that there would be about a 20% chance that the wall sustains damage. These results are consistent with the results of the ABAQUS mean value analysis. Again, the large deficiency may be explained in part by considering the lack of any form of reinforcement, the conservative assumption of pinned boundary conditions, and the fact that many people in regions similar to Norman often do not construct basements due to the likelihood of expansive soil damage.

It is clear from both the mean value and statistical analyses that the unreinforced masonry block basement wall lacks the tensile strength to withstand the expansive soil pressure loads

expected in Norman without sustaining damage. The composite tensile strength of the wall is the minimum of the concrete block tensile strength and the mortar bond strength. Generally, the mortar bond strength controls. This deficiency was anticipated due to the lack of tensile strength available in concrete and similar cementitious materials such as mortar. In Chapter 6, reinforcement strategies and other mitigation techniques to improve the wall performance will be discussed.

CHAPTER 6

PROPOSED BUILDING IMPROVEMENTS

6.1 Building System Improvements to Meet Target Fragilities

Potential building enhancements necessary to upgrade each basic quality archetype to meet the *Enhanced*, *Improved*, and *Resistant* performance targets are outlined herein. The purpose of this chapter is to highlight the weak points of each basic CQL archetype and indicate enhanced construction techniques and components that could be implemented at the current state of the art of residential building construction in order to meet the performance targets. Cost optimization of these enhancements is beyond the scope of this study but should be explored in future studies to reach an ideal balance between implementation costs and community resiliency and sustainability benefits.

Each CQL is considered to be met when the fragility obtained following building enhancement is either on top of, or shifted right of the target fragility. Because the calculated fragilities and target fragilities do not always share the same shape or slope, a critical value of the cumulative failure probability must be identified such that meeting or exceeding the target value at that point constitutes successfully meeting the target. It is assumed that this critical point is located at the tenth percentile of the cumulative probability distribution of the target fragilities. This assumption is based on the work of the ATC-63 project, in which it was concluded that an “*acceptably low probability of collapse is interpreted to be less than a 10% probability of collapse under the MCE (maximum considered event) ground motions*”. Because we do not currently have information about the maximum considered tornado (MCT) events at given locations, it is assumed that meeting the targets at the 10% fragility value will achieve

conservative but risk-consistent performance for the building portfolios. This assumption should be examined further in future work to validate the assumption or to determine a more appropriate value when evaluating tornado risk for light wood frame construction.

Considering the performance target matching criterion discussed above, Table 6.1 shows the tenth percentile fragility values for damage states slight, moderate, and complete for the lower bound case of A1-BQ in contrast to the tenth percentile fragility values for comparable damage states minor, moderate, and severe from Li (2005) for a building meeting minimum hurricane protection standards. The Li (2005) building is similar to A1-BQ in size (30'x40' *versus* 28'x40'), height (13' *versus* 12.5'), and construction (light wood frame residential). Li (2005) performed the analysis considering hurricanes, not tornados which is the reason that the lower bound case for A1-BQ is being considered. The lower bound case uses wind pressures determined directly from ASCE 7-10 without any amplification, so the wind pressures are calculated the same way that they would be if considering hurricane wind pressures; thus the lower bound case is similar to the case considered by Li (2005). Additionally, the definitions of the damage states used by Li (2005) differ from the ones used in this study, so for the sake of comparison, the A1-BQ values presented in Table 6.1 are the tenth percentile fragility values for the damage state definitions used by Li (2005), not the ones defined at the beginning of Chapter 5. The Li (2005) damage states are defined as follows; *Minor* – “one roof panel uplifted”, *Moderate* – “failure of two or more glass panels in windows or doors, combined with removal of at least one roof panel”, *Severe* – “failure of the roof-to-wall connection”.

TABLE 6. 1 – 10th percentile failure wind speed comparison; A1-BQ lower bound *versus* Li (2005)

Building	$V_{10\%}$ (mph)		
	Minor	Moderate	Severe
A1-BQ	90	95	122
Li (2005)	83	92	125

Observe that the values for the two studies are very comparable, especially for the moderate and severe damage states. Considering the discrepancies in the methods used to construct the damage fragilities, these values seem to be in good agreement. This serves as an additional check on building performance at the system level.

In addition to the similarities to the Li (2005) study, the upper and lower bound wind pressure case fragilities for damage states Slight, Moderate, and Complete bound the tenth percentile values for comparable damage states DOD2, DOD4, and DOD5 from Roueche et al. (2017). As discussed in Chapter 5, Roueche et al. (2017) uses tornado amplification factors that are significantly lower than those used for the upper bound case in this study. As such, it is sensible that the Roueche values fall between the upper and lower bound case values for this study. Figure 6.1 demonstrates this.

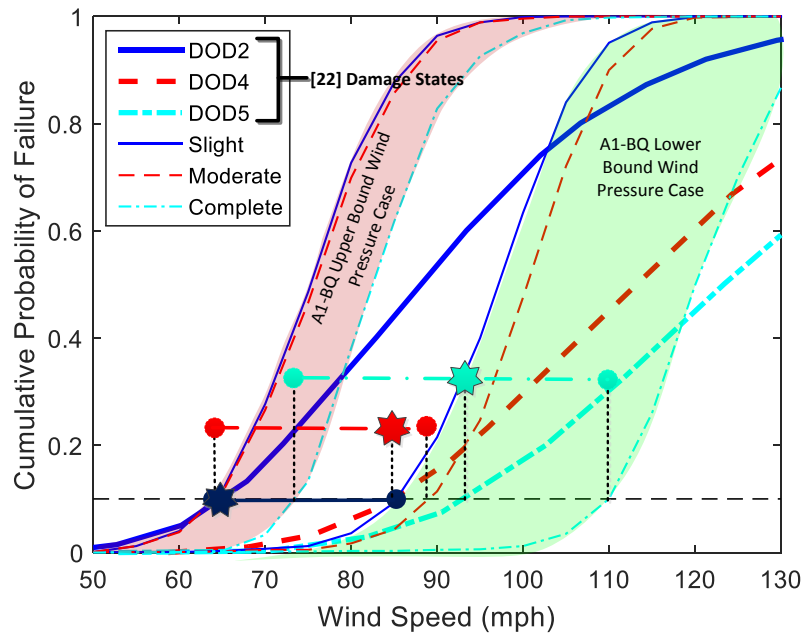


FIGURE 6. 1 - A1-BQ upper and lower bound fragilities versus Roueche et al. (2017) comparable damage states

The increase in component resistance for some of the improvement techniques is estimated because the experimental data available to quantify the performance of a wide variety of improvement techniques is limited. Ideally, all of these values would be validated experimentally as more research becomes available. The estimates and the assumptions used to formulate them are discussed herein. For components in which an anticipated failure mode is nail withdrawal such as rafter-sill connections and roof panel connections, two easily implemented component improvement methods are used. The first is to choose rafter or sill plate wood with a higher specific gravity than the basic quality SPF. This has been shown experimentally to increase nail pullout resistance, as discussed in Chapter 4. The relationship between specific gravity and pullout resistance given by equation 4.1 is used in this study to estimate the increased resistance associated with the use of higher specific gravity wood. The second is an increase in nail

diameter. It is assumed that nail pullout is a function of friction between the nail and the embedment wood and that the friction force is directly proportional to the contact area between the nail and wood. Therefore, increases in pullout resistance are assumed to be directly proportional to the increase in nail diameter. A nail sizing chart listing the diameters of nails of various size is provided in Appendix A, data on the specific gravity of various wood species can be found in Chapter 5 of the wood handbook (Kretschmann (2010)).

The roof panel connection can also be improved by decreasing the interior nailing pattern from 12" o.c. to 6" o.c. The estimated increase for this modification is assumed to be directly proportional to the number of nails used to fix the panel for each configuration. For the 12" interior spacing panels, a total of 33 nails are used and for the 6" interior spacing panels, 45 total nails are used. Therefore, the resistance increase is assumed to be $45/33$ (1.36).

Another component improvement that might be used specifically to strengthen the rafter to sill connections is the use of hurricane clips. Experimental data from Reed et al. (1997) is available for the uplift resistance of a single H2.5 hurricane clip. This data is compared to the recommended uplift loads from the manufacturer website which presumably has a factor of safety built in. For the use of different types of hurricane clips (made by the same manufacturer), the factor of safety associated with the H2.5 found by dividing the experimental mean strength found in Reed et al. (1997) by the manufacturer recommended load, is multiplied by the manufacturer recommended load for other hurricane clip models to find an estimated actual strength to be used in the model archetypes. The factor of safety for the H2.5 clip was found to be about 3. A list of various H2.5 hurricane clips and their recommended strength values is provided in Appendix A.

For the foundation connections, it is assumed that the equations defined by Alfano (2016) can be modified by a factor to account for changes in anchor bolt diameter and spacing. The connection strength is largely a function of the total area of steel that is in shear (lateral loading) and tension (uplift). Therefore, a factor is applied as shown in equation 6.1 to the equations given in Table 5.5 to account for increases in total steel area which is a function of both the number of bolts (spacing) and the diameter of the bolts.

Foundation connection resistance equation modification;

$$R = (-0.64 * S + 0.10 * F_{SA}) \quad (6.1)$$

where R is the uplift resistance in klf, S is shear in klf, and F_{SA} is the factor applied to account for changes in total area of steel. F_{SA} can be found simply by dividing the new area of steel in the foundation connection by the original area. The same factor is assumed to apply directly to the shear resistance for the case prior to uplift overcoming dead load, where the foundation connection is subject to pure shear as well. Observe that F_{SA} is not applied as a modifier to the product of the original equation but instead it is applied directly to a single variable in it. This is because the left side of the equation accounts for the reduction in uplift resistance due to applied shear and it would not make sense to effectively increase this reduction while increasing steel area. This method of estimating the foundation connection resistance increase has considerable uncertainty, due to the complex interaction between uplift and shear. However, there does not appear to be a definitive way to quantify the effect of increasing the foundation anchorage and so this method will be used as an estimate in this study. Future experimental testing of foundation connections with varying bolt spacings and diameters, etc. would be very beneficial in this area.

6.1.1 Enhanced Quality Target

The lowest of the target standards considered in this study, the *Enhanced* CQL target aims to improve life safety for light wood frame residential buildings subject to tornado hazards.

Damage state fragilities for versions of each archetype that meet the Enhanced quality targets, tables listing the improvements made to the archetypes, and brief summaries of the component deficiencies and proposed solutions are provided in this section.

6.1.1.1 Archetype A1

TABLE 6. 2 – A1 enhanced quality improvements

ARCHETYPE I ENHANCED QUALITY BUILDING IMPROVEMENTS - UPPER BOUND			
Component	Initial Condition	Modification	Nominal Strength Increase
Roof Panels ¹	6x12 Spa/8d nails/SPF rafters (G ≈ 0.37)	6x6 Spa./DF-L rafters (G ≈ 0.50)	2.9 (63 psf - 182 psf)
Rafter-Sill Connection	3-16d toe nails (pneumatically driven)	DF-L sill plate/4-16d toe nails (pneumatically driven)	2.8 (750 lb - 2123 lb)
Foundation Connection ³	0.5" dia. steel bolts @ 6' C-C	5/8" dia. steel bolts @ 1' C-C	7.5
Roof Cover	Class D asphalt shingles	Class F asphalt shingles	1.3 (74 psf - 98 psf)
Windows & Doors ²	DP25 windows/typical doors	DP30 windows	1.1 (40 psf - 45 psf)
Wall Sheathing	normal strenght stucco, 7" fastener spacing	None	1.0

1) 6x12 Spa. indicates panels nails are at 6" spacing at the edges and 12" spacing along the interior rafters. 6x6 Spa. Indicates 6" nail spacing along every rafter.

2) Actual window pressure rating is 1.5xDP value. I.e. DP30 is pressure tested to about 45 psf.

3) Resistance is dependant on shear load, so no nominal value is given.

Other wood species could be used in place of DF-L for the rafters and sill plates, so long as they have a specific gravity equal to or greater than that of DF-L.

TABLE 6.3 – A1 enhanced quality improvements (lower bound)

ARCHETYPE I ENHANCED QUALITY BUILDING IMPROVEMENTS - LOWER BOUND			
Component	Initial Condition	Modification	Nominal Strength Increase
Roof Panels ¹	6x12 Spa/8d nails/SPF rafters (G ≈ 0.37)	6x6 Spa.	1.4 (63 psf - 86 psf)
Rafter-Sill Connection	3-16d toe nails (pneumatically driven)	None	1.0
Foundation Connection ³	0.5" dia. steel bolts @ 6' C-C	None	1.0
Roof Cover	Class D asphalt shingles	None	1.0
Windows & Doors ²	DP25 windows/typical doors	DP30 windows	1.1 (40 psf - 45 psf)
Wall Sheathing	normal strength stucco, 7" fastener spacing	None	1.0

1) 6x12 Spa. indicates panels nails are at 6" spacing at the edges and 12" spacing along the interior rafters. 6x6 Spa. Indicates 6" nail spacing along every rafter.
 2) Actual window pressure rating is 1.5xDP value. I.e. DP30 is pressure tested to about 45 psf.
 3) Resistance is dependant on shear load, so no nominal value is given.

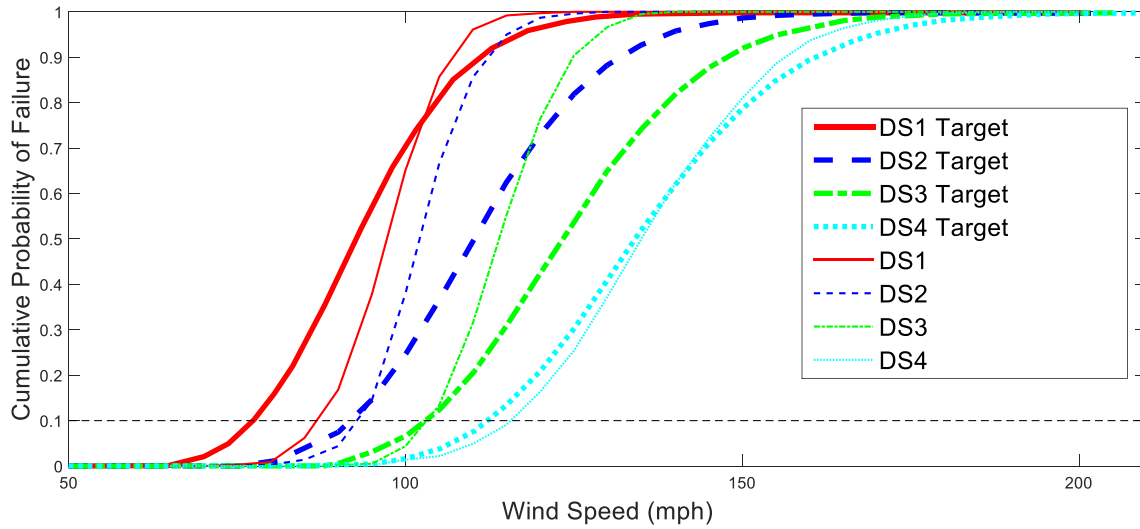


FIGURE 6.2 – A1 upper bound enhanced quality fragilities

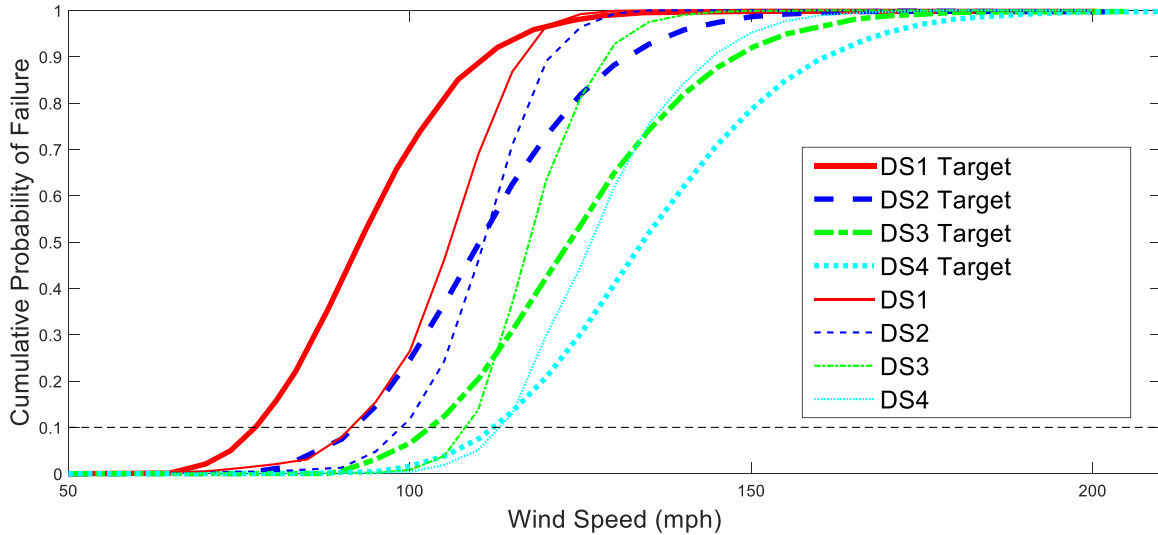


FIGURE 6.3 – A1 lower bound enhanced quality fragilities

Each damage state fragility meets or exceeds the 10th percentile target failure probability, and thus meets the Enhanced quality criteria. During the analysis, it was found that every component with the exception of the wall sheathing needed to be improved in some way in order to meet the targets for the upper bound case. The most substantial improvements appear to be needed for the foundation connections, roof panel connections, and rafter to sill connections, the other components required only minor upgrades to meet the quality standard for the upper bound case. Tables 6.2 and 6.3 summarize the improvements made to A1 for the Enhanced CQL for the upper and lower bound cases respectively. As anticipated, the lower bound case requires significantly less modification in order to meet the target.

6.1.1.2 Archetype A2

The component deficiencies and necessary improvements to achieve Enhanced quality for A2 are very similar to those determined in the analysis of A1. Again, each component requires some improvement with the exception of the wall sheathing for the upper bound case. The most

notable difference between the two archetypes is that A2 required slightly more substantial reinforcement of the rafter to sill connections, which makes sense considering the analyses of the basic quality archetypes for A1 and A2 discussed in Chapter 5.

TABLE 6. 4 - A2 enhanced quality improvements

ARCHETYPE II ENHANCED QUALITY BUILDING IMPROVEMENTS - UPPER BOUND			
Component	Initial Condition	Modification	Nominal Strength Increase
Roof Panels ¹	6x12 Spa/8d nails/SPF rafters (G ≈ 0.37)	6x6 Spa./DF-L rafters (G ≈ 0.50)	2.9 (63 psf - 182 psf)
Rafter-Sill Connection	3-16d toe nails (pneumatically driven)	2x H2.5 hurricane clips	3.5 (750 lb - 2624 lb)
Foundation Connection ³	0.5" dia. steel bolts @ 6' C-C	5/8" dia. steel bolts @ 1' C-C	7.5
Roof Cover	Class D asphalt shingles	Class F asphalt shingles	1.3 (74 psf - 98 psf)
Windows & Doors ²	DP25 windows/typical doors	DP30 windows	1.1 (40 psf - 45 psf)
Wall Sheathing	normal strenght stucco, 7" fastener spacing	None	1.0

1) 6x12 Spa. indicates panels nails are at 6" spacing at the edges and 12" spacing along the interior rafters. 6x6 Spa. Indicates 6" nail spacing along every rafter.

2) Actual window pressure rating is 1.5xDP value. I.e. DP30 is pressure tested to about 45 psf.

3) Resistance is dependant on shear load, so no nominal value is given.

TABLE 6. 5 – A2 enhanced quality improvements (lower bound)

ARCHETYPE II ENHANCED QUALITY BUILDING IMPROVEMENTS - LOWER BOUND			
Component	Initial Condition	Modification	Nominal Strength Increase
Roof Panels ¹	6x12 Spa/8d nails/SPF rafters (G ≈ 0.37)	6x6 Spa.	1.4 (63 psf - 86 psf)
Rafter-Sill Connection	3-16d toe nails (pneumatically driven)	Hem-Fir sill plate (G ≈ 0.43)	1.5 (750 lb - 1092 lb)
Foundation Connection ³	0.5" dia. steel bolts @ 6' C-C	5/8" dia. steel bolts @ 3' C-C	2.5
Roof Cover	Class D asphalt shingles	None	1.0
Windows & Doors ²	DP25 windows/typical doors	DP30 windows	1.1 (40 psf - 45 psf)
Wall Sheathing	normal strength stucco, 7" fastener spacing	None	1.0

1) 6x12 Spa. indicates panels nails are at 6" spacing at the edges and 12" spacing along the interior rafters. 6x6 Spa. Indicates 6" nail spacing along every rafter.

2) Actual window pressure rating is 1.5xDP value. I.e. DP30 is pressure tested to about 45 psf.

3) Resistance is dependant on shear load, so no nominal value is given.

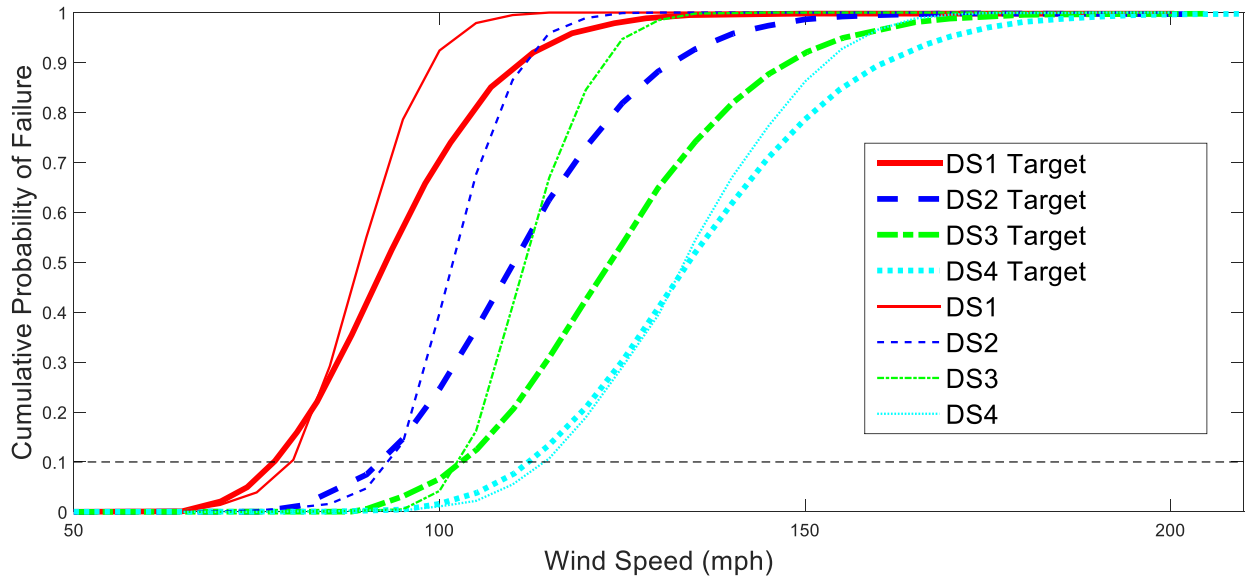


FIGURE 6. 4 – A2 upper bound enhanced quality fragilities

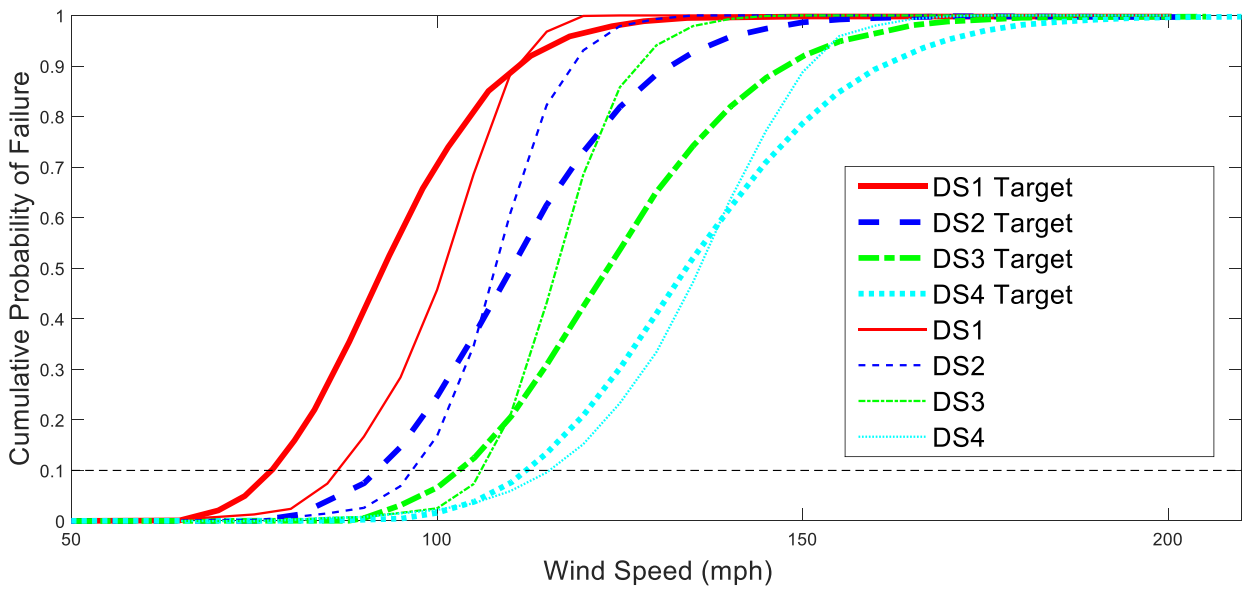


FIGURE 6. 5 – A2 lower bound enhanced quality fragilities

6.1.1.3 Archetype A3

Again, the component deficiencies and necessary improvements do not differ much from those related to A1.

TABLE 6. 6 – A3 enhanced quality improvements

ARCHETYPE III ENHANCED QUALITY BUILDING IMPROVEMENTS - UPPER BOUND			
Component	Initial Condition	Modification	Nominal Strength Increase
Roof Panels ¹	6x12 Spa/8d nails/SPF rafters (G ≈ 0.37)	6x6 Spa./DF-L rafters (G ≈ 0.50)	2.9 (63 psf - 182 psf)
Rafter-Sill Connection	3-16d toe nails (pneumatically driven)	DF-L sill plate/4-16d toe nails (pneumatically driven)	2.8 (750 lb - 2123 lb)
Foundation Connection ³	0.5" dia. steel bolts @ 6' C-C	3/4" dia. steel bolts @ 1' C-C	9.0
Roof Cover	Class D asphalt shingles	Class F asphalt shingles	1.3 (74 psf - 98 psf)
Windows & Doors ²	DP25 windows/typical doors	DP30 windows	1.1 (40 psf - 45 psf)
Wall Sheathing	normal strength stucco, 7" fastener spacing	None	1.0

1) 6x12 Spa. indicates panels nails are at 6" spacing at the edges and 12" spacing along the interior rafters. 6x6 Spa. Indicates 6" nail spacing along every rafter.

2) Actual window pressure rating is 1.5xDP value. I.e. DP30 is pressure tested to about 45 psf.

3) Resistance is dependant on shear load, so no nominal value is given.

TABLE 6. 7 – A3 enhanced quality improvements (lower bound)

ARCHETYPE III ENHANCED QUALITY BUILDING IMPROVEMENTS - LOWER BOUND			
Component	Initial Condition	Modification	Nominal Strength Increase
Roof Panels ¹	6x12 Spa/8d nails/SPF rafters (G ≈ 0.37)	6x6 Spa.	1.4 (63 psf - 86 psf)
Rafter-Sill Connection	3-16d toe nails (pneumatically driven)	None	1.0
Foundation Connection ³	0.5" dia. steel bolts @ 6' C-C	None	1.0
Roof Cover	Class D asphalt shingles	None	1.0
Windows & Doors ²	DP25 windows/typical doors	DP30 windows	1.1 (40 psf - 45 psf)
Wall Sheathing	normal strength stucco, 7" fastener spacing	None	1.0

1) 6x12 Spa. indicates panels nails are at 6" spacing at the edges and 12" spacing along the interior rafters. 6x6 Spa. Indicates 6" nail spacing along every rafter.

2) Actual window pressure rating is 1.5xDP value. I.e. DP30 is pressure tested to about 45 psf.

3) Resistance is dependant on shear load, so no nominal value is given.

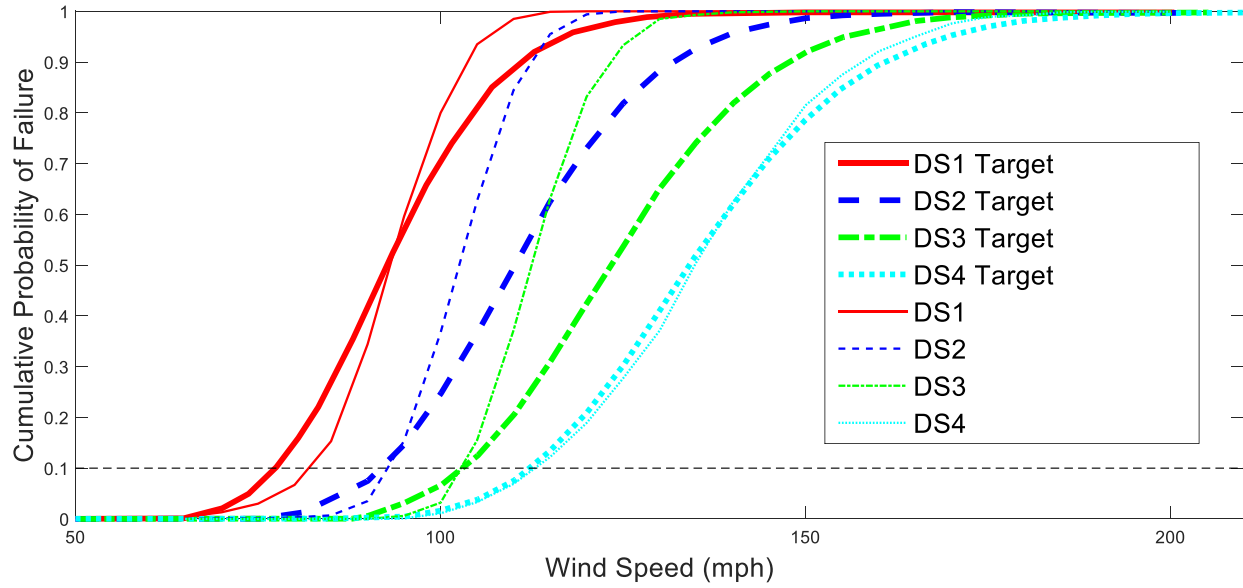


FIGURE 6. 6 - A3 upper bound enhanced quality fragilities

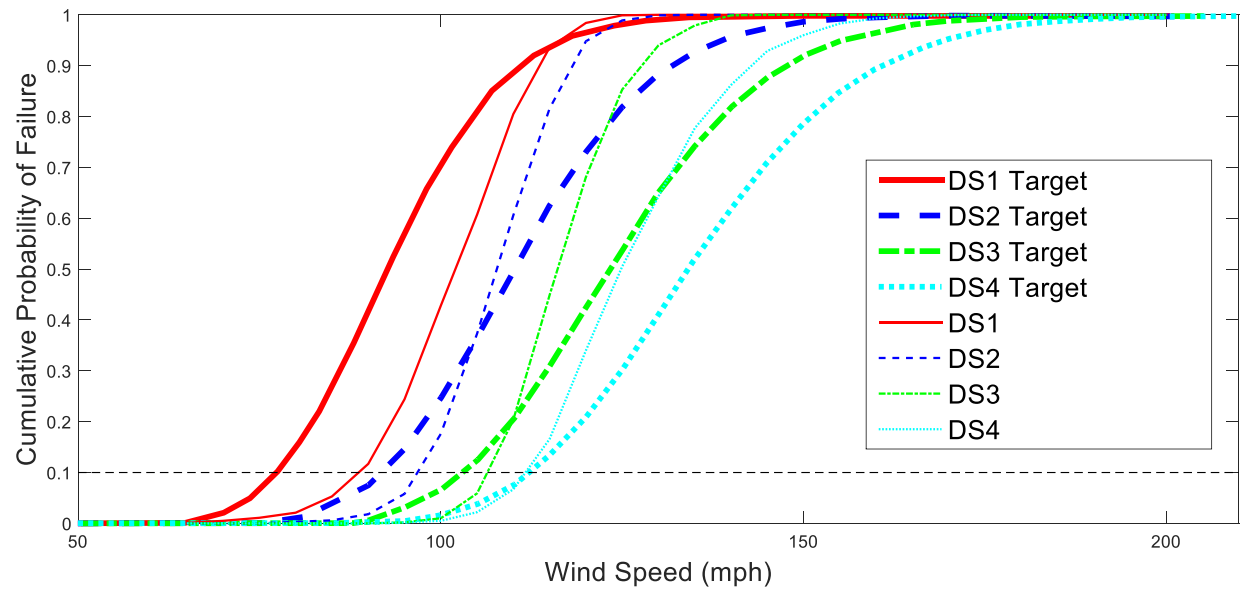


FIGURE 6. 7 – A3 lower bound enhanced quality fragilities

6.1.2 Improved Quality Target

The *Improved* CQL target focuses on reparability for light wood frame residential buildings subject to tornado hazards, meaning buildings that meet this standard are not likely to be destroyed or extensively damaged following a tornado event. A summary of the component deficiencies and proposed solutions necessary for each archetype to meet the Improved CQL target is provided in this section. Observe below that the component deficiencies and necessary improvements are similar to those determined for the Enhanced quality CQL for each archetype. They are basically just scaled up for the Improved and Resistant quality targets.

6.1.2.1 Archetype A1

TABLE 6. 8 – A1 improved quality improvements

ARCHETYPE I IMPROVED QUALITY BUILDING IMPROVEMENTS - UPPER BOUND			
Component	Initial Condition	Modification	Nominal Strength Increase
Roof Panels ¹	6x12 Spa/8d nails/SPF rafters ($G \approx 0.37$)	6x6 Spa./DF-L rafters ($G \approx 0.50$)/10D nails	3.2 (63 psf - 201 psf)
Rafter-Sill Connection	3-16d toe nails (pneumatically driven)	2x H2.5ASS hurricane clips	3.7 (750 lb - 2782 lb)
Foundation Connection ³	0.5" dia. steel bolts @ 6' C-C	3/4" dia. steel bolts @ 1' C-C	9.0
Roof Cover	Class D asphalt shingles	Class G asphalt shingles	1.6 (74 psf - 116 psf)
Windows & Doors ²	DP25 windows/typical doors	DP45 windows	1.7 (40 psf - 67.5 psf)
Wall Sheathing	normal strenght stucco, 7" fastener spacing	None	1.0

1) 6x12 Spa. indicates panels nails are at 6" spacing at the edges and 12" spacing along the interior rafters. 6x6 Spa. Indicates 6" nail spacing along every rafter.

2) Actual window pressure rating is 1.5xDP value. I.e. DP30 is pressure tested to about 45 psf.

3) Resistance is dependant on shear load, so no nominal value is given.

TABLE 6.9 – A1 improved quality improvements (lower bound)

ARCHETYPE I IMPROVED QUALITY BUILDING IMPROVEMENTS - LOWER BOUND			
Component	Initial Condition	Modification	Nominal Strength Increase
Roof Panels ¹	6x12 Spa/8d nails/SPF rafters (G ≈ 0.37)	6x6 Spa./Hem-Fir rafters (G ≈ 0.43)	2.0 (63 psf - 125 psf)
Rafter-Sill Connection	3-16d toe nails (pneumatically driven)	Hem-Fir top sill plate (G ≈ 0.43)	1.5 (750 lb - 1092 lb)
Foundation Connection ³	0.5" dia. steel bolts @ 6' C-C	5/8" dia. steel bolts @ 3' C-C	2.5
Roof Cover	Class D asphalt shingles	None	1.0
Windows & Doors ²	DP25 windows/typical doors	DP40 windows	1.5 (40 psf - 60 psf)
Wall Sheathing	normal strenght stucco, 7" fastener spacing	None	1.0

1) 6x12 Spa. indicates panels nails are at 6" spacing at the edges and 12" spacing along the interior rafters. 6x6 Spa. Indicates 6" nail spacing along every rafter.

2) Actual window pressure rating is 1.5xDP value. I.e. DP30 is pressure tested to about 45 psf.

3) Resistance is dependant on shear load, so no nominal value is given.

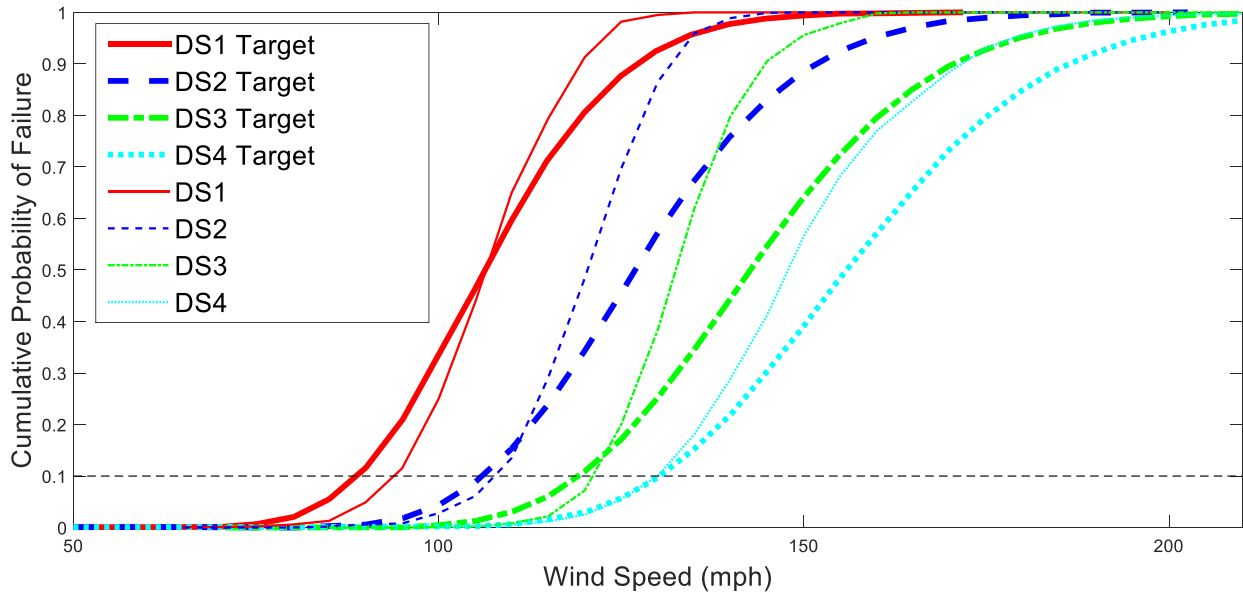


FIGURE 6.8 – A1 upper bound improved quality fragilities

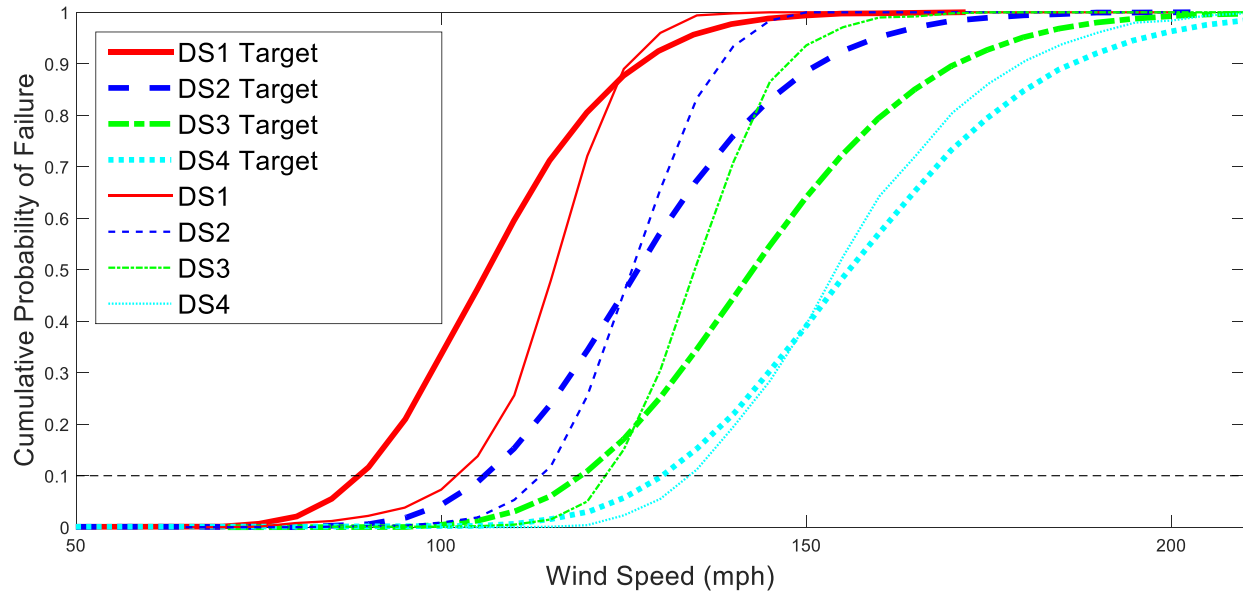


FIGURE 6.9 – A1 lower bound improved quality fragilities

6.1.2.2 Archetype A2

TABLE 6.10 – A2 improved quality improvements

ARCHETYPE II IMPROVED QUALITY BUILDING IMPROVEMENTS - UPPER BOUND			
Component	Initial Condition	Modification	Nominal Strength Increase
Roof Panels ¹	6x12 Spa/8d nails/SPF rafters ($G \approx 0.37$)	6x6 Spa./DF-L rafters ($G \approx 0.50$)/10D nails	3.2 (63 psf - 201 psf)
Rafter-Sill Connection	3-16d toe nails (pneumatically driven)	2x H2.5T hurricane clips	4.6 (750 lb - 3446 lb)
Foundation Connection ³	0.5" dia. steel bolts @ 6' C-C	7/8" dia. steel bolts @ 1' C-C	10.5
Roof Cover	Class D asphalt shingles	Class G asphalt shingles	1.6 (74 psf - 116 psf)
Windows & Doors ²	DP25 windows/typical doors	DP45 windows	1.7 (40 psf - 67.5 psf)
Wall Sheathing	normal strenght stucco, 7" fastener spacing	None	1.0

1) 6x12 Spa. indicates panels nails are at 6" spacing at the edges and 12" spacing along the interior rafters. 6x6 Spa. Indicates 6" nail spacing along every rafter.
2) Actual window pressure rating is 1.5xDP value. I.e. DP30 is pressure tested to about 45 psf.
3) Resistance is dependant on shear load, so no nominal value is given.

TABLE 6. 11 – A2 improved quality improvements (lower bound)

ARCHETYPE II IMPROVED QUALITY BUILDING IMPROVEMENTS - LOWER BOUND			
Component	Initial Condition	Modification	Nominal Strength Increase
Roof Panels ¹	6x12 Spa/8d nails/SPF rafters (G ≈ 0.37)	6x6 Spa.	1.4 (63 psf - 86 psf)
Rafter-Sill Connection	3-16d toe nails (pneumatically driven)	1xH2.5 hurricane clip	1.7 (750 lb - 1312 lb)
Foundation Connection ³	0.5" dia. steel bolts @ 6' C-C	5/8" dia. steel bolts @ 2' C-C	3.8
Roof Cover	Class D asphalt shingles	None	1.0
Windows & Doors ²	DP25 windows/typical doors	DP40 windows	1.5 (40 psf - 60 psf)
Wall Sheathing	normal strenght stucco, 7" fastener spacing	None	1.0

1) 6x12 Spa. indicates panels nails are at 6" spacing at the edges and 12" spacing along the interior rafters. 6x6 Spa. Indicates 6" nail spacing along every rafter.
 2) Actual window pressure rating is 1.5xDP value. I.e. DP30 is pressure tested to about 45 psf.
 3) Resistance is dependant on shear load, so no nominal value is given.

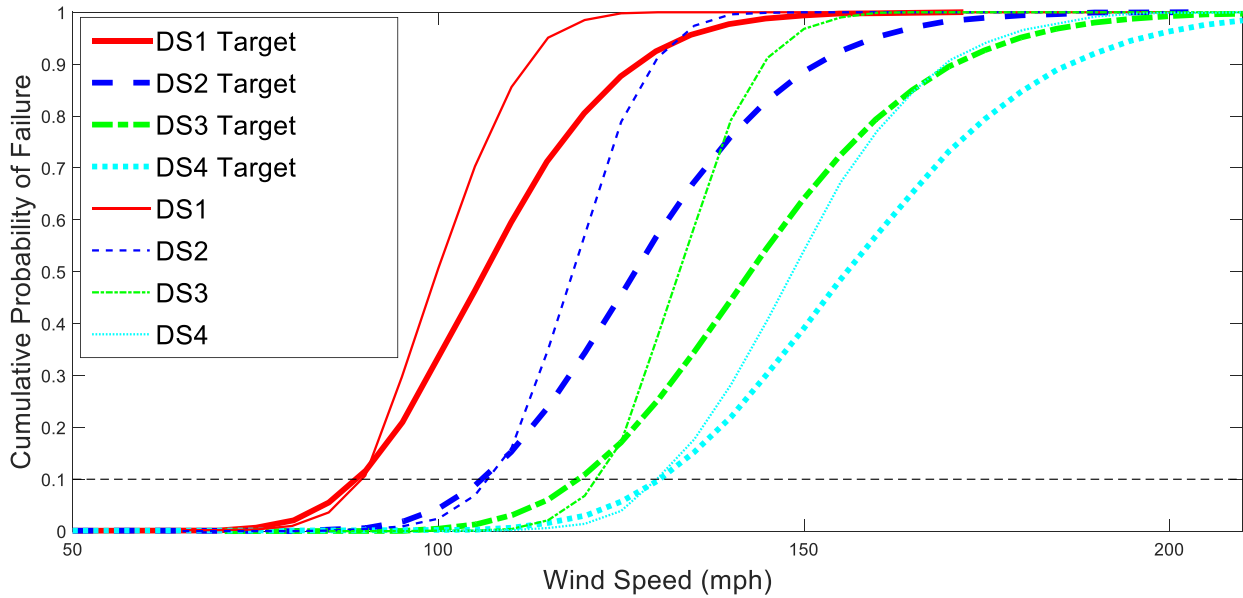


FIGURE 6. 10 – A2 upper bound improved quality fragilities

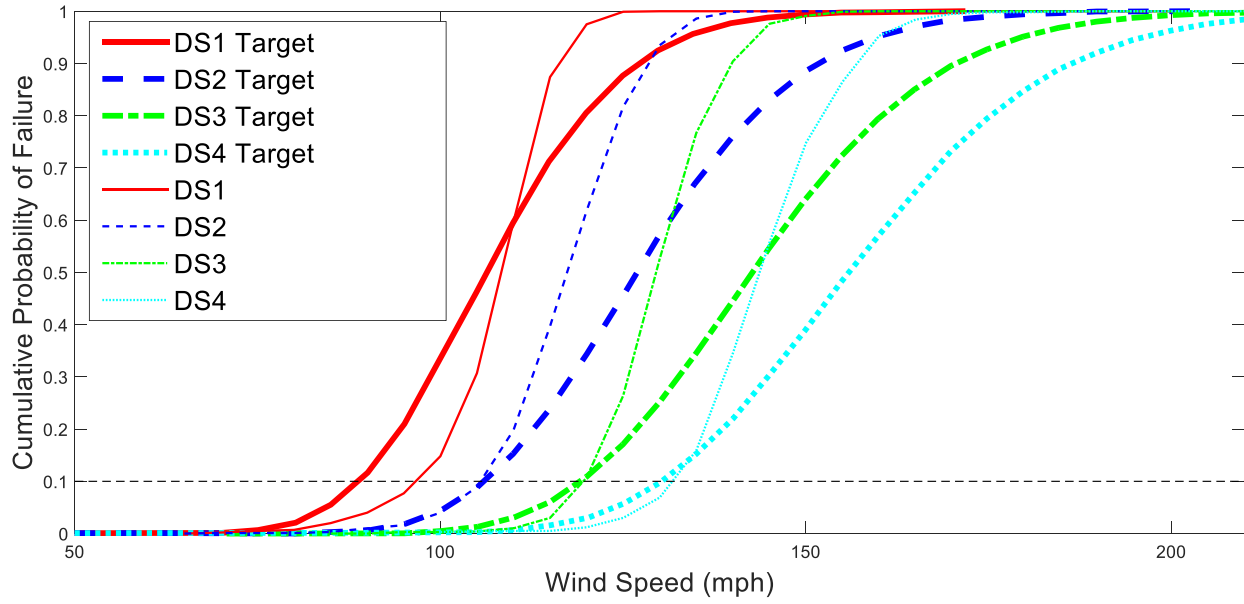


FIGURE 6. 11 – A2 lower bound improved quality fragilities

6.1.2.3 Archetype A3

TABLE 6. 12 – A3 improved quality improvements

ARCHETYPE III IMPROVED QUALITY BUILDING IMPROVEMENTS - UPPER BOUND			
Component	Initial Condition	Modification	Nominal Strength Increase
Roof Panels ¹	6x12 Spa/8d nails/SPF rafters (G ≈ 0.37)	6x6 Spa./DF-L rafters (G ≈ 0.50)/10D nails	3.2 (63 psf - 201 psf)
Rafter-Sill Connection	3-16d toe nails (pneumatically driven)	2x H2.5T hurricane clips	4.6 (750 lb - 3446 lb)
Foundation Connection ³	0.5" dia. steel bolts @ 6' C-C	1" dia. steel bolts @ 1' C-C	12.0
Roof Cover	Class D asphalt shingles	Class G asphalt shingles	1.6 (74 psf - 116 psf)
Windows & Doors ²	DP25 windows/typical doors	DP45 windows/wind resistant doors (min allowable pressure ~ 60 psf)	1.7 (40 psf - 67.5 psf) 1.2 (50 psf - 60 psf)
Wall Sheathing	normal strenght stucco, 7" fastener spacing	None	1.0

1) 6x12 Spa. indicates panels nails are at 6" spacing at the edges and 12" spacing along the interior rafters. 6x6 Spa. Indicates 6" nail spacing along every rafter.

2) Actual window pressure rating is 1.5xDP value. I.e. DP30 is pressure tested to about 45 psf.

3) Resistance is dependant on shear load, so no nominal value is given.

TABLE 6. 13 – A3 improved quality improvements (lower bound)

ARCHETYPE III IMPROVED QUALITY BUILDING IMPROVEMENTS - LOWER BOUND			
Component	Initial Condition	Modification	Nominal Strength Increase
Roof Panels ¹	6x12 Spa/8d nails/SPF rafters (G ≈ 0.37)	6x6 Spa./Hem-Fir rafters (G ≈ 0.43)	2.0 (63 psf - 125 psf)
Rafter-Sill Connection	3-16d toe nails (pneumatically driven)	Hem-Fir top sill plate (G ≈ 0.43)	1.5 (750 lb - 1092 lb)
Foundation Connection ³	0.5" dia. steel bolts @ 6' C-C	5/8" dia. steel bolts @ 3' C-C	2.5
Roof Cover	Class D asphalt shingles	None	1.0
Windows & Doors ²	DP25 windows/typical doors	DP40 windows	1.5 (40 psf - 60 psf)
Wall Sheathing	normal strength stucco, 7" fastener spacing	None	1.0

1) 6x12 Spa. indicates panels nails are at 6" spacing at the edges and 12" spacing along the interior rafters. 6x6 Spa. Indicates 6" nail spacing along every rafter.

2) Actual window pressure rating is 1.5xDP value. I.e. DP30 is pressure tested to about 45 psf.

3) Resistance is dependant on shear load, so no nominal value is given.

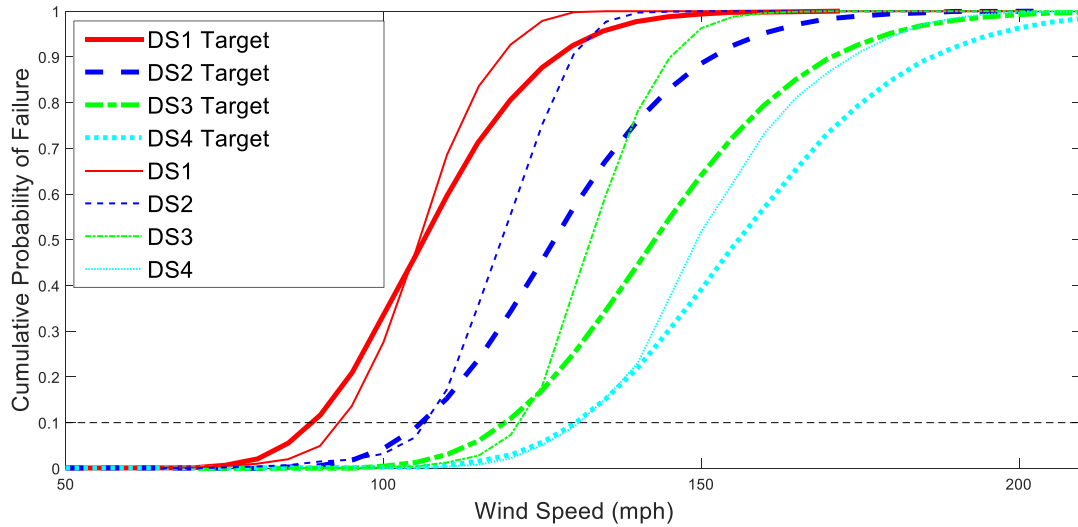


FIGURE 6.12 – A3 upper bound improved quality fragilities

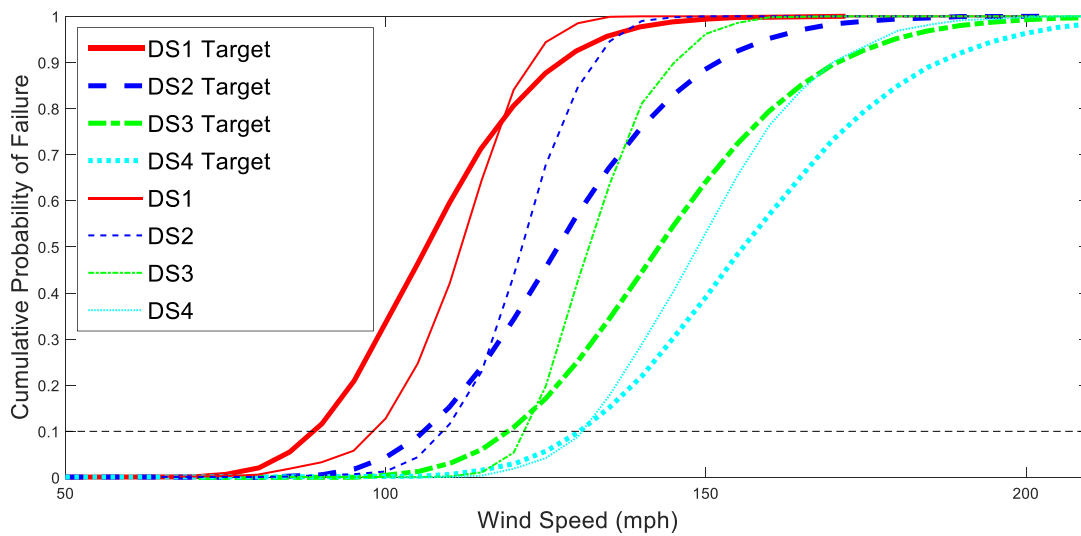


FIGURE 6.13 – A3 lower bound improved quality fragilities

6.1.3 Resistant Quality Target

The highest performance target for this study is the *Resistant* quality target. This standard aims for continued occupancy, use, and function of light wood frame residential buildings during

and after a tornado event. A summary of the component deficiencies and proposed solutions necessary for each archetype to meet the Resistant quality target is provided in this section.

6.1.3.1 Archetype A1

TABLE 6. 14 – A1 resistant quality improvements

ARCHETYPE I RESISTANT QUALITY BUILDING IMPROVEMENTS - UPPER BOUND			
Component	Initial Condition	Modification	Nominal Strength Increase
Roof Panels ¹	6x12 Spa/8d nails/SPF rafters (G ≈ 0.37)	6x6 Spa./W-L rafters (G ≈ 0.52)/10D nails	3.5 (63 psf - 222 psf)
Rafter-Sill Connection	3-16d toe nails (pneumatically driven)	2x H2.5T hurricane clips	4.6 (750 lb - 3446 lb)
Foundation Connection ³	0.5" dia. steel bolts @ 6' C-C	1" dia. steel bolts @ 1' C-C	12.0
Roof Cover	Class D asphalt shingles	Class H asphalt shingles	2.4 (74 psf - 181 psf)
Windows & Doors ²	DP25 windows/typical doors	DP50 windows	1.9 (40 psf - 75 psf)
Wall Sheathing	normal strenght stucco, 7" fastener spacing	None	1.0

1) 6x12 Spa. indicates panels nails are at 6" spacing at the edges and 12" spacing along the interior rafters. 6x6 Spa. Indicates 6" nail spacing along every rafter.

2) Actual window pressure rating is 1.5xDP value. I.e. DP30 is pressure tested to about 45 psf.

3) Resistance is dependant on shear load, so no nominal value is given.

TABLE 6. 15 – A1 resistant quality improvements (lower bound)

ARCHETYPE I RESISTANT QUALITY BUILDING IMPROVEMENTS - LOWER BOUND			
Component	Initial Condition	Modification	Nominal Strength Increase
Roof Panels ¹	6x12 Spa/8d nails/SPF rafters (G ≈ 0.37)	6x6 Spa./Hem-Fir rafters (G ≈ 0.43)	2.0 (63 psf - 125 psf)
Rafter-Sill Connection	3-16d toe nails (pneumatically driven)	1xH2.5 hurricane clip	1.7 (750 lb - 1312 lb)
Foundation Connection ³	0.5" dia. steel bolts @ 6' C-C	5/8" dia. steel bolts @ 3' C-C	2.5
Roof Cover	Class D asphalt shingles	None	1.0
Windows & Doors ²	DP25 windows/typical doors	DP45 windows	1.7 (40 psf - 67.5 psf)
Wall Sheathing	normal strenght stucco, 7" fastener spacing	None	1.0

1) 6x12 Spa. indicates panels nails are at 6" spacing at the edges and 12" spacing along the interior rafters. 6x6 Spa. Indicates 6" nail spacing along every rafter.

2) Actual window pressure rating is 1.5xDP value. I.e. DP30 is pressure tested to about 45 psf.

3) Resistance is dependant on shear load, so no nominal value is given.

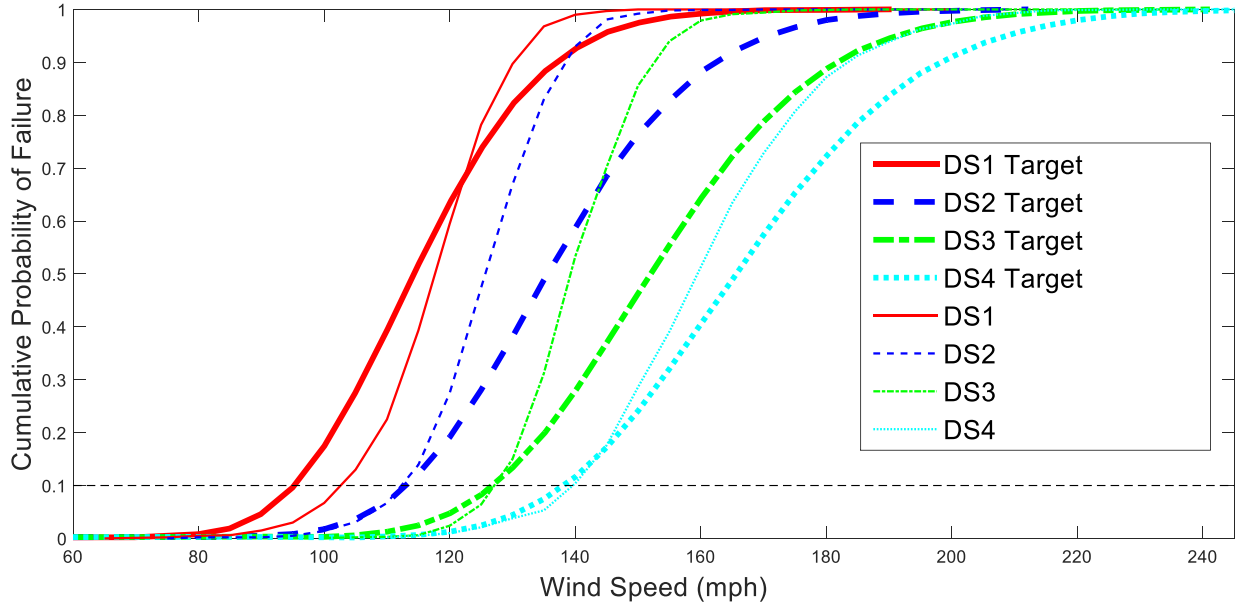


FIGURE 6.14 – A1 upper bound resistant quality fragilities

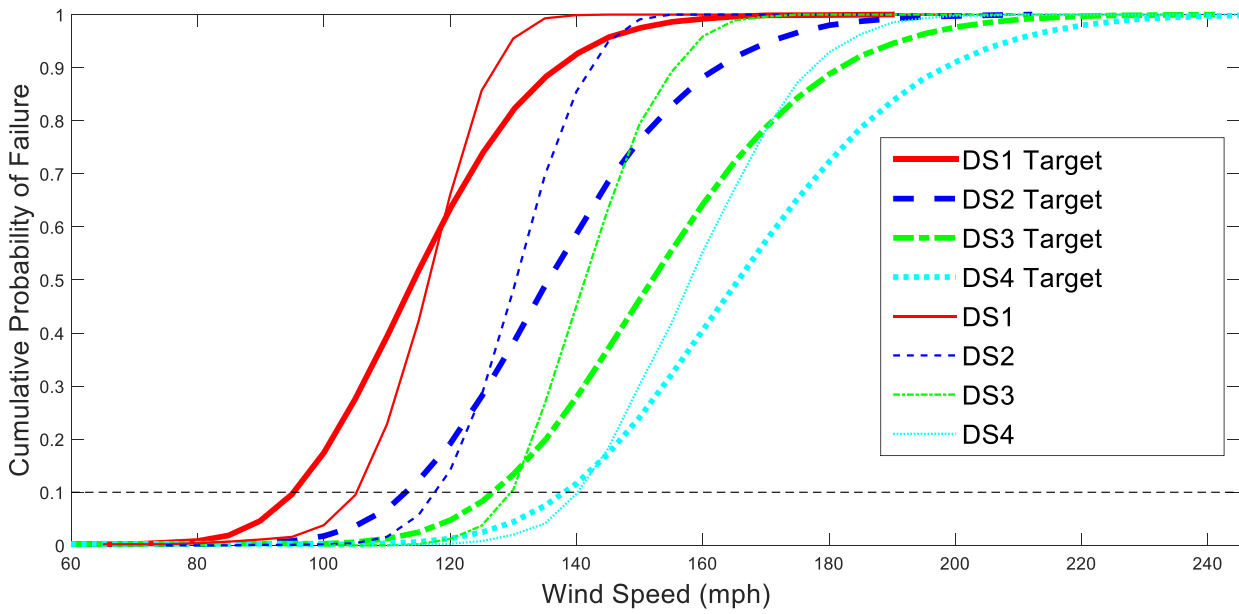


FIGURE 6.15 – A1 lower bound resistant quality fragilities

6.1.3.2 Archetype A2

TABLE 6. 16 – A2 resistant quality improvements

ARCHETYPE II RESISTANT QUALITY BUILDING IMPROVEMENTS - UPPER BOUND			
Component	Initial Condition	Modification	Nominal Strength Increase
Roof Panels ¹	6x12 Spa/8d nails/SPF rafters (G ≈ 0.37)	6x6 Spa./W-L rafters (G ≈ 0.52)/10D nails	3.5 (63 psf - 222 psf)
Rafter-Sill Connection	3-16d toe nails (pneumatically driven)	2x H2.5A hurricane clips	5.1 (750 lb - 3794 lb)
Foundation Connection ³	0.5" dia. steel bolts @ 6' C-C	1-1/8" dia. steel bolts @ 1' C-C	13.5
Roof Cover	Class D asphalt shingles	Class H asphalt shingles	2.4 (74 psf - 181 psf)
Windows & Doors ²	DP25 windows/typical doors	DP50 windows	1.9 (40 psf - 75 psf)
Wall Sheathing	normal strenght stucco, 7" fastener spacing	None	1.0

1) 6x12 Spa. indicates panels nails are at 6" spacing at the edges and 12" spacing along the interior rafters. 6x6 Spa. Indicates 6" nail spacing along every rafter.

2) Actual window pressure rating is 1.5xDP value. I.e. DP30 is pressure tested to about 45 psf.

3) Resistance is dependant on shear load, so no nominal value is given.

TABLE 6. 17 – A2 resistant quality improvements (lower bound)

ARCHETYPE II RESISTANT QUALITY BUILDING IMPROVEMENTS - LOWER BOUND			
Component	Initial Condition	Modification	Nominal Strength Increase
Roof Panels ¹	6x12 Spa/8d nails/SPF rafters (G ≈ 0.37)	6x6 Spa./Hem-Fir rafters (G ≈ 0.43)	2.0 (63 psf - 125 psf)
Rafter-Sill Connection	3-16d toe nails (pneumatically driven)	1xH2.5ASS hurricane clip	1.9 (750 lb - 1391 lb)
Foundation Connection ³	0.5" dia. steel bolts @ 6' C-C	5/8" dia. steel bolts @ 2' C-C	3.8
Roof Cover	Class D asphalt shingles	None	1.0
Windows & Doors ²	DP25 windows/typical doors	DP45 windows	1.7 (40 psf - 67.5 psf)
Wall Sheathing	normal strenght stucco, 7" fastener spacing	None	1.0

1) 6x12 Spa. indicates panels nails are at 6" spacing at the edges and 12" spacing along the interior rafters. 6x6 Spa. Indicates 6" nail spacing along every rafter.

2) Actual window pressure rating is 1.5xDP value. I.e. DP30 is pressure tested to about 45 psf.

3) Resistance is dependant on shear load, so no nominal value is given.

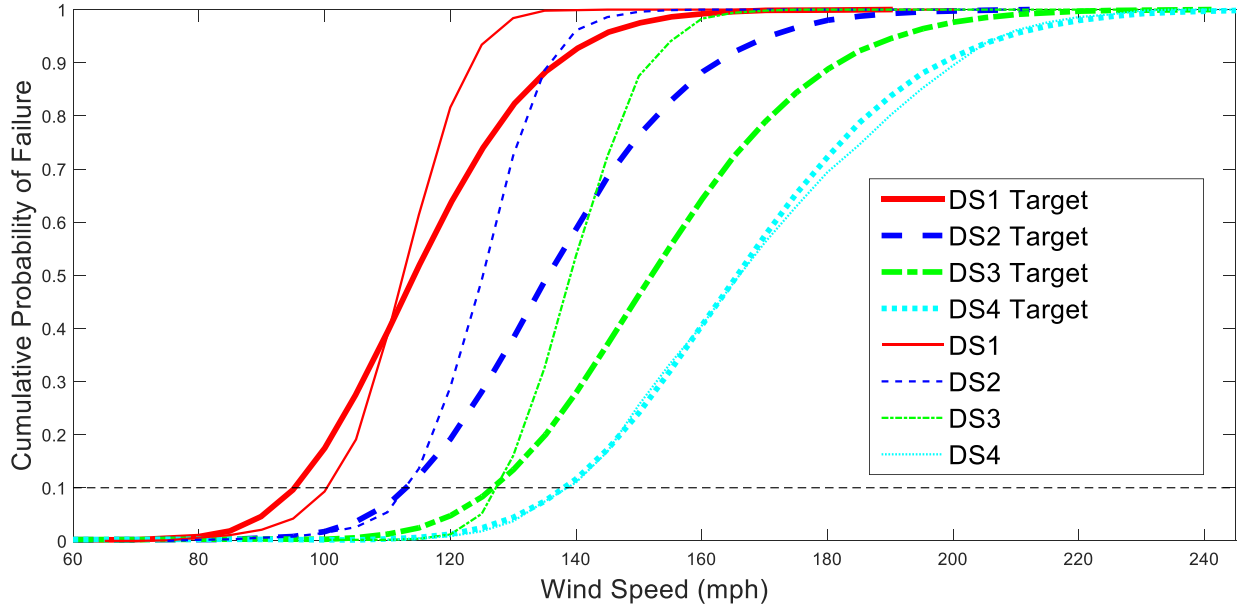


FIGURE 6. 16 - A2 upper bound resistant quality fragilities

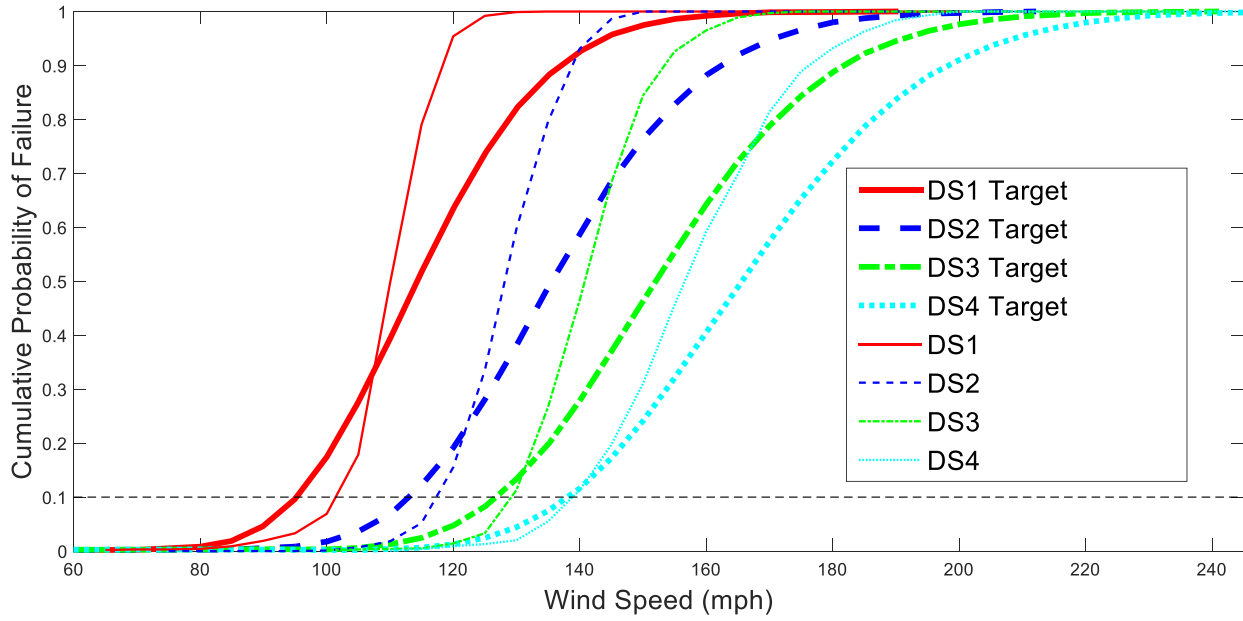


FIGURE 6. 17 – A2 lower bound resistant quality fragilities

6.1.3.3 Archetype A3

TABLE 6. 18 – A3 resistant quality improvements

ARCHETYPE III RESISTANT QUALITY BUILDING IMPROVEMENTS - UPPER BOUND			
Component	Initial Condition	Modification	Nominal Strength Increase
Roof Panels ¹	6x12 Spa/8d nails/SPF rafters (G ≈ 0.37)	6x6 Spa./W-L rafters (G ≈ 0.52)/16D nails	3.9 (63 psf - 248 psf)
Rafter-Sill Connection	3-16d toe nails (pneumatically driven)	2x H2.5T hurricane clips	4.6 (750 lb - 3446 lb)
Foundation Connection ³	0.5" dia. steel bolts @ 6' C-C	1-1/8" dia. steel bolts @ 1' C-C	13.5
Roof Cover	Class D asphalt shingles	Class H asphalt shingles	2.4 (74 psf - 181 psf)
Windows & Doors ²	DP25 windows/typical doors	DP50 windows/wind resistant doors (min allowable pressure ~ 60 psf)	1.9 (40 psf - 75 psf) 1.2 (50 psf - 60 psf)
Wall Sheathing	normal strenght stucco, 7" fastener spacing	None	1.0

1) 6x12 Spa. indicates panels nails are at 6" spacing at the edges and 12" spacing along the interior rafters. 6x6 Spa. Indicates 6" nail spacing along every rafter.

2) Actual window pressure rating is 1.5xDP value. I.e. DP30 is pressure tested to about 45 psf.

3) Resistance is dependant on shear load, so no nominal value is given.

TABLE 6. 19 – A3 resistant quality improvements (lower bound)

ARCHETYPE III RESISTANT QUALITY BUILDING IMPROVEMENTS - LOWER BOUND			
Component	Initial Condition	Modification	Nominal Strength Increase
Roof Panels ¹	6x12 Spa/8d nails/SPF rafters (G ≈ 0.37)	6x6 Spa./Hem-Fir rafters (G ≈ 0.43)	2.0 (63 psf - 125 psf)
Rafter-Sill Connection	3-16d toe nails (pneumatically driven)	1xH2.5 hurricane clip	1.7 (750 lb - 1312 lb)
Foundation Connection ³	0.5" dia. steel bolts @ 6' C-C	5/8" dia. steel bolts @ 2.5' C-C	3.0
Roof Cover	Class D asphalt shingles	None	1.0
Windows & Doors ²	DP25 windows/typical doors	DP45 windows	1.7 (40 psf - 67.5 psf)
Wall Sheathing	normal strength stucco, 7" fastener spacing	None	1.0

1) 6x12 Spa. indicates panels nails are at 6" spacing at the edges and 12" spacing along the interior rafters. 6x6 Spa. Indicates 6" nail spacing along every rafter.

2) Actual window pressure rating is 1.5xDP value. I.e. DP30 is pressure tested to about 45 psf.

3) Resistance is dependant on shear load, so no nominal value is given.

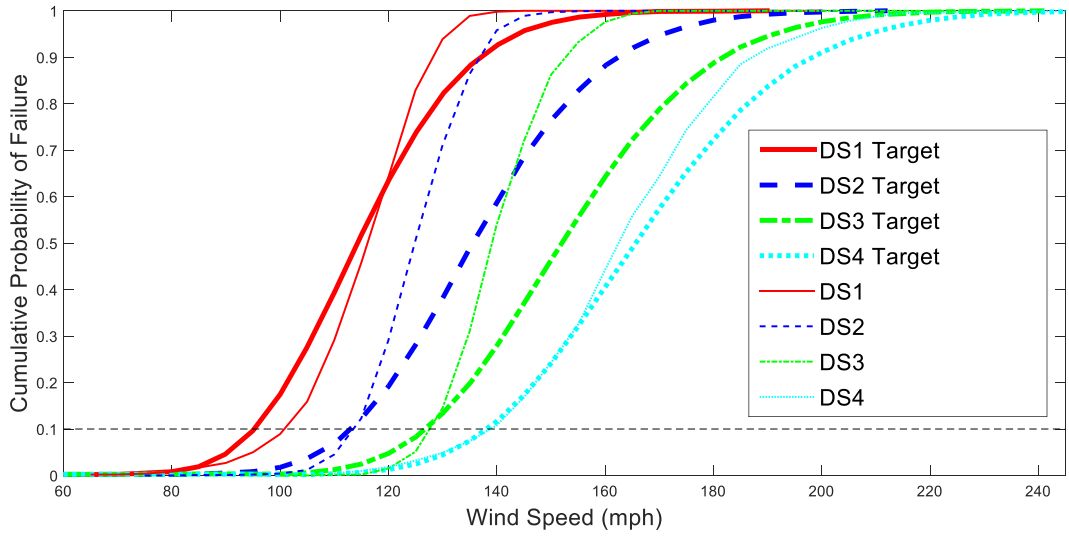


FIGURE 6.18 – A3 upper bound resistant quality fragilities

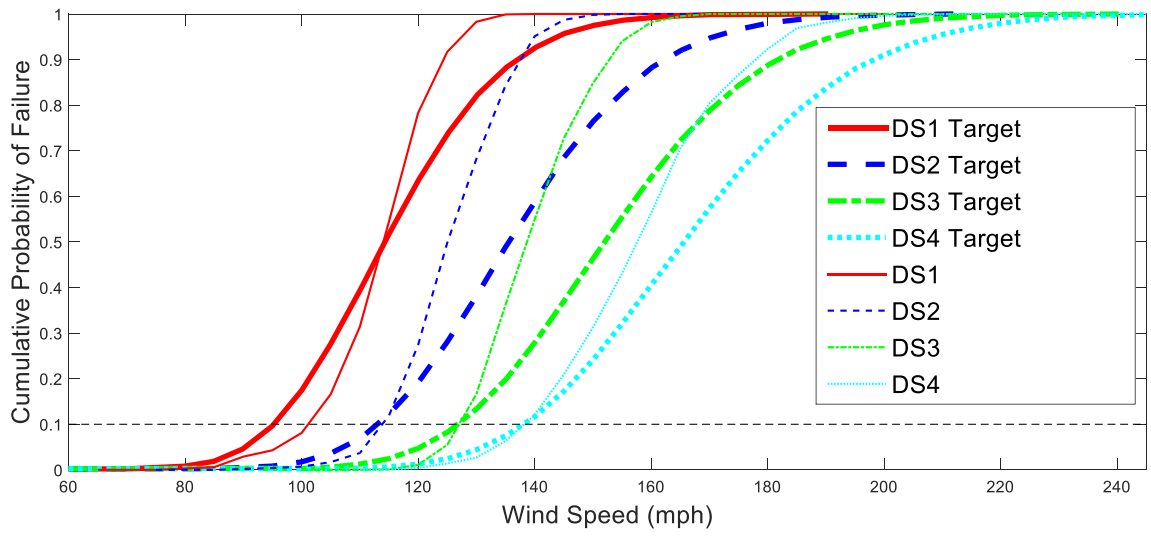


FIGURE 6.19 – A3 lower bound resistant quality fragilities

6.2 Building System Improvement Summary

The previous section makes it apparent that, while the baseline archetypes are all deficient to meet the target building portfolio performance levels, existing solutions can be implemented to

address the deficiencies for even the highest target performance level. These results are encouraging because if existing construction techniques and components can be used to achieve the target performance levels, it seems likely that implementing the improvements could be done in a cost effective and practical manner.

Future work should explore the cost of implementing such improvements versus the community resiliency benefits gained by doing so to determine which strategies are worthwhile and which are not. Furthermore, future work should use the knowledge gained in this study about the building system and component behavior, and the effects of each component's performance on the building system to examine the development of new and innovative methods of strengthening the components discussed in this study that are specifically tailored to optimizing community resiliency considering tornado and expansive soil hazards.

6.3 Masonry Basement Wall Improvements

Some potential methods of improving the performance of a typical masonry block basement wall under expansive soil pressures are examined in this section. As for the building system, cost-optimization of the improvement techniques is not attempted or discussed herein. The goal of this section is to give the reader an idea of what can be done to improve the performance of a typical masonry block basement wall so that the probability of expansive soil related damage is reduced to a reasonable degree. As discussed in Chapter 5, the target performance for this study is assumed to be achieved at a probability of damage less than or equal to 2% (1 of every 50 basements constructed).

The controlling damage mode for the typical masonry basement wall discussed in Chapter 5 is tensile damage. This is not a surprise given the lack of tensile strength common to

cementitious materials including both concrete block and mortar. Considering this, one obvious way to improve the masonry wall's performance is to add rebar to provide tensile strength. Additionally, as shown during the validation of the masonry wall model in Chapter 4, the wall's resistance to crack initiation can be improved significantly by applying a fixed boundary condition at the wall base. Given the increased moment resistance anticipated by utilizing cast-in-place anchor bolts to connect the basement wall to the slab in addition to the mortar joint used for the typical quality variation, it is assumed that this upgrade will achieve a boundary condition that can be idealized as fixed. More experimental data would be useful on this topic but for now, the assumption seems reasonable considering that the mortar joint alone out performs the idealized pinned base condition. Another method of increasing out-of-plane bearing strength is the application of fiber reinforced polymer (FRP) strips. As mentioned in Chapter 2, Bui et al. (2013) showed that the use of vertical and horizontal carbon fiber reinforced polymer (CFRP) strips can significantly increase the bearing capacity of a concrete block masonry wall subject to out-of-plane loading. The load associated with the initial wall cracking in Bui et al. (2013) was increased 135% by using the CFRP strips. The masonry walls tested by Bui et al. were used as a standard to construct and validate the masonry wall model used in this study, so it is assumed that the effect of the CFRP strips will be virtually the same for the wall considered herein.

A second general approach is considered to mitigate the effects of expansive soils. This method seeks not to increase wall resistance, but to decrease demand on the wall. This is achieved by the use of an expansive soil-rubber (ESR) mixture, such as the one described by Seda et al. (2007), as backfill for the basement wall. The same mix proportions used by Seda et al. will be used for the ESR considered herein. The mixture consists of 30% (by volume) fine ground ($\geq 6.7\text{mm}$) waste tire rubber and 70% in-situ expansive soil. Based on the results of Seda

et al., the application of the ESR mixture yields an approximate 75% reduction in swell pressure. The reduction is expected to vary based on the specific soil at a given site but due to a lack of comprehensive data, it is assumed that 75% is an applicable representative value. There is also generally a significant reduction in at-rest pressure load associated with the ESR mixture due to its reduced bulk density. Because the tire rubber is less dense than the typical in-situ soil, the composite bulk density of the ESR is generally less than that of the original soil. For the mean value case, the in-situ soil is approximately 25% more dense than the ESR mixture, corresponding to a 25% reduction of at-rest pressure load when using the ESR backfill.

Combinations of the mitigation techniques discussed above were considered to improve the performance of the concrete masonry block basement wall subject to expansive soil pressures to the target 2% probability of failure. ABAQUS analyses were performed to identify the total wall load-maximum stress relationship parameters for use in equation 5.40 for different combinations of rebar layouts (rebar sizing and spacing configurations) and wall base conditions (fixed or pinned). MATLAB statistical analyses were then performed to determine which combinations of wall reinforcement and swell pressure relief (by use of ESR backfill) would reach the target performance goal. Table 6.20 shows the combination of improvements that serve to most effectively achieve the target performance.

TABLE 6. 20 – Concrete Block Masonry Basement Wall Improvements

Component	Initial Condition	Modification	Effect	Source
Wall Reinforcement	None	CFRP Strips	~135% Increase in initial cracking load	Bui et al. (2013)
Wall Base	Mortar Joint (Pinned)	Cast-in-Place Anchor Bolts (Fixed)	Pinned to Fixed base condition	-
Backfill	In-Situ Soil	ESR Backfill	~75% Swell pressure reduction	Seda et al. (2007)

Making the improvements shown in Table 6.20 causes a reduction in the probability of failure to about 0.6%. This value is better than the target 2%. It was determined that most practical rebar layouts could not be used to achieve such a high level of performance and that wall base reinforcement and backfill treatment are both generally necessary to achieve the target performance considering the two methods of wall tensile strength reinforcement examined in this section.

Recall that the combination of methods used to mitigate expansive soil damage in this section has not been optimized. There are many other techniques that are being developed and that currently exist both to increase the strength of masonry walls and relieve the swell pressure loads exerted by expansive soils. Some of these techniques were discussed in Chapter 2. The process of exploring each of these techniques and the subsequent optimization of the masonry basement wall design is an in-depth process and is beyond the scope of this study.

CHAPTER 7

CONCLUSIONS AND RECOMMENDATIONS FOR FUTURE RESEARCH

7.1 Summary

The research reported herein was conducted as part of a large multi-investigator project aimed at the development of residential building design guidelines for engineers and planners to improve resilience and sustainability at the community level in regions of the US susceptible to tornadoes and expansive soils. To this end, the research examines the complex system behavior of three light wood frame residential building archetypes, considered as integrated systems, subject to tornado winds, and the behavior of masonry block basement walls subject to expansive soil pressures using ABAQUS finite element software. With the knowledge about system behavior gained through the ABAQUS analyses for the basic construction quality level (CQL) building archetypes and basement wall, the statistical performances of the three basic CQL archetypes and basement wall were evaluated independently using MATLAB Monte-Carlo simulations to form damage state fragilities for the building system archetypes and to calculate probability of failure for the basement wall.

Once the performance of each basic CQL archetype was quantified, a series of construction improvements was implemented for each archetype to raise its performance to meet the *Enhanced* (life-safety), *Improved* (reparability), and *Resistant* (continued function) CQL targets identified in concurrent project research. For the basement masonry block wall, non-expansive back-fill and wall reinforcement strategies were explored to reduce the probability of failure to the 2% target value.

The steps in the preceding paragraphs were taken to accomplish the goals of this study outlined in Chapter 1. Specifically, this study helps to accomplish those goals by providing an understanding of the relationship between the performance of individual building components and the performance of the building system. The level of modeling detail used herein allows this relationship to be captured more accurately than previously possible. Our research partners seek to link individual building performance to community resilience. Their work, coupled with the information provided in this study, will allow us to gauge the impact on community resilience made by the standardization of a single building component improvement (i.e. the use of hurricane clips). This, in turn, will allow for the optimization of community planning from cost, sustainability, and resiliency standpoints.

7.2 Conclusions

Details of the findings of this study for the basic CQL and upgraded CQLs for the building system archetypes and masonry basement wall are provided in this section.

7.2.1 Basic Quality Archetypes

Building System: It was found that each basic CQL building system archetype was deficient for both the upper and lower bound tornado wind pressure cases. Generally, the most deficient component was found to be the foundation connection. The roof panels and rafter-sill connections were significantly deficient for each archetype as well, while the roof cover and window/door components were only mildly deficient. The wall sheathing proved to be adequate for each archetype.

Masonry Block Basement Wall: The basic quality masonry block wall was unable to withstand the swell pressures associated with expansive soils in a region such as Norman, OK,

indicating that current basement construction practices in such locations are an unreliable method of providing shelter from tornados. The masonry wall deficiencies are primarily due to the lack of tensile strength available in an unreinforced masonry block wall.

7.2.2 Enhanced, Improved, and Resistant Quality Archetypes

Chapter 6 provides a comprehensive list of improvements made to each building archetype and basement wall for various CQLs. A brief summary of these improvements is given below:

Building System: General component improvements found to help the building system archetypes meet the target CQLs are as follows: *Roof Panels* – decrease nail spacing, increase nail size, upgrade rafter wood species; *Rafter-Sill Connections* – increase nail quantity, upgrade rafter wood species, use of hurricane clips; *Foundation Connection* – decrease bolt spacing, increase bolt size; *Roof Cover* – use of high wind rated shingles; *Windows/Doors* – use of higher pressure rated windows and doors.

Masonry Block Basement Wall: General improvements found to help the masonry block basement wall meet the target performance level include: *Wall Base* – strengthen wall base connection to footings with cast-in-place anchor bolts; *Wall Strength* – increase tensile strength by use of CFRP strips (Bui et al. 2013); *Swell Pressure Mitigation* – reduce swell pressure using ESR backfill (Seda et al. 2007).

7.3 Recommendations for Future Research

In order to best achieve the long term goals of this study described in Chapter 1, future research in the following areas would be useful:

- Development of performance targets for the basement wall, similar to those used for the building system performance. In this study, the target was assumed to be less than or equal to a 2% probability of failure. Providing the option for different performance levels which decrease probability of failure (i.e. increase performance) at additional life-cycle cost would be beneficial in balancing sustainability and cost against resiliency benefits.
- Development of cost optimized combinations of building component improvements that meet the target performance goals for both the building system archetypes and the basement wall. In this study, general combinations of improvements using existing techniques are provided (see Chapter 6). This analysis should be performed in greater detail considering a wider range of improvement options. Unique and innovative techniques should be explored, and developed, if necessary, to optimize cost and performance.
- Increased experimental and statistical data (mean, COV, probability distribution) describing the resistances of improved building components. In this study, for the improved building and basement wall components, experimental data was used when it was available but assumptions were made to fill in gaps in experimental data. Although such assumptions are logical and reasonable and are based on experimental data and physics, experimental validation should be sought in future studies.
- Development of design recommendations for maximum considered tornado (MCT) to better quantify the point at which we seek to match the archetype performance fragilities to the target values. In this study, the matching value (10% probability of failure) was chosen to achieve a risk-consistent but conservative level of design. This

is based on the work of ATC-63 which considered earthquake hazards. This value should be confirmed by future work, or a new value should be determined if 10% is not appropriate.

The research discussed above will help to bridge the gaps in the work included in this thesis and advance it towards the accomplishment of the goals outlined in Chapter 1.

REFERENCES

- Abdelnaby, A., Elnashai, A. (2013). "Integrity Assessment of the Pharos of Alexandria During the AD 1303 Earthquake". *Engineering Failure Analysis*. 33. 199-138.
- Alfano, C.D. (2016). Damage Analysis and Mitigation for Wood-Frame Structures Subjected to Tornado Loading (Doctoral Dissertation). Colorado State University.
- Amini, M. O., van de Lindt, J.W., (2014). "Quantitative Insight into Rational Tornado Design Wind Speeds for Residential Wood-Frame Structures Using Fragility Approach". *Journal of Structural Engineering*, July, 2014; 140(7). 04014033-1 – 04014033-15.
- Arnold, A.E., Uang, C., Filiatrault, A. (2003). "Cyclic Behavior and Repair of Stucco and Gypsum Sheathed Wood frame Walls: Phase I" Structural Systems Research Project. CUREE Report No. SSRP-2002/07.
- ASCE. (2010). "ASCE Standard Minimum Design Loads for Buildings and Other Structures". ASCE/SCI 7-10. Reston, VA.
- Bahmani, P., van de Lindt, J.W. (2014). "Experimental and Numerical Assessment of Wood frame Sheathing Layer Combinations for Use in Strength-Based and Performance-Based Design". *Journal of Structural Engineering*, ASCE, E4014001.
- Bruneau, M., S. Chang, R. Eguchi, G. Lee, T. O'Rourke, A.M. Reinhorn, M. Shinozuka, K. Tierney, W. Wallace, and D.V. Winterfelt. (2003). "A Framework to Quantitatively Assess and Enhance the Seismic Resilience of Communities." *Earthquake Spectra*, 19 (4); 733-752.
- Bui, T., Limam, A., David, B., Ferrier, E., Brun, M. (2013). "Masonry Walls Submitted to Out-of-Plane Loading: Experimental and Numerical Study". International Masonry Society. 8th International Masonry Conference, July 2010, Dresden, Germany. 2 (F-243), pp.1153-1162. <hal-00802207>
- Camelo, V., Beck, J., Hall, J. (2002). "Dynamic Characteristics of Wood frame Structures" The CUREE-Caltech Wood frame Project. CUREE Publication No. W-11.
- Chowdhury, I., Dasgupta, S. "Computation of Rayleigh Damping Coefficients for Large Systems".
- Dao, Thang N., van de Lindt, John W. (2008). "New Nonlinear Roof Sheathing Fastener Model for Use in Finite-Element Wind Load Applications". *Journal of Structural Engineering*, ASCE/October 2008/1668-1674.
- Deierlein, G.G., Kanvinde, A.M. (2003). "Seismic Performance of Gypsum Walls-Analytical Investigations" The CUREE-Caltech Wood frame Project. CUREE Publication No. W-23.
- Ellingwood, B.R., Rosowsky, D.V., Li, Y. K. (2004). "Fragility Assessment of Light-Frame Wood Construction Subjected to Wind and Earthquake Hazards" *Journal of Structural Engineering*, 10.1061/(ASCE)0733-9445(2004)130:12(1921), 1921-1930.
- Ellingwood, B.R., Tekie, P.B., (1999). "Wind Load Statistics for Probability-Based Structural Design". *Journal of Structural Engineering*, April 1999; 125(4): 453-463.
- Erzin, Y., Erol, O. (2007). "Swell Pressure Prediction by Suction Methods". *Engineering Geology*. 92 133-145.
- FEMA/NIBS. (2003). "Multi-hazard Loss Estimation Methodology Earthquake Model (HAZUS-MH MR4): Technical Manual." Washington, D.C.

- Fischer, D., Folz, B., Filiatrault, A., Uang, C., Seible, F. (2001). "Shake Table Tests of a Two-Story Wood frame House" The CUREE-Caltech Wood frame Project. CUREE Publication No. W-06.
- Grenier, Daniel, J. (2014). Contribution of Gypsum-board Sheathing to the Compressive Resistance of Wood Studs Subjected to Gravitational Loads. (Doctoral Dissertation). Western University – Scholarship@Western
- Gromko, G.J. (1974). "Review of Expansive Soils" *Journal of Geotechnical Engineering Division*, Vol. 100, Issue 6, pg 667-687.
- Grubler, J.J. (2012). Reliability and effect of partially restrained wood shear walls (Doctoral Dissertation). Wayne State University – DigitalCommons@WayneState
- Haan Jr., F.L., Balaramudu, V.K., Sarkar, P.P. (2010). "Tornado-Induced Wind Loads on a Low-Rise Building". *Journal of Structural Engineering*, ASCE 2010; 136(1): 106-116.
- Hadhazy, A. (2011). "Gone in Four Seconds – How a Tornado Destroys a House". *Popular Mechanics*. May 4, 2011.
- HAZUS. "Multi-hazard Loss Estimation Methodology, Hurricane Module, Hazus –MH 2.1 Technical Manual" Dept. of Homeland Security, FEMA Mitigation Division. Washington, D.C.
- Herzog, B., Yeh, B. "Nail Withdrawal and Pull-Through Strength of Structural-Use Panels". APA – The Engineered Wood Association. Tacoma, Washington, U.S.A.
- Hill K, Datin P, Prevatt DO, Gurley K, Kopp G. (2009). "A Case for Standardized Dynamic Wind Uplift Pressure Test for Wood Roof Structural Systems". 11th Americas Conference on Wind Engineering – San Juan, Puerto Rico. June 2009.
- Ho Lee, K., Rosowsky, D. (2005). "Fragility assessment for roof sheathing failure in high wind regions". *Engineering Structures*. 27: 857-868. Elsevier.
- Huang, G., He, H., Mehta, K.C., Liu, X. (2015). "Data-Based Probabilistic Damage Estimation for Asphalt Shingle Roofing". *Journal of Structural Engineering*, 141(12). 04015065-1 - 04015065-10.
- Huang, Z., Rosowsky, D., Sparks, P. (2001). "Long-term hurricane risk assessment and expected damage to residential structures". *Reliability Engineering & System Safety*. 74: 239-249. Elsevier.
- International Building Code (IBC). (2003). Ch. 21 – Masonry.
- Isoda, H., Foltz, B., Filiatrault, A. (2002). "Seismic Modeling Index of Wood frame Buildings" The CUREE-Caltech Wood frame Project. CUREE Publication No. W-12.
- Jankowiak, T., Lodygowski, T. (2005). "Identification of Parameters of Concrete Damage Plasticity Constitutive Model". *Foundations of Civil and Environmental Engineering*. No. 6.
- Jones, D.E., Jones, K.A. (1987). "Treating Expansive Soils" *Civil Engineering*, 57(8) (1987), pp. 62-65.
- Kassem, F., Bertrand, D., Brun, M., Limam, A. (2013). "Reliability Analysis of Reinforced Concrete Slab Subjected to Low Velocity Impact Accounting of Material Damage". *Safety, Reliability, Risk, and Life-Cycle Performance of Structures & Infrastructures – Deodatis, Ellingwood, and Frangopol (Eds)*. Taylor & Francis Group, London, ISBN 978-1-138-00086-5.
- Kmiecik, P., Kaminski, M. (2011). "Modelling of Reinforced Concrete Structures and Composite Structures with Concrete Strength Degradation Taken into Consideration". *Archives of Civil and Mechanical Engineering*. Vol. XI. No. 3.

- Kretschmann, David E. (2010). Wood Handbook, Wood as an Engineering Material, Chapter 05: Mechanical Properties of Wood. General Technical Report FPL-GTR-190. Madison, WI: U.S. Department of Agriculture, Forest Service, Forest Products Laboratory.
- Kuligowski, E., Lombardo, F., Phan, L., Levitan, M., Jorgensen, D. (2014). "Final Report, National Institute of Technology (NIST) Technical Investigation of the May 22, 2011, Tornado in Joplin, Missouri" NIST.
- Lee, K.H., Rosowsky, D.V. (2005). "Fragility Assessment for Roof Sheathing Failure in High Wind Regions" *Engineering Structures*, 27, 857-868.
- Li, Y. (2005). Fragility Methodology For Performance Based Engineering of Wood-Frame Residential Construction (Doctoral dissertation). Georgia Institute of Technology.
- Lin, P., Wang, N. (2016). "Building Portfolio Fragility Functions to Support Scalable Community Resilience Assessment". *Sustainable and Resilient Infrastructure*. Dec. 22nd, 2016, Pgs. 108-122.
- Luco, N., Ellingwood, B.R., Hamburger, R.O., Hooper, J.D., Kimball, J.K., Kircher, C.A. (2007). "Risk-Targeted versus Current Seismic Design Maps for Conterminous United States" SEAOC 2007 Convention Proceedings.
- Lytton, R., Aubeny, C., and Bulut, R (2005). "Design Procedure for Pavements on Expansive Soils". FHWA/TX-05/0-4518-1 Vol. 1.
- Mansour, E. (2011). Swell Pressure and Retaining Wall Design in Expansive Soils. (Masters Thesis). University of Dayton.
- McAllister, T. (2013). "Developing Guidelines and Standards for Disaster Resilience of the Built Environment: A Research Needs Assessment" National Institute of Standards and Technology (NIST) Technical Note 1795, Gaithersburg, MD.
- McMullin, K., Merrick, D. (2002). "Seismic Performance of Gypsum Walls: Experimental Test Program" The CUREE-Caltech Wood frame Project. CUREE Publication No. W-15.
- Melchers, R.E., (1999). "Structural Reliability Analysis and Prediction", Second Edition. John Wiley and Sons Ltd. West Sussex, England.
- NAHB. (2002). "Roof Framing Connections In Conventional Residential Construction". NAHB Research Center, Inc. U.S. Department of Housing and Urban Development Office of Policy Development and Research Contract No. H-21172CA. Upper Marlboro, MD. February 2002.
- Ploeger, S., G. Atkinson, and C. Samson. (2010). "Applying the HAZUS-MH Software Tool to Assess Seismic Risk in Downtown Ottawa, Canada." *Natural Hazards* 53(1); 1-20. doi:10.1007/s11069-009-9408-x.
- Reitherman, R., Cobeen, K. (2003). "Design Documentation of Wood frame Project Index Buildings." The CUREE-Caltech Wood frame Project. CUREE Publication No. W-29.
- Rosowsky DV, Cheng N. (1999). "Reliability of light-frame roofs in high-wind regions". II: Reliability Analysis. *Journal of Structural Engineering*, ASCE 1999; 125(7): 734-739.
- Roueche, D.B., Lombardo, F.T., Prevatt, D.O. (2017). "Empirical Approach to Evaluating the Tornado Fragility of Residential Structures" *J. Struct. Eng.*, 2017, 143(9): 04017123 – 1-10.
- Seda, J.H., Lee, J.C., Carraro, J.A.H., (2007). "Beneficial Use of Waste Tire Rubber for Swelling Potential Mitigation in Expansive Soils". ASCE , *Geotechnical Special Publication 172*, Geo-Denver 2007.

- Trendafiloski, G., M. Wyss, P. Rosset, and G. Marmureanu. (2009). "Constructing City Models to Estimate Losses Due to Earthquakes Worldwide: Application to Bucharest, Romania." *Earthquake Spectra*, 25(3); 665-685.
- van de Lindt, J. W., Pei, S., Dao, T., Graettinger, A., Prevatt, D.O., Gupta, R., Coulbourne, W. (2013). "Dual-Objective-Based Tornado Design Philosophy". *Journal of Structural Engineering*, 139(2): 251-263.
- Vieira, L., Schafer, B.W. (2009). "Experimental Results for Translational Stiffness of Stud-Sheathing Assemblies". AISI-COFS Project on Sheathing Braced Design of Wall Studs.
- Vitoontus, S., & Ellingwood, B. R. (2013). "Role of correlation in seismic demand and building damage in estimating losses under scenario earthquakes". In Proceedings of 11th International Conference on Structural Safety & Reliability (ICOSSAR 2013), New York, NY: Taylor & Francis; The Netherlands: A.A. Balkema.

APPENDIX A

FASTENER SPECIFICATIONS

TABLE A. 1 Nail Sizing Chart

NAIL SPECIFICATIONS				
Nail Size		Shank Diameter	Shank Length	Head Diameter
Penny Size	Guage	Nominal	Nominal	Apprx.
2D	15	0.072	1"	3/16"
	14	0.083	1"	13/64"
3D	14	0.083	1.25"	13/64"
4D	12	0.109	1.5"	1/4"
5D	12	0.109	1.75"	1/4"
6D	11	0.12	2"	17/64"
8D	10	0.134	2.5"	9/32"
10D	9	0.148	3"	5/16"
12D	9	0.148	3.25"	5/16"
16D	8	0.165	3.5"	11/32"
20D	6	0.203	4"	13/32"
30D	5	0.22	4.5"	7/16"
40D	4	0.238	5"	15/32"
60D	4	0.238	6"	17/32"
	2	0.284	6"	17/32"

TABLE A. 2 – Hurricane Clip Specifications (from Simpson Strong-Tie)

Model No.	Ga	Fasteners			DF/SP Allowable Loads			Uplift with 8dx1½ Nails (160)	SPF/HF Allowable Loads			Uplift with 8dx1½ Nails (160)
		To Rafter/Truss	To Plates	To Studs	Uplift (160)	Lateral (160)			Uplift (160)	Lateral (160)		
						F ₁	F ₂			F ₁	F ₂	
H1	18	6-8dx1½	4-8d	—	585	485	165	455	400	415	140	370
H2	Discontinued – See H2A											
H2A	18	5-8dx1½	2-8dx1½	5-8dx1½	575	130	55	—	495	130	55	—
H2ASS	18	5-SS8D	2-SS8D	5-SS8D	400	130	55	400	345	130	55	345
H2.5	18	5-8d	5-8d	—	415	150	150	415	365	130	130	365
H2.5A	18	5-8d	5-8d	—	600	110	110	480	535	110	110	480
H2.5ASS	18	5-SS8d	5-SS8d	—	440	75	70	365	380	75	70	310
H2.5T	18	5-8d	5-8d	—	545	135	145	425	545	135	145	425
H3	18	4-8d	4-8d	—	455	125	160	415	320	105	140	290
H4	20	4-8d	4-8d	—	360	165	160	360	235	140	135	235
H5	18	4-8d	4-8d	—	455	115	200	455	265	100	170	265
H6	16	—	8-8d	8-8d	950	—	—	—	820	—	—	—
H7Z	16	4-8d	2-8dx1½	8-8d	985	400	—	—	845	345	—	—
H8	18	5-10dx1½	5-10dx1½	—	745	75	—	630	565	75	—	510
H10	18	8-8dx1½	8-8dx1½	—	995	590	275	—	850	505	235	—
H10A	18	9-10dx1½	9-10dx1½	—	1140 ⁷	590	285	—	1015	505	285	—
H10ASS	18	9-SSN10	9-SSN10	—	970	565	195	—	835	485	195	—
H10AR	18	9-10dx1½	9-10dx1½	—	1050	490	285	—	905	420	285	—
H10S ^{3,10}	18	8-8dx1½	8-8dx1½ ¹⁰	8-8d	1010	660	215	550	870	570	185	475
H10A-2	18	9-10dx1½	9-10dx1½	—	1245	815	260	—	1070	700	225	—
H10-2	18	6-10d	6-10d	—	760	455	395	—	655	390	340	—
H11Z	18	6-16dx2½	6-16dx2½	—	830	525	760	—	715	450	655	—
H14	18	1 12-8dx1½	13-8d	—	1350 ⁷	515	265	—	1050	480	245	—
		2 12-8dx1½	15-8d	—	1350 ⁷	515	265	—	1050	480	245	—
TSP	16	9-10dx1½	6-10dx1½	—	740	310	190	—	635	265	160	—
		9-10dx1½	6-10d	—	890	310	190	—	765	265	160	—

APPENDIX B

CLEVELAND COUNTY, OKLAHOMA SOIL SURVEY DATA

TABLE B. 1 – Relevant Cleveland County Soil Parameters (from USDA Soil Survey Data)

Weighted average values - key soil parameters; Cleveland county, OK

USDA Soils Survey Database

Site #	w (%) (1/3 bar)	PI (%)	γ (g/cc)	γ (pcf)	γ_d (g/cc)	γ_d (pcf)
1	18.8	12.7	1.56	97.3908	1.31	81.98
2	19.6	16.1	1.54	96.1422	1.29	80.39
3	28.9	28.5	1.43	89.2749	1.11	69.26
4	14.9	2.8	1.59	99.2637	1.38	86.39
5	21.3	10.4	1.55	96.7665	1.28	79.77
6	26.8	20.4	1.62	101.1366	1.28	79.76
7	16.5	9.1	1.57	98.0151	1.35	84.13
8	20.7	10.1	1.64	102.3852	1.36	84.83
9	27.3	17.4	1.48	92.3964	1.16	72.58
10	18.2	9.6	1.54	96.1422	1.30	81.34
11	19	5.4	1.57	98.0151	1.32	82.37
12	10.4	0	1.68	104.8824	1.52	95.00
13	12.3	0	1.68	104.8824	1.50	93.39
14	9	0.8	1.59	99.2637	1.46	91.07
15	21.2	8	1.6	99.888	1.32	82.42
16	15.1	2.3	1.58	98.6394	1.37	85.70
17	13.5	1.2	1.58	98.6394	1.39	86.91
18	15.5	0.5	1.59	99.2637	1.38	85.94
19	19.3	8.5	1.55	96.7665	1.30	81.11
20	18.2	16.9	1.53	95.5179	1.29	80.81
21	24.9	10.8	1.48	92.3964	1.18	73.98
22	31.2	15.8	1.7	106.131	1.30	80.89
23	32	17.7	1.53	95.5179	1.16	72.36
24	30.8	13.7	1.49	93.0207	1.14	71.12
25	18.2	14.8	1.56	97.3908	1.32	82.39
26	22.5	15.7	1.52	94.8936	1.24	77.46
27	13.5	12.8	1.55	96.7665	1.37	85.26
28	22.3	8.8	1.56	97.3908	1.28	79.63
29	17.9	12.4	1.56	97.3908	1.32	82.60
30	28.6	11.3	1.52	94.8936	1.18	73.79
31	31	13.4	1.52	94.8936	1.16	72.44
32	26	11.4	1.53	95.5179	1.21	75.81

33	19.9	4.4	1.53	95.5179	1.28	79.66
34	20	25.1	1.53	95.5179	1.28	79.60
35	25.7	30.9	1.48	92.3964	1.18	73.51
36	28.1	30.1	1.41	88.0263	1.10	68.72
37	26.4	25	1.4	87.402	1.11	69.15
38	34	27.5	1.45	90.5235	1.08	67.55
39	11.4	3.6	1.49	93.0207	1.34	83.50
40	10.4	3.8	1.56	97.3908	1.41	88.22
41	12.4	8.6	1.58	98.6394	1.41	87.76
42	13.4	8.3	1.52	94.8936	1.34	83.68
43	14.8	24.3	1.52	94.8936	1.32	82.66
44	28	24.6	1.44	89.8992	1.13	70.23
45	28	24.6	1.44	89.8992	1.13	70.23
46	27	28.8	1.44	89.8992	1.13	70.79
47	27.1	29.3	1.4	87.402	1.10	68.77
48	28	31.9	1.4	87.402	1.09	68.28
49	33.5	22.4	1.39	86.7777	1.04	65.00
50	32.6	21.3	1.59	99.2637	1.20	74.86
51	31	33.5	1.62	101.1366	1.24	77.20
52	27.9	22.4	1.47	91.7721	1.15	71.75
53	21.1	22.4	1.57	98.0151	1.30	80.94
54	20	4.7	1.61	100.5123	1.34	83.76
55	19.4	4.2	1.56	97.3908	1.31	81.57
56	23.6	7.1	1.56	97.3908	1.26	78.80
57	19.1	4.1	1.56	97.3908	1.31	81.77
58	19.3	14.7	1.57	98.0151	1.32	82.16
59	24.7	19.2	1.54	96.1422	1.23	77.10
60	25.7	17.9	1.41	88.0263	1.12	70.03
61	22.1	15.1	1.42	88.6506	1.16	72.60
62	19.9	11.3	1.48	92.3964	1.23	77.06
63	19.4	11.1	1.52	94.8936	1.27	79.48
64	27.5	19.1	1.51	94.2693	1.18	73.94
65	27.5	20.2	1.46	91.1478	1.15	71.49
66	28.7	21.4	1.43	89.2749	1.11	69.37
67	32.2	15.5	1.41	88.0263	1.07	66.59
68	28	21.8	1.56	97.3908	1.22	76.09
69	27.9	20.4	1.41	88.0263	1.10	68.82
70	17.8	15.1	1.44	89.8992	1.22	76.32
71	20.9	15.6	1.55	96.7665	1.28	80.04
72	17.1	10	1.64	102.3852	1.40	87.43
73	15.8	2.6	1.51	94.2693	1.30	81.41
74	26.5	15.2	1.51	94.2693	1.19	74.52
75	27.8	15.5	1.42	88.6506	1.11	69.37

76	27.8	15.5	1.4	87.402	1.10	68.39
77	16.2	8	1.4	87.402	1.20	75.22
78	28.7	19	1.54	96.1422	1.20	74.70
79	17.8	3.4	1.4	87.402	1.19	74.20
80	16.1	12.8	1.55	96.7665	1.34	83.35
81	26.2	16.8	1.46	91.1478	1.16	72.22